CARLOS III UNIVERSITY OF MADRID
HIGHER POLYTECHNIC

Fluid-Dynamic Characterization and Modal Analysis of a Fluidized Bed Prototype

---

Industrial Engineering in Energy Technology
Thermal and Fluid Engineering Department

AUTHOR: *Eduardo Barta Pérez* ***TUTOR:*** *Antonio Soria Verdugo*

Leganés, 17 September 2009

A quién ha querido y ha hecho posible que yo haya llegado hasta aquí.
A mis padres, como siempre, por todo.
A mis amigos y compañeros, por estar ahí.
A mi tutor de proyecto, por su apoyo, dedicación y paciencia.
Y...a una persona muy especial para mí...

INDEX

"Fluidization is the operation by which solid particles are transformed into a fluid-like state through suspension in a gas or liquid"

1. MASTER SUMMARY

This document resume 9 months of investigations that from the beginning has had the aim of settle the conditions that let enlarge the current understanding of the fluid-dynamic behavior of a fluidized beds (FB) by developing experimental and theoretical studies working with a FB prototype in the *Carlos III University* of Madrid.

2. INTRODUCTION

Biomass and specially coal are projected to remain a dominant source of fuel for electric power generation, both domestically and globally, well into the 21st century. Biomass reaches 45% of production from renewable energies in Spain [1], while coal currently supplies more than 56 % of U.S. electric power needs [2], and near 42 % of world electric power consumption [3].

In the early part of the next decade, power generators will select the next generation of base-load power plants [2]. In an era of tight environmental standards, new plants will have to meet very stringent air quality requirements. Coal and biomass is expected to remain a fuel of choice for many of these plants, and fluidized bed combustor (FBC) technology could provide an important option for a power company that must meet these air quality standards while producing the most affordable electricity possible for its consumers.

The understanding of the behavior and performance of any system in modern industry is a vital tool in establishing a previous diagnosis. This knowledge could shows the better way for installation design improvement, allowing to predict which

components should be evolved, sometimes because of its still inefficient operation, minimizing their maintenance costs and maximizing the quality of the system.

The compelling advantage of overall economy of fluidized contacting has been responsible for its successful use in industrial operations. But such a success depends on understanding and overcoming its disadvantages [4]. The study of the fluid-dynamic proprieties of the FBC is important to ensure the reliability of the reactor operation. Creating the knowledge base in both general and particular vision of the behavior of the elements under fluidization is essential to progress in developing new methods to increase the efficiency of this technology.

FBC is a technology used in power plants. FBC plants are more flexible than conventional plants since they can be fired on coal and biomass, among other fuels giving fluidization bed technology a greater flexibility in fuel use [5]. Fluidized beds suspend solid fuels on upward-blowing jets of air during the combustion process. The result is a turbulent mixing of gas and solids. The tumbling action, much like a bubbling fluid, provides more effective chemical reactions and heat transfer.

As in any other high technology design, the fluidized bed reactor does have it draw-backs, which any reactor designer must take into consideration. Among others, current understanding of the actual behavior of the materials in a fluidized bed is rather limited. It is very difficult to predict and calculate the complex mass and heat flows within the bed. Due to this lack of understanding, a pilot plant for new processes is required. Even with pilot plants, the scale-up can be very difficult [6].

The concept of a fluidized bed emerged in the early 50’s in the United States (US) and the United Kingdom (UK), but did not attract the interest of utilities, primarily because of the high cost and low importance of the emission of pollutants at that time. In 1968 a pilot plant was built in the UK where the technology was improved and tested the potential of such plants, but the British government did not have much interest in the plant, so most of the studies were financed by Swedish companies. In the early 70's was built the first plant that supplied electricity to the net. It was a small coal plant in Rivesville, West Virginia. After many technical and economic problems due to the high

maintaining cost, the plant was closed at the end of that decade. Other pioneer plants also experienced many problems with erosion, air inlet and coal feed. In the mid 70's began building plants in US and UK which finally managed to prove its effectiveness and benefits, some of these plants are still in operation. Parallel in the early 80's, there was a high development and new constructions of few plants in Spain and the Scandinavian countries, which served to improve existing technology and so to the creation of new concepts. Currently, the fluidized bed is experiencing a boom due to better utilization of coal and lower emissions of polluting gases.

Since the beginning of the twentieth century, several techniques have been used to study the better way to fire fuel to provide energy. From classical theoretical analysis based basically in using only the P-u (pressure-velocity) curve to determine minimum fluidization velocity (u_{mf}) to actual computer simulations. Whatever the methods used, it is first necessary to determine a complete theoretical behavior on which to settle the subsequence system evolutions, by which ensure high efficiency in the comprehension of fluid-dynamics FB performance. This project is including in the *Carlos III University* of Madrid ambitious purpose of compromise with the development of this technology.

2.1. REASONS AND IMPORTANCE OF THE PROJECT

When a new commercial-scale energy production plant or other physical or chemical process is designed, proper selection of technology is critical. Nowadays the world, in its particular technological career, is competing in another parallel hard race: the environmental care. Human is growing not only in knowledge and science fields, but in the necessity of a bigger compromise with himself and his environment too. Possible fluidization applications in the energy production industry, among other fields, could be an answer for twinning energy necessities and efficiency demand.

According to forecasts by the *European Commission* expressed in its *White Paper on Renewable Energy*, the energy input due to biomass (including municipal solid waste, *MSW*), estimated at 44.8 *Mtoe* in 1995, should now be 135 *Mtoe* in 2010 [2].

According to these data, biomass should triple its current contribution to achieve the goal.

At present, biomass reaches almost 50% of Spanish production from renewable energies, equivalent to 2.9% of total primary energy consumption, including conventional [2]. Both electrical and thermal resources are used more waste from forestry and agricultural industries.

According to *IEO 2007*, coal consumption will see growth of 74% for the period between 2004 and 2030 from 114.4 *quadrillion Btu* (2004) to 199.0 *quadrillion*. Until 2015 the average consumption is 2.6%, growth will slow to 1.8% in the period 2015-2030 [2]. Although the increase in the use of this fuel is for all geographic areas, are the non-OECD countries responsible for 85% of the increase, as in the advanced economies remains the coal replaced the natural gas and renewable energy.

In 2004, coal accounted for 26% of global energy consumption. Of this amount, two thirds was devoted to electricity production, 31% for industrial use and only 4% for residential and commercial uses. A 2007 *Ciemat* investigation report [1] estimates that by 2030 the relative importance of coal will increase 2 percentage points (to 28%), and its participation in power production worldwide will grow from 43 to 45%.

A substantial part of the electricity is generated nowadays in thermo-electrical plants or, by simply, thermal plants. Most of these facilities operate according to a simple process, in which the chemical energy of a fossil fuel is used to produce heat in a boiler, which will generate steam at high temperature and pressure, which in turn is transformed into mechanical energy in a *Rankine cycle*, which spins an alternator finally where mechanical energy is transformed into electricity.

Although coal is currently the second source of carbon dioxide after the oil, it is expected to be the first in 2010 [2]. The liability of the coal on the emissions of greenhouse gases will grow until the end of the period, when it reaches 43% of emissions, compared to 36% of oil or 21% of natural gas.

The FBC technology reduces the amount of sulfur emitted in the form of *SOx* emissions [7]. Limestone is used to precipitate out sulfate during combustion, which also allows more efficient heat transfer from the boiler to the apparatus used to capture the heat energy (usually water tubes). The heated precipitate coming in direct contact with the tubes (heating by conduction) increases the efficiency. Since this allows coal plants to burn at cooler temperatures, less *NOx* is also emitted [7]. However, burning at low temperatures could also cause an increase in polycyclic aromatic hydrocarbon emissions.

Increasing the current understanding of the actual behavior of the materials in a fluidized bed is, among others necessities, one of the definitive via to develop the FBC technology. So establish the particular proprieties and limitations and of the fluid-dynamic behavior by characterized the FB prototype‘s reactor is essential to settle the conditions to begin future decisive investigations.

2.2. APPROACH TO THE PROBLEM

As previously indicated, determine the fluid-dynamic behavior of the FB is an essential tool to increase the efficiency and, as a consequence, to improve the design of the system. However, the task is not simple, since the fluid-dynamic performance of a FB is a complex state consisting of multiple elements that has to be taken into account, each with a specific function and behavior. It is necessary to focus the study on at the right direction to extract correct information avoiding management of complex information unnecessary to solve the problem.

A FBC reactor is composed basically of a distributor (perforated plate distributor in prototype), a plenum chamber and the bed in which combustion and fluidization occurs. Is in this structure where soil, air, fuel, solid-liquid residues, exhaust gases and temperature is playing together the main roll of the reactor producing energy. Because of the huge amount of variables, all the elements involved in the operation, first detailed account, the acquisition data equipment and the facilities for experiment with prototype, have to be design, create and set up meticulously for better experimental results.

The problem is to implement a new strategy for assessment an FB fluid-dynamic guideline. To characterize the fluid-dynamic proprieties of the prototype theoretical techniques based in the *"Institute Of Chemicals Process Fundamentals"* investigation "*Evaluation of Minimum Fluidization Velocity in Gas Fluidized Bed from Pressure Fluctuation"* will be used working parallel with *Matlab* mathematical software to analyze the signals obtained from experiments.

2.3. PROJECT OBJECTIVES

The project ***"Fluid-Dynamic Characterization and Modal Analysis of a Fluidized Bed Prototype"*** is part of the research of the *Thermal and Fluids Department* of the *Carlos III University* of Madrid. For the development of the project has been raised the following objective:

CHARACTERIZATION OF ITS FLUID-DYNAMIC BEHAVIOR BASED ON THE MINIMUM FLUIDIZATION VELOCITY ANALYSIS AND DESIGN SUPPORTING OF THE FLUIDIZATION BED BASED ON THEORETICAL MODELS.

2.4. METHODOLOGY

In order to carry out this work, the methodology undergone has been as follows:

a) Literature collection on the following topics:

- Composition and operation of a standard fluidization bed model like the one used in the project.
- Work performed by other authors in the fluid-dynamic studies of u_{mf} for fluidized beds.
- Documentation of specialize hardware for the right data capture of the fluidized bed prototype experimentation.
- Mathematical and engineer software applications.

b) Study and analysis of the previous information.

c) Experimental work

- Calibration and tuning of all the intake measures equipment involved in the simulation of an on charge fluidized bed.
- Operative simulation of the fluidized bed with different regulated air charges blowing.

d) Results and data

- Analysis and study of the data obtained.
- Preparation of preliminary results.

e) Conclusions and findings.

All the project information collected and obtained along the project evolution has been analyzed and compiled divided into 7 different chapters. The structure appears as this:

- ✓ In the first and second ones, as it has been seen, the introduction gives a first approximation to the project environment.

- ✓ In the third chapter is treaty an overview of the particular description of all the elements from the prototype.

- ✓ The fourth one is all the facility design description.

- ✓ In chapter five will be the distributor design description, as an entire chapter is needed to develop the designing of this critical element.

- ✓ The main chapters are the sixth and seventh ones, in which fluid-dynamic analysis is carried out.

- ✓ Chapter number eight, is the structural analysis of vibration modes.

- ✓ Nine and ten chapters of the project are the findings and future prospects respectively, in which important results and studding propositions are given as a result of the intense investigation.

3. FLUIDIZED BED PROTOTYPE

3.1. PROTOTYPE GENERAL VIEW

For the development of the investigations a FB prototype was designed and constructed in the laboratories of the *Carlos III University* of Madrid. The prototype recreate a FB reactor, see Figure 3.1.1, by developing detailed all the important elements as the air intake, the plenum chamber, the distributor and the reactor that make up the principal system of the prototype. The equipment used during the experimental session involves:

Figure 3.1.1. FB Prototype of Carlos III University of Madrid laboratory used in the investigation.

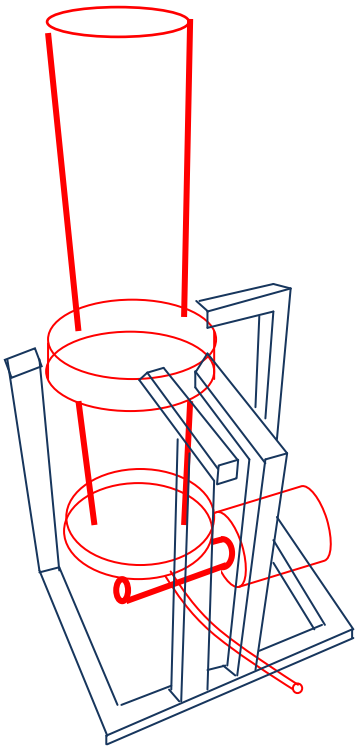

Figure 3.1.2. FB Prototype scheme obtain from the real prototype.

1 - A mainstay where reactor is located, conformed by aluminum beams supporting the whole structure, represented in blue in the scheme of Figure 3.1.2, will be analyzed and studied in *Chapter 8* also with prototype.

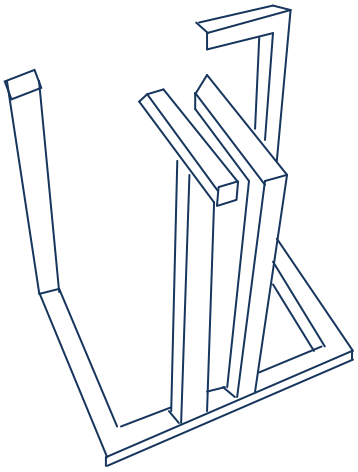

Figure 3.3. Main aluminum structure

2 - A *Plexiglas* cylinder, the reactor, filled with sand and with the following specifications:

Transverse Diameter: Ø 19,2 *cm*.

Height of vessel: 55,5 *cm*.

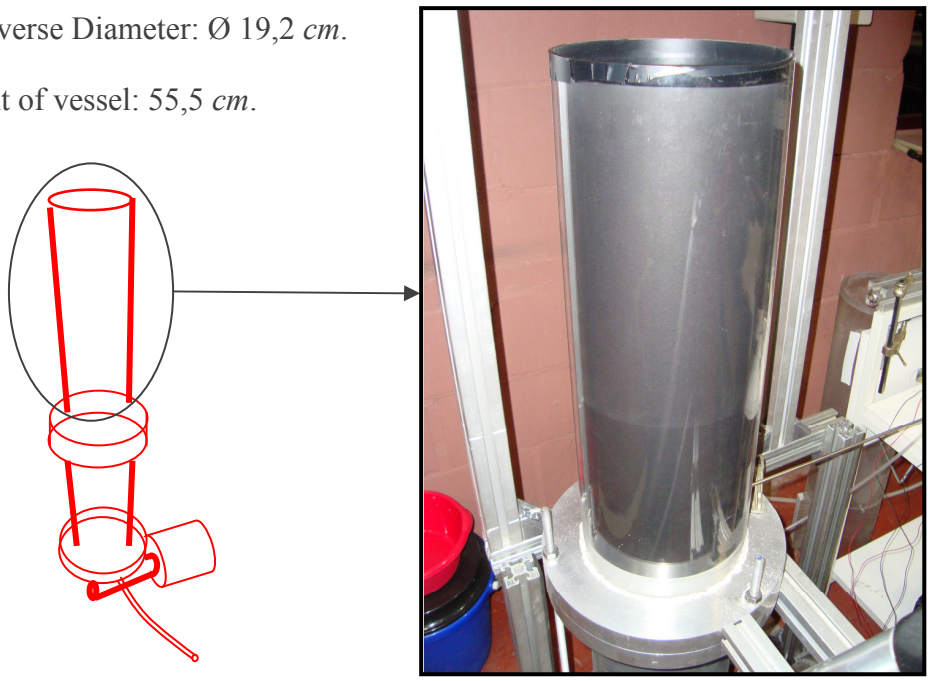

Figure 3.1.4. FB prototype reactor

3 – Plenum Chamber, where the air is conditioned after the air intake and before the distributor, with the following specifications.

Transverse Diameter: Ø 19,2 *cm*.

Height of the plenum: 39,5 *cm*

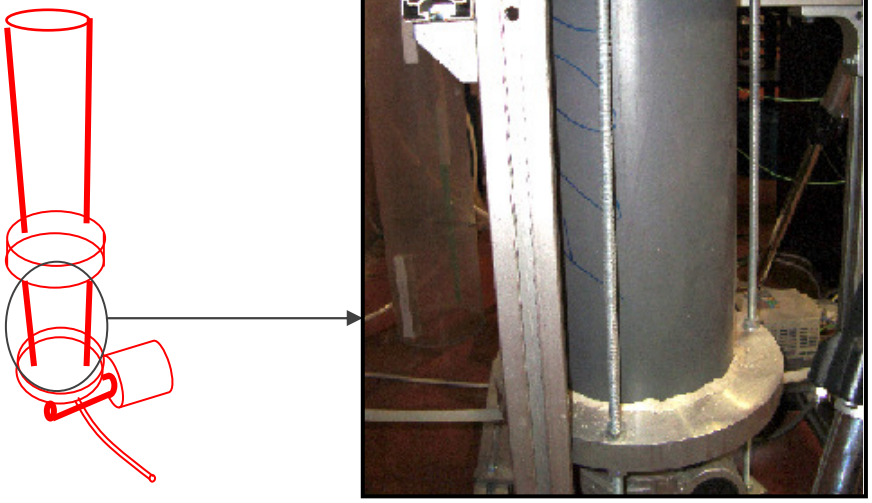

Figure 3.1.5. FB prototype plenum chamber

4 – The distributor, a perforated plate, with the following specifications:

Throat diameter: Ø 19,2 *cm*.

Thickness: 6 *mm*.

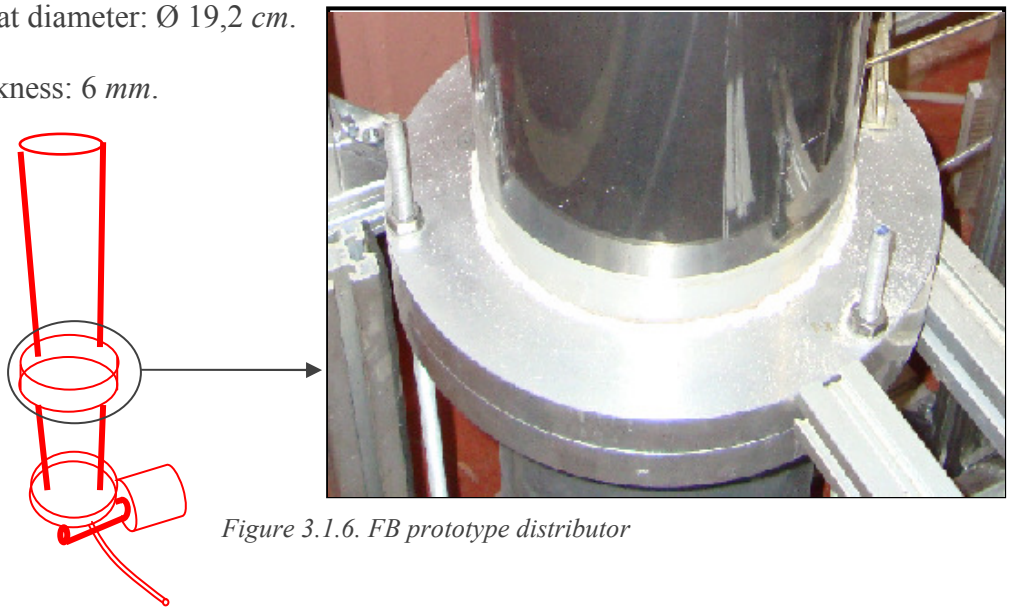

Figure 3.1.6. FB prototype distributor

5 – The air inlet, an adapted mechanism to incorporate air in below the plenum chamber:

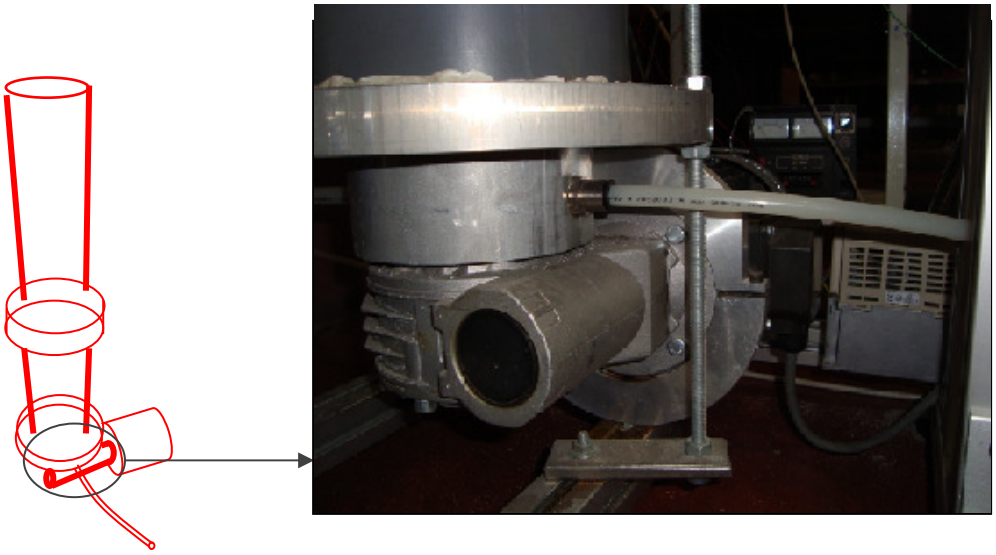

Figure 3.1.7. FB prototype air inlet

6 – Electrical motor, allows the swirl of the distributor by a conical transmission mechanism trough the plenum chamber:

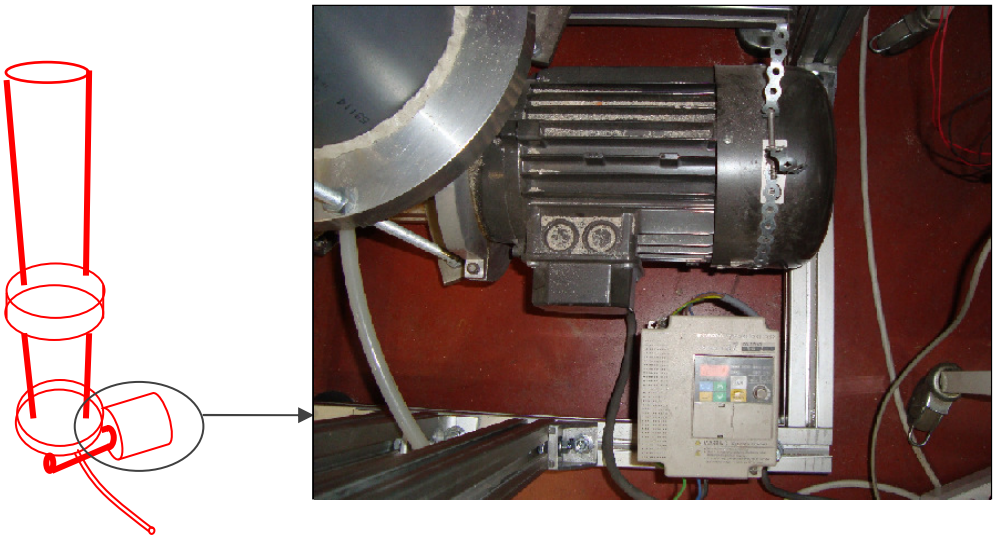

Figure 3.1.7. FB prototype electrical motor

3.2. THE PHENOMENON OF FLUIDIZATION [3]

Fluidization is the operation by which solid particles are transformed into a fluid-like state through suspension in a gas or liquid. This method of contacting has some unusual characteristics, and fluidization engineering puts them to good use.

The Phenomenon of Fluidization [3]

If a fluid is passed upward through a bed of fine particles, as shown in Figure 3.2.1.(a), at a low flow rate, the fluid merely percolates through the void spaces between stationary particles. This is the so called fixed bed. With an increase in flow rate, particles move apart and a few vibrate and move in restricted regions. This is known as expanded bed.

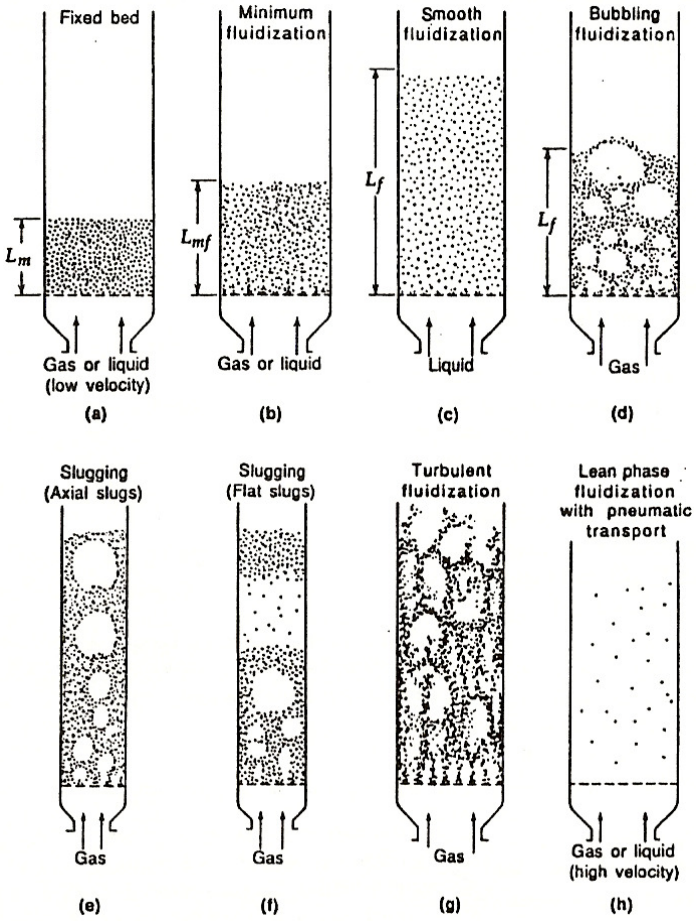

Figure 3.2.1. Various forms of contacting of a batch of solids by fluid, depending on the fluid up velocity.

At a still higher velocity, a point is reached where all the particles are just suspended by the upward-flowing gas or liquid. At this point the frictional force between particle and fluid just counterbalances the weight of the particles, the vertical component of the compressive force between adjacent particles disappears, and the pressure drop through any section of the bed about equals the weight of fluid and particles in that section. The bed is considered to be just fluidized and is referred to as an incipiently fluidized bed or a bed at minimum fluidization; see Figure 3.2.1.(b).

In liquid-solid systems, an increase in flow rate above minimum fluidization usually results in a smooth, progressive expansion of the bed. Gross flow instabilities are damped and remain small, and heterogeneity, or large-scale voids of liquid, are not observed under normal conditions. A bed such as this is called a particularly fluidized bed, a homogeneously fluidized bed, or a smoothly fluidized bed; see Figure. 3.2.1. (c). In gas-solid systems, such beds can be observed only under special conditions of fine light particles with dense gas at high pressure.

Generally, gas-solid systems behave quite differently. With an increase in flow rate beyond minimum fluidization, large instabilities with bubbling and channeling of gas are observed. At higher flow rates, agitation becomes more violent and the movement of` solids becomes more vigorous. In addition, the bed does not expand much beyond its volume at minimum fluidization. Such a bed is called an aggregative fluidized bed, a heterogeneous fluidized bed, or a bubbling fluidized bed; see Figure 3.2.1. (d). In a few rare cases, liquid-solid systems also behave as bubbling beds. This occurs only with very dense solids fluidized by low-density liquids.

Both gas and liquid fluidized beds are considered to be dense-phase fluidized beds as long as there is a fairly clearly defined upper limit or surface to the bed.

In gas solid systems, gas bubbles coalesce and grow as they rise, and in a deep enough bed of small diameter they may eventually become large enough to spread across the vessel. In the case of fine particles, they flow smoothly down by the wall around the rising void of gas. This is called slugging, with axial slugs, as shown in Figure 3.2.1. (e). For coarse particles, the portion of the bed above the bubble is pushed

upward, like a piston. Particles rain down from the slug, which finally disintegrates. At about this time another slug forms, and this unstable oscillatory motion is repeated. This is called a flat slug; see Figure 3.2.1. (f). Slugging is especially serious in long, narrow fluidized beds.

When fine particles are fluidized at a sufficiently high gas flow rate, the terminal velocity of` the solids is exceeded, the upper surface of the bed disappears, entrainment becomes appreciable, and, instead of bubbles, one observes a turbulent motion of solid clusters and voids of gas of various sizes and shapes. This is the turbulent fluidized bed, shown in Figure 3.2.1. (g). With a limiter increase in gas velocity, solids are carried out of the bed with the gas. In this state we have a disperse-, dilute-, or lean-phase fluidized bed with pneumatic transport of solids; see Figure 3.2.1. (h).

In both turbulent and lean-phase fluidization, large amounts of particles are entrained, precluding steady state operations. For steady state operation in these contacting modes, entrained particles have to be collected by cyclones and returned to the beds. In turbulent fluidized beds, inner cyclones can deal with the moderate rate of entrainment, as shown in Figure 3.2.2. (a), and this system is sometimes called a fluid bed. On the other hand, the rate of entrainment is far larger in lean-phase fluidized beds, which usually necessitates the use of big cyclone collectors outside the bed, as shown in Figure 3.2.2. (b). This system is called a fluidized bed or circulatory reactor.

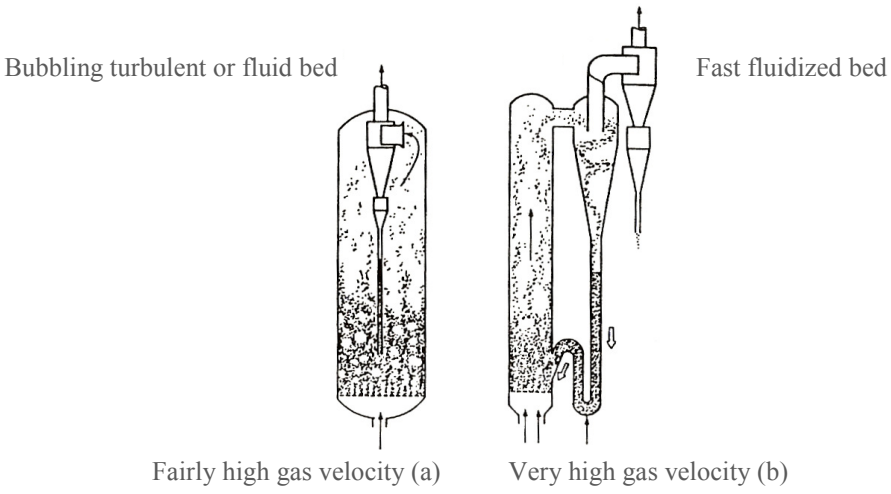

Figure 3.2.2. Various forms of contacting of a batch of solids by fluid.

Figure 3.2.3. Spouted bed.

In fluid beds and fast fluidized beds, smooth and steady recirculation of solids through the dipleg or other solid trapping device is crucial to good operations. These beds are called circulating fluidized beds. For systems with particles from *Geldart D* group, the spouted bed, sketched in Figure 3.2.3, represents a somewhat related contacting mode wherein comparatively coarse uniformly sized solids are contacted by gas. In this operation, a high-velocity spout of gas punches through the bed of solids, thereby transporting particles to the top of the bed. The rest of the solids move downward slowly around the spout and through gently upward- percolating gas. Behavior somewhere between bubbling and spouting is also seen, and this may be called spouted fluidized bed behavior.

Compared to other methods of gas-solid contacting, fluidized beds have some rather unusual and useful properties. This is not the case with liquid-solid fluidized beds. Thus, most of the important industrial applications of fluidization to date are with gas-solid systems, and for this reason this work deals primarily with these systems. It describes their characteristics and shows how they can be used.

Liquid-like Behavior of a Fluidized Bed [3]

A dense-phase gas fluidized bed looks very much like a boiling liquid and in many ways exhibits fluid-like behavior. This is shown in Figure 3.2.4. For example, a large, light object is easily pushed into a bed and, on release, will pop up and float on the surface. When the container is tipped, the upper surface of the bed remains horizontal, and when two beds are connected their levels equalize. Also, the difference in pressure between any two points in n bed is roughly equal to the static head of bed between these points. The bed also has liquid-like flow properties. Solids will gush in a jet from a hole in the side of a container and can be made to flow like a liquid from vessel to vessel.

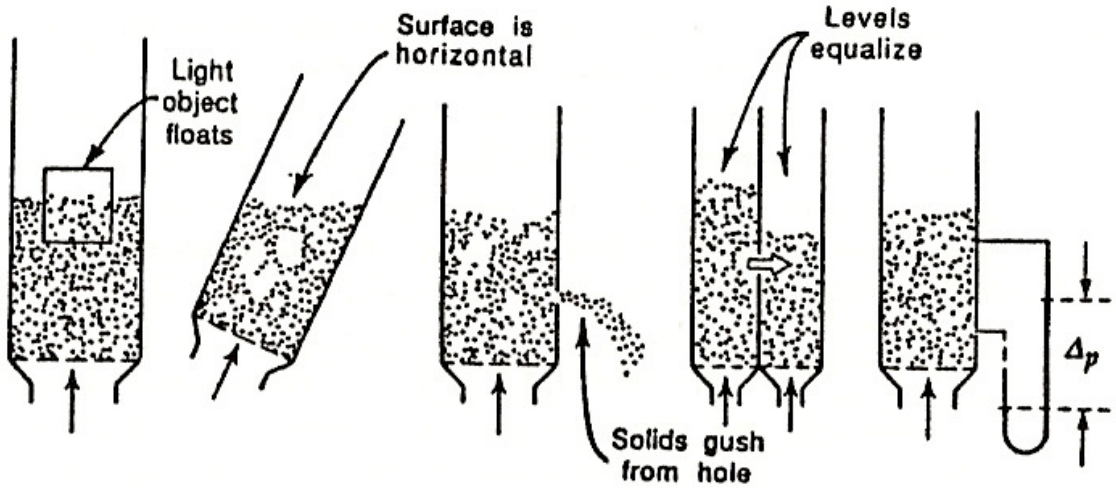

Figure 3.2.4. Liquid-like behavior of gas fluidized beds.

This liquid-like behavior allows various contacting schemes to be devised. As shown in Figure 3.2.5, these schemes include staged countercurrent contacting in a vessel containing perforated plates and down comers, crosscurrent contacting in a sectioned bed, and solid circulation between two beds.

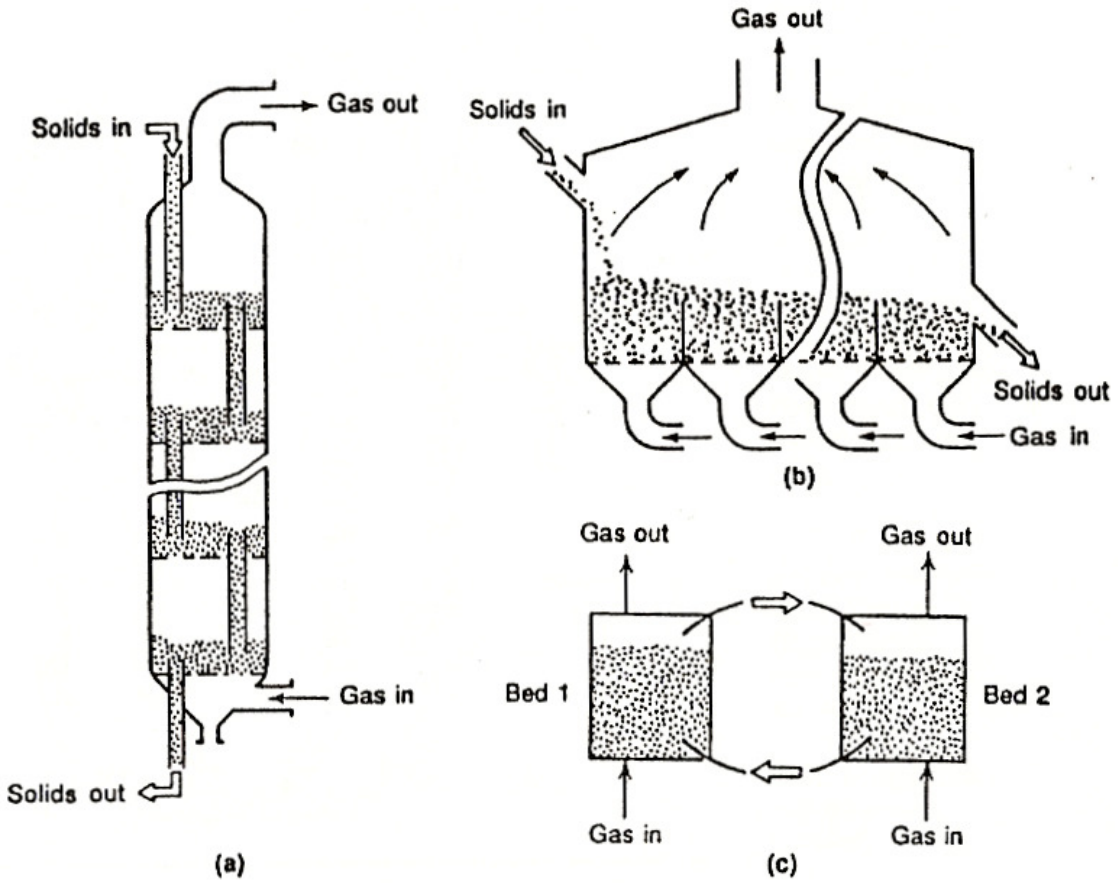

Figure 3.2.5. Contacting schemes with gas fluidized beds: (a) countercurrent; (b) crosscurrent; (c) solid circulation between two beds

To give some insight into the workings of a contacting scheme, consider a solids circulation system between two fluidized beds, as shown in Figure 3.2.6, if gas is injected into U-tube C connecting fluidized beds A and B and if the solids everywhere are fluidized, then it can be shown that the difference in static pressure in the two arms of the U-tube will be the driving force causing particles to flow from A to B. A combination of two such U-tubes will then allow complete circulation of solids. The faster the flow, the higher the frictional resistance, and so, as in any hydraulic system of this kind, the rate of circulation is determined by a balance between this frictional resistance and the previously mentioned pressure differences. The circulation is controlled by changing the frictional resistance of the system to flow, say, by slide valves or by varying the average densities of the flowing mixtures in the various portions of the connecting circuit, a procedure that modifies the pressure differences.

For proper operation of circulation and other solids flow systems, the solids must be maintained in dynamic suspension throughout, because any settling of particles can clog the lines and cause a complete shutdown of operations. Thus, special care is needed in the design of such systems: gas injectors must be properly sized, piping liable to settling and clogging should be avoided, and reliable start-up and shutdown procedures must be used.

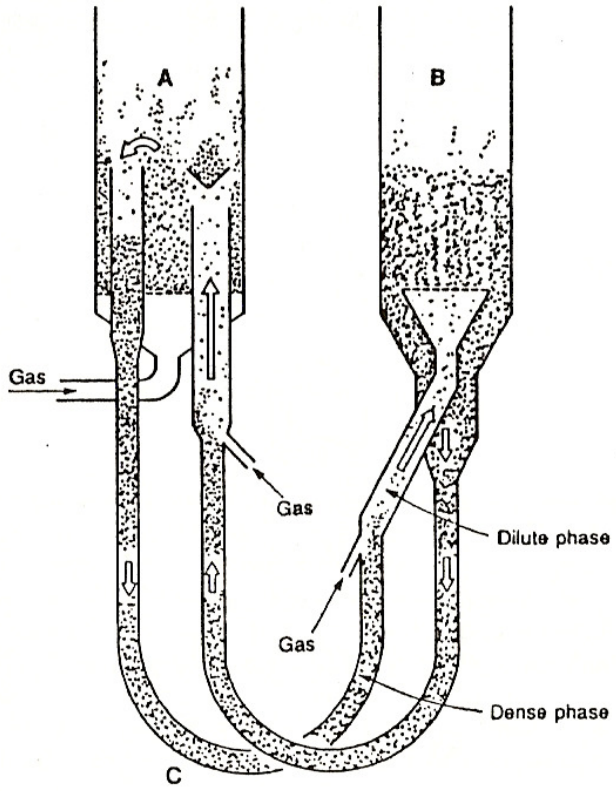

Figure 3.2.6. Operating principal for stable circulation between two beds.

Circulation systems such as shown in Figure 3.2.6 are used primarily for solid-catalyzed gas-phase reactions. Here, catalyst flows smoothly and continuously between reactor and regenerator. Because of the large specific heat of the solids, their rapid flow between reactor and regenerator can transport vast quantities of heat from one to the other and thus effectively control the temperature of the system. Actually, in highly endothermic or exothermic reactions, the circulation rate of the solids is chosen not only on the basis of the rate of solids deactivation but also as a means of achieving favorable temperature levels in reactor and regenerator. Automatic control of such operations is the rule.

This fluid-like behavior of solids with its rapid, easy transport and its intimate gas contacting is often the most important property recommending fluidization for industrial operations. These systems have the transport proprieties of fluids while retaining the thermal proprieties from solids.

Comparison with Other Contacting Methods [3]

Figure 3.2.7 sketches the different ways of contacting solids and gas streams, and compares fluidized beds and pneumatic conveying lines (or fast fluidized beds) with the other contacting modes.

In many of the conventional contacting modes, such as fixed beds, moving beds, and rotary cylinders, the gas flow or solid flow closely approximates the ideal of plug flow. Unfortunately, this is not the case for single fluidized beds where solids are best represented by well-mixed flow and the gas follows some intermediate and difficult-to-describe flow pattern. Nevertheless, with proper baffling and staging of units and negligible entrainment of solids, contacting in fluidized beds can approach the usually desirable extreme of countercurrent plug flow.

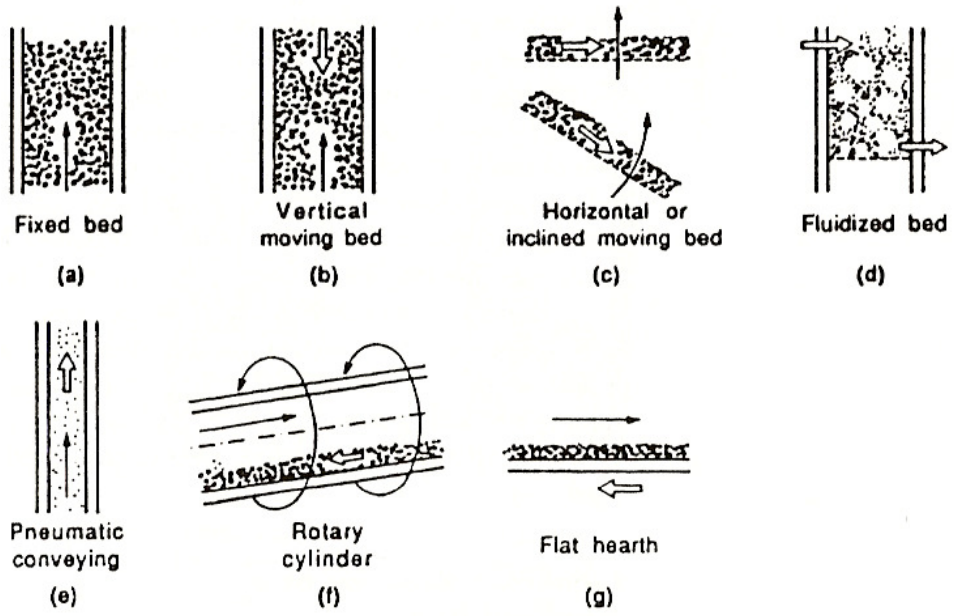

Figure 3.2.7. Contacting modes for gas solid reactors.

3.3. APPLICATIONS [8]

In 1920s, the Winkler process was developed to gasify coal in a fluidized bed, using oxygen. It was not commercially successful.

The first large scale commercial implementation, in the early 1940's, was the fluid catalytic cracking (FCC) process, which converted heavier petroleum cuts into gasoline. Carbon-rich "coke" deposits on the catalyst particles and deactivates the catalyst in less than 1 second. The fluidized catalyst particles are shuttled between the fluidized bed reactor and a fluidized bed burner where the coke deposits are burned off, generating heat for the endothermic cracking reaction.

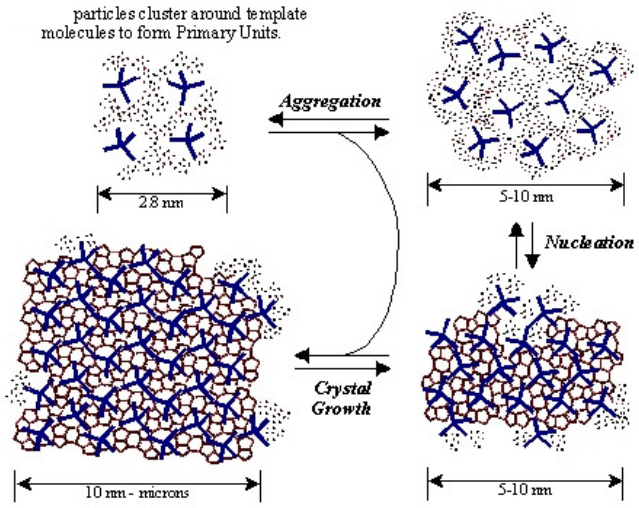

Figure 3.3.1. Fluid catalytic cracking process.

By the 1950's fluidized bed technology was being applied to mineral and metallurgical processes such as drying, *calcining*, and *sulfide roasting*.

In the 1960's, several fluidized bed processes dramatically reduced the cost of some important monomers. Examples are the *Sohio* process for *acrylonitrile* and the *oxychlorination* process for vinyl chloride.

In the late 1970's, a fluidized bed process for the synthesis of polyethylene dramatically reduced too the cost of this important polymer, making its use economical in many new applications. The polymerization reaction generates heat and the intense mixing associated with fluidization prevents hot spots where the polyethylene particles would melt. A similar process is used for the synthesis of polypropylene.

Currently, most of the processes that are being developed for the industrial production of carbon *nanotubes* use a fluidized bed.

The new potential application of fluidization technology is chemical looping combustion, which has not yet been commercialized. One solution to reduce the potential effect of carbon dioxide generated by fuel combustion (e.g. in power stations) on global warming is carbon dioxide sequestration.

Regular combustion with air produces a gas that is mostly nitrogen (as it is air's main component at about 80% in volume), which prevents economical sequestration. Chemical looping uses a metal oxide as a solid oxygen carrier. These metal oxide particles replace air (specifically oxygen in the air) in a combustion reaction with a solid, liquid or gaseous fuel in a fluidized bed, producing solid metal particles from the reduction of the metal oxides and a mixture of carbon dioxide and water vapor, the major products of any combustion reaction. The water vapor is condensed, leaving pure carbon dioxide which can be sequestered. The solid metal particles are circulated to another fluidized bed where they react with air (and again, specifically oxygen in the air), producing heat and oxidizing the metal particles to metal oxide particles that are recirculated to the fluidized bed combustor.

Nowadays, commercially available fluidized bed boilers of different technologies are manufacturers in a wide range of powers, from 5 *MWe* to 500 *MWe*, with technology continually adapted to meet a variety of industrial applications, particularly in the field of electricity generation. In this area, most of the operating facilities are based on the technology of Atmospheric bubbling fluidized bed (ABFB) and the Atmospheric Circulating Fluidize Bed (ACFB) [9].

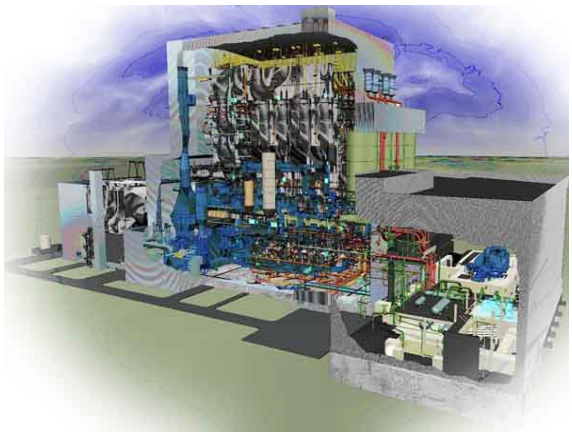

Figure 3.3.2. Foster Wheeler 500 - MWe supercritical circulating fluidized bed power plant.

4. FACILITY DESIGN

4.1. BED MATERIAL

In 1973, Professor *D. Geldart* proposed the grouping of powders in to four so-called "*Geldart* Groups" [10]. The groups are defined by their locations on a diagram of solid-fluid density difference and particle size. Design methods for fluidized beds can be tailored based upon the particle's *Geldart* grouping.

- Group A. For this group the particle size is between 20 μm and 100 μm, and the particle density is typically 1400 kg/m^3. Prior to the initiation of a bubbling bed phase, beds from these particles will expand by a factor of 2 to 3 at incipient fluidization, due to a decreased bulk density. Most powder-catalyzed beds utilize this group.

- Group B. The particle size lies between 200 μm and 10 mm and the particle density between 1400 and 4500 kg/m^3. Bubbling typically forms directly at incipient fluidization.

- Group C. This group contains extremely fine and subsequently the most cohesive particles. With a size of 20 μm to 30 μm, these particles fluidize under very difficult to achieve conditions, and may require the application of an external force, such as mechanical agitation.

- Group D. The particles in this region are above 1 mm and typically have high particle densities. Fluidization of this group requires very high fluid energies and is typically associated with high levels of abrasion. Drying grains and peas, roasting coffee beans, gasifying coals, and some roasting metal ores are such solids, and they are usually processed in shallow beds or in the spouting mode.

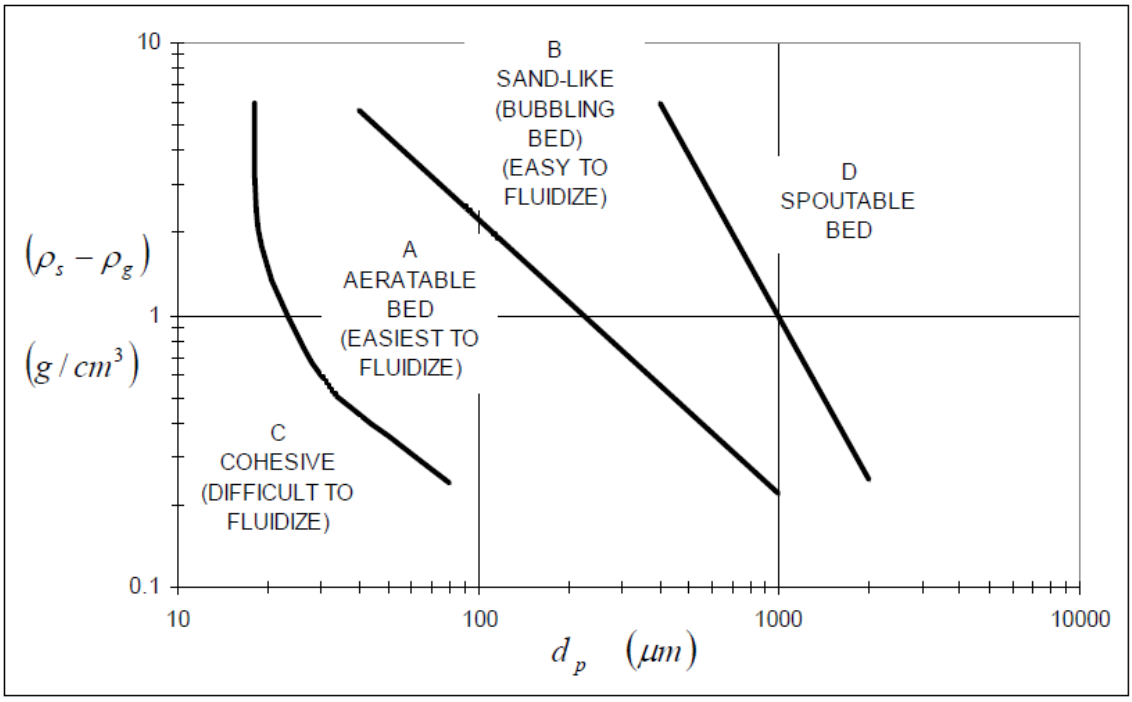

Figure 4.1.1. Geldart classification of fluidized beds. Particle properties are related to the type of fluidized beds.

Regardless of density, below 20 *μm* particles present a cohesive behavior (region C) that makes difficult fluidization, as they tend to form among themselves heavy particles. Above 3 *mm* particles show a jet-type behavior (region D), not suitable too for the operation of a fluidized bed. The regions A and B define the conditions to be met by the solid particles to achieve adequate fluidization [9].

The commercial sand in which the authors of the experiment have had accessed has determine the composition of the bed particles. For characterize sand, previously has received a preparation treatment based in mechanical sieves. The quantity deposited in the prototype to conform the bed reactor has been 4,5 kg occupying 9,6 *cm* (½ diameter) high in the bed reactor. That gives a relative density of 1620 kg/m^3, being 1,16 kg/m^3 used as air density, and supposing a typical *packing factor* of 0,63 [19] for this kind of sands, that gives a real density of 2640 kg/m^3.

Experimentally has been determined the *packing factor* as a result of direct measures in prototype sand. For 8,15 *kg* of material by occupying 5 *liters* in vessel and

supposing a typical density for sand of 2600 kg/m^3 packing factor is calculated as follow:

$$\left.\begin{array}{l} \varepsilon_s = \dfrac{\rho\ relative}{\rho\ real} \\ \\ \varepsilon_s = \dfrac{(8{,}15\ kg\ /\ 5.10^{-3}\ m^3)}{2600\ kg/m^3} \end{array}\right\} \quad \begin{array}{c} \varepsilon_s = 0{,}627 \\ \approx \\ theory\ \varepsilon_s\ 0{,}63 \end{array}$$

The results of the mechanical sieves treatment are shown in Table 4.1.1:

Sieve (mm)	Sieve weight (g)	Sieve weight + sample (g)	Sample weight (g)	Mass fraction (%)	Cumulative mass fraction (%)
2	337,02	337,02	0,00	0,00	100,00
1	323,85	365,04	41,19	5,85	100,00
0,85	302,58	472,96	170,38	24,18	94,15
0,6	312,73	756,85	444,12	63,03	69,97
0,425	296,35	339,97	43,62	6,19	6,94
0,25	275,65	280,93	5,28	0,75	0,75
0,18	245,75	245,77	0,02	0,00	0,00
0,106	242,01	242,01	0,00	0,00	0,00
0,053	233,7	233,7	0,00	0,00	0,00
0	362,38	362,38	0,00	0,00	0,00

Table 4.1.1. Results for the sample sift, giving results for the sieve weight, the sieve weight plus sample weight, the sample weight, the mass fraction and the cumulative mass fraction.

The great predominant particle diameter, as could be reflected in the Graphic 4.1.1 and Graphic 4.1.2, is around 0,6 mm.

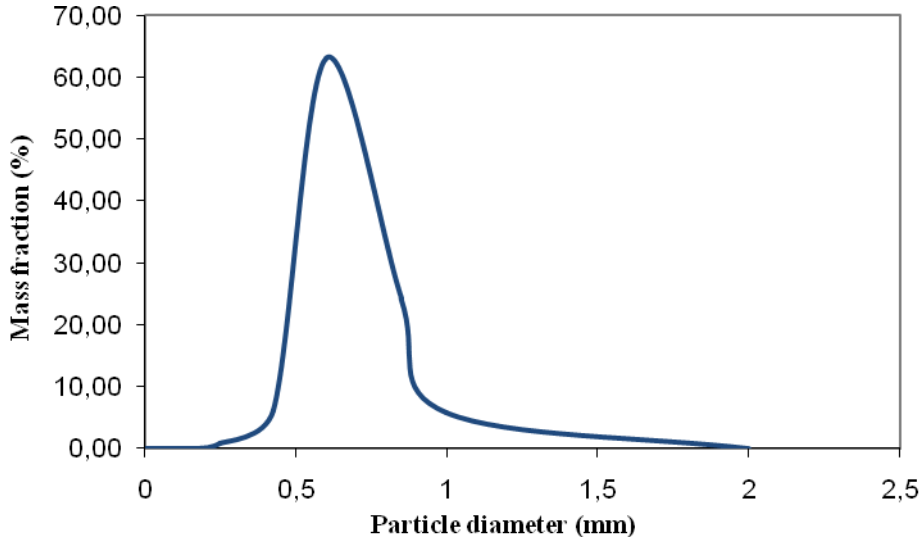

Graphic 4.1.1. Particle diameter distribution.

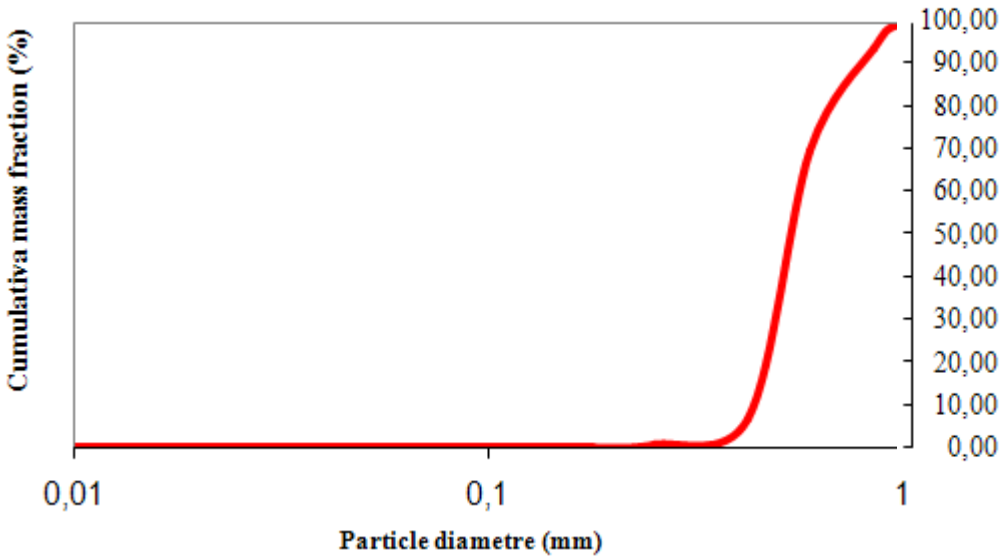

Graphic 4.1.2. Cumulative mass factor of the inert material.

In this context, particles from group B have been selected as a result.

In beds of *Geldart* B particles solids, bubbles form as soon as the gas velocity exceeds u_{mf}. Thus, u_{mb} (minimum velocity as which bubbles appears) / $u_{mf} \approx 1$. This kind of particles is appropriate for recreate a fluidization bed reactor as behaves as follow[3]:

• Small bubbles form at the distributor and grow and coalesce as they rise trough the bed.

• Bubble size increases roughly linearly with the distance above the distributor and excess gas velocity.

• Bubble size is roughly independent of mean particle size.

• Vigorous bubbling encourages the gross circulation off solids.

The majority of gas-solid reactions, metallurgical and other ones, are run in this regime because the mean size and size distribution of feed particles are usually determined by the upstream processing of the raw materials.

4.2. BED

The height reached by the sand in the boiler prototype has been set as a result of the scale up gives by the typical design of a FB reactor. The procedure to establish the bed height is to find a relation between the fix fluidized bed height and bed diameter (aspect ratio $a_r = H/D$).

Although the effect of the aspect ratio on fluidized bed performance is an important topic, not much research work seems to have been carried out on this aspect with distributor swirl[11]. For example, in high-temperature chlorination of *zireon*, there are no stable internals that can withstand the aggressive reaction environment. In such situations, the aspect ratio should be selected judiciously [11].

But generally, in a bed with internals the bubble size is close to constant, so for a given weight of solids and volumetric gas flow rate, the aspect ratio has only a small effect on conversion. However, to avoid possible short-circuiting of gas and to ensure good temperature control, very shallow beds should be avoided. As a safe value the minimum aspect ratio should be about unity [3].

As this scale-up designing pattern is only suitable for large units[3], also will be consider half of diameter aspect ratio for fix bed height in order to cover all the commercial possibilities of FB applications.

As a result, two parallel experiments (with and without distributor rotation) will be carried out under three different suppositions for large and commercial units with ¾, ½ and ¼ aspect ratio aspect ratio respectively. So that, sand will raise three different fix bed heights of *14,4 cm*, *9,6 cm* and *4,8 cm* in the boiler.

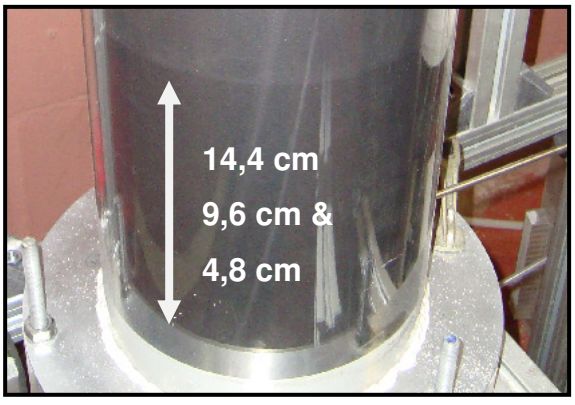

Figure 4.2.1. Height of the sand deposited in the bed reactor equal to 1 and ½ times reactor diameter.

4.3. SAMPLE MEASURE SYSTEM

All information intakes from the prototype need a reliable acquisition system for the experimental data capture, so for the plenum chamber as for the mid-height bed reactor measurements too.

Carlos III University has offer for working with the prototype to the *Thermal and Fluid Department* three sensors highly proved in other departmental tests. These are two *Kistler* sensors for measurement pressure variations, one in the plenum chamber and other one in the mid-height bed reactor, and a differential sensor for measuring the pressure difference between ambient and the pressure in the mid-height bed reactor, see Figure 4.3.1. These pressure signals, converted by the sensors into electrical signals, will be sending to the acquisition system. This system is conformed by two amplifiers connected to the *Kistlers* sensors and a data acquisition board connected to the computer. So the two amplifiers and the pressure difference sensor send directly the signals to the acquisition board that will implement the information for it posterior treatment, see Figure 4.3.1.

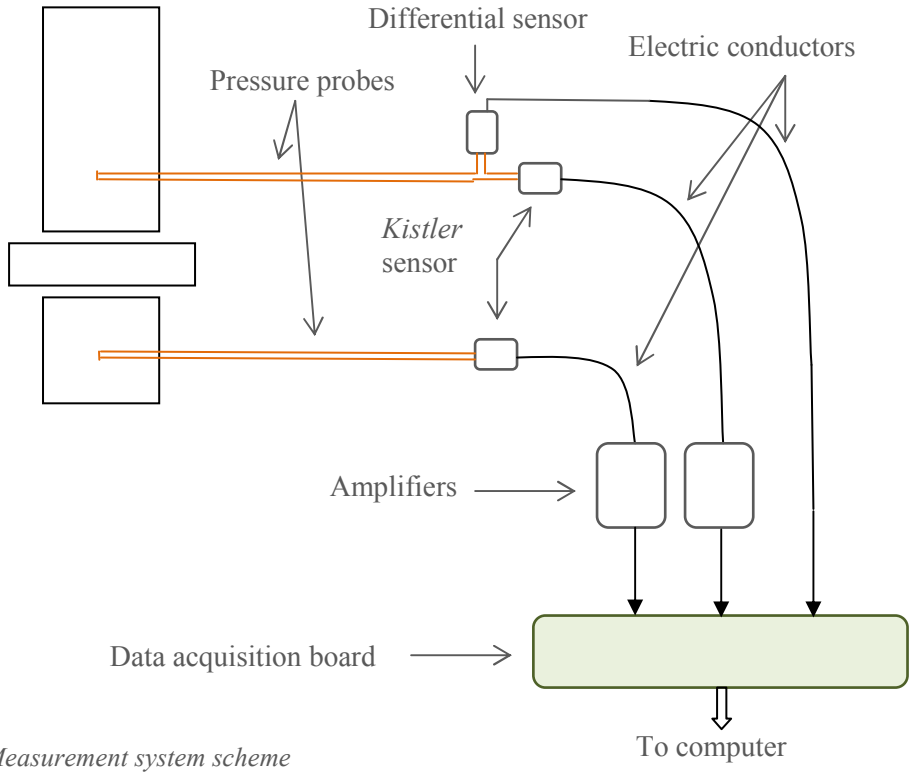

Figure 4.3.1. Measurement system scheme

4.3.1 PROBE DESIGN

Experiments in a bench-scale fluidized bed of *Geldart* B particles, as this prototype is, show that a probe–transducer system can severely distort a measured pressure signal. Generally speaking, for a wide range of transducer volumes from 500 up to 2500 mm^3, a pressure probe with an internal diameter between 2 and 5 mm will give minimum distortion of the pressure signal. The longer the probe, the more critical the choice of the probe diameter becomes. In smaller fluidized beds, or when applying smaller particles, the frequency range of interest will shift to higher frequencies. This will not influence the optimum probe diameter range from 2 to 5 mm, but the higher the frequency range of interest, the more important it becomes to keep the probe lengths limited[12].

So that, the pressure probe form the sensor to the acquisition system will need to be designed taking into account a maximum length and an interior diameter value below which, the signal, will not be disturbed until could be interpreted in the acquisition system.

In order to elect a criterion to design the probe, it was found that the *Delft University of Technology* has widely experimented with pressure probes for fluidized bed. In its investigations, *Van Ommen et al* discover that the *Bergh and Tijdeman* model, originally developed for wind-tunnel testing, is the only model that gives a good prediction of the frequency response characteristics of a probe–transducer system for a wide range of probe dimensions [12]. As a visual way for explain the process by which conclusion were obtained could be checked in the next graphical experimental results, see Graphics 4.3.1.1.

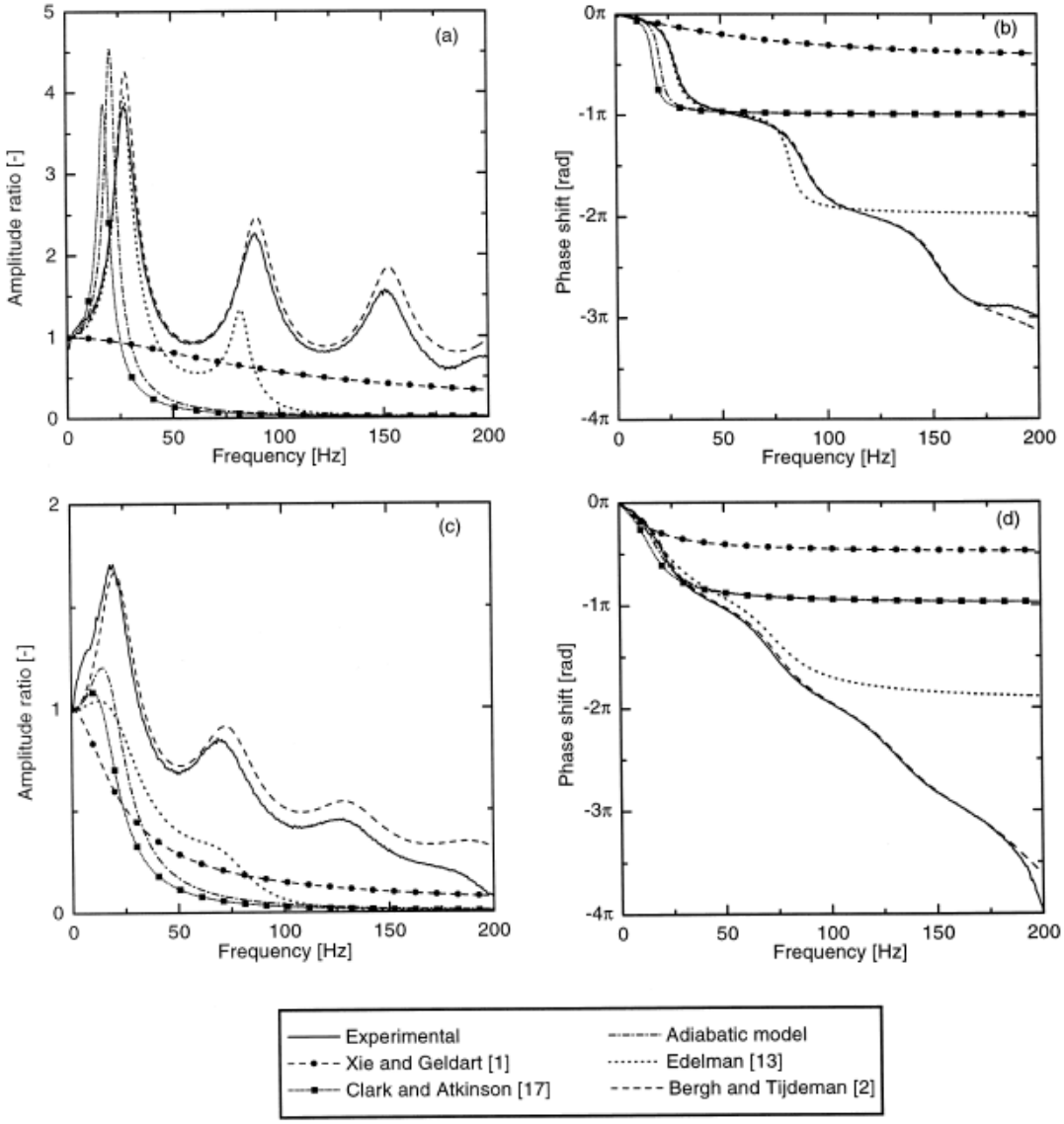

Graphic 4.3.1.1. Amplitude ratio curves determined from fluidized bed experiments (type B) for varying probe lengths at a limited internal diameter of˙4 mm. The lines give the experimental results; the symbols give the Bergh and Tijdeman prediction model.

It is shown in the graphic above, Graphic 4.3.1.1., how the *Bergh and Tijdeman* model fit with the experimental results carried out. As now has came upon a theory model for probe designing, so valid for fluidized bed pressure measuring, found the dimensions of a probe based in the *Bergh and Tijdeman* model was the next step.

New experiments carried out by *Johnson el al* used a probe for pressure testing in fluidized bed according to the report conclusion [13]. Then, a 50 *cm* length and 4 *mm*

interior diameter probe base in the *Bergh and Tijdeman* model was defined for measuring pressure. Investigations based in this model showed that this dimension gives a resonance frequency of 670 *Hz*; frequency much higher that the typical ones for fluidized beds (1-5 *Hz*) [13].

So that, the dimensions of the probe for the prototype will be the ones used in the *Chalmers University of Technology* experiments (50 cm length; 4 mm of interior diameter), as those probes were design based in the *Bergh and Tijdeman* theory model outweigh validated.

4.3.2 ACQUISTION SYSTEM

The sensors used to measure the pressure variation were two *Kistlers* Type 5015A. These sensors gives the versatility needed for adjust the acquisitions conditions to the experiment parameters.

The functional behavior is based in the piezoelectric effect. Piezoelectric sensors convert mechanical quantities such as pressure, directly into an electric charge. The charge produced is proportional to the force acting on the quartz crystal contained in the sensor. In addition, an integrated amplifier circuit is included with these sensors. This converts the high impedance charge signal of the piezoelectric sensor element into a low impedance voltage. The great advantage of the charge amplifier principle is that it allows quasi-static measurement as it let keep interference in a very low level [14].

As the acquisition board received the electrical signal from amplifier between two electrical limits from 0 to 5 V, a conversion factor for the *Kistler* amplifier system has to be defining in order to obtain the certain precision for appropriate data working. Some test revealed that pressure variation was between 0 to 5.10^{-2} bar limits. So the amplifier factor to be introduced for a proper data precision has to be calculated as follow:

$$\left.\begin{array}{l} \textit{acquisition board card limits: } 0 - 5\ V \\ \textit{pressure variation limits: } 0 - 5.10^{-2}\ bar \end{array}\right\} \quad \begin{array}{c} \textit{Conversion factor} = \dfrac{5.10^{-2}}{5}\ \dfrac{bar}{V} \\ C_f = 0{,}01\ bar / V \end{array}$$

When first samples were taken, the work team realizes an increasing drift appears in the measuring.

As the pressure variation oscillate around a mean value different form 0, for proper future analysis is interest to reset the mean pressure variation to the 0 value. High pass filter could help for solve this action.

The high pass filter of the *Kistler* has to set up by defining a time constant. For the time constant setting has been studied the experiments carried out by *Johnson et al* report [13]. This fluidized bed research reveal that the measures were picked with the same *Kistler* sensor Type 5015A by setting a time constant based in a frequency of 0,1 *Hz* [13]. Time constant selection will be the one based in a frequency of 0,16 *Hz* (close to the 0,1 *Hz* valid one). This time constant fit the better conditions to analyze the prototype frequency response as this value became a divisor of the intake data frequency (200 *Hz*) not to high, for an unnecessary huge amount of information, not too low for a better data precision.

The high pass filter works as a *"subtract mean variation pressure"* in 0,16 *Hz* intervals of the real time pressure measured. That is shown in the next Graphic 4.3.2.2.

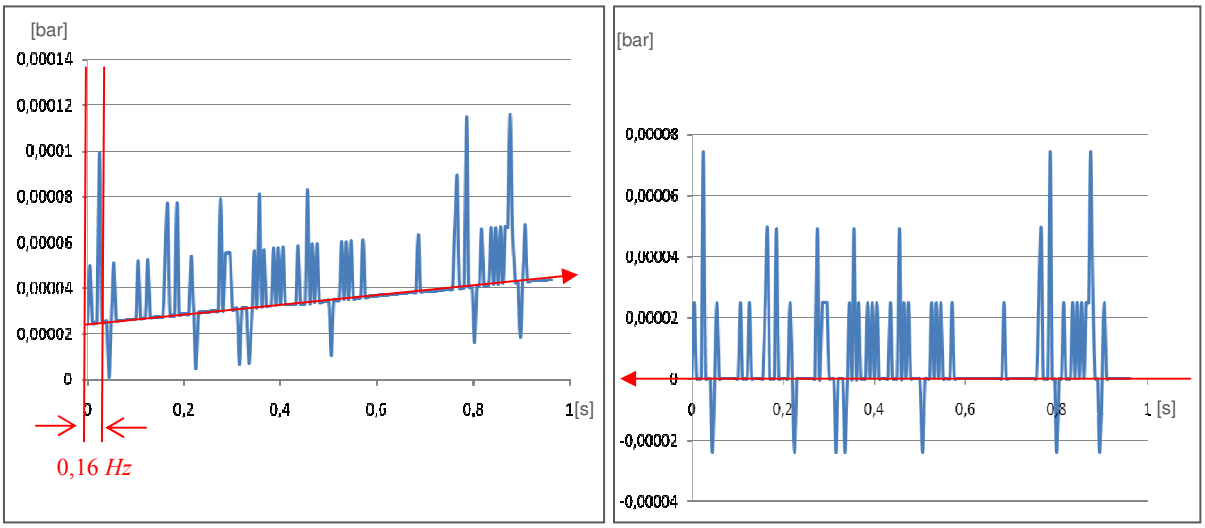

Graphic 4.3.2.2. High pass filter effect for one second registered measurements in mid-height bed. Left graphic is the original register; right graphic is the final evaluation, where mean pressure variation of every 0,16 Hz interval has been subtract to the real time pressure.

Higher frequency interference signals can be attenuated with a low-pass filter, as this *Kistler* amplifier has. The cutoff frequency can be varied in this *Kistler* between 5 *Hz* and 30 *Hz* and the cutoff frequency could be calculated by the *Nyquist Criteria*: the signal obtained from this reconstruction process can have no frequencies higher than one-half the sampling frequency. According to the theorem, the reconstructed signal will match the original signal provided that the original signal contains no frequencies at or above this limit. So that, the cutoff frequency is calculate as shown:

$$f_{cutoof} = \frac{sampling\ frequency}{2}$$

$$f_{cutoof} = \frac{200}{2}\ Hz \longrightarrow f_{cutoof} = 100\ Hz$$

The final sensor disposition is shown in next Figure 4.3.2.1. :

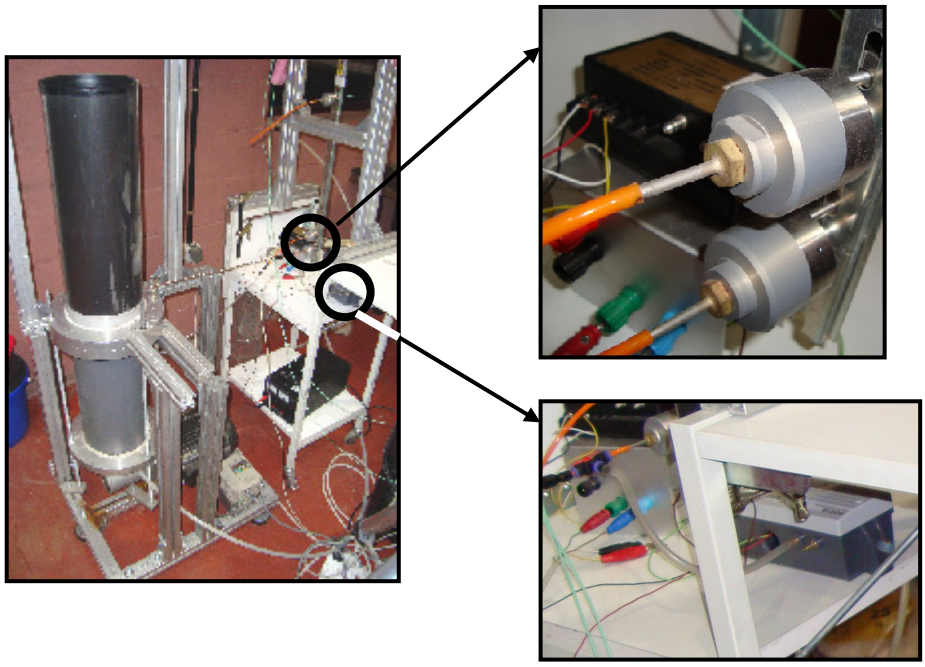

Figure 4.3.2.1. The three sensors. The uppers ones for measuring the variations pressure and the lower one for measuring the total pressure in the mid-bed.

4.4. AIR SYSTEM

As the normal operation of a FBC is based in the gas pumping through the particles, not also to provide sustentation but to providing oxidizing too, the prototype needs an external gas supply.

The gas composition depends on the FBC final application. For example, pioneering FBC for coal gasification (*Winkler gas generator*) or a *BASF* fluidized coke unit, for *thermal cracking,* work with oxygen fluxes; inert gas is suitable for *drying very wet feedstock*; or air fluxes for *synthesis reactions*, *hydrocarbons catalytic cracking* or *heat exchange applications* [3].

From a global perspective, the future of atmospheric circulating fluidized bed mainly using coal as fuel looks really promising, since, at it has been said, it is estimated at 150 *GWe* power for 2020 based on this technology [9].

As these combustion systems work mostly with a primary air flux [3], it seems to be suitable to work with air flows. In the *Carlos III University* facilities a compressed air system is available, to which it could be accessed by the department team.

Situated in the nearby of the prototype is located an external valve. The facility let control the air flux by a graduated *rotameter* connected to it, see Figure 4.5.1.

Figure 4.5.1. Graduated rotameter from 50 to 1400 liters per minute.

Also, the prototype is endowed with an axial motor connected to the air inlet for pumping the flux into the plenum chamber, see Figure 4.5.2, working at a constant velocity of 100 *rpm*. Is in the plenum chamber where the conditions of the air are stabilize seems to be a continuous axial vertical flow with minimum radial velocity component until arrive to the distributor.

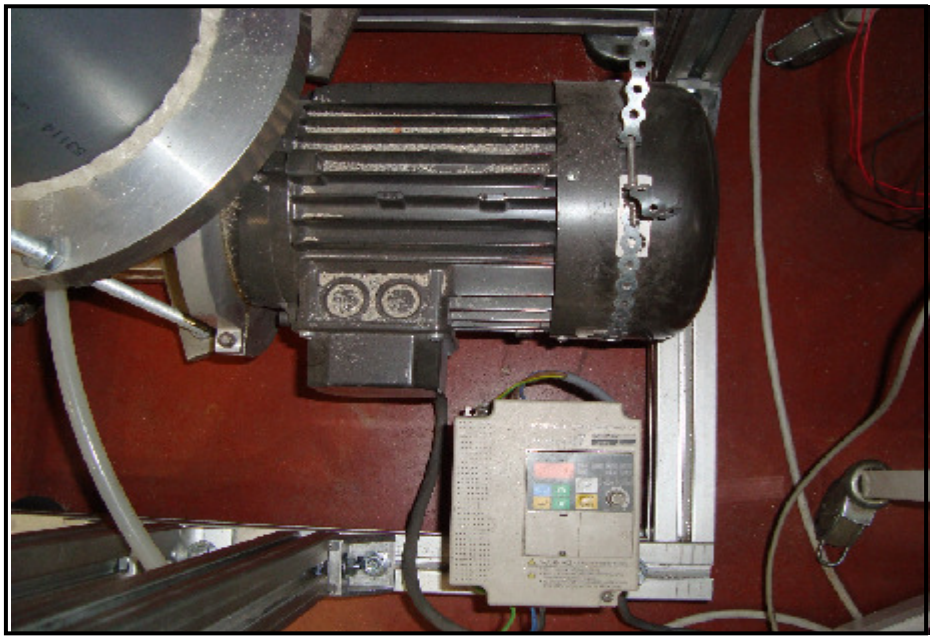

Figure 4.5.2. Axial motor to rotate the distributor.

Both dispositives are connected trough two tubes from the external valve to the air inlet. The objective is to have the desire air flux at the *rotameter* outlet. Three first different tube disposition test demonstrated that the drop was over the limit: at the *rotameter* output could not be obtain the 1200 *lpm* necessary to complete the future experiments. Diminish the drop in the pipe line link became the guide line of the air connection designing.

First design had only one tube of 1.5 cm diameter from air valve to the prototype. Then, as the drop was too high, it was decided to take two tubes of the same diameter. Proved insufficient. The next strategy then, was to increase the diameter tubes. Maintaining the two tubes lines from external valve to the motor, were found a tube with a lower thickness. For the time being enough, but still result over the limit as one

new difficulty appeared when the prototype. Because department space reasons, prototype had to be taken out of the laboratory, increasing with it the tube length. As the diameter reduction dimension were now a difficult task, as the radius were commercially fixed, the new strategy was in this occasion to minimize the longitude of the pipe line between the two points, now larger than first disposition. Then, the only way to address this approach was to go trough the laboratory window by drilling the frame to arrive as straight as possible out of the working room. Solution was success, see Figure 4.5.4.

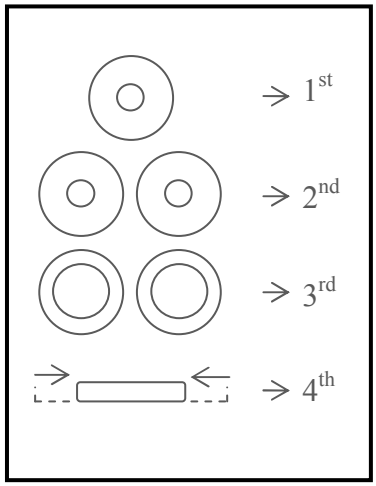

Figure 4.5.3. Pipe line connection designing.

The final disposition pipe line connection is shown as follow:

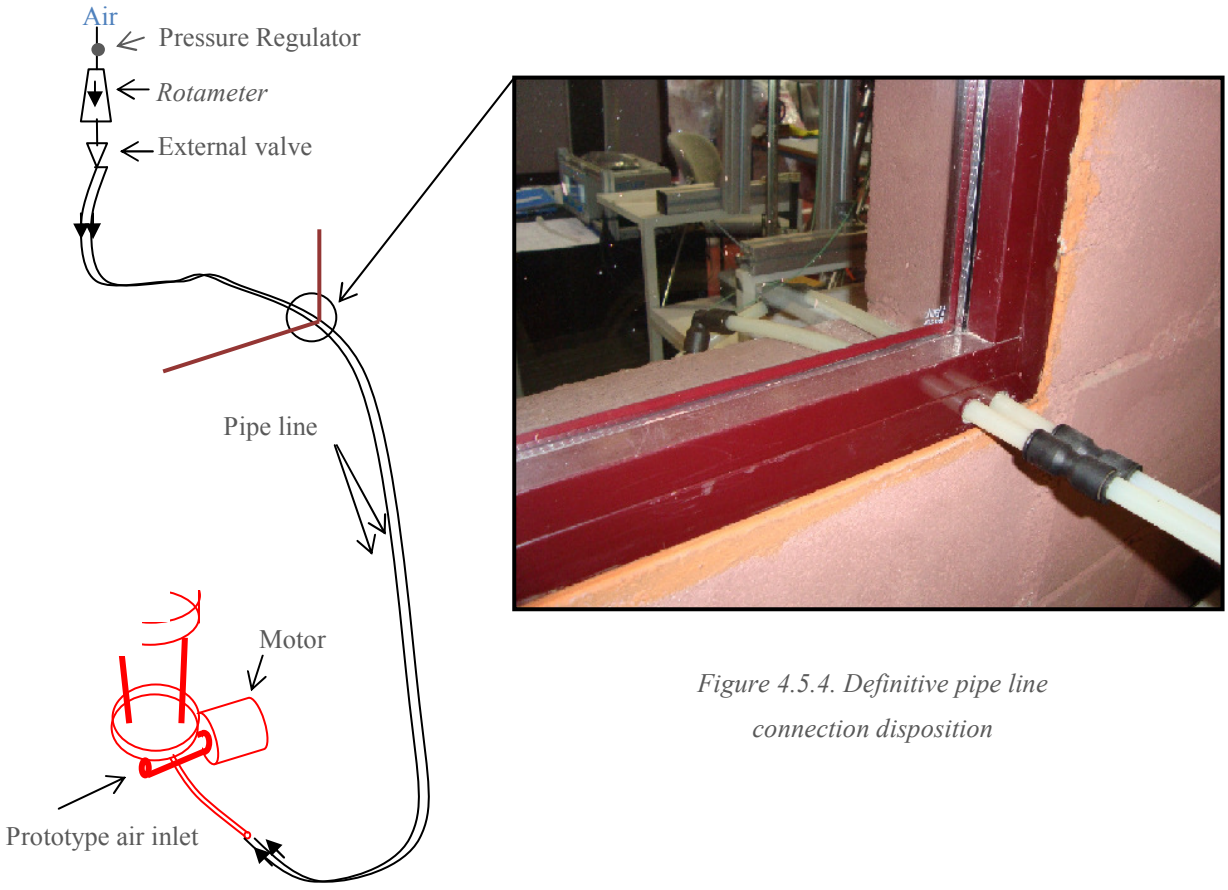

Figure 4.5.4. Definitive pipe line connection disposition

5. DISTRIBUTOR DESIGNING

5.1. JUSTIFY DESIGN

Most small-scale studies in fluidization use ceramic or sintered metal porous plate distributors, because they have a sufficiently high flow resistance to give a uniform distribution of gas across the bed. This situation is ideal. Many other materials can do this - for instance, filter cloth, compressed fibers, compacted wire plate or even a thin bed of small particles [3].

In addition, because they are cheap and easy to fabricate, perforated plate distributors are widely used in industry [3].

But perforated plate distributors cannot be used under severe operating conditions, such as high temperature or in highly reactive environment. Also, special precautions must be taken to ensure that the incoming gas is free of filter-clogging material. Place a slit is frequently used to prevent solids from falling through the distributor. However, in all designs, particles are apt to settle, sinter, and stick on the distributor plate itself. Because of their complicated construction, slit type distributors are much more expensive that only perforated plate [3].

However, a slit perforated plate distributor has been designed for the experiment as is economically assumable for the *Carlos III University Thermal and Fluids Department* and experimentally more interesting for the investigation, as this design will ensure the better distributor operation.

5.1.1 FIRST DISTRIBUTOR

Although all the installations have been design by the actual department team, the first intention was to utilize a first distributor already designed by anterior department team.

First testing demonstrates that was not so much difference between the values obtained by the three sensors when distributor rotated and when not. This experience made think the new department team the drop was high enough to keep fluidized the bed but not to make it commercially interesting.

High drop values (with an upper limit for distributor drop $\Delta p_d = (0,2 - 0,4) \cdot \Delta p_b$ [15], see point *5.1.2. Distributor Design*) for working velocity (around $u_0 = 0,5$ *m/s)* in distributor, force to increase the power in the air supplier system, making it unnecessary more expensive and consequently for the project far from real ones, see Graphic 5.1.1.1.

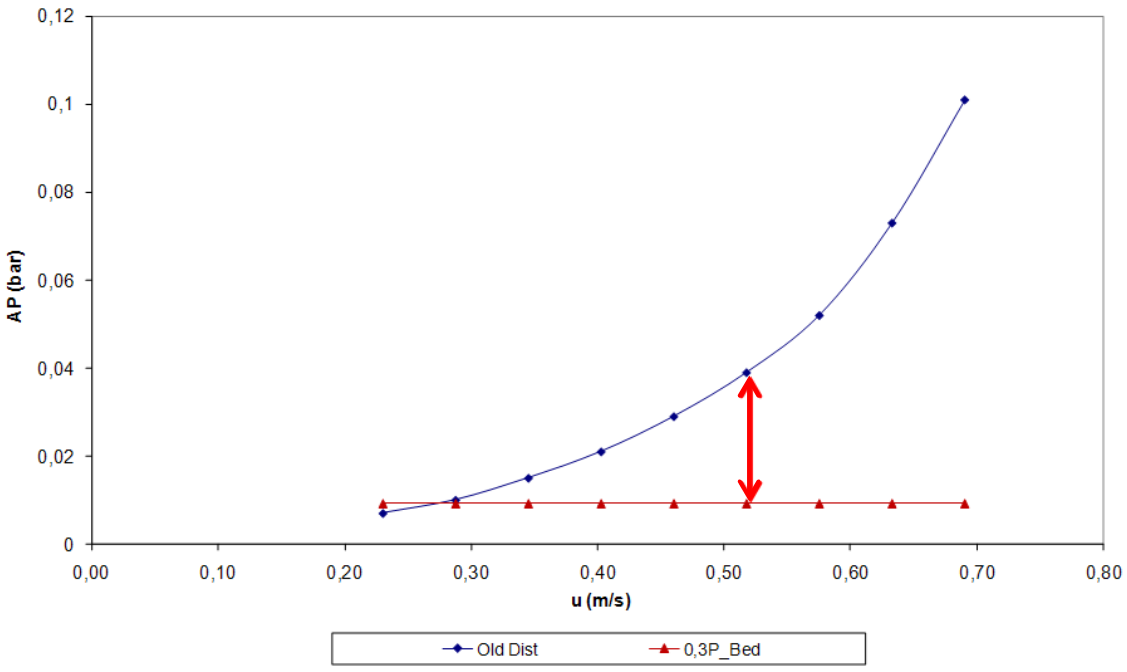

Graphic 5.1.1.1. First distributor. (For H/D = 1) Distributor drop face to velocity inlet. Also 30 % bed pressure drop is presented as maximum drop limit. Definitely rejected by the department team because of its high pressure losses.

Finally, the decision taken by the *Carlos III University Thermal and Fluids Department* was to design a new distributor fitted with commercial ones based on a designing commercial guideline.

Figure 5.1.1.1. First distributor. Rejected by the department team because of it high pressure drop.

5.1.2 DISTRIBUTOR DESIGN

The prototype distributor will be composed by two items: the slit, which mission is to prevent solids from falling through the distributor, and the perforated plate, entrust of air distribution. The designing condition will be determining a maximum value for the total drop in the distributor.

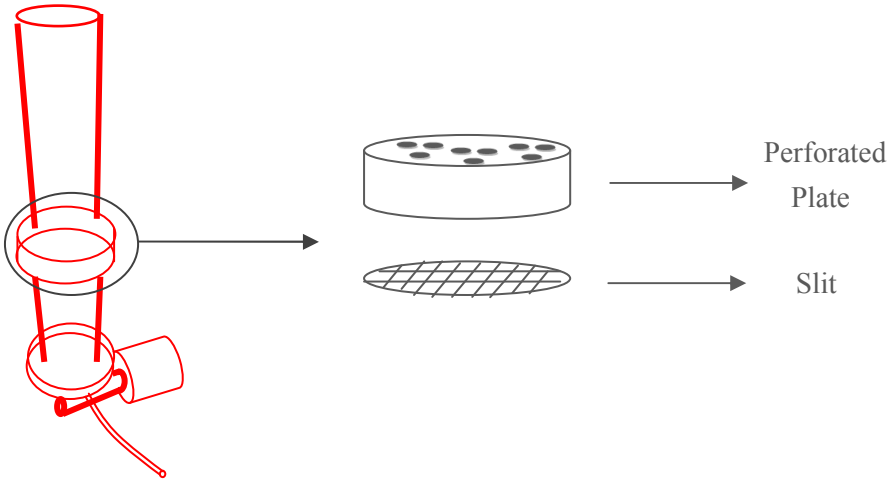

Figure 5.1.2.1. Distributor elements. Perforated plate and slit.

Experience shows that distributors should have a sufficient pressure drop Δp_d to achieve equals flows over the entire cross section of the bed [3]. In the early years of fluidization engineering rules of thumb were followed:

$$\Delta p_d = (0{,}2 - 0{,}4) \cdot \Delta p_b \text{ [15]}$$

Where Δp_b is the pressure drop across the bed. It is also clear that increased Δp_d will ensure a more even distribution of entering gas. However, an excessive Δp_d could have its drawbacks [3].

Moreover, the drop of the distributor (Δp_d) will be subdivided into two different losses: the one corresponding to the grid and the ones corresponding to the perforated plate. That is:

$$\Delta p_d = \Delta p_{slit} + \Delta p_{perf\_plate}$$

So the condition pattern imposed will be that the maximum drop in distributor (Δp_d) be 30 % the drop corresponding to the bed drop Δp_b (H/D =1) in the working point (where minimum velocity of fluidization is smaller than working velocity; $u_{mf} < u_0$).

As the slit is already designed (is a commercial slit), the perforated plate is now the unique distributor element under designing.

The diameter of orifices in perforated plate distributors may range from 1 to 2 *mm* in small experimental beds to as much as 50 mm in large FB units with their solid-entrained gases [3]. For this distributor, 2 *mm* will be the drilled diameter.

Now the hole diameter is already fixed; the diameter of the distributor is determined by the bed dimensions (19,2 *cm*); and the height of the perforated plate is not a critical parameter (as the height drop is negligible in front of the perforated drop). So that, the pressure losses in perforated plate could be calculate as a *number of holes* (N_{holes}) and *separation between them (or pitch)* function as will be shown later, being able to determine this parameters with the maximum drop condition.

Hence, the slit drop will be calculated as a *number of holes* and *separation between them*.

The approach to the problem will be then:

$$\boxed{CONDITION \rightarrow \Delta p_d = 0{,}3 \cdot \Delta p_b\,(u_0)} \quad ;WHERE:$$

$$\begin{cases} \Delta p_b\,(u_0) = \rho(u_0) \cdot g \cdot h \\ \boxed{\Delta p_d = \Delta p_{slit} + \Delta p_{perf\ plate}} \end{cases} \quad ;WHERE:$$

$$\begin{cases} \Delta p_{perf\ plate}\,(N_{holes}) = \tau(N_{holes}) \cdot \frac{1}{2} \rho_{air} \cdot v^2 \\ \Delta p_{slit}\,(N_{holes}) = \tau(N_{holes}) \cdot \frac{1}{2} \rho_{air} \cdot v^2 \end{cases}$$

The τ value is a fluid-dynamic correction constant [16] dependent on the *number of holes* and the *pitch*. As the resolution of the problem requires long formulation and an iteration process, for solving has been used the *Engineer Calculation Software "Mathcad "* and the popular *Spreadsheet Software* "*Excel"*, now considered to have the largest market share on the *Windows* and *Macintosh* platforms. The resolution process is shown in the next calculation from the *Mathcad* program:

Basic parameters:

$D_{bed} := 192mm$

$D_{hole} := 2mm$

$u_{sup} = 0.48\frac{m}{s}$; is an initialization velocity (1,5 times the $\approx u_{mf}$).

Grid drop calculation:

$$f := \frac{A_{free.hole}}{A_{hole}}$$

$$A_{hole} := \frac{\pi \cdot D_{hole}^{2}}{4} \qquad A_{hole} = 3.142mm^2$$

$A_{free.hole} := 0.33 \cdot A_{hole}$ $\qquad A_{free.hole} = 1.037mm^2$

$f = 33\%$; is the percentage of free area respect to the hole.

Flow resistance:

$$\tau_{grid} := \tau \cdot \left(\frac{A_{bed}}{N_{hole} \cdot A_{hole}} \right)^2 \qquad \tau := 1.3 \cdot (1 - f) + \left(\frac{1}{f} - 1 \right)^2 \text{ [16] ; } \tau = 4.993$$

N_{hole} ; *number of holes* is one the unknown variable of the fluid-dynamic correction constant.

For initialize the calculus, *number of holes* is given a value (here is shown the calculus for the definitive *number of holes*):

$$N_{hole} := 275$$

$$A_{bed} := \frac{\pi \cdot D_{bed}^{2}}{4} \qquad A_{bed} = 2.895 \times 10^{4}\ mm^{2}$$

So, the constant value for *275 number of holes* is:

$$\tau_{grid} = 5.608 \times 10^{3} \quad ; \text{refer to } u_{sup}.$$

Orifice drop calculation:

$$\tau_{orifice} := \left[\frac{1}{C_D} \cdot \left(\frac{A_{bed}}{N_{hole} \cdot A_{hole}} \right)^{2} \right]$$

As C_D is a *Reynolds number function*, this coefficient must be calculated through the grid for checking the working field by the condition Re > 3000 [16]:

$$Re_l := \frac{\rho \cdot u_{grid} \cdot \delta}{\mu} \quad ; \text{where } \rho = 1{,}2\ Kg/m^3,\ \delta = 0{,}1\ mm\ (grid\ diameter),\ \mu = 1{,}8.10^{-5}\ Pa.s$$

$$u_{grid} := \frac{u_{hole}}{f}$$

The velocity through the hole will be calculated by the non accumulation of mass supposition, by the equal flow equation as shown below:

$$u_{hole} := \frac{u_{sup}}{\frac{A_{hole} \cdot N_{hole}}{A_{bed}}} \qquad u_{hole} = 16.086 \frac{m}{s} \quad ; \text{refer to } u_{sup}.$$

$u_{grid} = 48.746\frac{m}{s}$; then:

$$Re_l := \frac{\rho_{air} \cdot u_{hole} \cdot D_{hole}}{\mu_{air}} \qquad Re_l = 2.024 \times 10^3$$

Drag coefficient is calculated as:

$$C_D := Ktd \cdot \left(\frac{p}{D_{hole}} \right)^{-0.1}$$ [17]

; where Ktd is obtain from graphic:

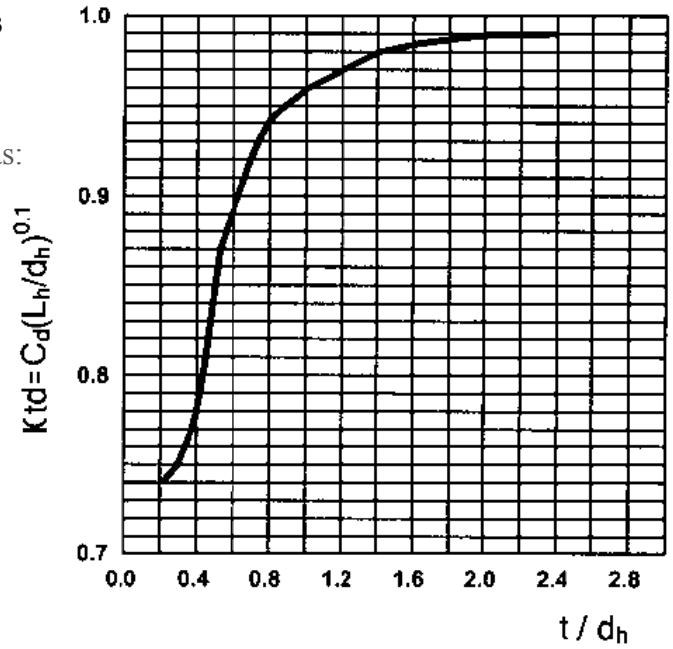

$e_{dist} := 6mm$ $\qquad \frac{e_{dist}}{D_{hole}} = 3$

So that, the orifice constant result:

$\tau_{orifice} = 1.345 \times 10^3$

The disposition of the holes would be grouped in equilateral triangles. The side length of the triangle would be calculated as shown:

$$p := \sqrt{\frac{A_{bed}}{\frac{\sqrt{3}}{2} \cdot N_{hole}}}$$

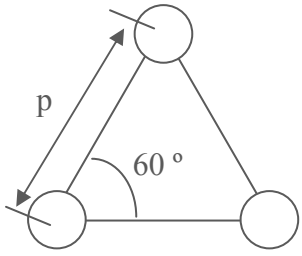

$p = 11.026mm$

For validating the pitch value, in order to avoid death zones between distributor orifices, is necessary to fulfill the next restriction [18]:

$$p < \lambda \cdot d_{eq}$$

For particles type B, λ take the next value [18]:

$$\lambda := 1$$

Where the equivalent diameter is calculated as by the next equation [18]:

$$d_{eq} := 1.3 \cdot \left(\frac{u_{sup}^{2}}{g \cdot N_{holem2}^{2}} \right)^{0.2}$$; where:

$$N_{holem2} := \frac{N_{hole}}{A_{bed}} \qquad N_{holem2} = 9.498 \times 10^{3} \frac{1}{m^{2}}$$

$d_{eq} = 15.743mm$; and finally:

$p = 11.026mm < \lambda \cdot d_{eq} = 15.743mm$; so that, the condition is fulfilled making valid the pitch value.

The strategy is now to iterate the number of holes and checking the fist condition imposed ($\Delta p_d = 0,3 \; . \; \Delta p_b (u_0)$), where for the prototype u_0 it supposed to be around 0,5 *m/s*, greater than the minimum fluidization velocity, supposed to be around 0,3 *m/s*. (later on, in the Chapter 6 will be found this supposed values are valid for the prototype). In the next graphic is shown the iteration process, see Graphic 5.1.2.1. :

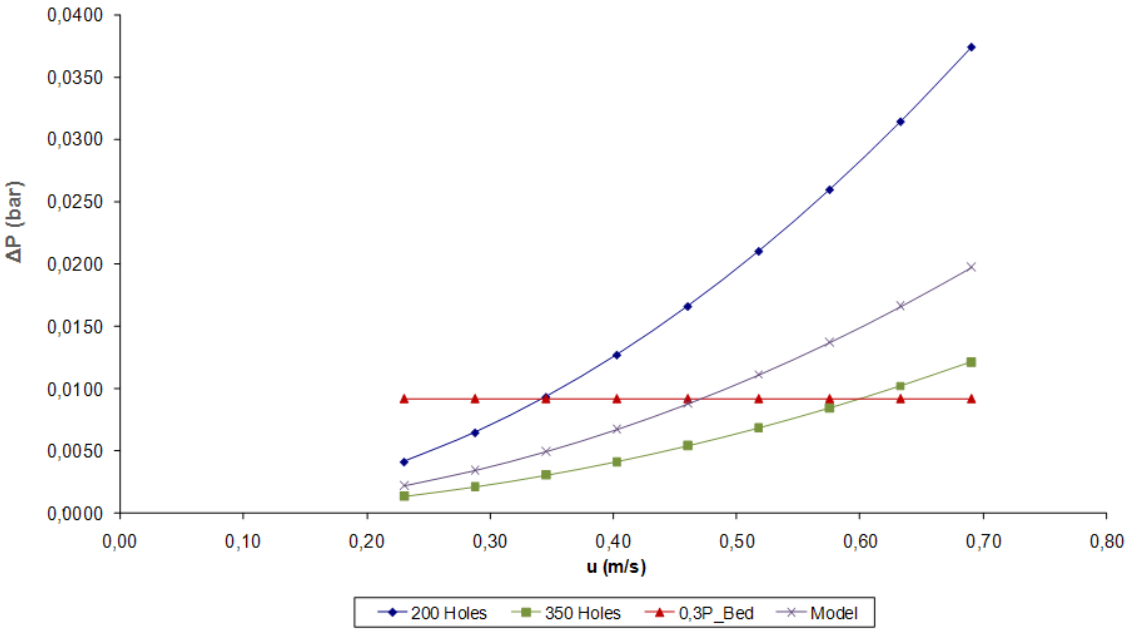

Graphic 5.1.2.1. Pressure face to velocity inlet as a number of holes function for 200 holes, 350 holes and the model with 275 holes. Also ⅓ bed pressure drop is presented.

As the condition was the distributor to have 30 % of the bed drop at the working velocity, and was supposed to be around 0,5 *m/s*, hence the *275 holes* perforated plate is going to be taken as the theory model to fabricate the distributor, see Figure 5.1.2.2. :

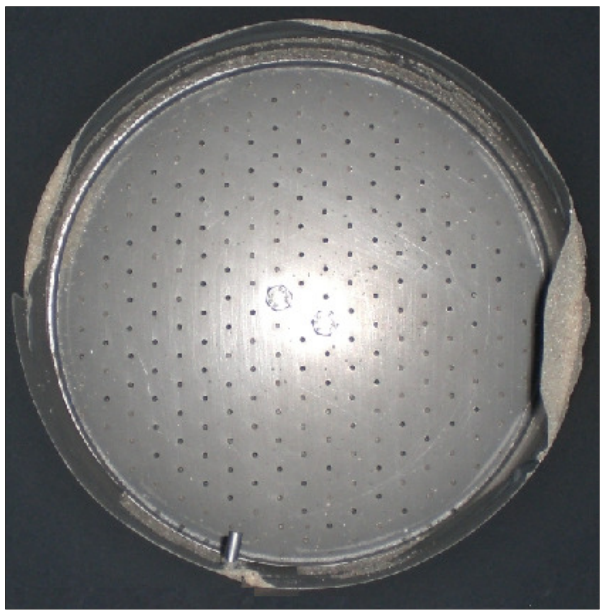

Figure 5.1.2.2. Final distributor designed based in the theory model.

One time the distributor is already manufactured, is necessary to check if the drop at the working velocity is near enough to ⅓ the bed drop, see Graphic 5.1.2.2.

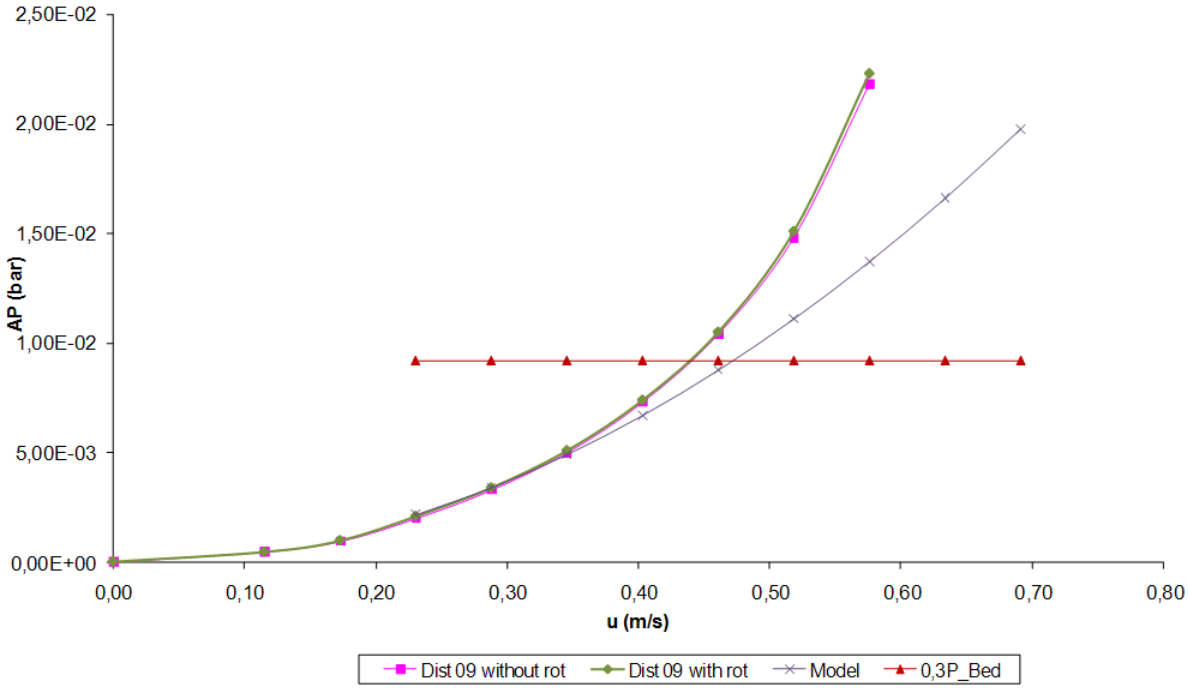

Graphic 5.1.2.2. Pressure face to velocity inlet for 30 % bed pressure drop, the theory model and the final prototype distributor manufactured with and without rotation.

It could be observed that real model do not fit exactly to the theory model along the entire curve. This misalignment is not only a first supposition consequence, but as well as other manufacturing and assembly mismatches. Remember that it was said to neglect the drop across the height of the perforate plate and non turning distributor model was calculated in front of the turning real one. All this deviation from the theory model is perfectly assumable as the original designing condition has a tolerance for the distributor pressure drop:

$$CONDITION \rightarrow \Delta p_d = (0{,}2 - 0{,}4) \cdot \Delta p_b\,(u_0)$$

So that, the new working point will be at $u_0 = 0{,}48\ m/s$, where the distributor pressure drop is $\Delta pd = 0{,}4 \cdot \Delta pb$, only a 4 % far form the initial supposition of working velocity $u_0 = 0{,}5\ m/s$, see Graphic 5.1.2.3.

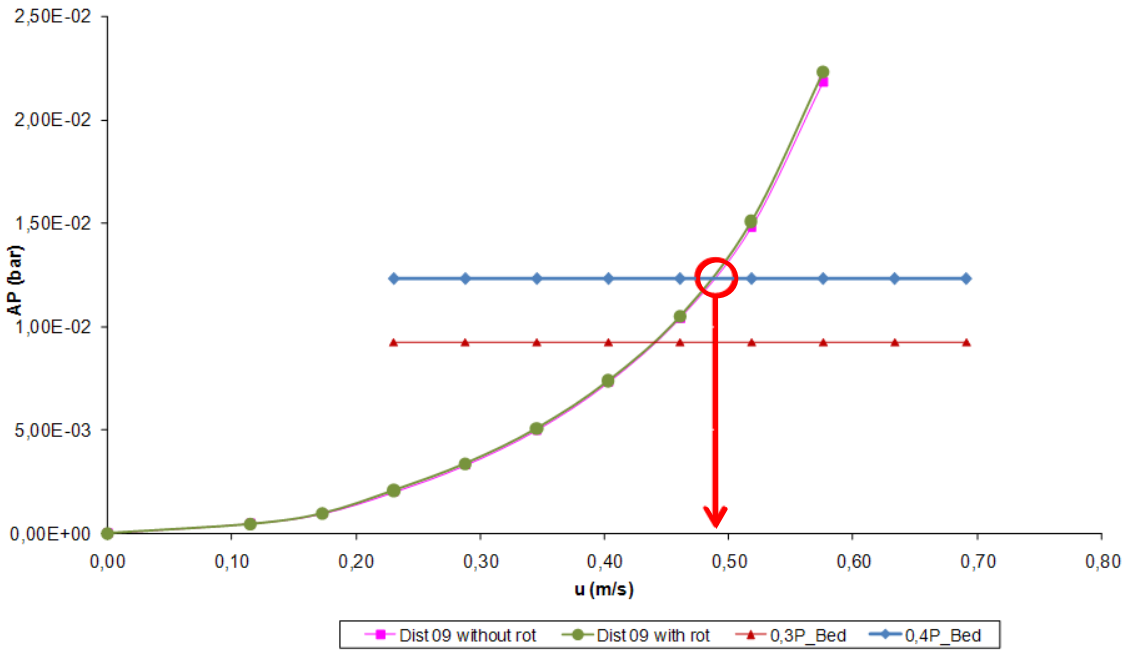

Graphic 5.1.2.3. Pressure face to velocity inlet for ⅓ bed pressure drop, upper condition limit 40 % bed pressure drop and the final prototype distributor manufactured. New working point in the tolerance limits.

The definitive distributor designed when making compared with the old distributor, gives an improvement for the pressure drop of *66 %* less losses, permitting the new perforated plate to situate as a great commercial reproduction distributor itself and compare with an original one, see Graphic 5.1.2.4. :

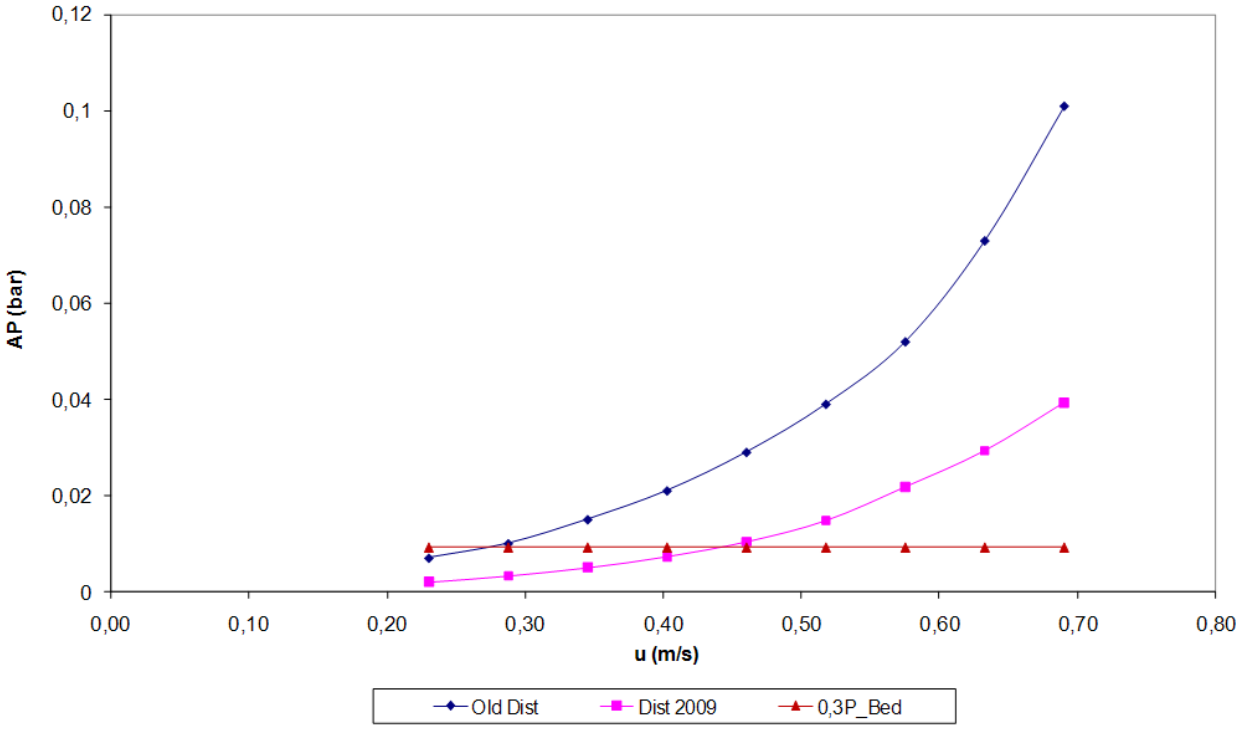

Graphic 5.1.2.3. Pressure face to velocity inlet for ⅓ bed pressure drop, old distributor and the final prototype distributor manufactured. A 66 % drop gain from old distributor to the new one.

6. MINIMUM FLUIDIZATION VELOCITY

6.1. INTRODUCTION

[20] The minimum fluidization velocity, u_{mf}, is one of the basic parameters characterizing the process of fluidization. It is defined as the linear velocity at which the net downward force due to the effects of gravity is compensated by the upward force due to the frictional action of the fluid on the particles:

$$P_{mf} = (\rho_s - \rho_f) \cdot (1 - \varepsilon_{mf}) \cdot g \cdot H_{mf}$$

Because of the uncertainty in estimating the bed voidage at incipient fluidization, ε_{mf}, especially for beds of mixed particle sizes, the accuracy of prediction of u_{mf} from available correlations based on above equation is rather low.

Thus, the experimental way is preferred and u_{mf} is usually evaluated from the dependence of bed pressure drop on fluid velocity. The minimum fluidizing velocity is taken as that corresponding to the intersection of pressure drop lines for regimes of developed fluidization and fixed bed, respectively. The shortcoming of this approach is that two different sets of experimental data including the complicated transition region are necessary for evaluating u_{mf} which reduces the accuracy of the method.

Moreover, this method cannot be used for the on-line determination of u_{mf} during the process, e.g. for the industrial circulating fluidized bed reactors when u_{mf}, may change in time due to changes in temperature or granulometry and density of particles.

The purpose of this work is to take advantage of an experimental method for the evaluation of the minimum fluidization velocity from pressure measurements. This method is based only on the fluidized bed regime and can be also used for monitoring of u_{mf}, in the process of online control of fluidized bed reactors.

[13] But, interpretation of results in time domain, such as standard deviation of the pressure fluctuations to calculate u_{mf}, may lead to erroneous conclusions about the flow

regime. The results from the frequency domain (power spectra) of the pressure fluctuations are generally in agreement and can be used complementary to each other. The power spectra can be divided into three regions, a region corresponding to the macro-structure (due to the bubble flow) and, at higher frequencies, two regions representing liner structures that are not predominantly governed by the macro structure of the flow.

Several methods have been proposed to characterize the fluidization regimes: visual observations, study of time averaged entities such as the axial solids concentration profile and interpretation of fluctuating signals from in-bed measurements.

For a qualitative classification of regimes visual observation is important, but subjective in nature; what is regarded to be a turbulent regime by some observers may be described as bubbling by others. In quantitative measurements, frame by frame analysis of motion pictures has been used to determine bubble and cluster velocities and bubble frequency. Although recent developments in video techniques make such an analysis easier, it is still a tedious method.

Changes in the vertical distribution of time-averaged solids concentration (from pressure drop measurements) have been used as an indirect measure of the bed dynamics. But, the solids concentration is only recorded in a certain point or in a certain region of the bed. Methods based on the study of time averaged values of solids concentration do not directly quantify the flow dynamics and may lead to pitfalls.

All this methods result imprecise and subjective in nature. But a real quantitative description of flow regimes can be obtained from time-series analysis of fluctuating signals of in-bed measurements of pressure. The key to such quantification is an appropriate measurement method, as well as appropriate methods of time-series analysis of the measured fluctuating signals. Time-series analysis for this purpose operates in time domain and the frequency domain, the latter being used in non-linear time-series analysis.

6.2. EXPERIMENTAL DATA ANALISYS PROCEDURE [20]

Experimental data on the pressure fluctuations measured by the pressure probe tube in cool fluidized bed reactor has been analyzed for various experimental conditions. The standard deviation of pressure fluctuations, σ_p, is a practically linear function of the gas velocity, u:

$$\sigma_p = A + Bu$$

where parameters A and B can be determined by a linear regression analysis.

Assuming that the **pressure fluctuations in the bed arise at gas velocities higher than u_{mf}**, it is obtain from equation above:

$$u_{mf} = -\frac{A}{B}$$

The above equations can be interpreted using the concept of the mechanical energy of vibrational motion of particles in a fluidized bed. The average mechanical energy of particles in unit volume of bed at gas velocity $u > u_{mf}$, E(u), can be generally expressed as:

$$E(u) = E(u_{mf}) + W$$

where W is the energy contribution due to inhomogeneities characterizing the given fluidizing state. *Furukawa and Ohmae* (1958) found that E(u) is proportional to the velocity and it can be written:

$$E(u) = k_1 u$$

where k_1 is a complex function of particle properties and temperature. For the regimes when all particles move in phase with the same frequency and the fluid moves in phase with particles (*Verloop and Heertjes*, 1974) could be supposed that W can be expressed by the amplitude of pressure fluctuations:

$$W = k_2 \sigma_p$$

By combining the three last equations a reasonable physical interpretation of first one will be obtained in which $A = -E(u_{mf})\ k_1/k_2$ and $B = k_l/k_2$.

All computations were carried out from the time series of 60 *s*. The standard deviation of pressure fluctuations in the bed was computed as:

$$\sigma_P = \left\{ \frac{1}{N-1} \sum_{i=1}^{N} (P_i - \bar{P})^2 \right\}^{1/2}$$

where N is the number of sampled points, $N = 12037$, P is the instantaneous value of pressure and the mean pressure, $\overline{P}$, is given by:

$$\bar{P} = \frac{1}{N} \sum_{i=1}^{N} P_i$$

From the parameters A and B obtained by linear regression and the minimum fluidizing velocities computed using the equation $u_{mf} = -A/B$, value of u_{mf} will be determined from the plot of σ_p *vs.* u, see an example on Graphic 6.2.1. :

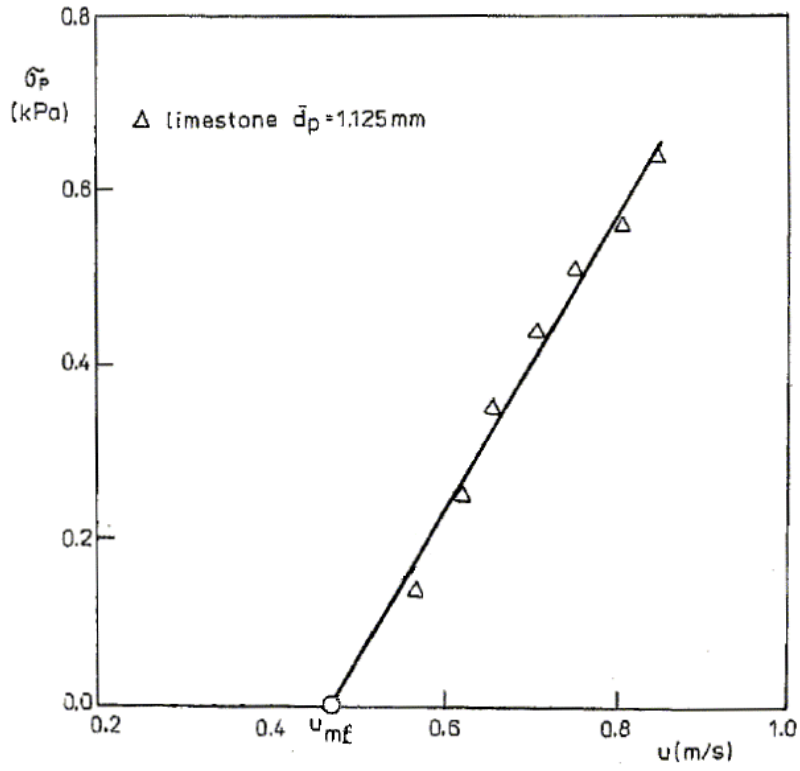

Graphic 6.2.1. Example of u_{mf} prediction for a d_p = 1,125 mm limestone in bed reactor.

[13] Attending to the analysis of frequency distribution, *Fast Fourier Transform*, *FFT,* power spectra analysis has been applied on time series of pressure from fluidized bed in previous experiments, giving a fluid-dynamic guideline for characterize new fluidization systems.

[13] The differences in the dynamics of four fluidization regimes (multiple bubble regime, single bubble regime, exploding regime and transport conditions) are clearly seen in the frequency domain by *Johnson et al*, see Figure 6.2.2. . This plot show the first 10 *Hz* (of 200 *Hz* measured) of the power spectra with linear scales on both axes, a representation which is suitable to illustrate dominant frequencies. Comparison plots with prototype power spectrum results from *Carlos III University of Madrid* fluidized prototype will give a complementary fluid-dynamic characterization.

[13] The multiple bubble regime has a broad band of frequencies between 0 and 10 *Hz* with a maximum at about 2,5-3 *Hz*, see Graphic. 6.2.2.a. Pressure fluctuations are influenced by a multitude of bubbles in the bed. In the single bubble regime, the dominant frequency of about 0,7 *Hz* of the bed pressure fluctuations represents the passage of single bubbles (the second lower peak should be due to a period doubling). The strong periodicity appears as a narrow peak in the power spectrum. The difference in amplitude (that is in the energy of the signal) of pressure fluctuations is seen on the vertical axes scales of the power spectra in Graphic 6.2.2.a and 6.2.2.b. The exploding bubble regime is characterized by large voids, but the flow pattern is more complex than the one of the single bubble regime, and the dominant frequency is not readily estimated from the time sequence. However, the power spectrum of Graphic 6.2.2.c shows a pronounced peak (at about 1,3 *Hz*) with only a minor part of the energy in the range of 2-10 *Hz*. On one hand, the single and exploding bubble regimes appear different in time domain but similar in frequency domain. On the other hand, the time series of the exploding bubble regime and in the transport conditions look similar in frequency-content, but they have quite different power spectra. Under transport conditions no pronounced dominant frequency is measured, although the major energy is located below 4 *Hz*, see Graphic 6.2.2.d.

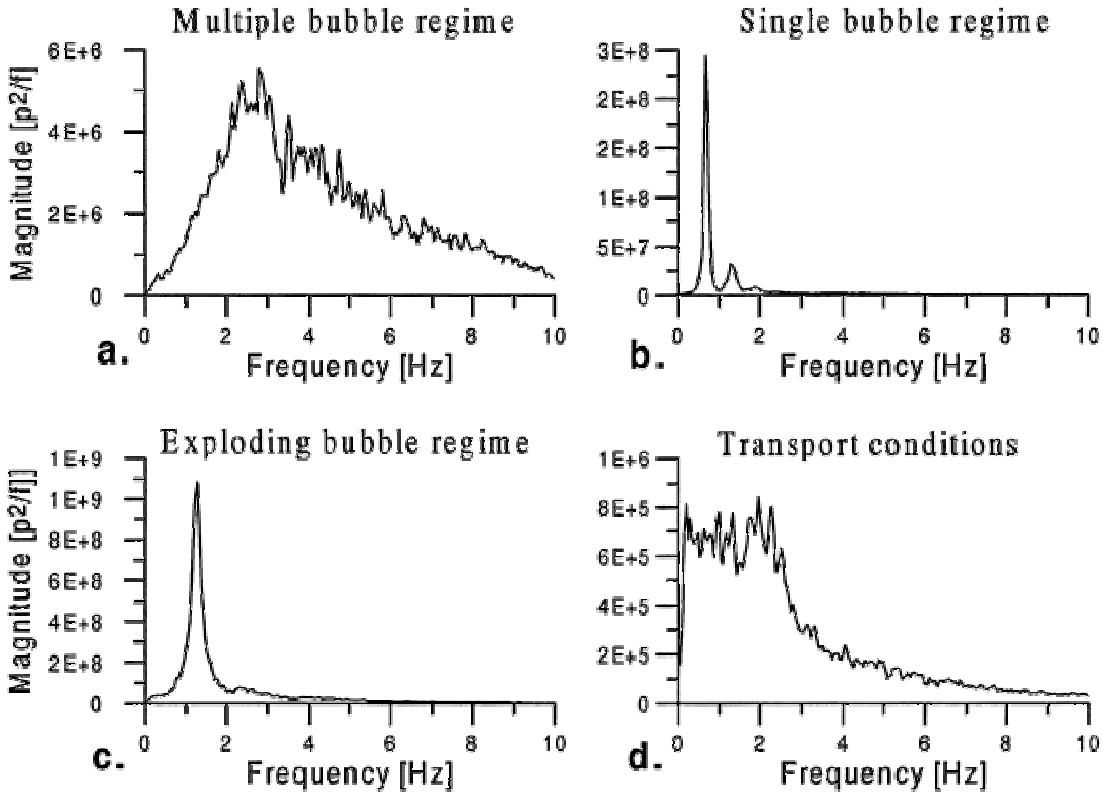

Graphic 6.2.2. Power spectra of: [a] multiple bubble regime, [b] single bubble regime, [c] exploding bubble regime, and [d] transport conditions. The spectra, which are zoom-ins of the first 10 Hz, are averages of 96 sub-spectra, each consisting of 8192 samples [corresponding to x20 s of measurement time].

6.3. U_{mf} ANALITICAL CALCULATION

For the interest of the investigation, first the minimum fluidization velocity will be estimated, u_{mf}, from the theory calculations with traditional method.

The Δp-versus-u_0 diagram is particularly useful as a rough indication of the quality of fluidization, especially when visual observation is not possible. For the relatively low flow rates in a fixed bed, the pressure drop is approximately proportional to gas velocity, and usually reaching a maximum, Δp_{max}, slightly higher than the static pressure of the bed. With a further increase in gas velocity, the timed bed "unlocks"; in other words, the voidage increases from e_m to e_{mf}, resulting in a decrease in pressure drop to the static pressure of the bed. With gas velocities beyond minimum fluidization, the bed expands and gas bubbles are seen to be present, resulting in nonhomogeneity. Usually, u_{mf} is taken as the intersection of the Δ_p-versus-u_0, line for the fixed bed of voidage e_{mf}, with the horizontal line corresponding to W/A_t [4], see Figure 6.3.1. In order to avoid the hysteresis phenomena, *Slope 2*, experiments will be carried out from higher velocities to lower ones, where inter-granular attraction forces do not appear, *Slope 1*.

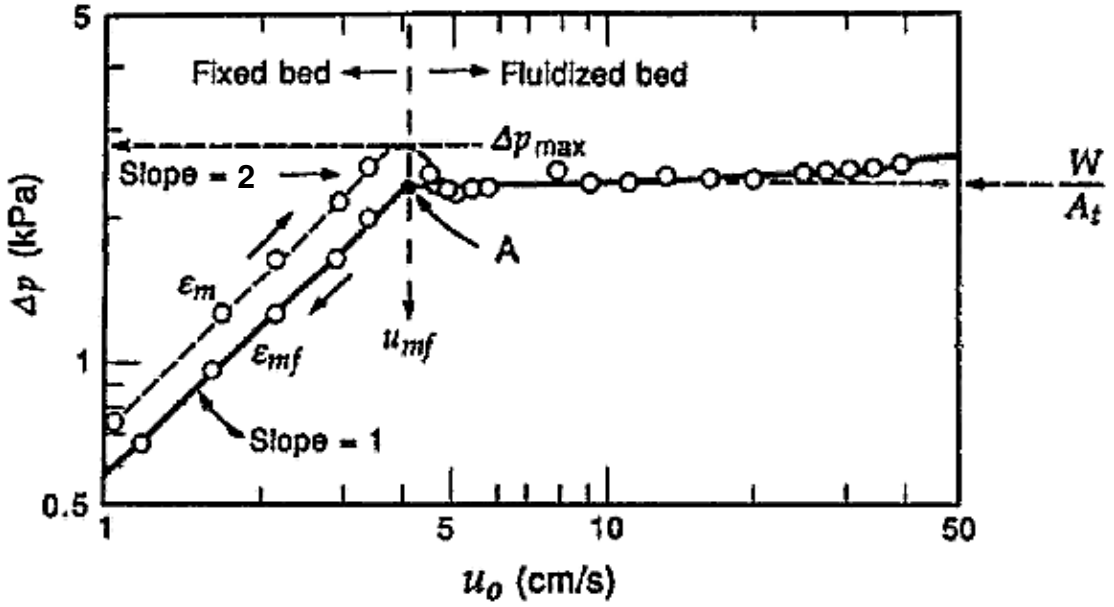

Graphic 6.3.1. Δ_P versus u_0 for uniformly size sharp sand gives ideal behavior with distributor consisting in a fixed bed of larger solids.

According to *Brawn et al* [21], the void fraction ε_m in a packed bed is related to particle sphericity; in addition, for vessels of small diameter the wall effect becomes important and influences the bed voidage. Since ε_m is easy to measure, an experimental determination, as has been already obtained, is more adequate.

The frictional pressure drop always positive, through fixed beds of length L_b containing a single size of monodisperse solids of screen size d_p was correlated by *Ergun equation* [22], so it was calculated as:

$$\Delta p = \frac{150\mu u_0 L_b}{(d_p \phi_s)^2}\frac{(1-\varepsilon_m)^2}{\varepsilon_m{}^3} + \frac{1.75\rho u_0^2 L_b}{d_p \phi_s}\frac{(1-\varepsilon_m)}{\varepsilon_m{}^3}$$

This equation is valid for *intermediate flows* under the *Blake-Kozeny* equation condition, with air proprieties at work velocity $u_0 = 0,5\ m/s$;

$$\left.\begin{array}{l} 10 < Re < 1000 \quad ; \text{where:} \\ Re_p = \dfrac{1}{1-\varepsilon_m}\dfrac{d_p u_0 \rho_f}{\mu} \end{array}\right\} \quad Re = 31,04 \quad ; OK$$

The hydrostatic pressure at mid bed, assuming the sand proprieties and a bed height $L_b = 0,096\ m$ with void fraction $\varepsilon_m = 0,37$, could be calculated as:

$$\Delta p_h = (1-\varepsilon_m).\rho.g.L_b$$

$$\Delta p_h = 1564,74 Pa$$

Fluidization theory affirms that fluidization starts when sustentation of particles appears. At high enough velocities fluid drag plus buoyancy overcomes the gravity force and the bed fluidize. This condition thus, will be fulfilling when pressure frictional drop equals hydrostatic pressure:

$$\Delta p(u_0) = \Delta p_h$$

Graphically obtained, see Graphic 6.3.2. :

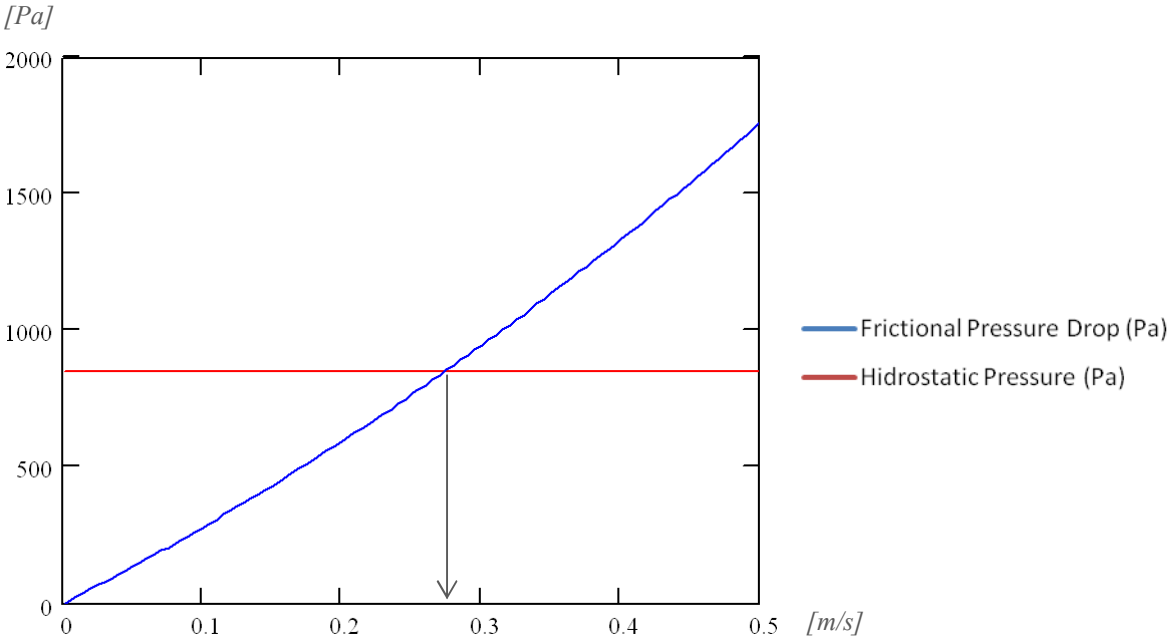

Graphic 6.3.2. Δ_P versus u_0 for ideal behavior with distributor consisting in a fixed bed of larger solids with prototype proprieties.

Finally, minimum fluidization velocity could be found as a result:

$$u_{mf} \approx 0{,}28\ m/s$$

Besides the reasons already stated in the introduction by which this method is not as accurate as the deviation method is, the value obtained for the minimum fluidization velocity seems to be lower than experimental one obtain onwards, as theory calculus for the u_{mf} do not take into account heterogeneous particle distribution size, heterogeneity of mass distribution, different viscosity proprieties along bed, boundary conditions and the real inherent conditions of the prototype reactor. All this conditions undertaken will underestimates the real frictional pressure drop, giving as a result lower pressure drop values for the same gas flow decreasing the minimum fluidization velocity u_{mf}.

6.4. EXPERIMENTAL DATA

For an integral fluid-dynamic characterization of 3 different bed height experiments fluidized bed prototype will be carried out, with aspect ratios of a_r = $^1/_4$, ½, ¾, (will be repeated the one with a_r = ½ for being representative) with and without rotation of the distributor respectively, making a total of 8 different experiments.

For each aspect ratio, in order to analyze the plot of σ_p *vs.* u, see Graphic 6.4.1., data will be taken from sensors, during 60 *seconds* with a sampling frequency of 200 *Hz*, for 13 different air flows from 0 to 1200 *lpm* with 100 *lpm* increments. Graphically:

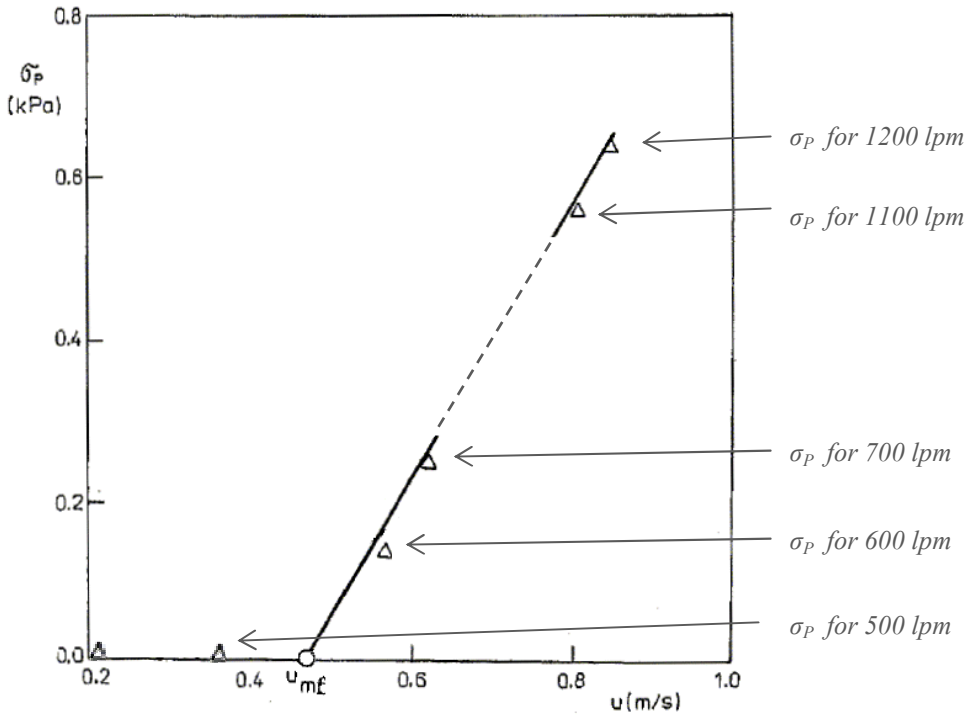

Graphic 6.4.1. Creating process of the plot of σp vs. u for calculating u_{mf}.

The information collected, because of the great number of test and, nevertheless, with the high frequency data acquisition, will generate a great volume of information. It is needed to be post processed with a powerful mathematical software. In this context, data will be treated with *Excel* and *Matlab* due to the flexibility required for the exigent data analysis. Because of the great amount of information collected, it will be shown

only for this time an example of *Excel* data collection for a 100 *lpm* flow (take into account that only for one flow value exist an *Excel* file with 3 columns of information with 12039 rows that results about 3 million of pressure datum).

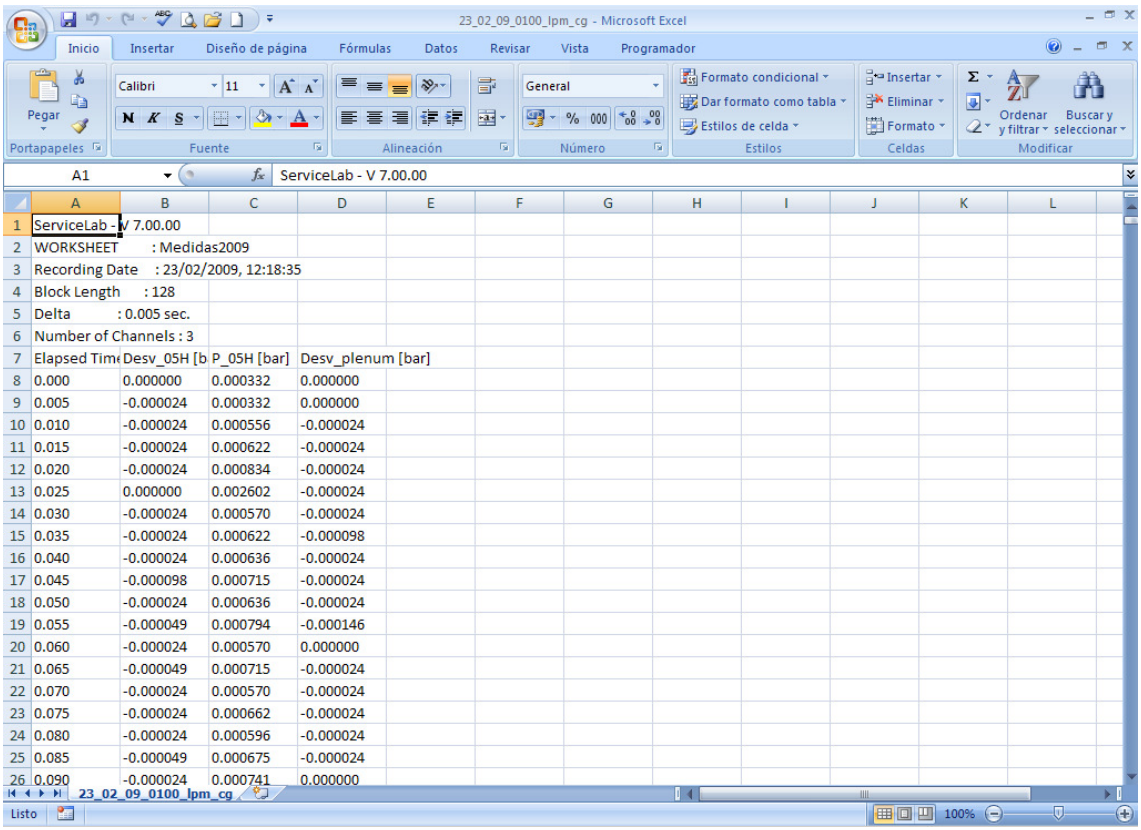

	A	B	C	D
1	ServiceLab - V 7.00.00			
2	WORKSHEET	: Medidas2009		
3	Recording Date	: 23/02/2009, 12:18:35		
4	Block Length	: 128		
5	Delta	: 0.005 sec.		
6	Number of Channels : 3			
7	Elapsed Tim	Desv_05H [b	P_05H [bar]	Desv_plenum [bar]
8	0.000	0.000000	0.000332	0.000000
9	0.005	-0.000024	0.000332	0.000000
10	0.010	-0.000024	0.000556	-0.000024
11	0.015	-0.000024	0.000622	-0.000024
12	0.020	-0.000024	0.000834	-0.000024
13	0.025	0.000000	0.002602	-0.000024
14	0.030	-0.000024	0.000570	-0.000024
15	0.035	-0.000024	0.000622	-0.000098
16	0.040	-0.000024	0.000636	-0.000024
17	0.045	-0.000098	0.000715	-0.000024
18	0.050	-0.000024	0.000636	-0.000024
19	0.055	-0.000049	0.000794	-0.000146
20	0.060	-0.000024	0.000570	0.000000
21	0.065	-0.000049	0.000715	-0.000024
22	0.070	-0.000024	0.000570	-0.000024
23	0.075	-0.000024	0.000662	-0.000024
24	0.080	-0.000024	0.000596	-0.000024
25	0.085	-0.000049	0.000675	-0.000024
26	0.090	-0.000024	0.000741	0.000000

Figure 6.4.2. Excel file for 100 lpm flow containing 36096 different data.

The acquisition system has three different external data input (2 *Kistlers* and 1 differential pressure sensor), so to avoid a huge amount of information, among other technical reasons, the three sensors only will operate at time for aspect ratio ½ and ¾ experiments in order to test if u_{mf} is independent of sensors. If finally so, next experiments could only be carried out with plenum one avoiding insert pressure sensors in bed reactor.

6.4.1. BED ASPECT RATIO $^1/_2$

Next graphic, build in *Matlab* software, presents all the original pressure data intake from sensors versus time, for a bed height of ***h_b = 9,6 cm* without distributor rotation**, from the pressure samples collected by the three sensors, for the first series of experiments for this bed height, see Graphic 6.4.1.1. :

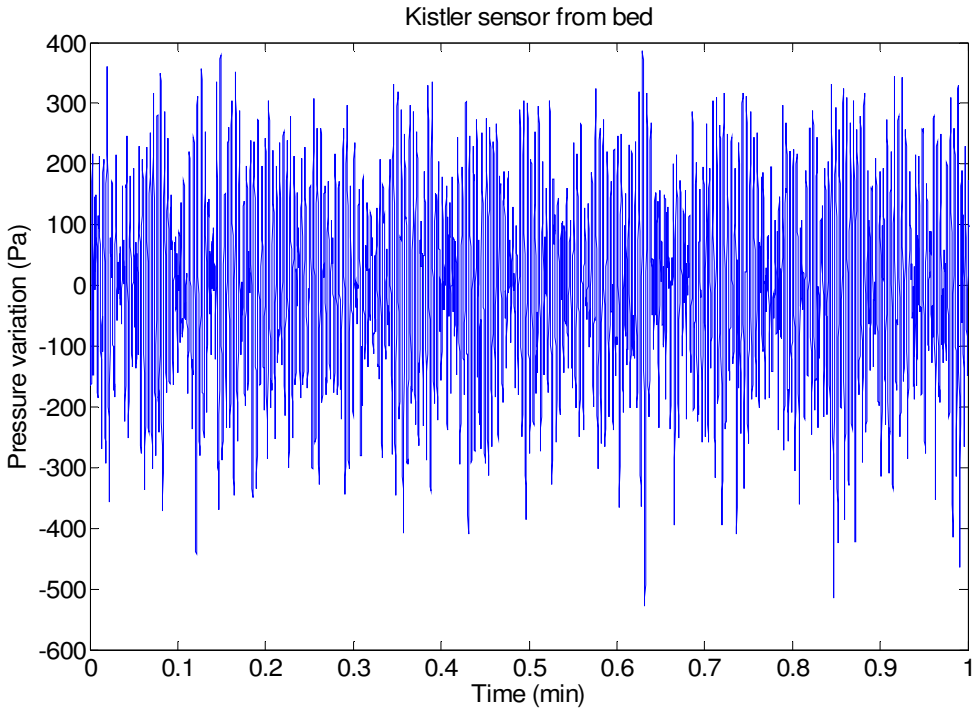

Graphic 6.4.1.1. Original pressure samples intake for a bed height of h = 9.6 cm without distributor rotation collected by Kistler sensors in bed reactor.

Pressure samples, as could be observed so for Graphic 6.4.1.1 so for Graphic 6.4.1.2., vary around the mean pressure reset at 0 *Pa* as a result of the high pass filter effect of the amplifier connected to the probes.

These data, also for Graphic 6.4.1.3., is collected without any mathematical treatment directly from the amplifiers for a time period of 60 *s* with a 200 *Hz* rate collection frequency.

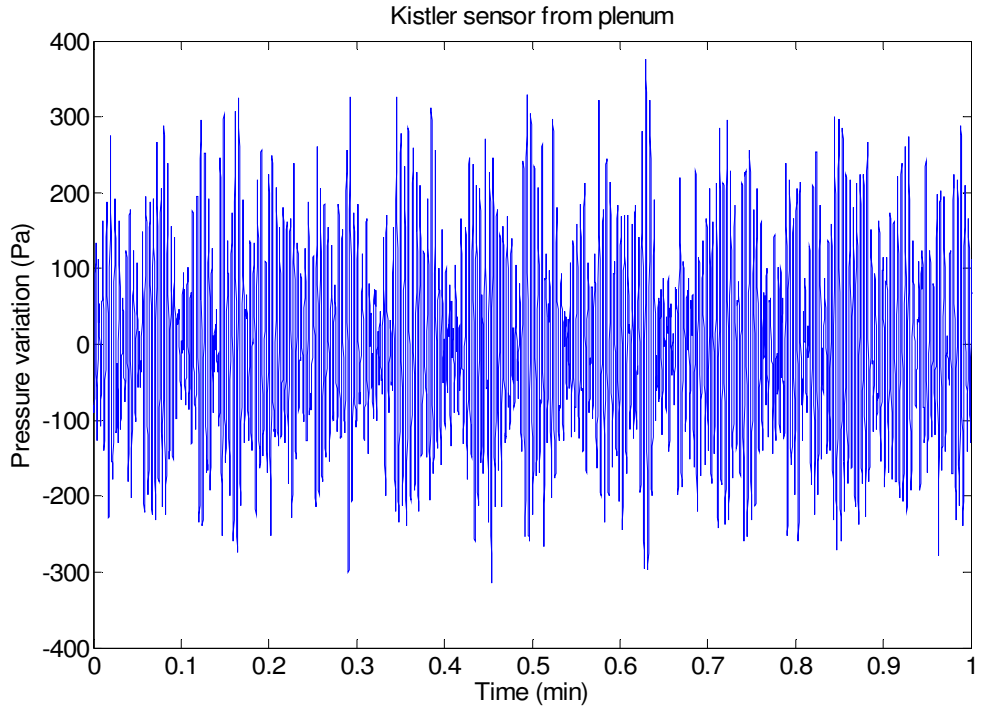

Graphic 6.4.1.2. Original pressure samples intake for a bed height of h = 9.6 cm without distributor rotation collected by Kistler sensor in plenum .

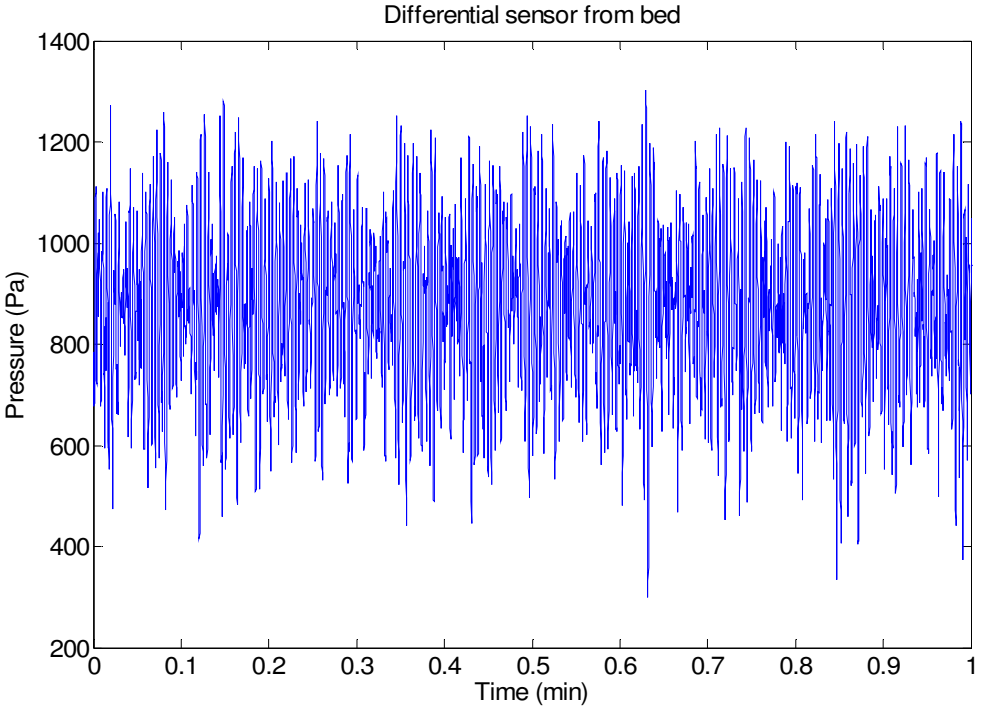

Graphic 6.4.1.3. Original pressure samples intake for a bed height of h = 9.6 cm without distributor rotation collected by differential sensor in bed reactor .

Unlike *Kistlers* pressure signal that was pretreated with amplifiers, in Graphic 6.4.1.3. could be observed that pressure form differential sensor vary around a value above 800 *Pa* because data is directly intake without electronic modulation.

Next graphic, build in *Matlab* software, presents all the pressure standard deviation versus gas velocity, for the same bed height of $h_b = 9,6\ cm$ without distributor rotation, from the pressure samples collected by the three sensors, for the first series of experiments for this bed height, see Graphic 6.4.1.4. :

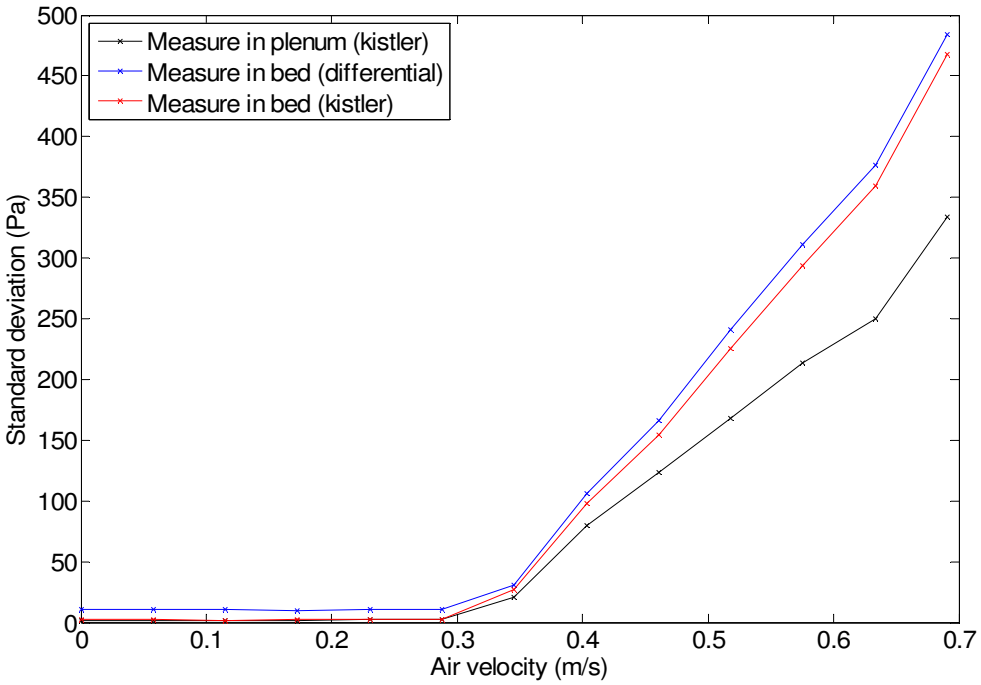

Graphic 6.4.1.4.Pressure samples for bed height of h = 9.6 cm without distributor rotation collected by the three sensors .

Could be observed how the two curves from *Kistlers* sensors fit one each other closer than the one from differential sensor. The same nature of the *Kistlers*, technically different from differential sensor, made the data intake potentially closer.

Also could be check that deviation, as *Puncochar et al* [20] supposed, is 0 until fluidization appears around 0,3 *m/s*, growing almost linearly with velocity.

In the next graphic it is shown the mean pressure versus gas velocity for a bed height of $h_b = 9,6$ cm without distributor rotation in the mid bed height, $H = 4,8\ cm$, see Graphic 6.4.1.5. :

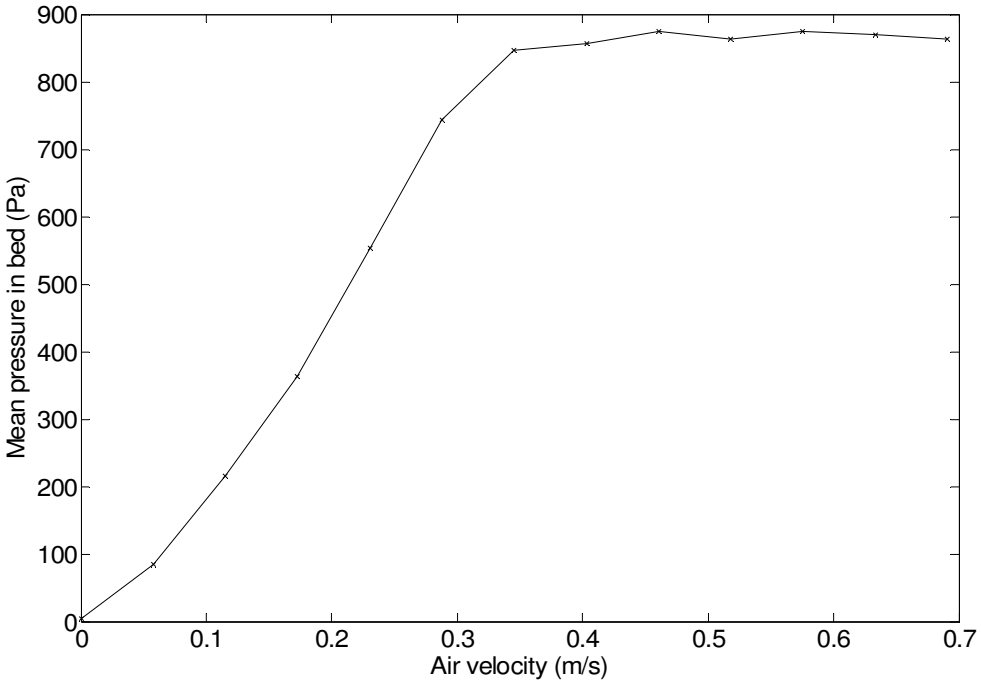

Graphic 6.4.1.5. Mean pressure for bed height of h = 9.6 cm without distributor rotation.

Could be observed how hydrostatic pressure grow almost linearly with velocity until fluidization, point from which hydrostatic pressure reaches a constant value equal to the weight of the column of *"fluid"* above the sensor. This result certifies that sand bed has reached a fluid behavior in the fluidization regime.

Next graphic, build also in *Matlab* software, presents all the original pressure data intake from sensors versus time, for a bed height of ***h_b = 9,6 cm* with distributor rotation**, from the pressure samples collected by the three sensors, for the first series of experiments for this bed height, see Graphic 6.4.1.6. :

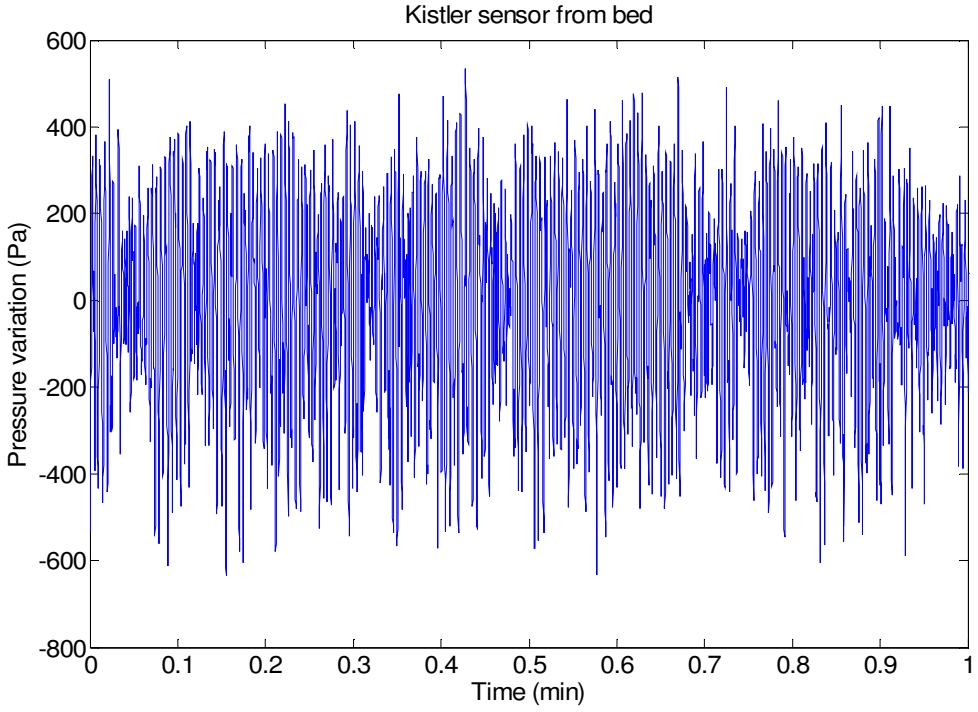

Graphic 6.4.1.6. Original pressure samples intake for a bed height of h = 9.6 cm with distributor rotation collected by Kistler sensors in bed reactor.

Pressure samples, as could be observed so for Graphic 6.4.1.6 so for Graphic 6.4.1.7., vary also around the mean pressure reset at 0 *Pa* as a result of the high pass filter effect of the amplifier connected to the probes.

These data, also for Graphic 6.4.1.8., is collected without any mathematical treatment directly from the amplifiers for a time period of 60 *s* with a 200 *Hz* collection frequency.

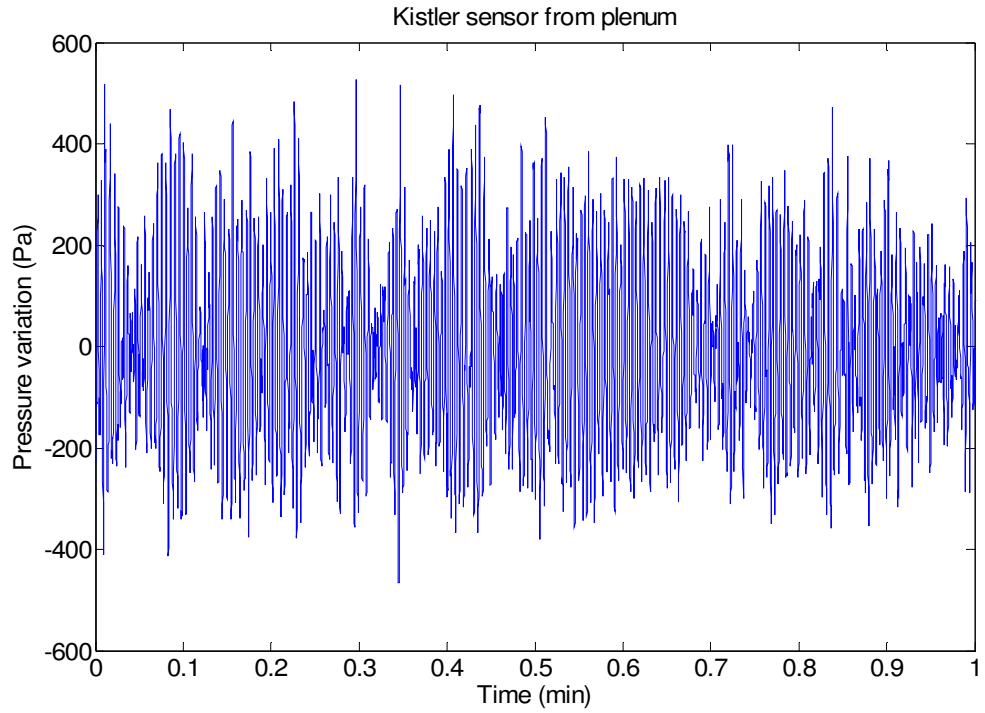

Graphic 6.4.1.7. Original pressure samples intake for a bed height of h = 9.6 cm with distributor rotation collected by Kistler sensor in plenum .

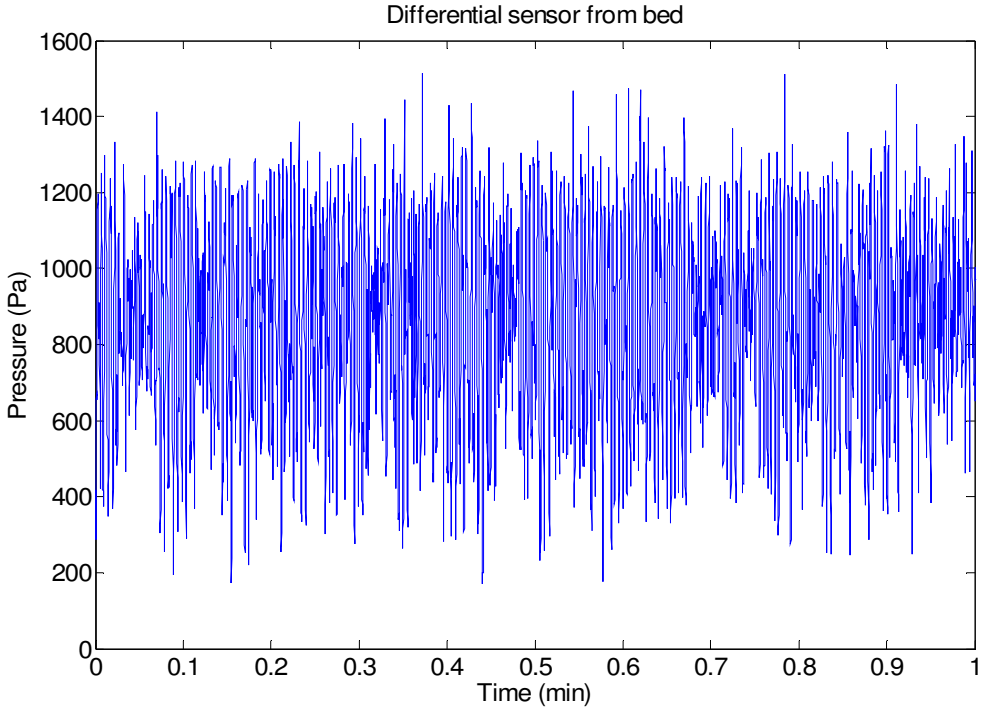

Graphic 6.4.1.8. Original pressure samples intake for a bed height of h = 9.6 cm with distributor rotation collected by differential sensor in bed reactor.

Unlike *Kistlers* pressure signal that was pretreated with amplifiers, in Graphic 6.4.1.8. could be observed that pressure form differential sensor vary around a value above 850 *Pa* because data is directly intake in this occasion too without modulation.

Next graphic, build with *Matlab* software, presents all the pressure standard deviation versus gas velocity, for the same bed height of h_b = *9,6 cm* with distributor rotation, from the pressure samples collected by the three sensors, for the first series of experiments for this bed height, see Graphic 6.4.1.9. :

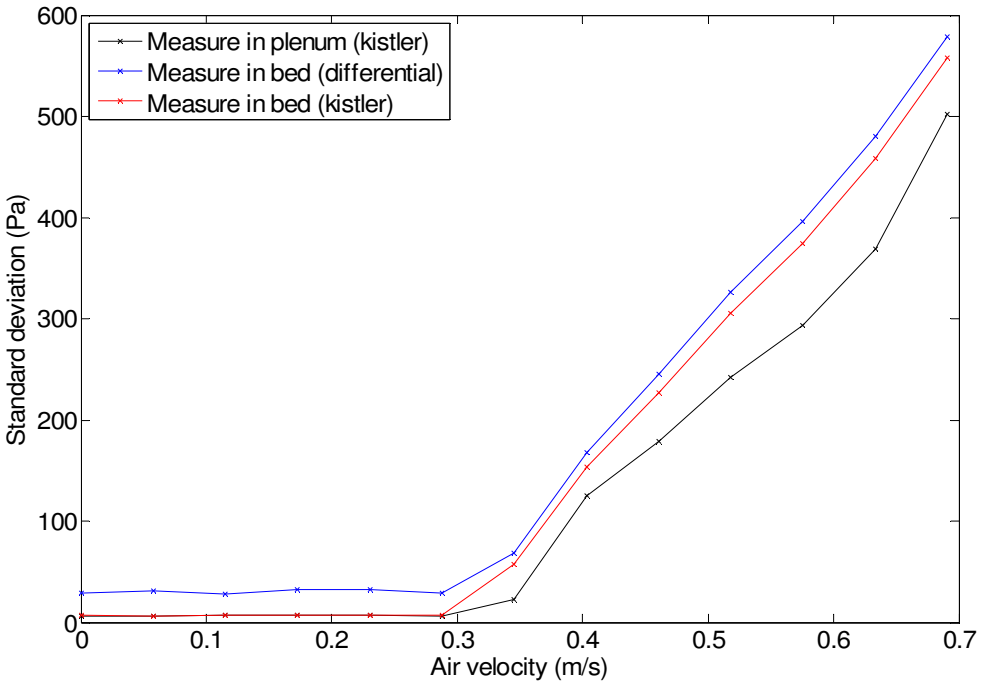

Graphic 6.4.1.9.Pressure samples for bed height of h = 9.6 cm with distributor rotation collected by the three sensors.

Could be observed how the two curves from *Kistlers* sensors fit one each other closer, as without distributor rotation, than the one from differential sensor. The same nature of the *Kistlers*, technically different from differential sensor, made the data intake potentially closer.

Also could be check that deviation, as Puncochar et al [20] supposed, is 0 until fluidization appears around 0,3 *m/s*, growing almost linearly with velocity.

In the next graphic it is shown the mean pressure versus gas velocity for a bed height of h_b = *9,*6 cm with distributor rotation in the mid bed height, H = *4,8 cm*, see Graphic 6.4.1.10. :

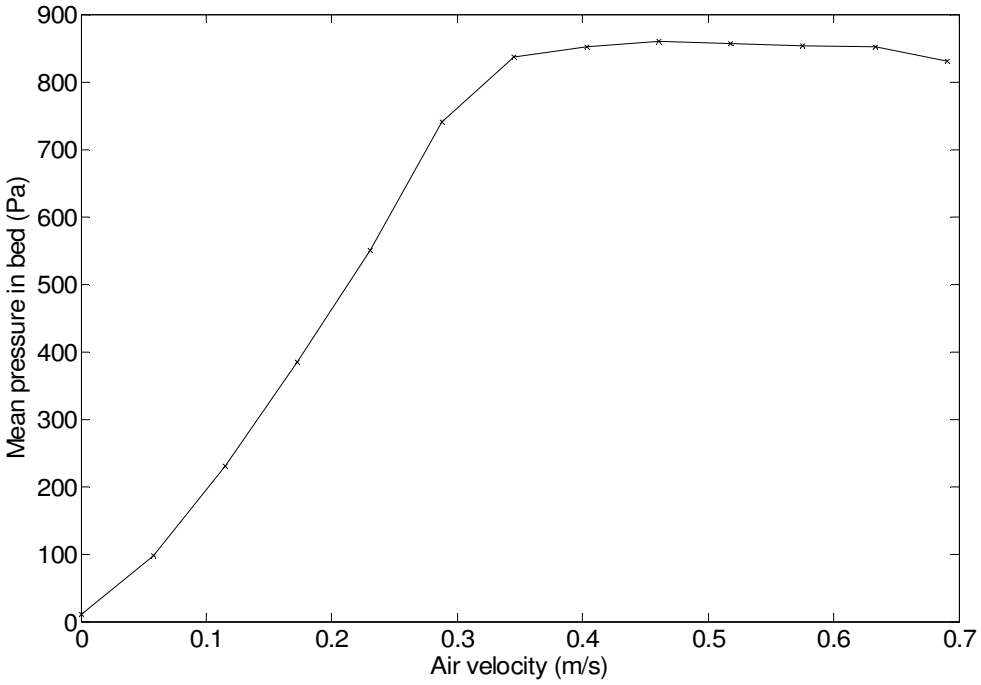

Graphic 6.4.1.10. Mean pressure for bed height of h = 9.6 cm with distributor rotation.

Could be observed in this case how hydrostatic pressure grow almost linearly with velocity until fluidization too, point from which hydrostatic pressure reaches a constant value equal to the weight of the column of *"fluid"* above the sensor. This result certifies that sand bed has reached a fluid behavior in the fluidization regime.

Could be observed that all the sensors for the two series of experiments, see Graphic 6.4.1.4 and Graphic 6.4.1.9., measure real pressure with a very high fitness with very close margin in data.

6.4.2. 2nd TEST FOR BED ASPECT RATIO 1/2

Because of the great amount of information collected by the three sensors, the strategy consist on evaluating the results obtained with three sensors in order to validate the three to avoid used them at time. For a better analysis of the data, second experiment with three sensors will be done for same height, $h = 9,6\ cm$ with and without rotation, to ensure reliability of information by using any sensor in future experiments. From now, original data input and different comments for next graphics will be not display for the document clarity as fundamental information for analysis and interpretation of data is already exposed.

It is presented then the all the pressure samples versus gas velocity, for a bed height of ***h_b = 9,6 cm* without distributor rotation**, collected by the three sensors, for the second series of experiments for this bed height, see Graphic 6.4.2.1. :

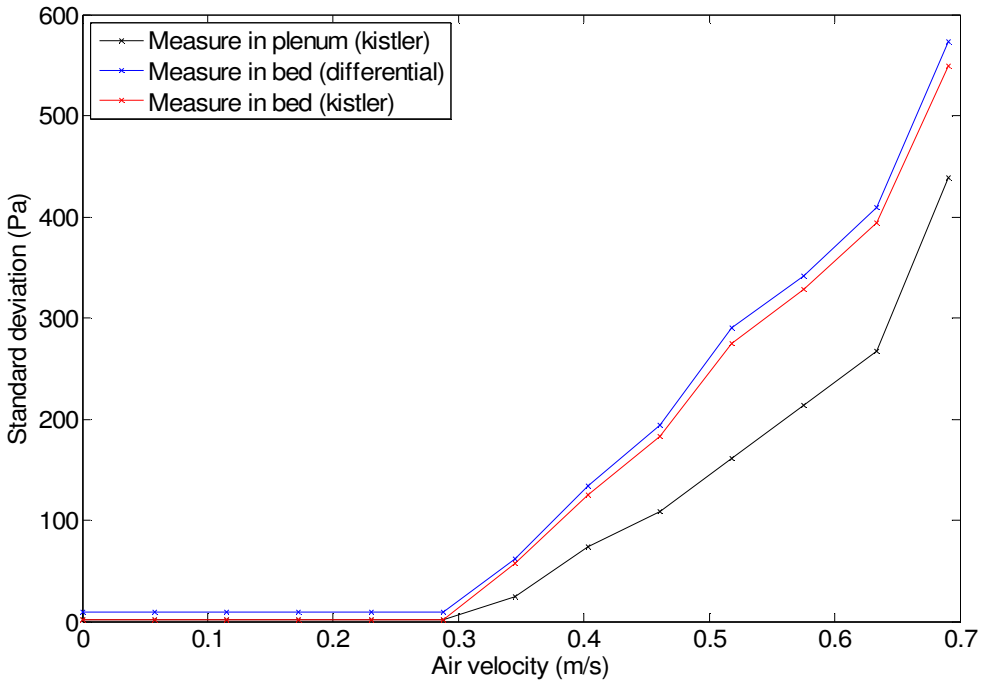

Graphic 6.4.2.1.Pressure samples for bed height of h = 9.6 cm without distributor rotation collected by the three sensors for second series of experiments for this bed height .

In next graphic it is shown the mean pressure versus gas velocity for a bed height of $h_b = 9,6$ cm without distributor rotation in the mid bed height, $H = 4,8\ cm$, for the second series of experiments for this bed height, see Graphic 6.4.2.2. :

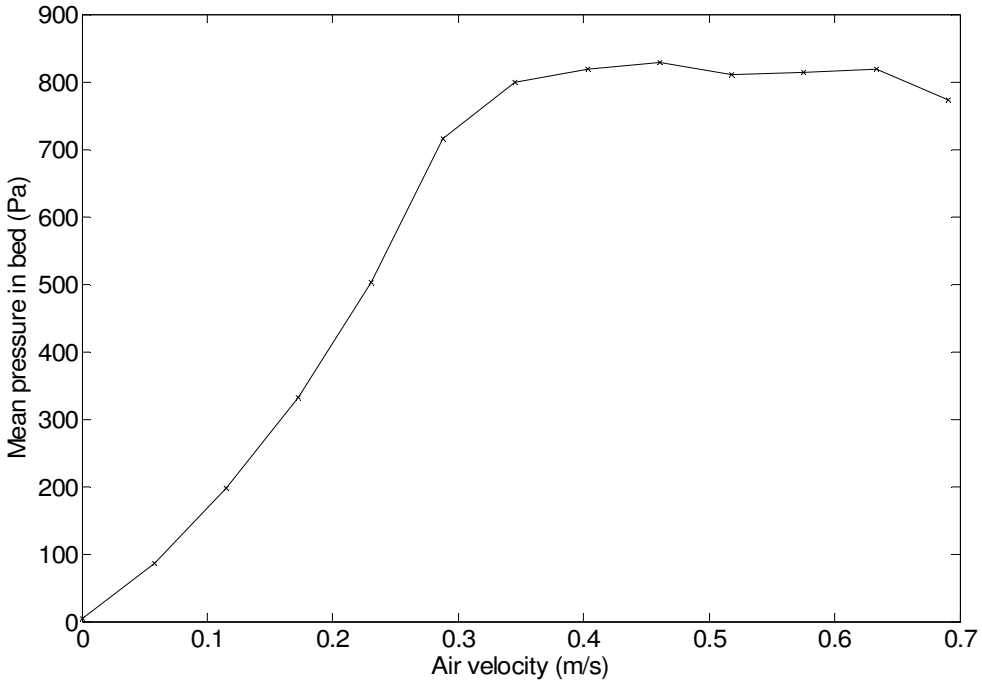

Graphic 6.4.2.2. Mean pressure for bed height of h = 9.6 cm without distributor rotation.

It is presented then the all the pressure samples versus gas velocity, for a bed height of ***h_b = 9,6 cm* with distributor rotation**, collected by the three sensors, for the second series of experiments for this bed height, see Graphic 6.4.2.3. :

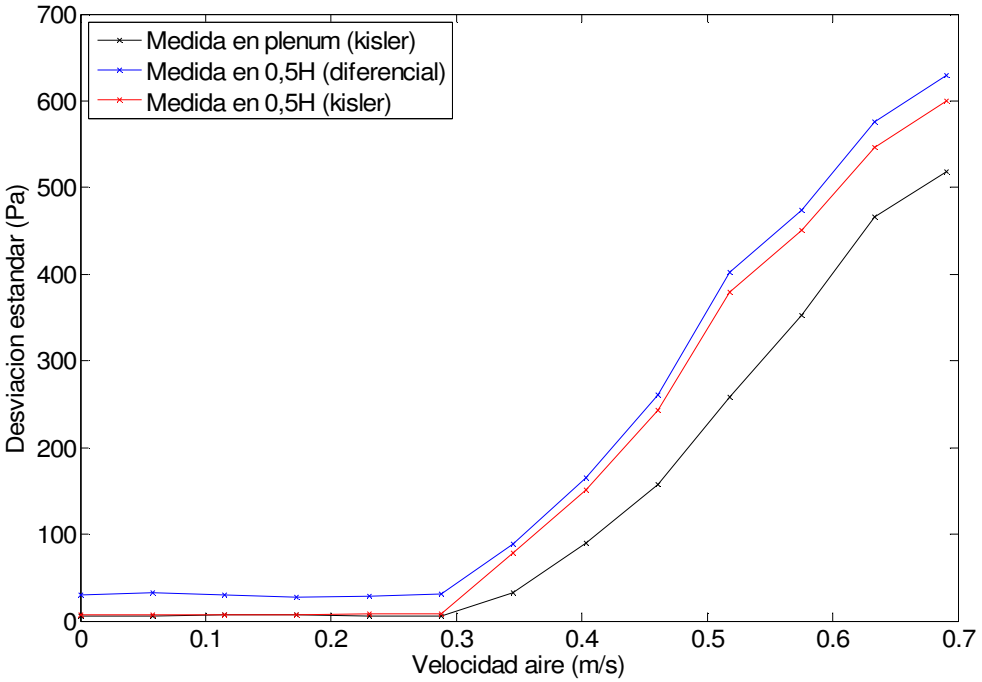

Graphic 6.4.2.3. Pressure samples versus velocity for bed height h = 9.6 cm with distributor rotation e three sensors.

It is shown, in next graphic, the mean pressure versus gas velocity for a bed height of $h_b = 9,6$ cm with distributor rotation in the mid bed height, $H = 4,8$ *cm*, for the second series of experiments for this bed height, see Graphic 6.4.2.4. :

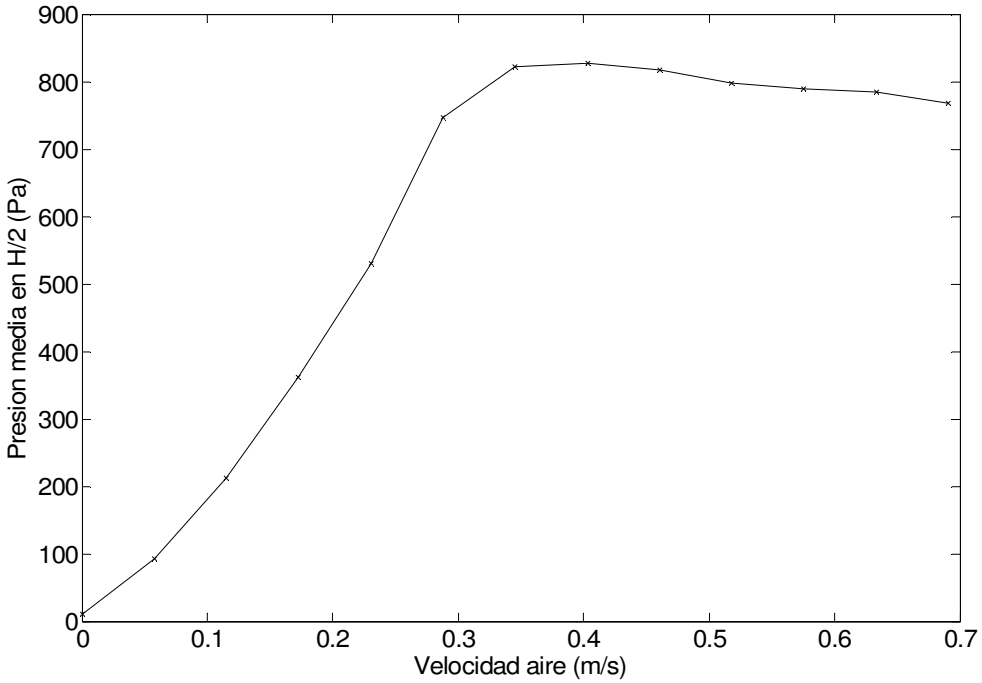

Graphic 6.4.2.4. Mean pressure for bed height of h = 9.6 cm with distributor rotation.

Could be observed that all the sensors for the two series of experiments, see Graphic 6.4.2.1 and Graphic 6.4.2.3., measure real pressure with a very high fitness with very close margin in data.

Finally could be assume that all the sensors, as this preliminary test reveal, see Graphic 6.4.1.4., Graphic 6.4.1.9., Graphic 6.4.2.1 and Graphic 6.4.2.3., are valid separately for pressure data collection from prototype.

6.4.3. BED ASPECT RATIO $^3/_4$

Once preliminary analysis of the data already collected from the *h = 9,6 cm* bed height experiment reveal that three sensors measures with the same accuracy could be affirm that sensors are validated. So that, hereinafter experiments with different bed heights could be carried out with only one sensor for avoid manage huge amount redundant information. Nevertheless, in order to certify it, will be obtained pressure samples with the three different sensors but with another bed aspect ratio.

It is presented then the all the pressure samples versus gas velocity, for a bed height of ***h_b = 14,4 cm* without distributor rotation**, collected by the three sensors, see Graphic 6.4.3.1. :

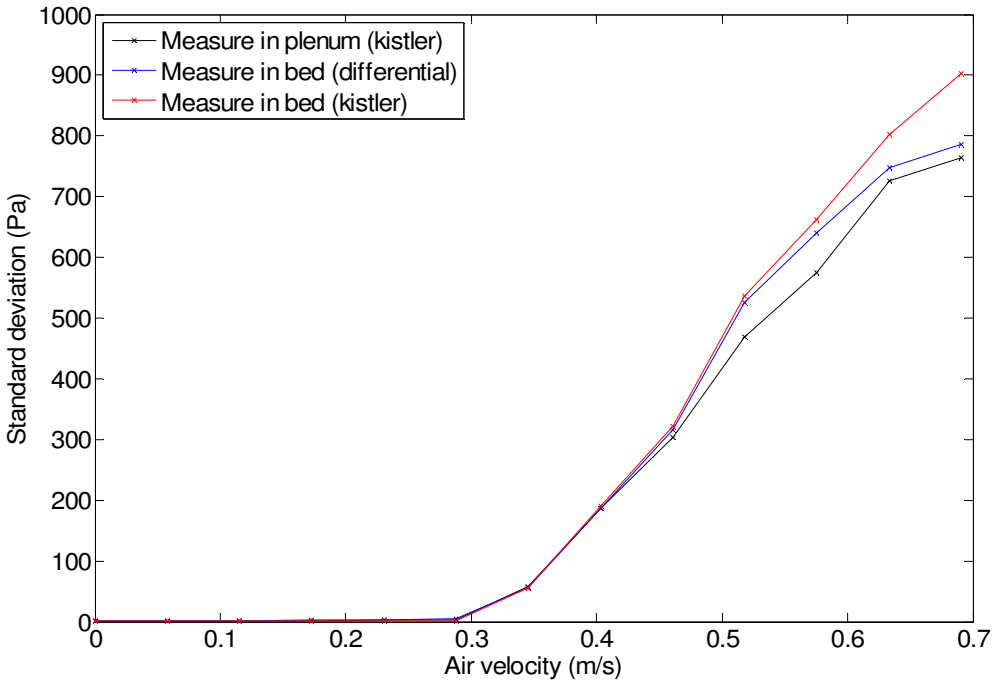

Graphic 6.4.3.1.Ppressure samples for bed height of h = 14,4 cm without distributor rotation collected by the three sensors .

In next graphic it is shown the mean pressure versus gas velocity for a bed height of h_b = *14,4* cm without distributor rotation at same height than previous aspect ratio experiment *H = 4,8 cm*, as the steel probe is a fixed probe, see Graphic 6.4.3.2. :

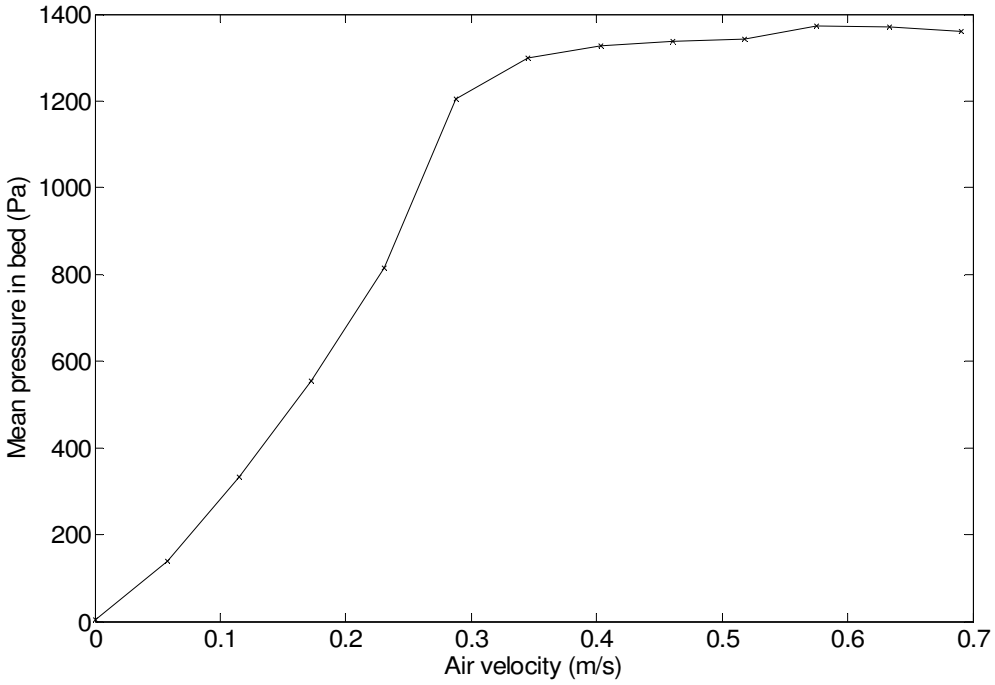

Graphic 6.4.3.2. Mean pressure for bed height of h = 9.6 cm without distributor rotation.

It is presented then the all the pressure samples versus gas velocity, for a bed height of ***h_b = 14,4 cm* with distributor rotation**, collected by the three sensors, see Graphic 6.4.3.3. :

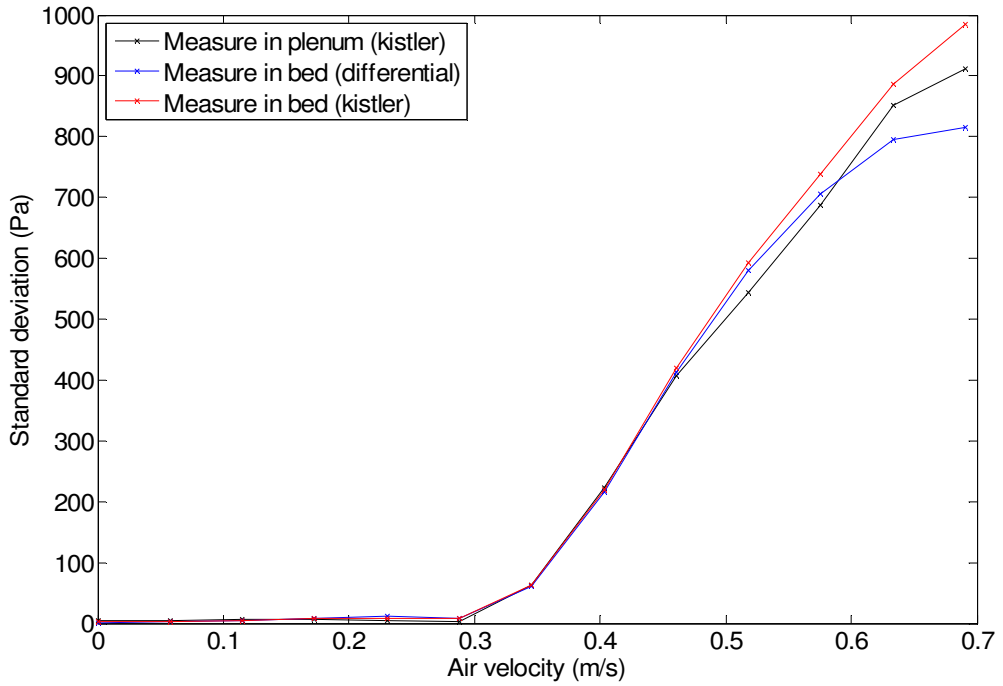

Graphic 6.4.3.3. Pressure samples versus velocity for bed height h = 14,4 cm with distributor rotation e three sensors.

It is shown, in next graphic, the mean pressure versus gas velocity for a bed height of $h_b = 14,4$ cm with distributor rotation at $H = 4,8$ *cm*, see Graphic 6.4.3.4. :

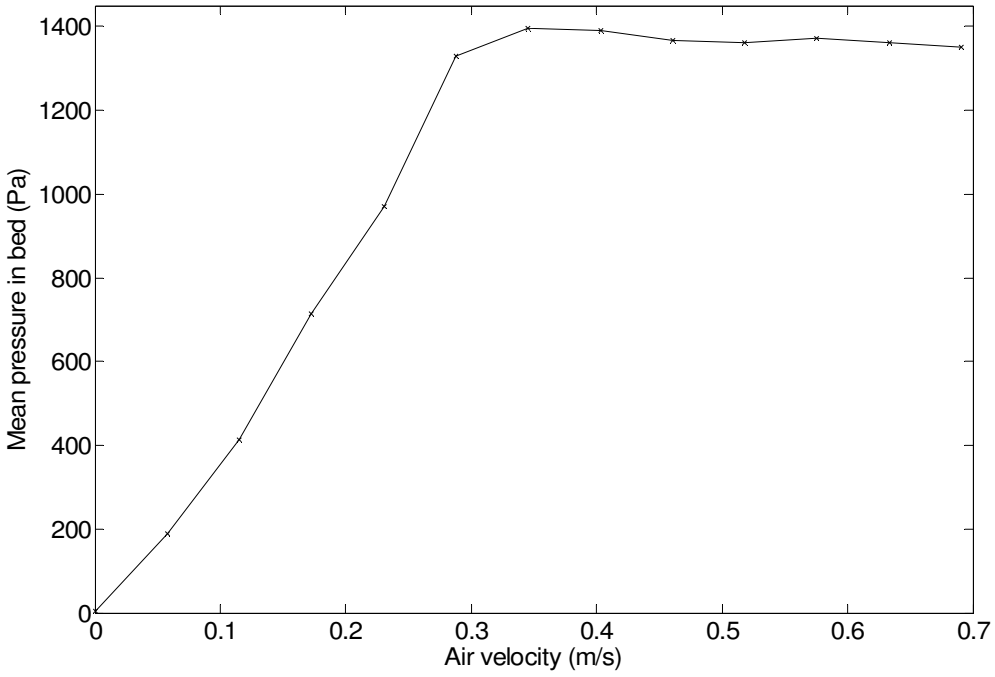

Graphic 6.4.3.4. Mean pressure for bed height of h = 14,4 cm with distributor rotation.

Could be observed that all the sensors, see Graphic 6.4.3.1 and Graphic 6.4.3.3., measure real pressure with a very high fitness with very close margin in data, confirming the validation of the three sensors separately.

6.4.4. BED ASPECT RATIO $^1/_4$

As the height of the *Kistler* sensor inside the bed reactor is at $H = 4,8\ cm$, and the freeboard in this experiment is at the same height, only one sensor will be used, the plenum chamber one, for bed to decrease amount of information and increase for test quality of data input in this particular disposition.

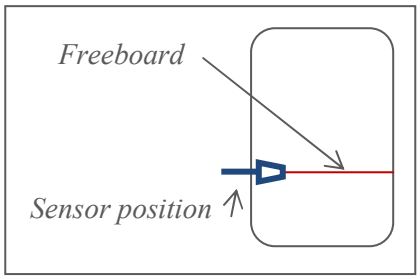

Figure 6.4.4.1. Sensor position and freeboard at same height.

Department team firstly supposed that sensors at freeboard height will not record data correctly. The great particles movement at this position makes difficult a certain pressure sample transmission to the sensor. In fact, after a first data post process, the study revealed that data measured at this sensor position certify the supposition, as all the prototype test done with different heights above that sensor bed height has been successfully carried out, except data collected with *Kistlers* and differential sensors at $h_b = 4,8\ cm$ ($^D/_4$) with significant distortions.

When the department team obtained the data the from *Kistler*, they realize about the serious data distortions going on. In the standard deviation plot, from pressure samples versus gas velocity, the curve presented so many peaks that made it not enough smoothness for the u_{mf} prediction.

In order to get sure that experiment had been done under properly conditions, a new test was done under the same characteristics. But the data obtained present the same outline as the previous one, with peaks that do not let the certain u_{mf} prediction for this method.

In addition, the fact that a at great gas velocities the sand pulled by the air is mostly the same whatever bed height used, has a negative impact for this aspect ratio experiment. Supposing that dragged sand is equal for all aspect ratios (as $\frac{\delta m}{\delta t} = 0$), the mass that is under fluidization for aspect ratio ¼ is closer to the one that is under

suspension. That is traduce in a different bed behavior as mass under fluidization is not the same for attenuate the particle falling under suspension.

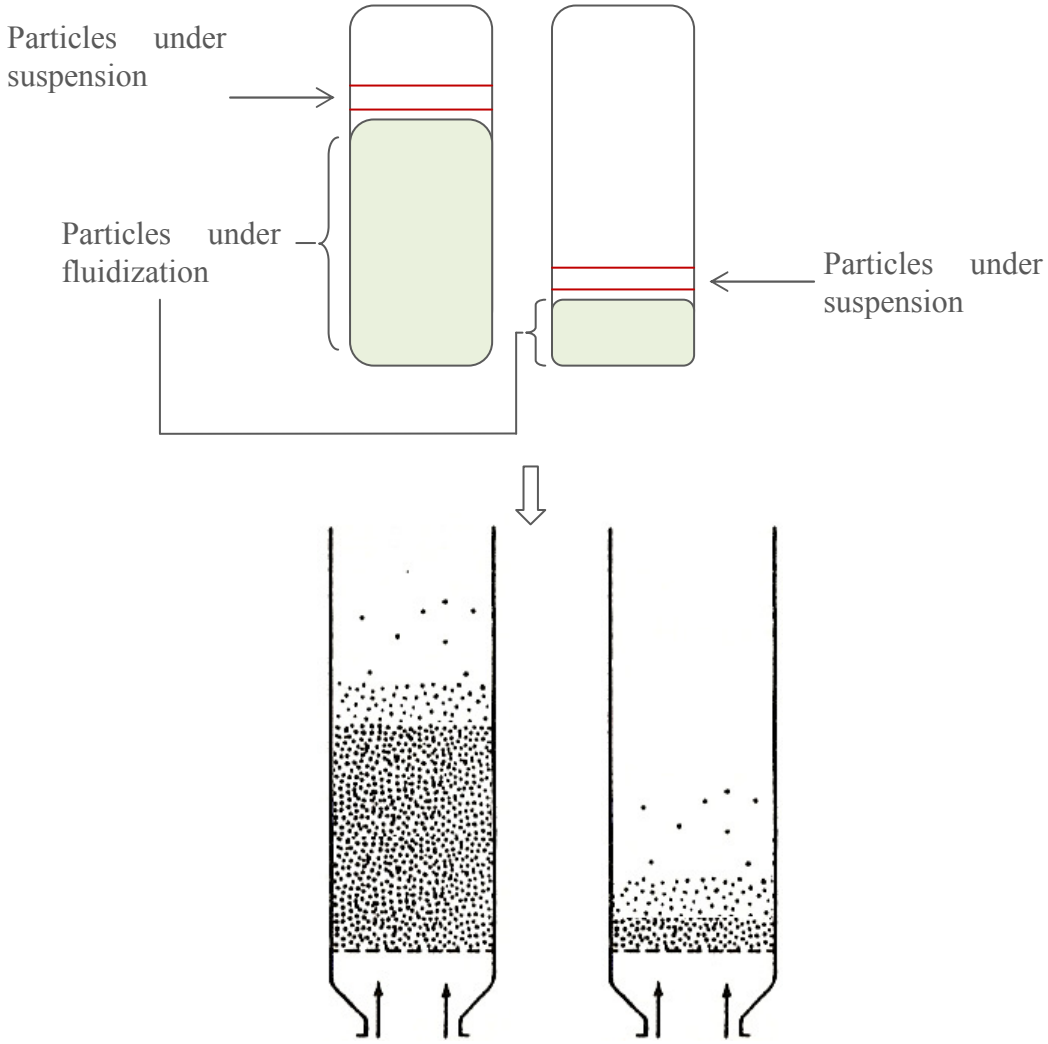

Figure 6.4.4.2. Mass percentage under suspension and under fluidization for different bed heights.

So that, when higher velocity gas fluxes are insufflate, the mass percentage of particles in suspension increase and lower percentage of sand under fluidization for mitigate particle fallings.

Because of this new experimental findings and because of the fact that this aspect ratio ($^1/_4$) commercially is not as usual at higher ones, the data process for this particular bed height could not be carry on with this sensors for this special conditions.

6.5. DATA POST-PROCESS

The analysis of the data will have the aim of settle the minimum fluidization velocity, u_{mf}, to characterize the flow with all the different bed heights of the prototype.

Also, the power spectra analysis will carry out for all the flows above u_{mf} to determine the different fluidization regime.

The method already exposed, based on assuming that the **pressure fluctuations in the bed increase linearly at gas velocities higher than u_{mf}** will be used to determine this velocity. As fluctuations for the different flow rates are already known, the velocity at which fluidization begins is the intersection of the curve $\sigma_p = A + Bu$ and fluctuation value equals to $\sigma_p = 0\ Pa$. The curve will be fitted by linear regression with *Matlab* software and the standard deviation values taken into account to solve the curve $\sigma_p = A + Bu$ values will be above $\sigma_p = 10\ Pa$ to ensure been in the fluidization regime.

In addition, calculus of u_{mf} with the mean pressure values in bed will give a new value for comparing traditional and applied method to predict that velocity.

For the regime determination *Johnson et al* [13] plots will be used, see Graphic 6.2.2., as the guideline to establish the fluid-dynamic regime by the *FFT power spectra* analysis of each rates.

Last point will summarize all the data conclusions for u_{mf} prediction and regime determination, for the three bed heights and for all the flow rates experimentations.

6.5.1. BED ASPECT RATIO $^1/_2$

The graphic determination of u_{mf} *with* the curve $\sigma_p = A + Bu$ values, fitted by linear regression, for those pressure fluctuations for a bed height of ***h_b = 9,6 cm* in the plenum and bed without distributor rotation** above σ_p *=20 Pa,* and the intersection with σ_p *= 0 Pa*, at u_{mf} velocity, see Graphic 6.5.1.1., Graphic 6.5.1.2., Graphic 6.5.1.3. , and the mean pressure values in bed, Graphic 6.5.1.4. :

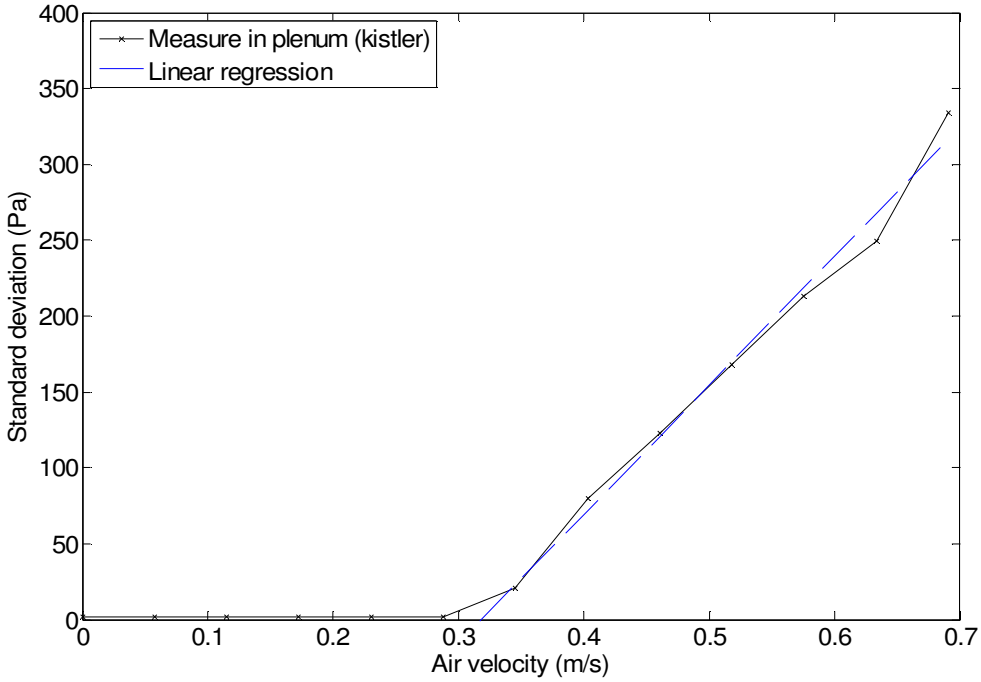

Graphic 6.5.1.1. Standard deviation curve (0 to 1200 lpm) in plenum chamber; and regression curve without distributor rotation.

Could be observed how the regression curve fit closer to the standard deviation curve from data for plenum chamber. The regression curve has been constructed with those standard deviation values already in fluidization regime (above σ_p *=20 Pa*), see Graphic 6.5.1.1.

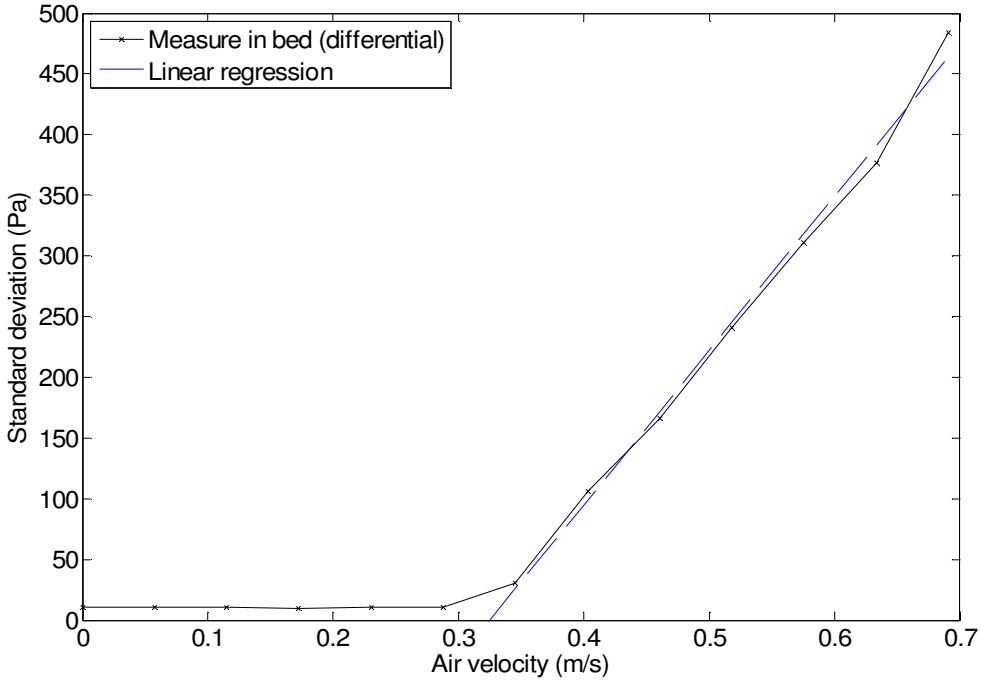

Graphic 6.5.1.2. Standard deviation curve (0 to 1200 lpm) in bed (differential); and regression curve, without distributor rotation.

Could be observed how the regression curve fit closer too the standard deviation curve from data for bed differential sensor, see Graphic 6.5.1.2.

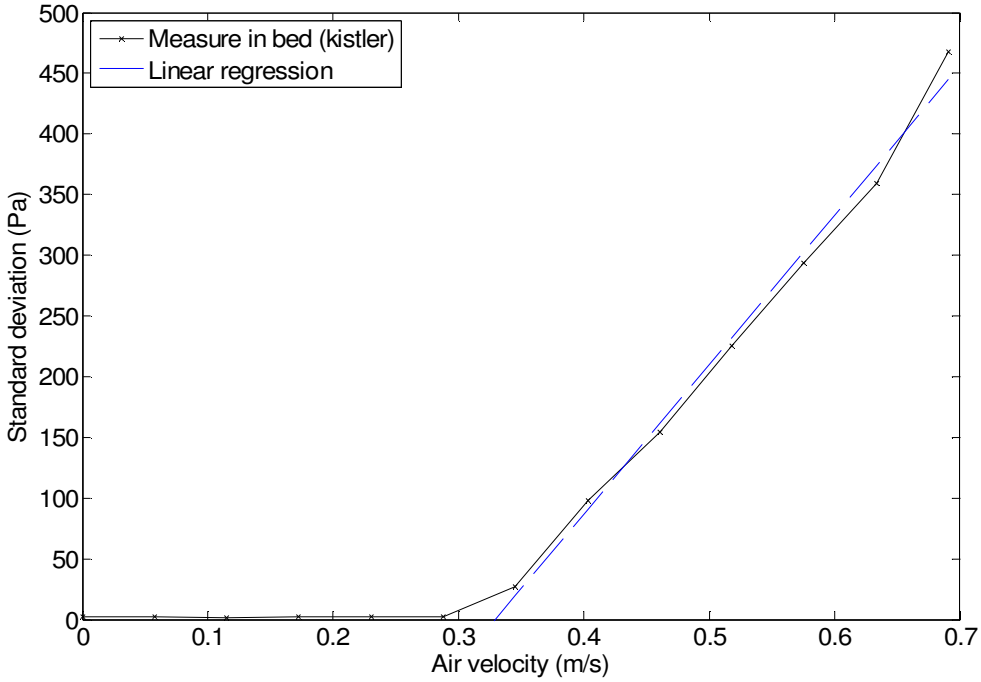

Graphic 6.5.1.3. Standard deviation curve (0 to 1200 lpm) in bed (Kistler); and regression curve, without distributor rotation.

Also, the regression curve for bed *Kistler* sensor fit closer too the standard deviation curve from data, see Graphic 6.5.1.3.

It is presented now graphically the mean pressure in bed for all flow rates, see Graphic 6.5.1.4. :

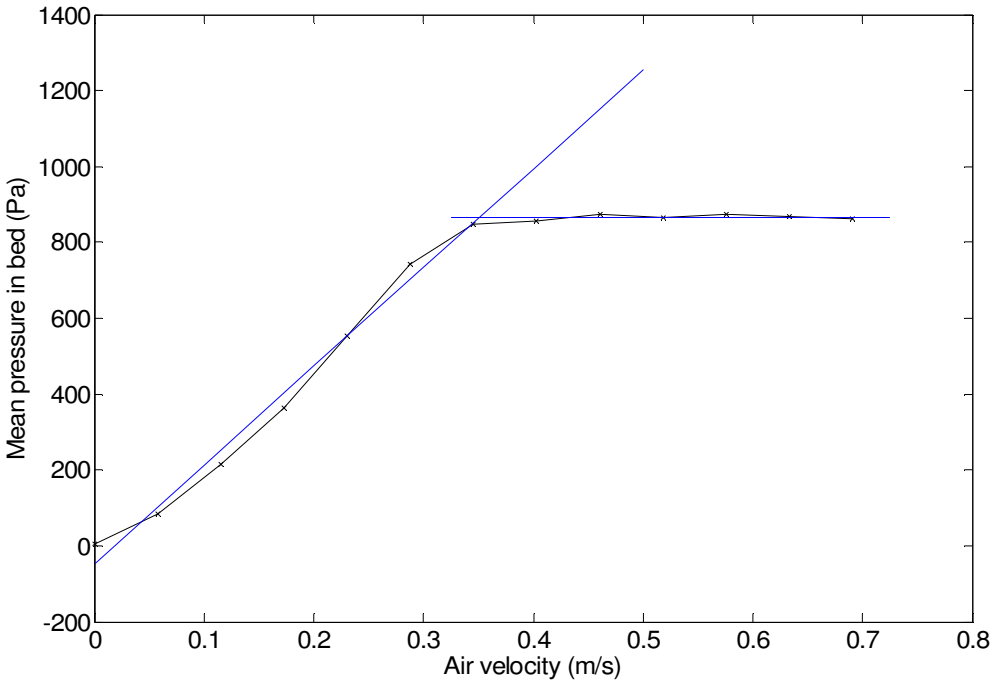

Graphic 6.5.1.4. Mean pressure curve for flow rates from 0 to 1200 lpm in bed; and regression curves for growing and constant pressure values with velocity, without distributor rotation.

As has been already said, one of the first methods to predict minimum fluidization velocity was the mean pressure plot. The pressure grows linearly until fluidization phenomena appear to maintain hydrostatic pressure constant.

In order to compare this method with deviation one, has been generate two regression curves, see Graphic 6.5.1.4., for linear growing pressure region and for constant pressure region. Intersection of both curves indicates minimum fluidization velocity.

Despite well fitness between the two different pressure region and its linear regression curves, this method has a greater uncertainty because of the difficulty to decided which pressure data sample belong to which fluid-dynamic region.

Results for the umf determination are summarized on Table 6.5.1.1. The table shows minimum fluidization velocity with the final values extract from *Matlab* both for plenum chamber, bed (with differential sensor and *Kistler* respectively) and the mean value of the three sensors. The u_{mf} calculated with the mean pressure values in bed and the mean is presented too.

	Plenum Chamber	***Bed (differential sensor)***	***Bed (Kistler)***	***Bed Mean Pressure***	***Mean u_{mf} Fluctuation Method***	***Mean u_{mf} with bed mean pressure value***
m/s	0,3182	0,325	0,3294	0,3499	0,3242	0,3306
lpm	552,8	564,6	572,2	607,8	563,2	574,4

Table 6.5.1.1. Values of u_{mf} for plenum chamber, bed (with differential sensor and Kistler respectively) and the mean value; u_{mf} calculated with the mean pressure values in bed and the total mean.

Results fit well between each other with the pressure deviation method purposed in *Puncochar et al* [20] (*97 %*). This results evidence that could be used separately any sensor as all of them arrive at the same minimum fluidization velocity, $u_{mf,}$ prediction.

Results from mean pressure deviation method are close to deviation ones but still at a certain distance (*8 %* greater than the mean u_{mf} calculated with the fluctuation method). Knowing that deviation method is a more accurate method for minimum fluidization velocity prediction, could be said that, without distributor rotation, mean pressure method predicts a greater u_{mf}.

The power spectrum analysis will be carried out, as said, with those flow rates already in fluidization regime. After applied the *FFT*, results obtained from *Matlab* are shown in Graphic 6.5.1.5., 6.5.1.6. and 6.5.1.7. for the three sensors without distributor rotation:

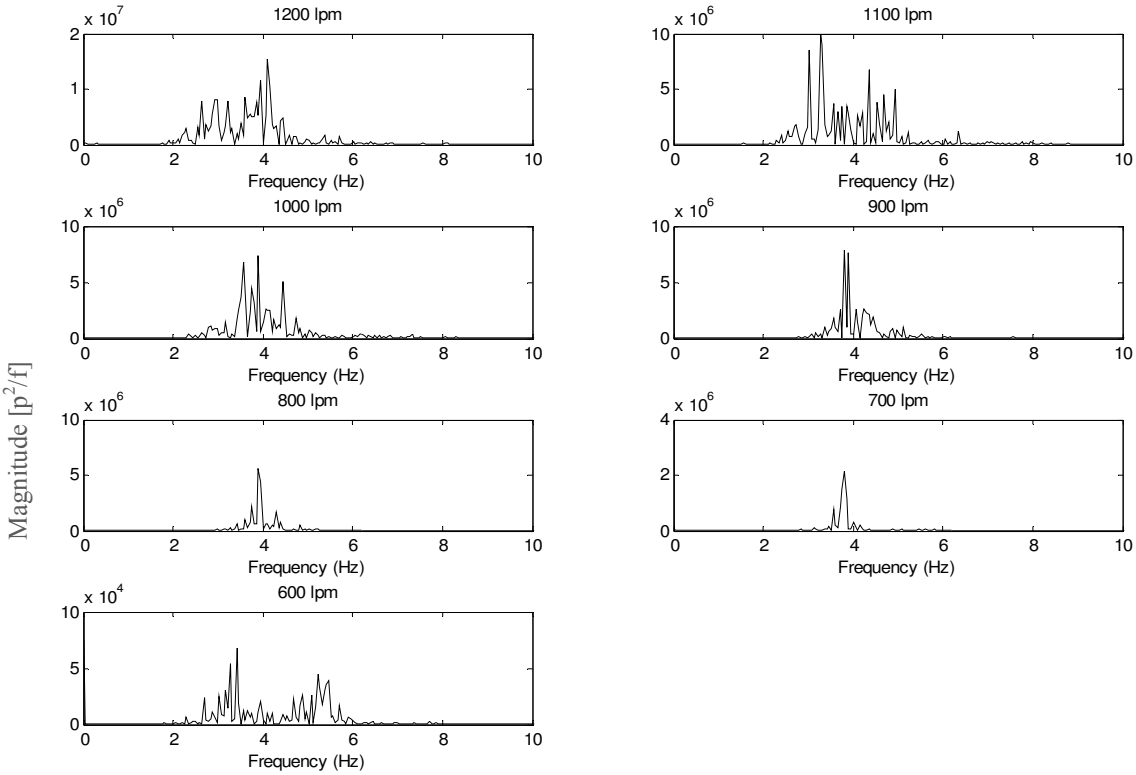

Graphic 6.5.1.5. Power spectra for flow rates from 600 to 1200 lpm in fluidization regime for plenum chamber with Kistler sensor, without distributor rotation .

Results from power spectrum analysis reveal, as *Johnson et al* [13] predicts, that in plenum chamber, without distributor rotation and under fluidization regime all the fundamental frequencies are between 1 to 5 *Hz*.

Because of clarity reasons for document, from now will be show power spectrum analysis in smaller size as all the plots has the same structure than Graphic 6.5.1.5.

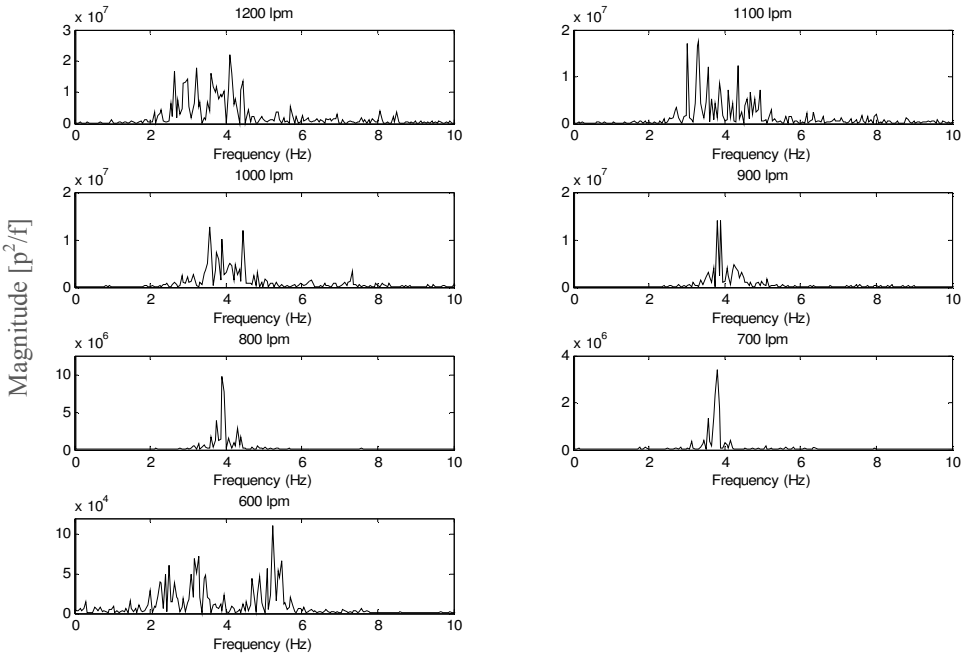

Graphic 6.5.1.6. Power spectra for (600 to 1200 lpm) for bed with differential pressure sensor, without distributor rotation .

Results from power spectrum analysis for bed (with differential sensor) reveal too that and under fluidization all the fundamental frequencies are between 1 to 5 *Hz*.

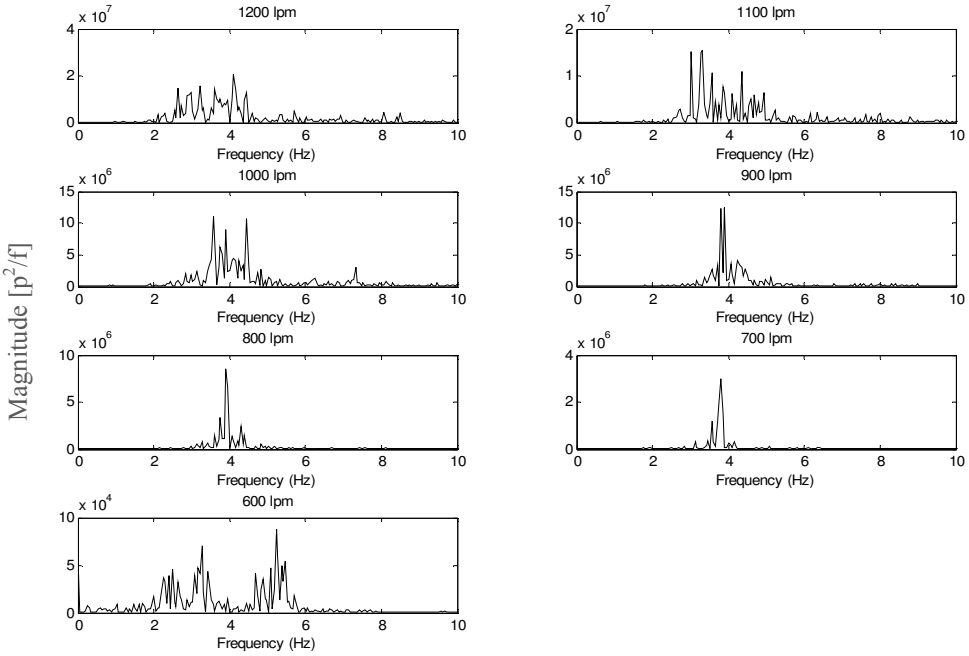

Graphic 6.5.1.7. Power spectra (600 to 1200 lpm) for bed with Kistler sensor, without distributor rotation.

Also, from power spectrum analysis for bed (with *Kistler* sensor) is revealed too that and under fluidization all the fundamental frequencies are between 1 to 5 *Hz*.

Results for the fundamental frequency are summarized on Table 6.5.1.2. The table shows fundamental frequencies with the final values extract from *Matlab* both for plenum chamber, bed (with differential sensor and *Kistler* respectively) and the mean value of the three sensors. Also it is presented the total mean fundamental frequency for plenum and bed.

	[lpm]	***600***	***700***	***800***	***900***	***1000***	***1100***	***1200***	***Mean Frequency [Hz]***
[Hz]	***Plenum Chamber***	*3,0*	*4,0*	*4,0*	*4,0*	*4,0*	*3,0*	*4,0*	***3,7***
	Bed (differential sensor)	*5,0*	*4,0*	*4,0*	*4,0*	*3,6*	*3,3*	*4,1*	***4,0***
	Bed (Kistler)	*5,2*	*3,8*	*3,9*	*3,9*	*3,6*	*3,3*	*4,1*	***4,0***
									3,9

Table 6.5.1.2. Values of fundamental frequencies for plenum chamber, bed (with differential sensor and Kistler respectively) the mean value respectively and the total mean fundamental frequency.

From the *Johnson et al* [13] power spectra plots obtained, the regime has been determine from which prototype evolve from fluidization to maximum flow rate experimented. All the final regimes for plenum chamber, bed (with differential sensor and *Kistler* respectively) for bed without distributor rotation are presented in Table 6.5.1.3.

The fluid-dynamic determination for each flow rate will be carried out by visual analysis by possible correlation of the prototype signal with any of the power spectrum *Johnson et al* [13] ones.

	Flow rate (lpm)	*Fluid-dynamic regime*
Plenum Chamber	600	Multiple Bubble regime
	700	Multiple Bubble regime
	800	Multiple Bubble regime
	900	Multiple Bubble regime
	1000	Multiple Bubble regime
	1100	Single Bubble regime
	1200	Single Bubble regime
Differential Sensor (bed)	600	Multiple Bubble regime
	700	Multiple Bubble regime
	800	Multiple Bubble regime
	900	Multiple Bubble regime
	1000	Multiple Bubble regime
	1100	Single Bubble regime
	1200	Single Bubble regime
Kistler (bed)	600	Multiple Bubble regime
	700	Multiple Bubble regime
	800	Multiple Bubble regime
	900	Multiple Bubble regime
	1000	Multiple Bubble regime
	1100	Single Bubble regime
	1200	Single Bubble regime

Table 6.5.1.3. Final regimes for plenum chamber, bed (with differential sensor and Kistler respectively) for all the flow rates in fluidization regime, without distributor rotation.

Results for the three sensors reveal that, when bed is already under fluidization, the fluid-dynamic regime seems to evolve from a multiple bubble regime to a single bubble regime, as all these the regimes are expected to operate far from transport regimes.

The graphic determination of u_{mf} *with* the curve $\sigma_p = A + Bu$ values, fitted by linear regression, for those pressure fluctuations for a bed height of **h_b = 9,6 *cm* in the plenum and bed with distributor rotation** above σ_p =*20 Pa,* and the intersection with σ_p = *0 Pa*, at u_{mf} velocity, see Graphic 6.5.1.8., Graphic 6.5.1.9., Graphic 6.5.1.10. , and the mean pressure values in bed, Graphic 6.5.1.11. :

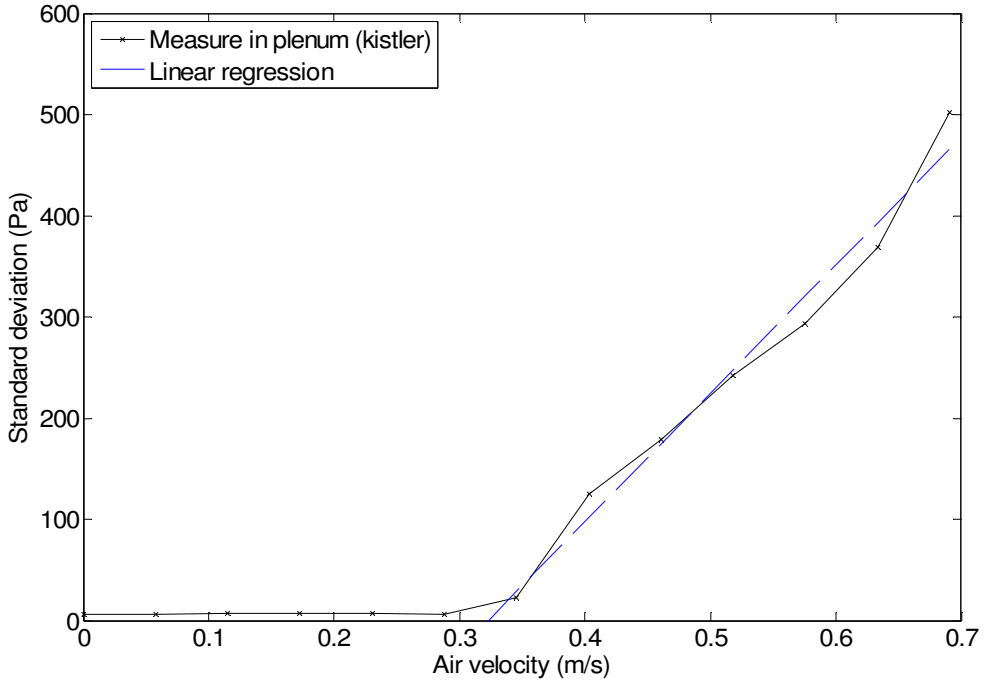

Graphic 6.5.1.8. Standard deviation curve (0 to 1200 lpm) in plenum chamber; and regression curve, with distributor rotation.

Could be observed how the regression curve fit closer to the standard deviation curve from data for plenum chamber. The regression curve has been constructed with those standard deviation values already in fluidization regime (above σ_p =*20 Pa*), see Graphic 6.5.1.8.

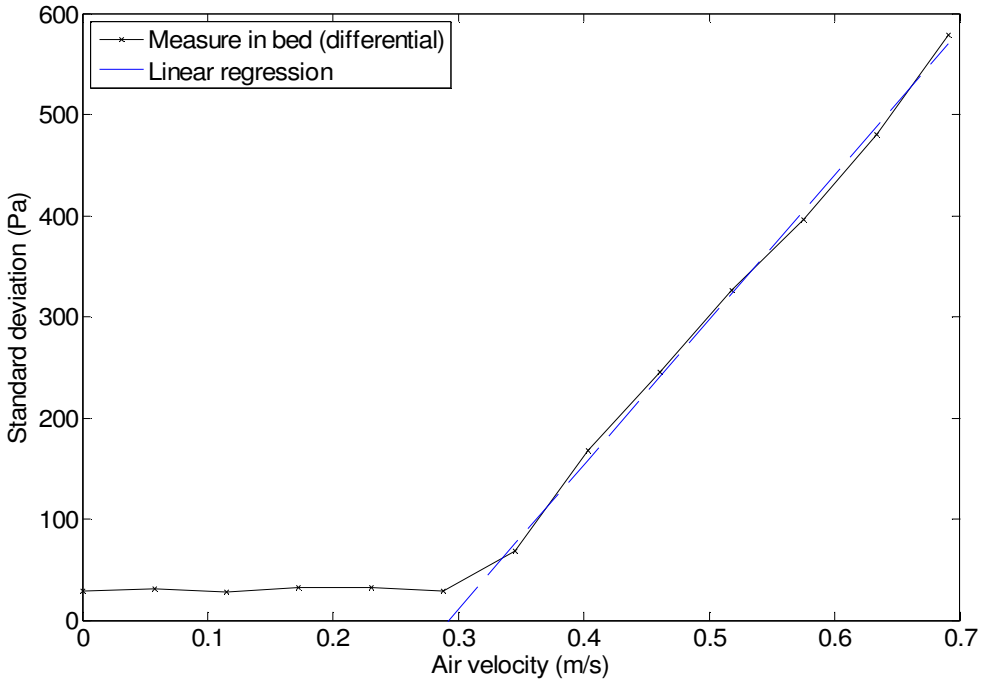

Graphic 6.5.1.9. Standard deviation curve (0 to 1200 lpm) in bed (differential); and regression curve, with distributor rotation.

Could be observed how the regression curve fit closer too the standard deviation curve from data for bed differential sensor, see Graphic 6.5.1.9.

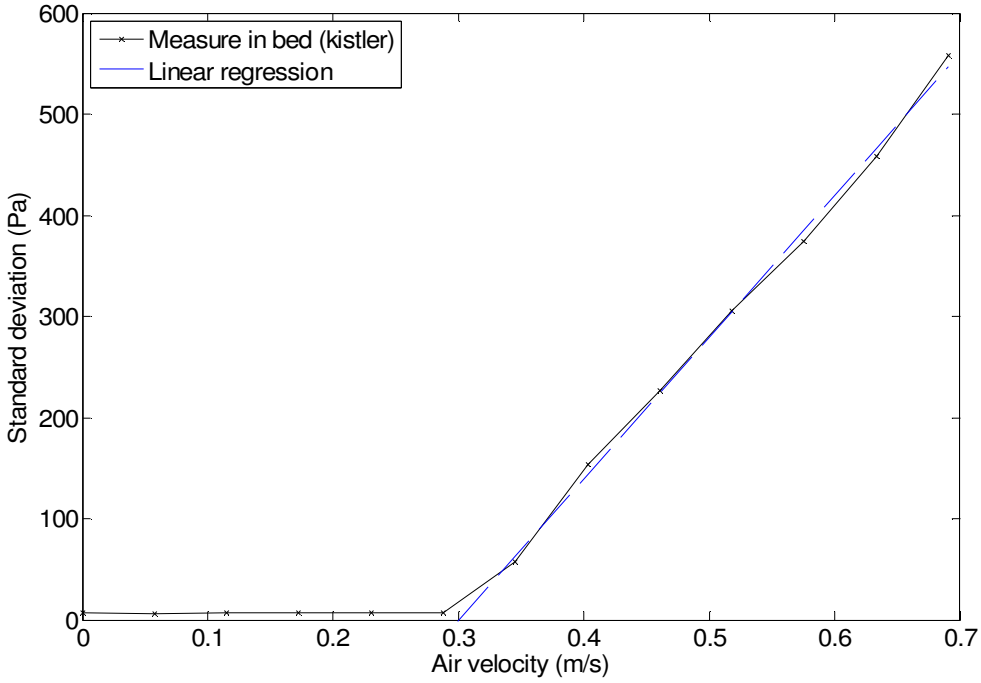

Graphic 6.5.1.10. Standard deviation curve (0 to 1200 lpm) in bed (Kistler); and regression curve, with distributor rotation.

Also, the regression curve for bed *Kistler* sensor fit closer too the standard deviation curve from data, see Graphic 6.5.1.10.

It is presented now graphically the mean pressure in bed for all flow rates, see Graphic 6.5.1.11. :

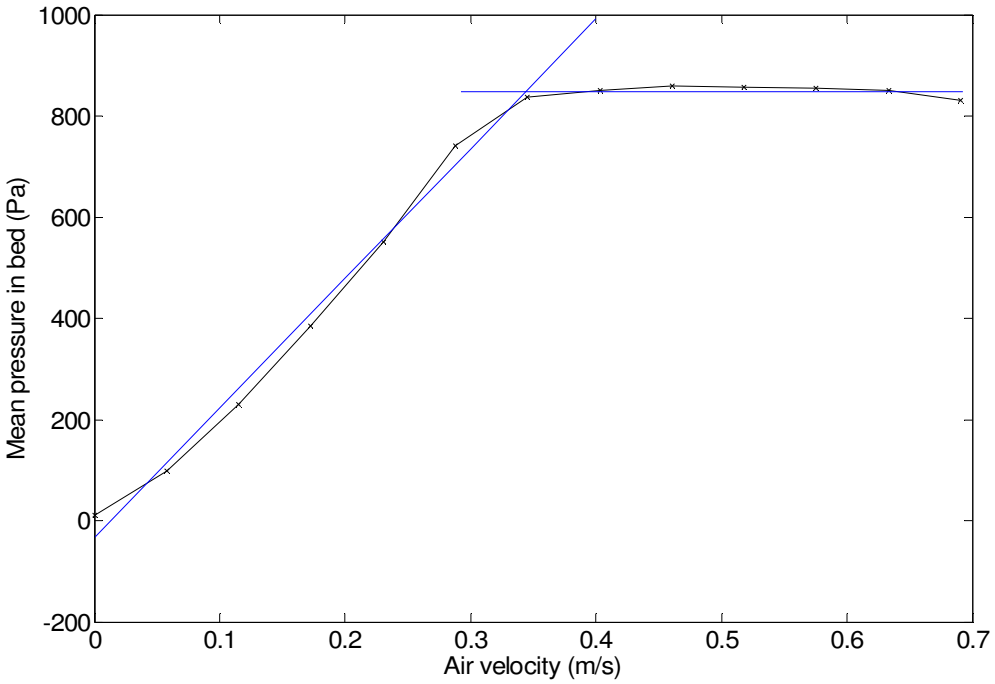

Graphic 6.5.1.11. Mean pressure curve for flow rates from 0 to 1200 lpm in bed; and regression curves for growing and constant pressure values with velocity, with distributor rotation.

As in case of no distributor rotation will be studied too to predict minimum fluidization velocity the mean pressure plot. Remember that pressure grow linearly until fluidization phenomena appears to maintain hydrostatic pressure constant.

One more time, in order to compare this method with deviation one, has been generate two regression curves, see Graphic 6.5.1.11., for linear growing pressure region and for constant pressure region. Intersection of both curves indicates minimum fluidization velocity.

In this case too, despite well fitness between the two different pressure region and its linear regression curves, this method has a greater uncertainty because of the difficulty to decided which pressure data sample belong to which fluid-dynamic region.

Results for the umf determination are summarized on Table 6.5.1.4. The table shows minimum fluidization velocity with the final values extract from *Matlab* both for plenum chamber, bed (with differential sensor and *Kistler* respectively) and the mean value of the three sensors. The u_{mf} calculated with the mean pressure values in bed and the mean is presented too.

	Plenum Chamber	***Bed (differential sensor)***	***Bed (Kistler)***	***Bed Mean Pressure***	***Mean umf Fluctuation Method***	***Mean umf with bed mean pressure value***
(m/s)	0,3227	0,2823	0,3003	0,3441	0,3018	0,3124
lpm	560,6	490,4	521,7	597,8	524,2	542,6

Table 6.5.1.4. Values of u_{mf} for plenum chamber, bed (with differential sensor and Kistler respectively) and the mean value; u_{mf} calculated with the mean pressure values in bed and the total mean.

Results fit well between each other with the pressure deviation method purposed in *Puncochar et al* [20] (*88 %*). This results evidence definitely that could be used separately any sensor as all of them arrive at the same minimum fluidization velocity, $u_{mf,}$ prediction.

Results from mean pressure deviation method are close to deviation ones but still at a certain distance (*14 %* greater than the mean u_{mf} calculated with the fluctuation method). Knowing that deviation method is a more accurate method for minimum fluidization velocity prediction, could be said that, without distributor rotation, mean pressure method predicts a greater u_{mf}.

Could be observed too, that fitness between data from no distributor rotation are closer each other for three sensors than with distributor rotation. Take into account that a rotational mechanism enter in the system with direct effects in bed performance.

The power spectrum analysis will be carried out, as said, with those flow rates already in fluidization regime. After applied the *FFT*, results obtained from *Matlab* are shown in Graphic 6.5.1.12., 6.5.1.13 and 6.5.1.14 for the three sensors without distributor rotation:

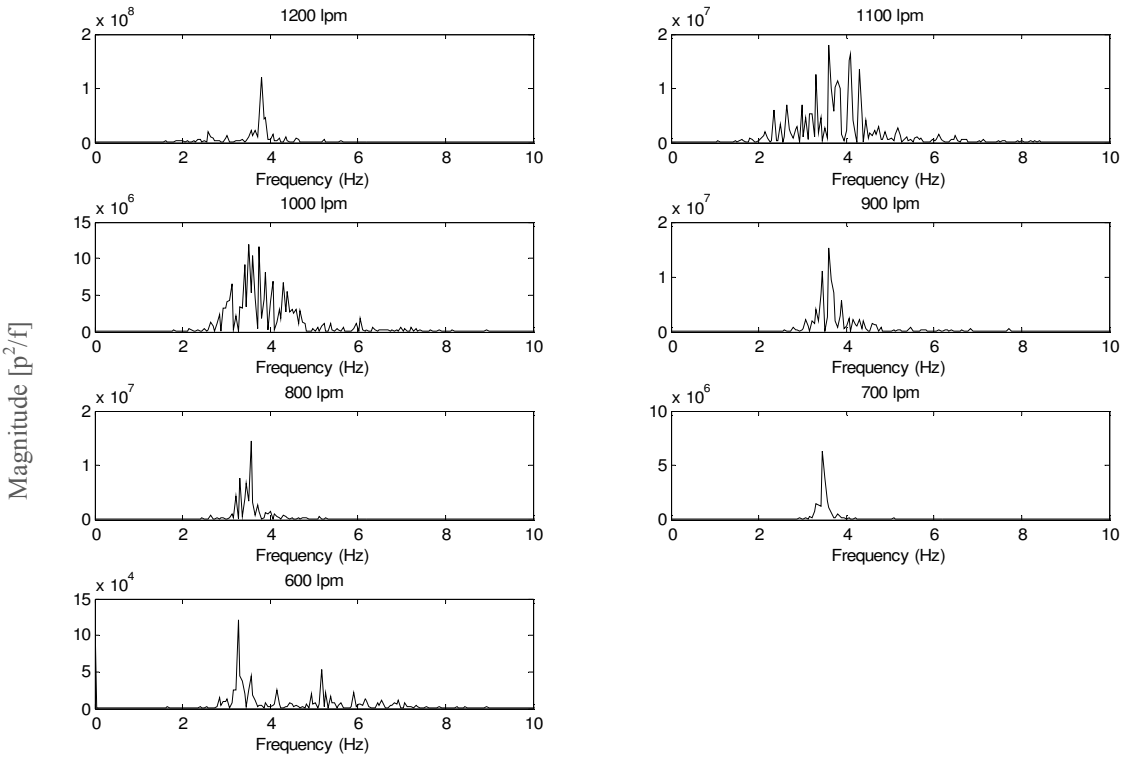

Graphic 6.5.1.12. Power spectra for flow rates from 600 to 1200 lpm in fluidization regime for plenum chamber with Kistler sensor, with distributor rotation.

Results from power spectrum analysis reveal, as *Johnson et al* [13] predicts, that in plenum chamber, with distributor rotation and under fluidization regime all the fundamental frequencies are between 1 to 5 *Hz*.

Because of clarity reasons for document, from now will be show power spectrum analysis in smaller size as all the plots has the same structure than Graphic 6.5.1.12.

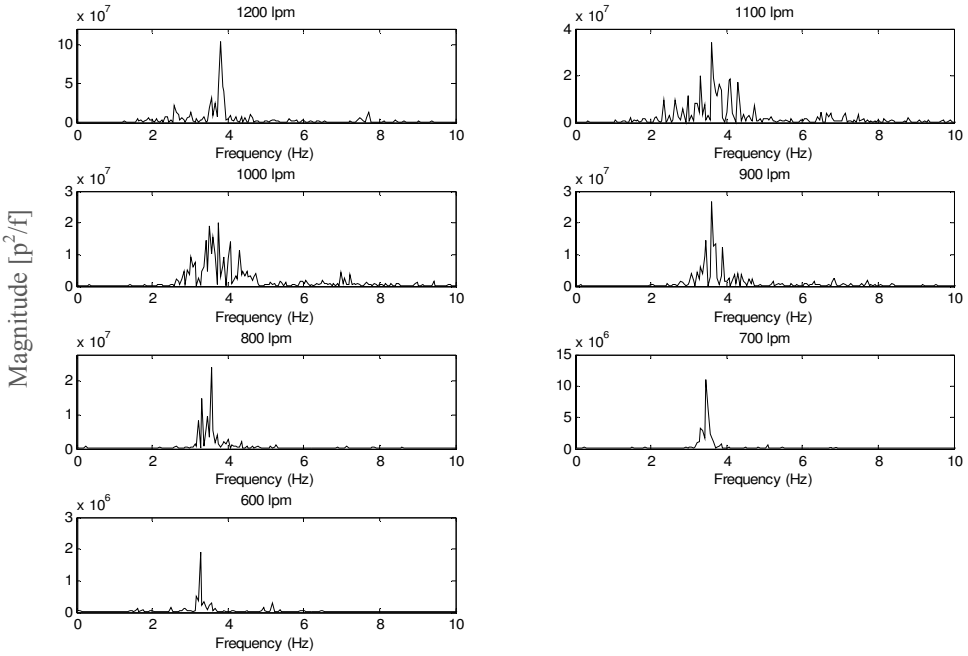

Graphic 6.5.1.13. Power spectra for (600 to 1200 lpm) for bed with differential pressure sensor, with distributor rotation .

Results from power spectrum analysis for bed (with differential sensor) reveal too that and under fluidization all the fundamental frequencies are between 1 to 5 *Hz*.

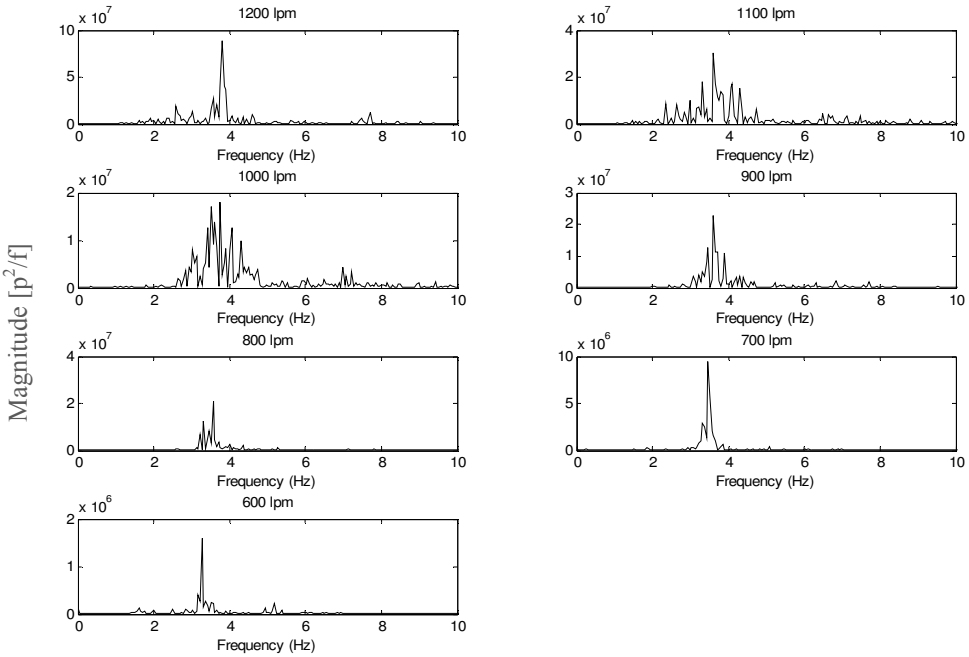

Graphic 6.5.1.14. Power spectra (600 to 1200 lpm) for bed with Kistler sensor, with distributor rotation.

Also, from power spectrum analysis for bed (with *Kistler* sensor) is revealed too that and under fluidization all the fundamental frequencies are between 1 to 5 *Hz*.

Results for the fundamental frequency are summarized on Table 6.5.1.5. The table shows fundamental frequencies with the final values extract from *Matlab* both for plenum chamber, bed (with differential sensor and *Kistler* respectively) and the mean value of the three sensors. Also it is presented the total mean fundamental frequency for plenum and bed.

	[lpm]	***600***	***700***	***800***	***900***	***1000***	***1100***	***1200***	***Mean Frequency [Hz]***
[Hz]	***Plenum Chamber***	*3,3*	*3,5*	*3,6*	*3,6*	*3,5*	*3,6*	*3,8*	***3,6***
	Bed (differential sensor)	*3,3*	*3,5*	*3,6*	*3,6*	*3,6*	*3,8*	*3,6*	***3,6***
	Bed (Kistler)	*3,3*	*3,5*	*3,6*	*3,6*	*3,6*	*3,8*	*3,6*	***3,6***
									3,6

Table 6.5.1.5. Values of fundamental frequencies for plenum chamber, bed (with differential sensor and Kistler respectively) the mean value respectively and the total mean fundamental frequency.

From the *Johnson et al* [13] power spectra plots obtained, the regime has been determine from which prototype evolve from fluidization to maximum flow rate experimented. All the final regimes for plenum chamber, bed (with differential sensor and *Kistler* respectively) for bed without distributor rotation are presented in Table 6.5.1.6.

The fluid-dynamic determination for each flow rate will be carried out by visual analysis by possible correlation of the prototype signal with any of the power spectrum *Johnson et al* [13] ones.

	Flow rate (lpm)	*Fluid-dynamic regime*
Plenum Chamber	600	Multiple Bubble regime
	700	Multiple Bubble regime
	800	Multiple Bubble regime
	900	Multiple Bubble regime
	1000	Multiple Bubble regime
	1100	Single Bubble regime
	1200	Single Bubble regime
Differential Sensor (bed)	600	Multiple Bubble regime
	700	Multiple Bubble regime
	800	Multiple Bubble regime
	900	Multiple Bubble regime
	1000	Multiple Bubble regime
	1100	Single Bubble regime
	1200	Single Bubble regime
Kistler (bed)	600	Multiple Bubble regime
	700	Multiple Bubble regime
	800	Multiple Bubble regime
	900	Multiple Bubble regime
	1000	Multiple Bubble regime
	1100	Single Bubble regime
	1200	Single Bubble regime

Table 6.5.1.6. Final regimes for plenum chamber, bed (with differential sensor and Kistler respectively) for all the flow rates in fluidization regime, with distributor rotation.

Result for the three sensors reveal that, when bed is already under fluidization, the fluid-dynamic regime seems to evolve from a multiple bubble regime to a single bubble regime as all these the regimes are expected to operate far from transport regimes.

6.5.2. 2nd TEST FOR BED ASPECT RATIO $^1/_2$

Is presented then the resolution of the curve $\sigma_p = A + Bu$ values, solved by linear regression, for those pressure fluctuations for **second test series experiments for a bed height of h_b = 9,6 cm in plenum chamber, and bed without distributor rotation** above σ_p =20, and the intersection with σ_p = 0, at u_{mf} velocity, see Graphic 6.5.2.1., Graphic 6.5.2.2., Graphic 6.5.2.3. , and the mean pressure values in bed, Graphic 6.5.2.4. :

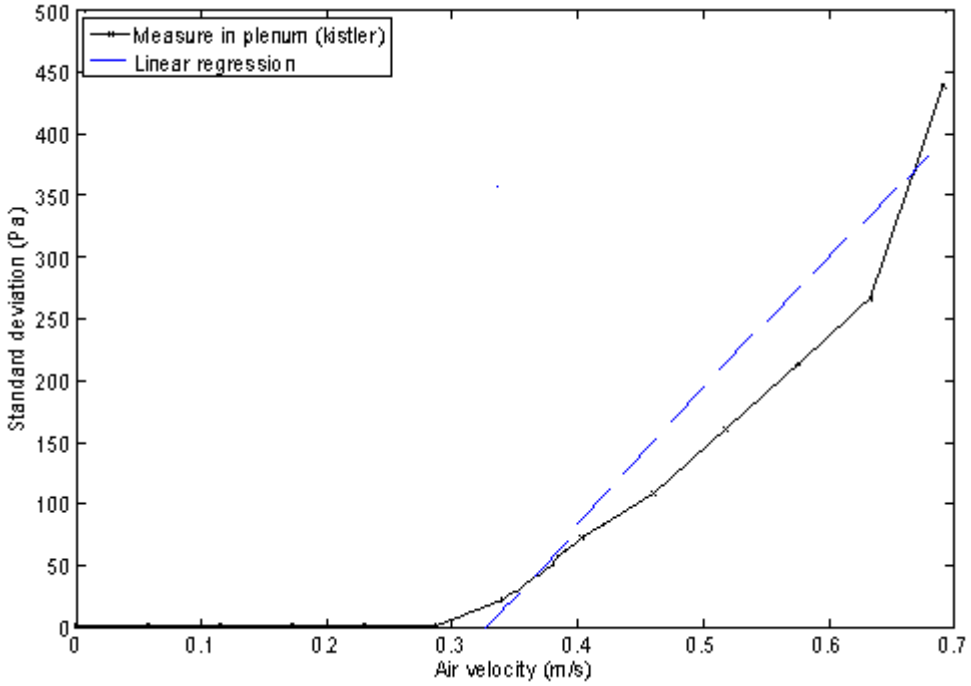

Graphic 6.5.2.1. Standard deviation curve (0 to 1200 lpm) in plenum chamber; and regression curve, without distributor rotation.

Could be observed how the regression curve fit closer to the standard deviation curve from data for plenum chamber. The regression curve has been constructed with those standard deviation values already in fluidization regime (above σ_p =20 Pa), see Graphic 6.5.1.1.

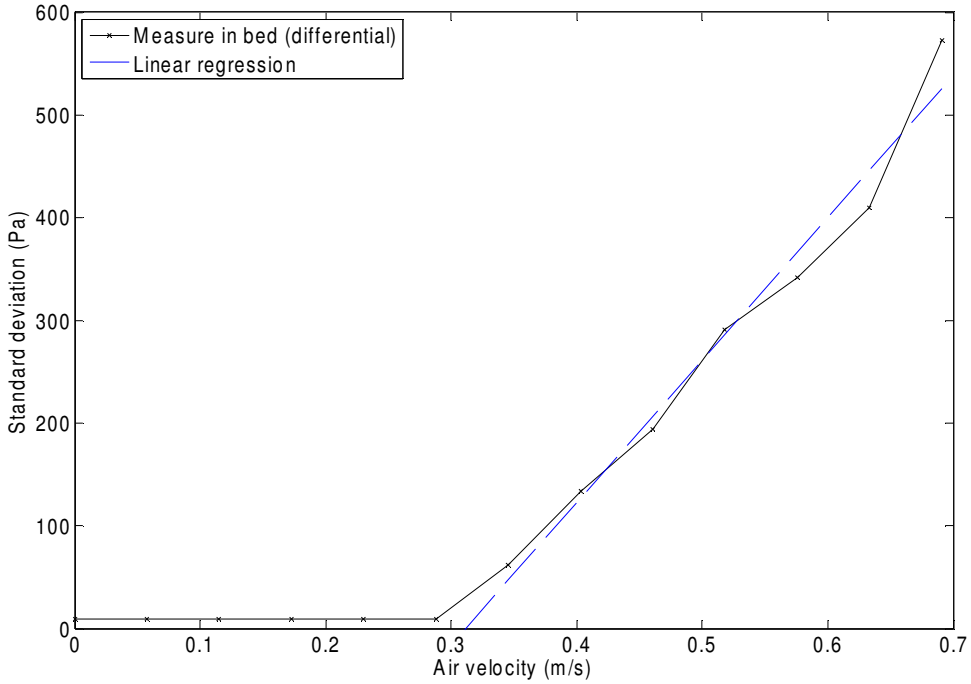

Graphic 6.5.2.2. Standard deviation curve (0 to 1200 lpm) in bed (differential); and regression curve, without distributor rotation.

Could be observed how the regression curve fit closer too the standard deviation curve from data for bed differential sensor, see Graphic 6.5.2.2.

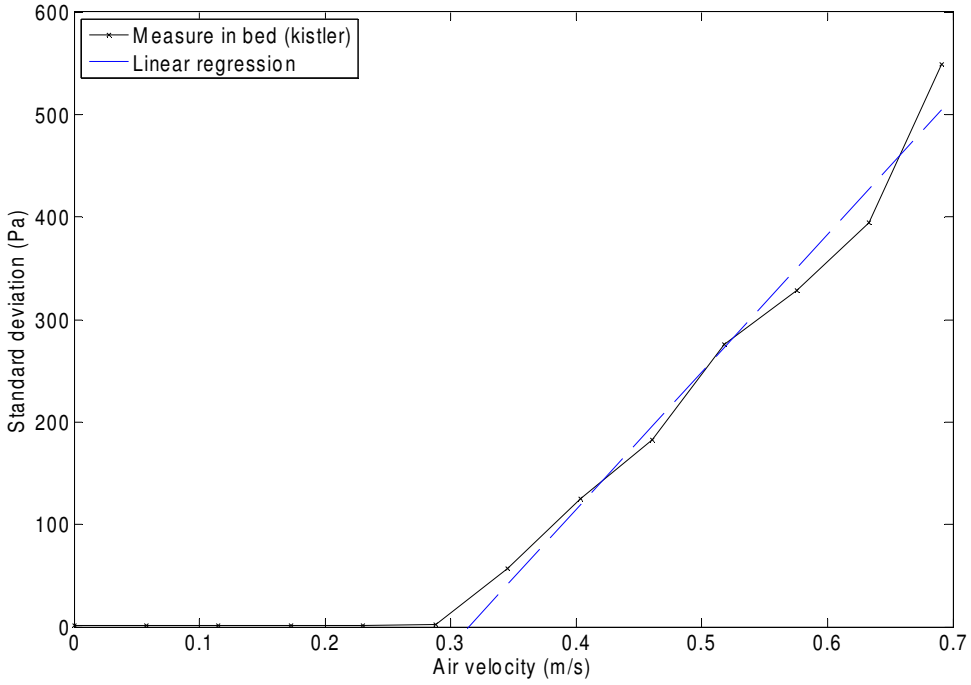

Graphic 6.5.2.3. Standard deviation curve (0 to 1200 lpm) in bed (Kistler); and regression curve, without distributor rotation.

Also, the regression curve for bed *Kistler* sensor fit closer too the standard deviation curve from data, see Graphic 6.5.2.3.

It is presented now graphically the mean pressure in bed for all flow rates, see Graphic 6.5.2.4. :

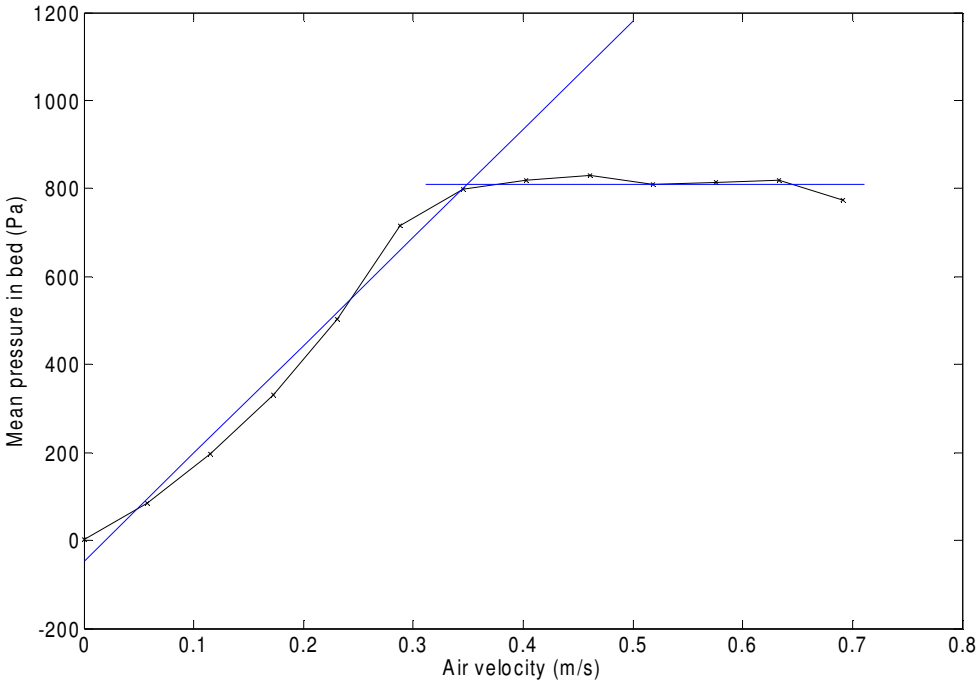

Graphic 6.5.2.4. Mean pressure curve for flow rates from 0 to 1200 lpm in bed; and regression curves for growing and constant pressure values with velocity, without distributor rotation.

As has been already said, one of the first methods to predict minimum fluidization velocity was the mean pressure plot. The pressure grows linearly until fluidization phenomena appear to maintain hydrostatic pressure constant.

In order to compare this method with deviation one, has been generate two regression curves, see Graphic 6.5.2.4., for linear growing pressure region and for constant pressure region. Intersection of both curves indicates minimum fluidization velocity.

Despite well fitness between the two different pressure region and its linear regression curves, this method has a greater uncertainty because of the difficulty to decided which pressure data sample belong to which fluid-dynamic region.

Result for the u_{mf} determination is summarized on Table 6.5.2.1. The table shows minimum fluidization velocity with the final values extract from *Matlab* both for plenum chamber, bed (with differential sensor and *Kistler* respectively) and the mean value of the three sensors. The u_{mf} calculated with the mean pressure values in bed and the mean is presented too.

	Plenum Chamber	***Bed (differential sensor)***	***Bed (Kistler)***	***Bed Mean Pressure***	***Mean umf Fluctuation Method***	***Mean umf with bed mean pressure value***
(m/s)	0,3215	0,3287	0,3346	0,3386	0,3283	0,3309
lpm	558,5	571,0	581,3	588,3	570,3	574,8

Table 6.5.2.1. Values of u_{mf} for plenum chamber, bed (with differential sensor and Kistler respectively) and the mean value; u_{mf} calculated with the mean pressure values in bed and the total mean.

Results fit well between each other with the pressure deviation method purposed in *Puncochar et al* [20] (*90 %*). This results evidence, this time too, that could be used separately any sensor as all of them arrive at the same minimum fluidization velocity, $u_{mf,}$ prediction.

Results from mean pressure deviation method are close to deviation ones but still at a certain distance (8 % greater than the mean u_{mf} calculated with the fluctuation method). Knowing that deviation method is a more accurate method for minimum fluidization velocity prediction, could be said that, with distributor rotation, mean pressure method predicts a greater u_{mf}.

The power spectrum analysis will be carried out, as said, with those flow rates already in fluidization regime. After applied the *FFT*, results obtained from *Matlab* are shown in Graphic 6.5.2.5., 6.5.1.6. and 6.5.2.7. for the three sensors without distributor rotation:

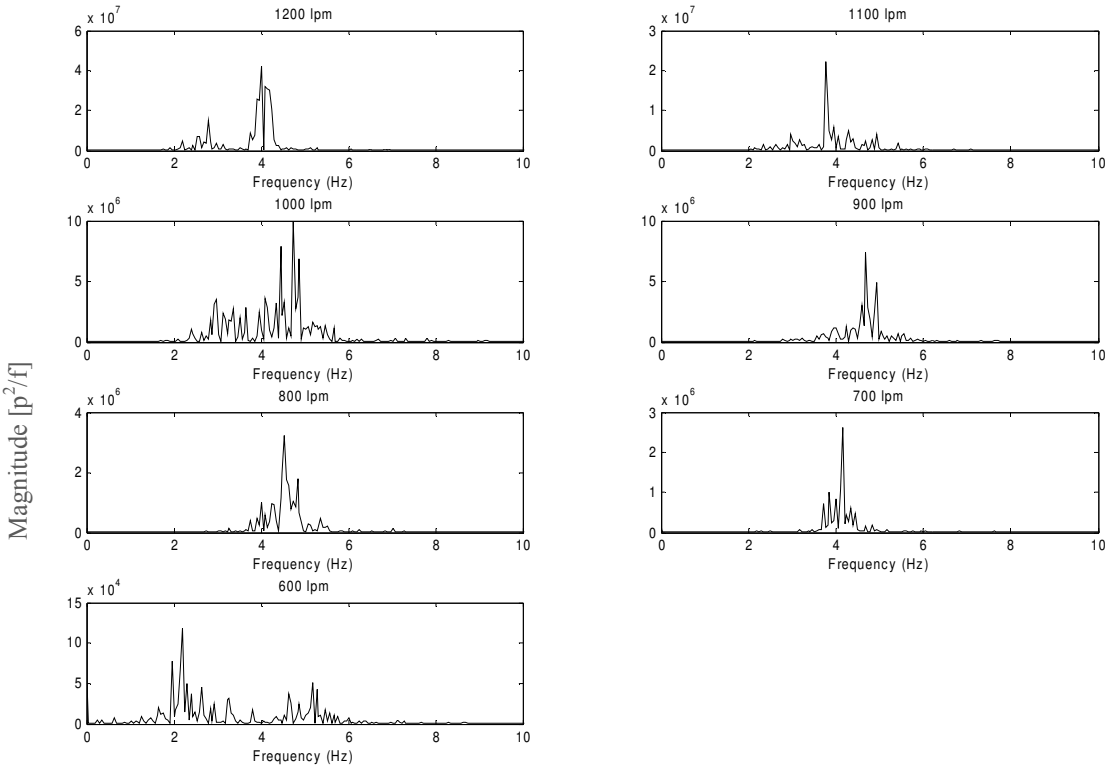

Graphic 6.5.2.5. Power spectra for flow rates from 600 to 1200 lpm in fluidization regime for plenum chamber with Kistler sensor, without distributor rotation.

Results from power spectrum analysis reveal, as *Johnson et al* [13] predicts, that in plenum chamber, without distributor rotation and under fluidization regime all the fundamental frequencies are between 1 to 5 *Hz*.

Because of clarity reasons for document, from now will be show power spectrum analysis in smaller size as all the plots has the same structure than Graphic 6.5.2.5.

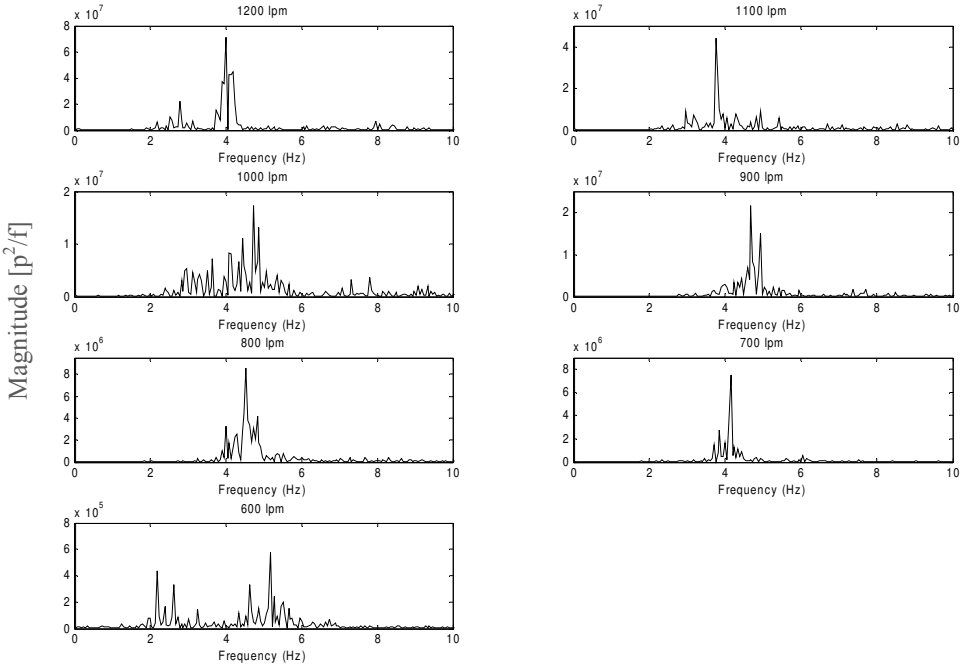

Graphic 6.5.2.6. Power spectra for (600 to 1200 lpm) for bed with differential pressure sensor, without distributor rotation.

Results from power spectrum analysis for bed (with differential sensor) reveal too that and under fluidization all the fundamental frequencies are between 1 to 5 *Hz*.

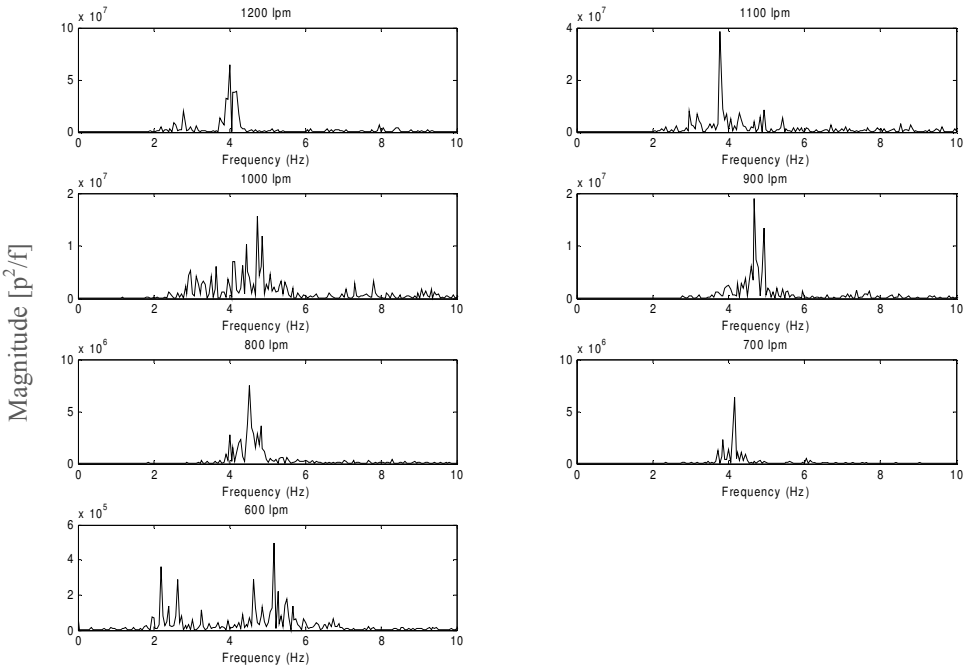

Graphic 6.5.2.7. Power spectra (600 to 1200 lpm) for bed with Kistler sensor.

Also, from power spectrum analysis for bed (with *Kistler* sensor) is revealed too that and under fluidization all the fundamental frequencies are between 1 to 5 *Hz*.

Results for the fundamental frequency are summarized on Table 6.5.2.2. The table shows fundamental frequencies with the final values extract from *Matlab* both for plenum chamber, bed (with differential sensor and *Kistler* respectively) and the mean value of the three sensors. Also it is presented the total mean fundamental frequency for plenum and bed.

	[lpm]	***600***	***700***	***800***	***900***	***1000***	***1100***	***1200***	***Mean Frequency [Hz]***
[Hz]	***Plenum Chamber***	*2,2*	*4,2*	*4,2*	*4,7*	*4,7*	*3,8*	*4,0*	***4,0***
	Bed (differential sensor)	*5,2*	*4,2*	*4,5*	*4,7*	*4,7*	*3,8*	*4,0*	***4,4***
	Bed (Kistler)	*5,2*	*4,2*	*4,5*	*4,7*	*4,7*	*3,8*	*4,0*	***4,4***
									4,3

Table 6.5.2.2. Values of fundamental frequencies for plenum chamber, bed (with differential sensor and Kistler respectively) the mean value respectively and the total mean fundamental frequency.

From the *Johnson et al* [13] power spectra plots obtained, the regime has been determine from which prototype evolve from fluidization to maximum flow rate experimented. All the final regimes for plenum chamber, bed (with differential sensor and *Kistler* respectively) for bed without distributor rotation are presented in Table 6.5.2.3.

The fluid-dynamic determination for each flow rate will be carried out by visual analysis by possible correlation of the prototype signal with any of the power spectrum *Johnson et al* [13] ones.

	Flow rate (lpm)	*Fluid-dynamic regime*
Plenum Chamber	600	Multiple Bubble regime
	700	Multiple Bubble regime
	800	Multiple Bubble regime
	900	Multiple Bubble regime
	1000	Multiple Bubble regime
	1100	Single Bubble regime
	1200	Single Bubble regime
Differential Sensor (bed)	600	Multiple Bubble regime
	700	Multiple Bubble regime
	800	Multiple Bubble regime
	900	Multiple Bubble regime
	1000	Multiple Bubble regime
	1100	Single Bubble regime
	1200	Single Bubble regime
Kistler (bed)	600	Multiple Bubble regime
	700	Multiple Bubble regime
	800	Multiple Bubble regime
	900	Multiple Bubble regime
	1000	Multiple Bubble regime
	1100	Single Bubble regime
	1200	Single Bubble regime

Table 6.5.2.3. Final regimes for plenum chamber, bed (with differential sensor and Kistler respectively) for all the flow rates in fluidization regime, without distributor rotation.

Results for the three sensors reveal that, when bed is already under fluidization, the fluid-dynamic regime seems to evolve from a multiple bubble regime to a single bubble regime as all these the regimes are expected to operate far from transport regimes.

The graphic determination of u_{mf} *with* the curve $\sigma_p = A + Bu$ values, fitted by linear regression, for those pressure fluctuations for a bed height of **h_b = 9,6 *cm* in the plenum and bed with distributor rotation** above σ_p =*20 Pa,* and the intersection with σ_p = *0 Pa*, at u_{mf} velocity, see Graphic 6.5.2.8., Graphic 6.5.2.9., Graphic 6.5.2.10. , and the mean pressure values in bed, Graphic 6.5.2.11. :

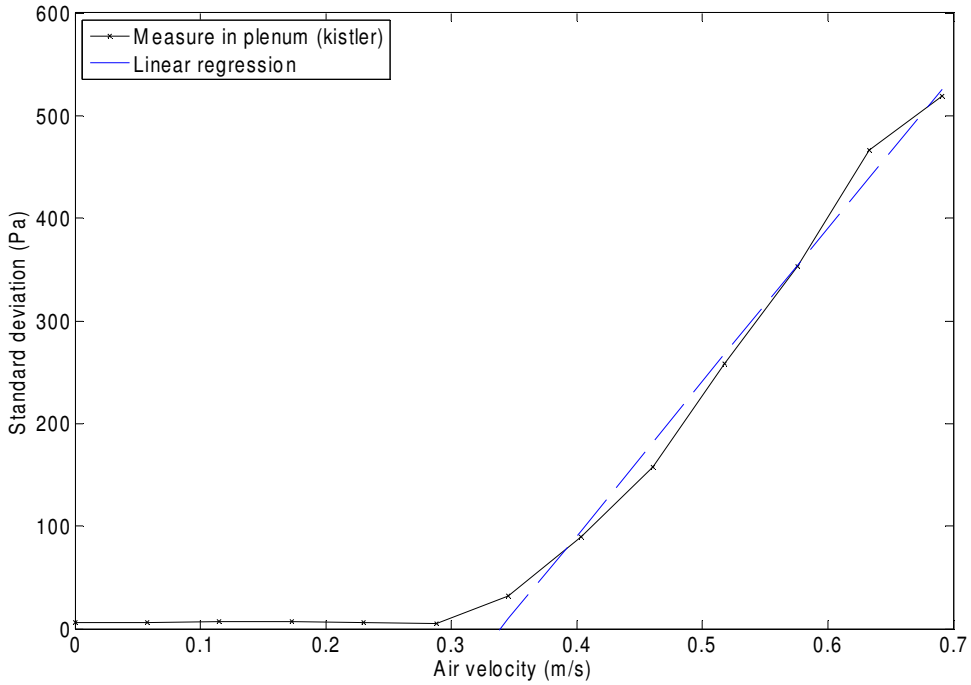

Graphic 6.5.2.8. Standard deviation curve (0 to 1200 lpm) in plenum chamber; and regression curve, with distributor rotation.

Could be observed how the regression curve fit closer to the standard deviation curve from data for plenum chamber. The regression curve has been constructed with those standard deviation values already in fluidization regime (above σ_p =*20 Pa*), see Graphic 6.5.2.8.

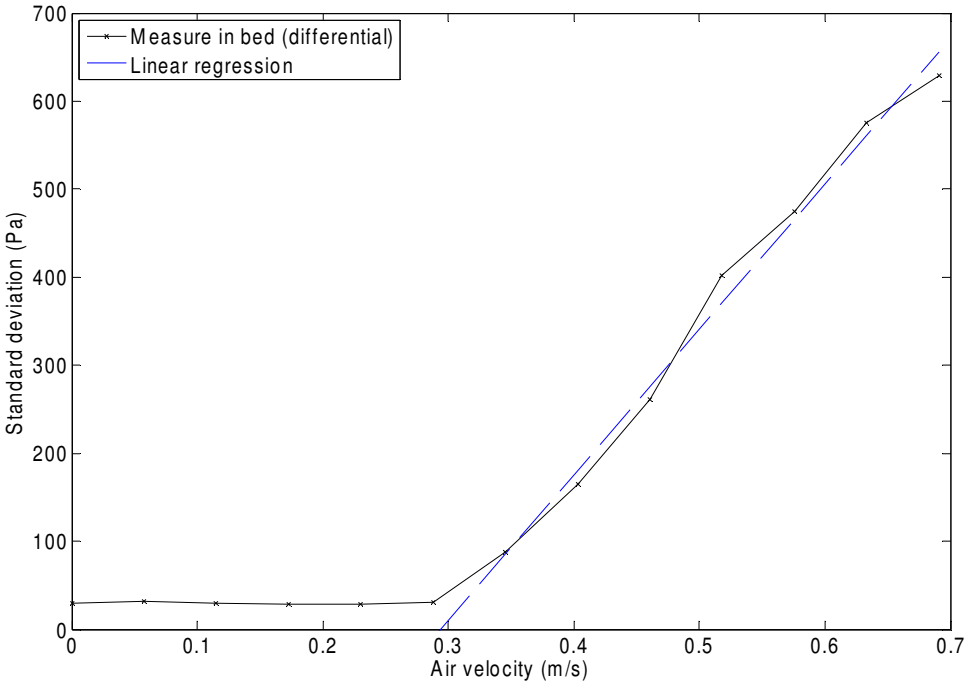

Graphic 6.5.2.9. Standard deviation curve (0 to 1200 lpm) in bed (differential); and regression curve, with distributor rotation.

Could be observed how the regression curve fit closer too the standard deviation curve from data for bed differential sensor, see Graphic 6.5.2.9.

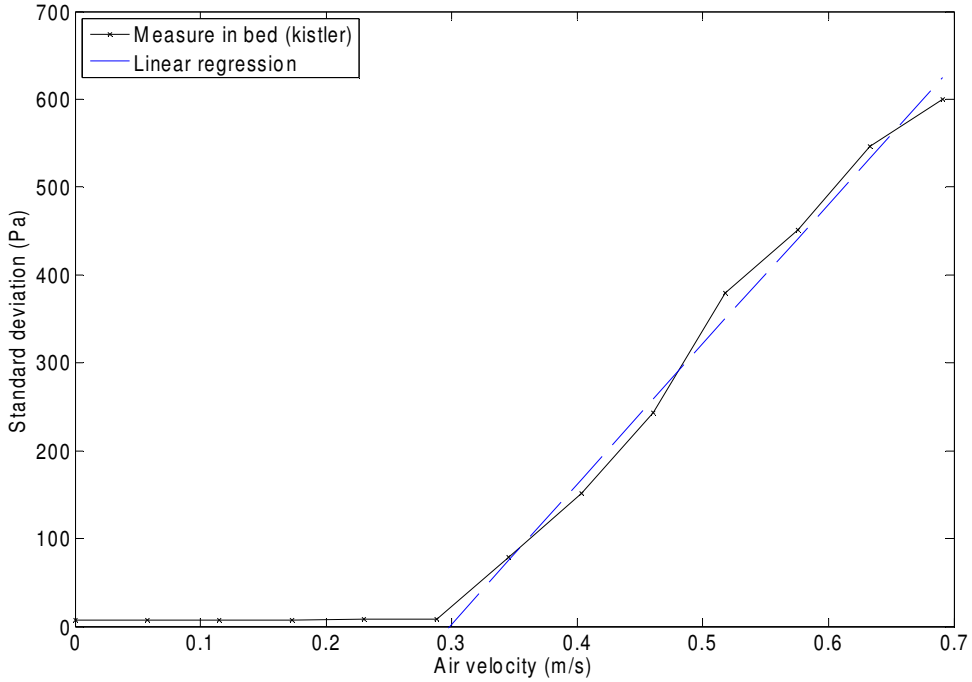

Graphic 6.5.2.10. Standard deviation curve (0 to 1200 lpm) in bed (Kistler); and regression curve, with distributor rotation.

Also, the regression curve for bed *Kistler* sensor fit closer too the standard deviation curve from data, see Graphic 6.5.2.10.

It is presented now graphically the mean pressure in bed for all flow rates, see Graphic 6.5.2.11. :

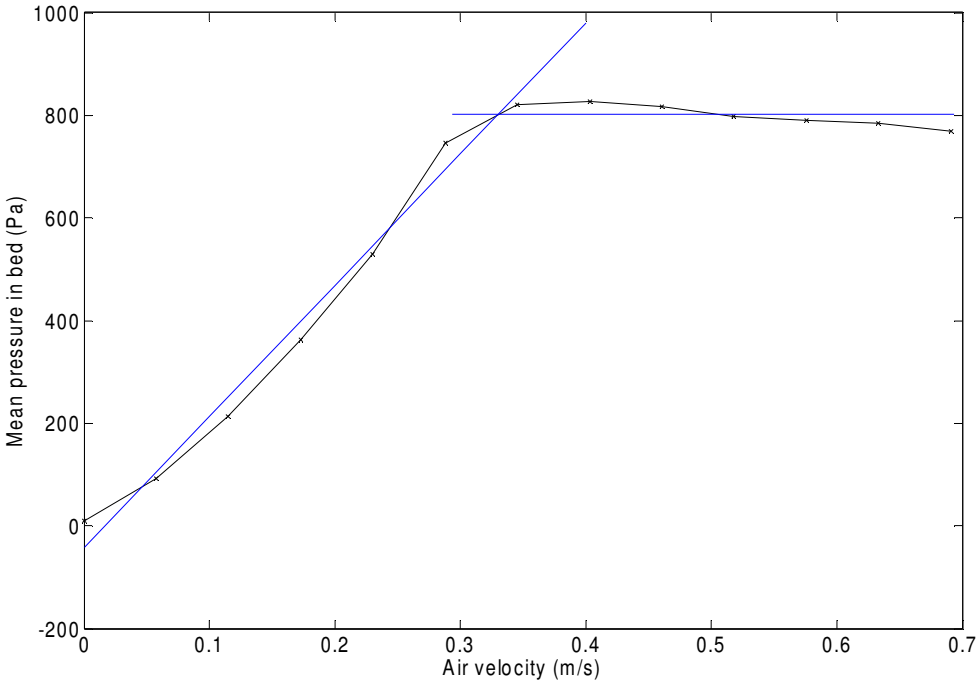

Graphic 6.5.2.11. Mean pressure curve for flow rates from 0 to 1200 lpm in bed; and regression curves for growing and constant pressure values with velocity, with distributor rotation.

As in case of no distributor rotation will be studied too to predict minimum fluidization velocity the mean pressure plot. Remember that pressure grow linearly until fluidization phenomena appears to maintain hydrostatic pressure constant.

One more time, in order to compare this method with deviation one, has been generate two regression curves, see Graphic 6.5.2.11., for linear growing pressure region and for constant pressure region. Intersection of both curves indicates minimum fluidization velocity.

In this case too, despite well fitness between the two different pressure region and its linear regression curves, this method has a greater uncertainty because of the difficulty to decided which pressure data sample belong to which fluid-dynamic region.

Results for the umf determination are summarized on Table 6.5.2.4. The table shows minimum fluidization velocity with the final values extract from *Matlab* both for plenum chamber, bed (with differential sensor and *Kistler* respectively) and the mean value of the three sensors. The u_{mf} calculated with the mean pressure values in bed and the mean is presented too.

	Plenum Chamber	***Bed (differential sensor)***	***Bed (Kistler)***	***Bed Mean Pressure***	***Mean umf Fluctuation Method***	***Mean umf with bed mean pressure value***
(m/s)	0,3389	0,2934	0,2979	0,33	0,3101	0,3151
lpm	588,7	509,7	517,5	573,3	538,6	547,3

Table 6.5.2.4. Values of u_{mf} for plenum chamber, bed (with differential sensor and Kistler respectively) and the mean value; u_{mf} calculated with the mean pressure values in bed and the total mean.

Results fit well between each other with the pressure deviation method purposed in *Puncochar et al* [20] (*86 %*). This results evidence finally too, that could be used separately any sensor as all of them arrive at the same minimum fluidization velocity, $u_{mf,}$ prediction.

Results from mean pressure deviation method are close to deviation ones but still at a certain distance (6 % greater than the mean u_{mf} calculated with the fluctuation method). Knowing that deviation method is a more accurate method for minimum fluidization velocity prediction, could be said that, without distributor rotation, mean pressure method predicts a greater u_{mf}.

Could be observed too, that fitness between data from no distributor rotation are closer each other for three sensors than with distributor rotation. Take into account that a rotational mechanism enter in the system with direct effects in bed performance.

The power spectrum analysis will be carried out, as said, with those flow rates already in fluidization regime. After applied the *FFT*, results obtained from *Matlab* are shown in Graphic 6.5.2.12., 6.5.2.13 and 6.5.2.14 for the three sensors without distributor rotation:

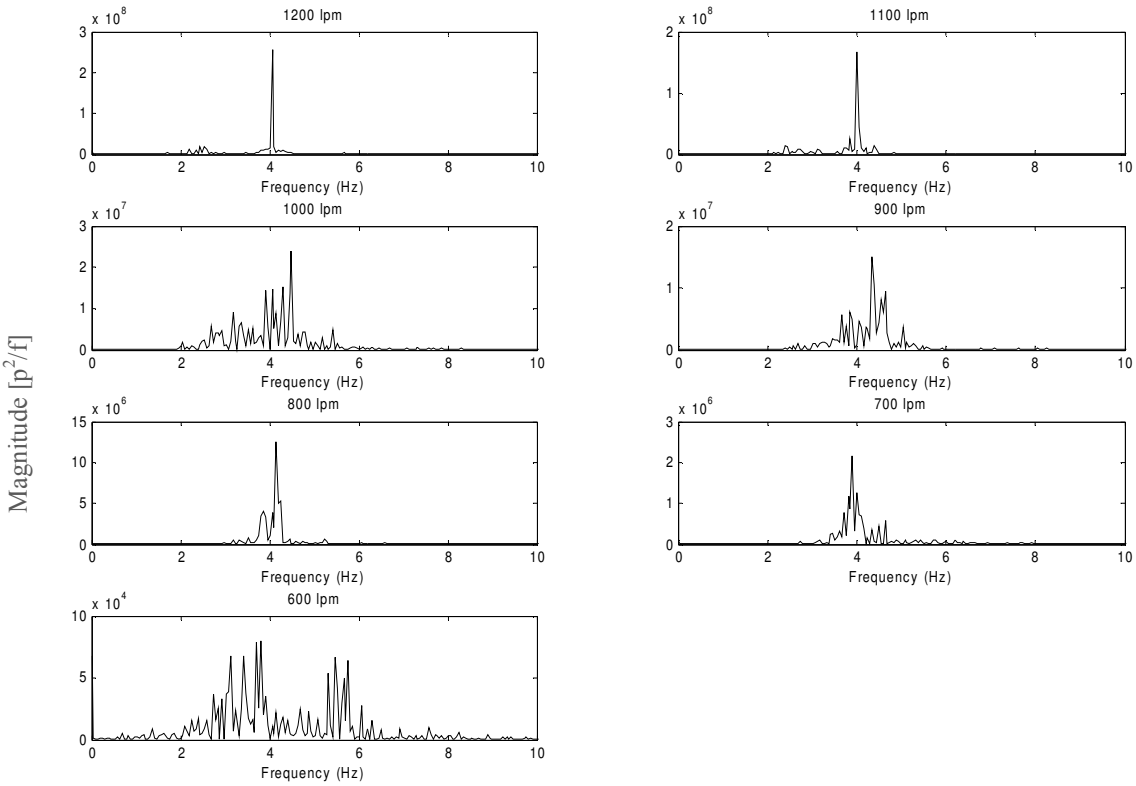

Graphic 6.5.2.12. Power spectra for flow rates from 600 to 1200 lpm in fluidization regime for plenum chamber with Kistler sensor, with distributor rotation.

Results from power spectrum analysis reveal, as *Johnson et al* [13] predicts, that in plenum chamber, with distributor rotation and under fluidization regime all the fundamental frequencies are between 1 to 5 *Hz*.

Because of clarity reasons for document, from now will be show power spectrum analysis in smaller size as all the plots has the same structure than Graphic 6.5.2.12.

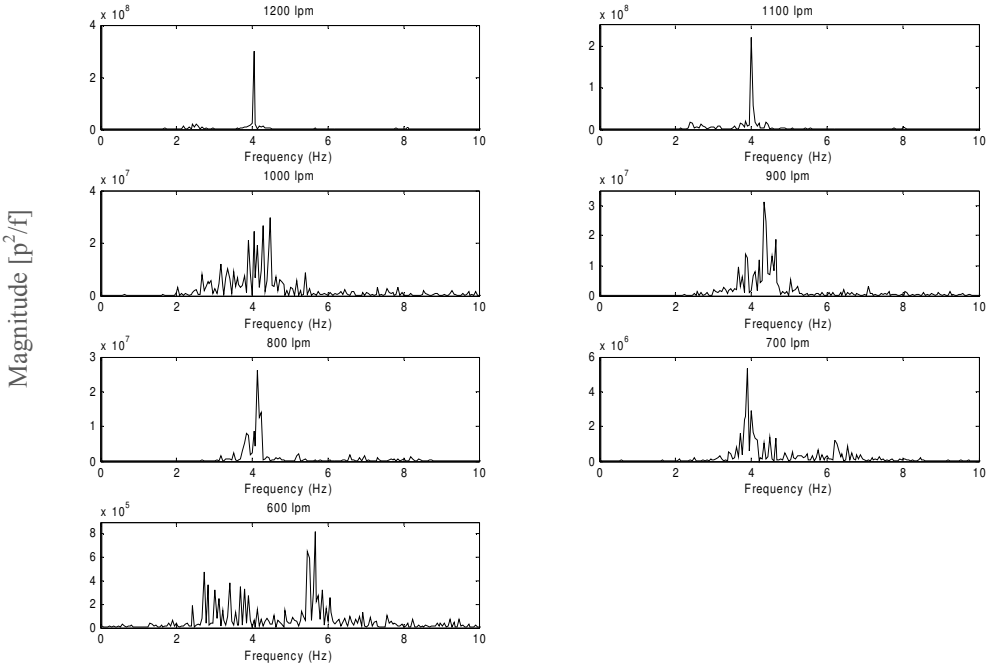

Graphic 6.5.2.13. Power spectra for (600 to 1200 lpm) for bed with differential pressure sensor, with distributor rotation.

Results from power spectrum analysis for bed (with differential sensor) reveal too that and under fluidization all the fundamental frequencies are between 1 to 5 *Hz*.

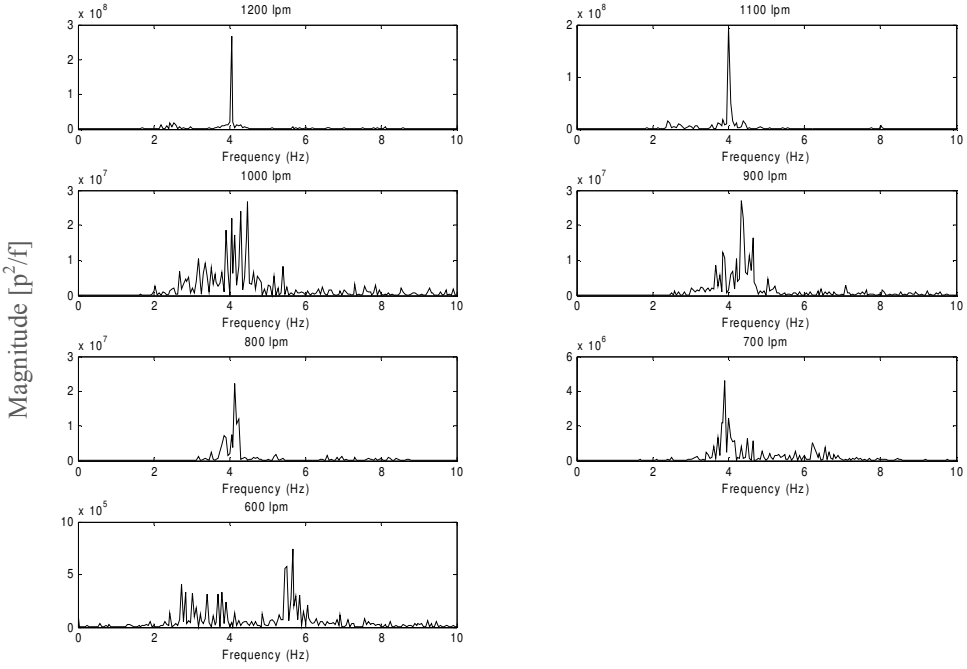

Graphic 6.5.2.14. Power spectra (600 to 1200 lpm) for bed with Kistler sensor, with distributor rotation.

Also, from power spectrum analysis for bed (with *Kistler* sensor) is revealed too that and under fluidization all the fundamental frequencies are between 1 to 5 *Hz*.

Results for the fundamental frequency are summarized on Table 6.5.2.5. The table shows fundamental frequencies with the final values extract from *Matlab* both for plenum chamber, bed (with differential sensor and *Kistler* respectively) and the mean value of the three sensors. Also it is presented the total mean fundamental frequency for plenum and bed.

	[lpm]	***600***	***700***	***800***	***900***	***1000***	***1100***	***1200***	***Mean Frequency [Hz]***
[Hz]	***Plenum Chamber***	*3,8*	*3,9*	*4,2*	*4,3*	*4,5*	*4,0*	*4,1*	***4,1***
	Bed (differential sensor)	*5,2*	*4,2*	*4,5*	*4,7*	*4,7*	*3,8*	*4,0*	***4,4***
	Bed (Kistler)	*5,2*	*4,2*	*4,5*	*4,7*	*4,7*	*3,8*	*4,0*	***4,4***
									4,3

Table 6.5.2.5. Values of fundamental frequencies for plenum chamber, bed (with differential sensor and Kistler respectively) the mean value respectively and the total mean fundamental frequency.

From the *Johnson et al* [13] power spectra plots obtained, the regime has been determine from which prototype evolve from fluidization to maximum flow rate experimented. All the final regimes for plenum chamber, bed (with differential sensor and *Kistler* respectively) for bed without distributor rotation are presented in Table 6.5.2.6.

The fluid-dynamic determination for each flow rate will be carried out by visual analysis by possible correlation of the prototype signal with any of the power spectrum *Johnson et al* [13] ones.

	Flow rate (lpm)	*Fluid-dynamic regime*
Plenum Chamber	600	Multiple Bubble regime
	700	Multiple Bubble regime
	800	Multiple Bubble regime
	900	Multiple Bubble regime
	1000	Multiple Bubble regime
	1100	Single Bubble regime
	1200	Single Bubble regime
Differential Sensor (bed)	600	Multiple Bubble regime
	700	Multiple Bubble regime
	800	Multiple Bubble regime
	900	Multiple Bubble regime
	1000	Multiple Bubble regime
	1100	Single Bubble regime
	1200	Single Bubble regime
Kistler (bed)	600	Multiple Bubble regime
	700	Multiple Bubble regime
	800	Multiple Bubble regime
	900	Multiple Bubble regime
	1000	Multiple Bubble regime
	1100	Single Bubble regime
	1200	Single Bubble regime

Table 6.5.1.6. Final regimes for plenum chamber, bed (with differential sensor and Kistler respectively) for all the flow rates in fluidization regime, with distributor rotation.

Result for the three sensors reveal that, when bed is already under fluidization, the fluid-dynamic regime seems to evolve from a multiple bubble regime to a single bubble regime as all these the regimes are expected to operate far from transport regimes.

6.5.3. BED ASPECT RATIO $^{3}/_{4}$

Is presented then the resolution of the curve $\sigma_p = A + Bu$ values, solved by linear regression, for those pressure fluctuations for a bed height of ***h_b = 14,4 cm* in the plenum chamber, and bed without distributor rotation** above σ_p =20, and the intersection with $\sigma_p = 0$, at u_{mf} velocity, see Graphic 6.5.3.1., Graphic 6.5.3.2., Graphic 6.5.3.3. , and the mean pressure values in bed, Graphic 6.5.3.4. :

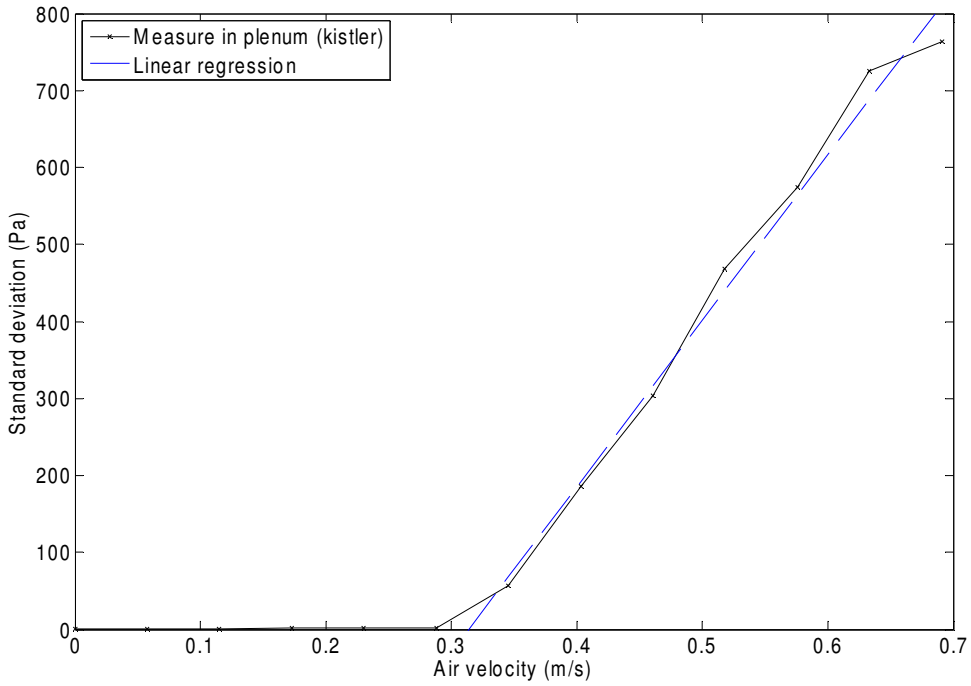

Graphic 6.5.3.1. Standard deviation curve (0 to 1200 lpm) in plenum chamber; and regression curve, without distributor rotation.

Could be observed how the regression curve fit closer to the standard deviation curve from data for plenum chamber. The regression curve has been constructed with those standard deviation values already in fluidization regime (above σ_p =20 *Pa*), see Graphic 6.5.3.1.

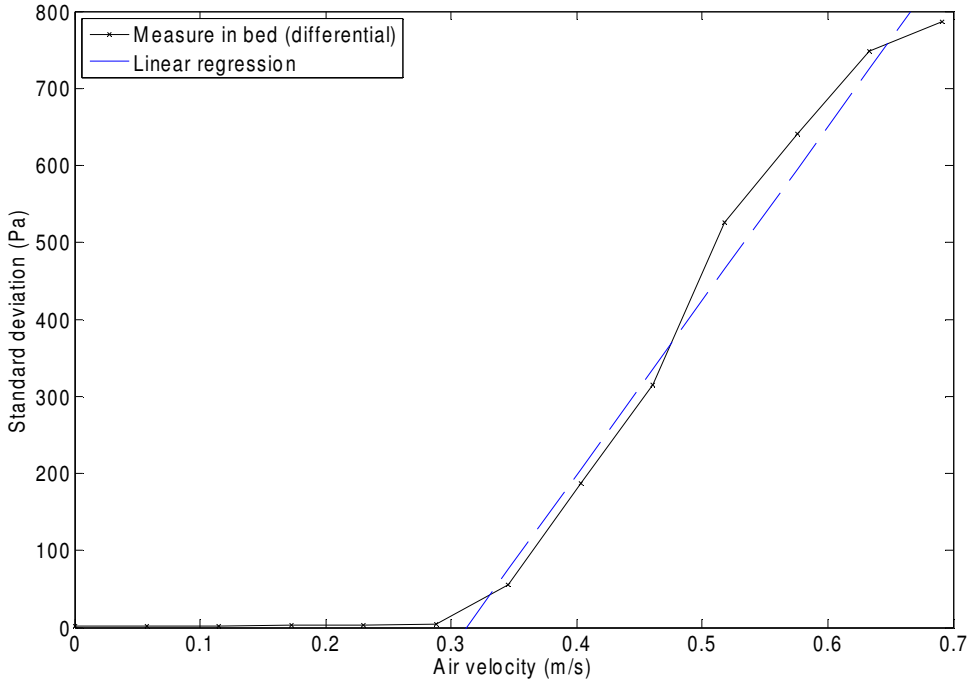

Graphic 6.5.3.2. Standard deviation curve (0 to 1200 lpm) in bed (differential); and regression curve, without distributor rotation.

Could be observed how the regression curve fit closer too the standard deviation curve from data for bed differential sensor, see Graphic 6.5.3.2.

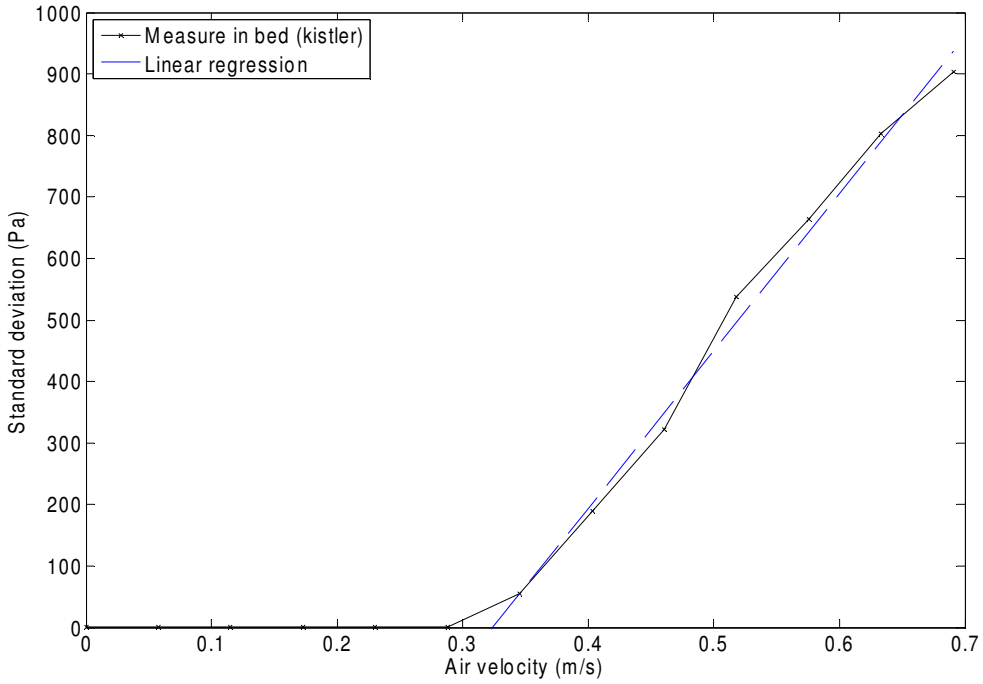

Graphic 6.5.3.3. Standard deviation curve (0 to 1200 lpm) in bed (Kistler); and regression curve, without distributor rotation.

Also, the regression curve for bed *Kistler* sensor fit closer too the standard deviation curve from data, see Graphic 6.5.3.3.

It is presented now graphically the mean pressure in bed for all flow rates, see Graphic 6.5.3.4. :

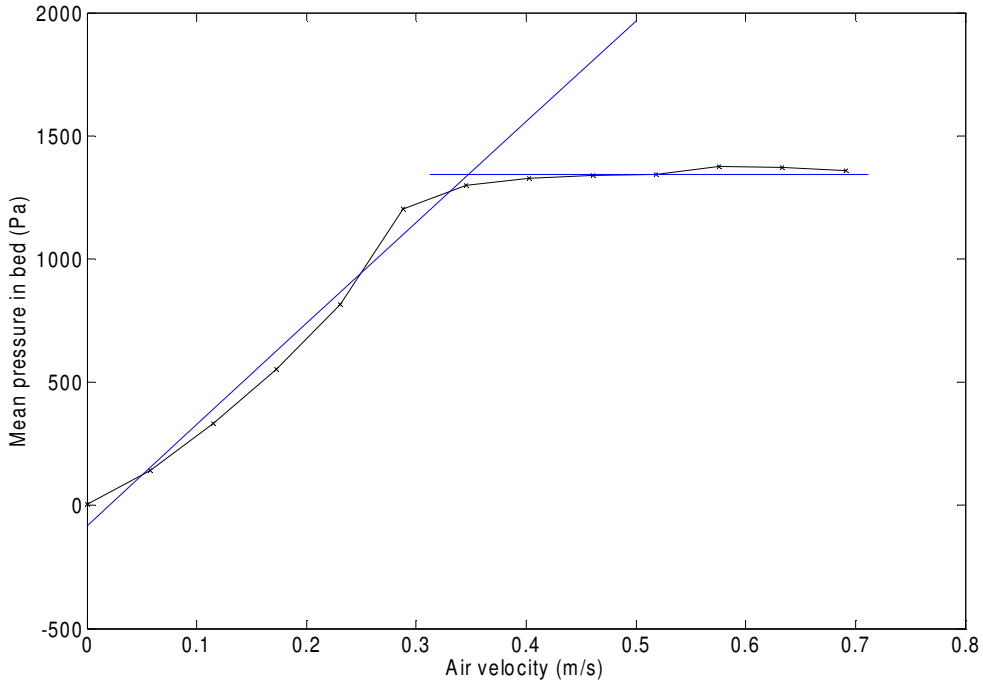

Graphic 6.5.3.4. Mean pressure curve for flow rates from 0 to 1200 lpm in bed; and regression curves for growing and constant pressure values with velocity, without distributor rotation.

As has been already said, one of the first methods to predict minimum fluidization velocity was the mean pressure plot. The pressure grows linearly until fluidization phenomena appear to maintain hydrostatic pressure constant.

In order to compare this method with deviation one, has been generate two regression curves, see Graphic 6.5.3.4., for linear growing pressure region and for constant pressure region. Intersection of both curves indicates minimum fluidization velocity.

Despite well fitness between the two different pressure region and its linear regression curves, this method has a greater uncertainty because of the difficulty to decided which pressure data sample belong to which fluid-dynamic region.

Results for the umf determination are summarized on Table 6.5.3.1. The table shows minimum fluidization velocity with the final values extract from *Matlab* both for plenum chamber, bed (with differential sensor and *Kistler* respectively) and the mean value of the three sensors. The u_{mf} calculated with the mean pressure values in bed and the mean is presented too.

	Plenum Chamber	***Bed (differential sensor)***	***Bed (Kistler)***	***Bed Mean Pressure***	***Mean umf Fluctuation Method***	***Mean umf with bed mean pressure value***
(m/s)	0,3138	0,3119	0,3236	0,3481	0,3164	0,3244
lpm	545,1	541,8	562,1	604,7	549,7	563,5

Table 6.5.3.1. Values of u_{mf} for plenum chamber, bed (with differential sensor and Kistler respectively) and the mean value; u_{mf} calculated with the mean pressure values in bed and the total mean.

Results fit well between each other with the pressure deviation method purposed in *Puncochar et al* [20] (*97 %*). This results evidence, this time too, that could be used separately any sensor as all of them arrive at the same minimum fluidization velocity, $u_{mf,}$ prediction.

Results from mean pressure deviation method are close to deviation ones but still at a certain distance (10 % greater than the mean u_{mf} calculated with the fluctuation method). Knowing that deviation method is a more accurate method for minimum fluidization velocity prediction, could be said that, with distributor rotation, mean pressure method predicts a greater u_{mf}.

The power spectrum analysis will be carried out, as said, with those flow rates already in fluidization regime. After applied the *FFT*, results obtained from *Matlab* are shown in Graphic 6.5.3.5., 6.5.3.6. and 6.5.3.7. for the three sensors without distributor rotation:

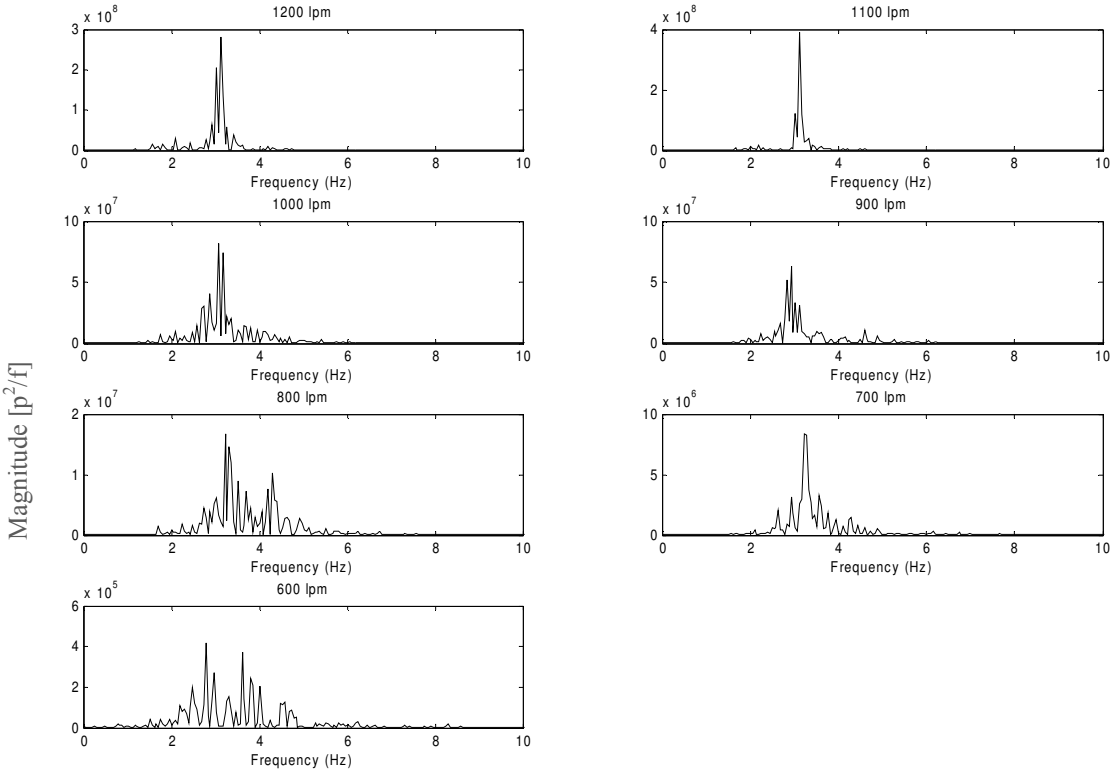

Graphic 6.5.3.5. Power spectra for flow rates from 600 to 1200 lpm in fluidization regime for plenum chamber with Kistler sensor, without distributor rotation.

Results from power spectrum analysis reveal, as *Johnson et al* [13] predicts, that in plenum chamber, without distributor rotation and under fluidization regime all the fundamental frequencies are between 1 to 5 *Hz*.

Because of clarity reasons for document, from now will be show power spectrum analysis in smaller size as all the plots has the same structure than Graphic 6.5.3.5.

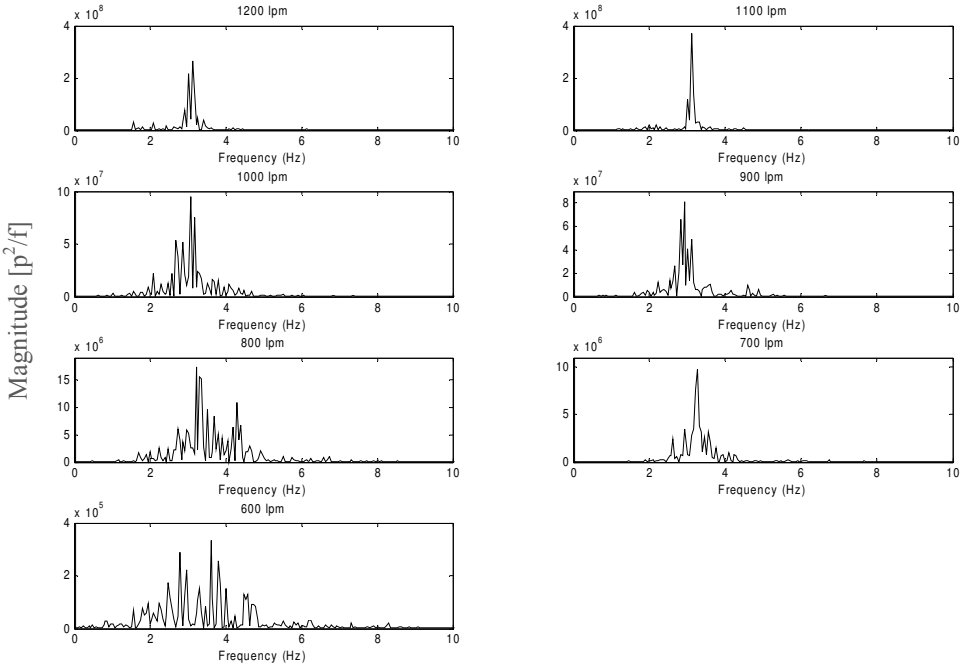

Graphic 6.5.3.6. Power spectra for (600 to 1200 lpm) for bed with differential pressure sensor, without distributor rotation .

Results from power spectrum analysis for bed (with differential sensor) reveal too that and under fluidization all the fundamental frequencies are between 1 to 5 *Hz*.

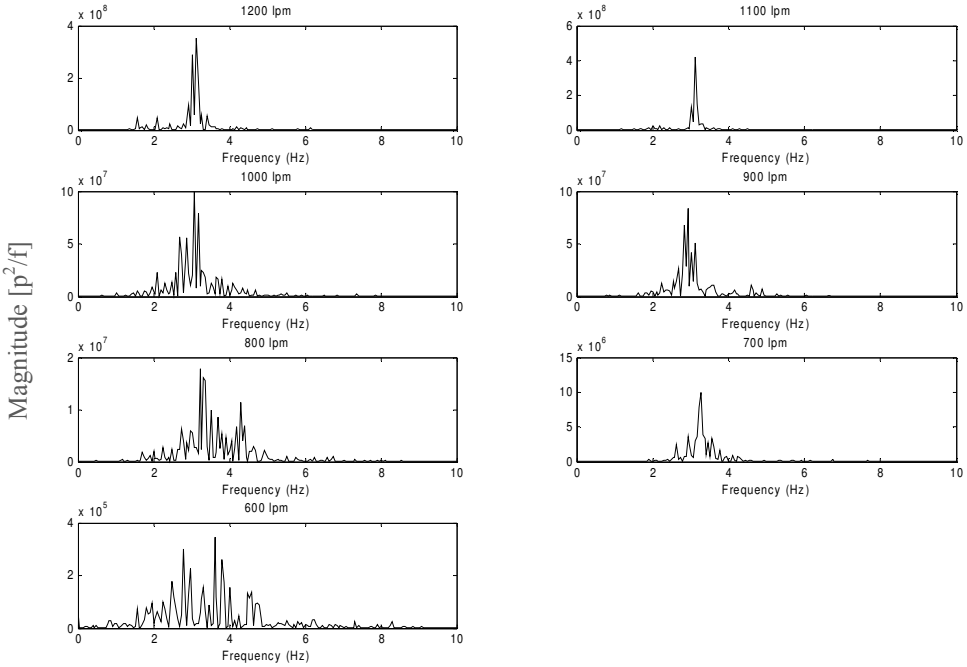

Graphic 6.5.3.7. Power spectra (600 to 1200 lpm) for bed with Kistler sensor, without distributor rotation.

Also, from power spectrum analysis for bed (with *Kistler* sensor) is revealed too that and under fluidization all the fundamental frequencies are between 1 to 5 *Hz*.

Results for the fundamental frequency are summarized on Table 6.5.3.2. The table shows fundamental frequencies with the final values extract from *Matlab* both for plenum chamber, bed (with differential sensor and *Kistler* respectively) and the mean value of the three sensors. Also it is presented the total mean fundamental frequency for plenum and bed.

	[lpm]	***600***	***700***	***800***	***900***	***1000***	***1100***	***1200***	***Mean Frequency [Hz]***
[Hz]	***Plenum Chamber***	*2,8*	*3,2*	*3,2*	*2,9*	*3,1*	*3,1*	*3,1*	***3,1***
	Bed (differential sensor)	*3,6*	*3,3*	*3,2*	*2,9*	*3,1*	*3,1*	*3,1*	***3,2***
	Bed (Kistler)	*3,6*	*3,3*	*3,2*	*2,9*	*3,1*	*3,1*	*3,1*	***3,2***
									3,1

Table 6.5.3.2. Values of fundamental frequencies for plenum chamber, bed (with differential sensor and Kistler respectively) the mean value respectively and the total mean fundamental frequency.

From the *Johnson et al* [13] power spectra plots obtained, the regime has been determine from which prototype evolve from fluidization to maximum flow rate experimented. All the final regimes for plenum chamber, bed (with differential sensor and *Kistler* respectively) for bed without distributor rotation are presented in Table 6.5.3.3.

The fluid-dynamic determination for each flow rate will be carried out by visual analysis by possible correlation of the prototype signal with any of the power spectrum *Johnson et al* [13] ones.

	Flow rate (lpm)	*Fluid-dynamic regime*
Plenum Chamber	600	Multiple Bubble regime
	700	Multiple Bubble regime
	800	Multiple Bubble regime
	900	Multiple Bubble regime
	1000	Multiple Bubble regime
	1100	Single Bubble regime
	1200	Single Bubble regime
Differential Sensor (bed)	600	Multiple Bubble regime
	700	Multiple Bubble regime
	800	Multiple Bubble regime
	900	Multiple Bubble regime
	1000	Multiple Bubble regime
	1100	Single Bubble regime
	1200	Single Bubble regime
Kistler (bed)	600	Multiple Bubble regime
	700	Multiple Bubble regime
	800	Multiple Bubble regime
	900	Multiple Bubble regime
	1000	Multiple Bubble regime
	1100	Single Bubble regime
	1200	Single Bubble regime

Table 6.5.3.3. Final regimes for plenum chamber, bed (with differential sensor and Kistler respectively) for all the flow rates in fluidization regime, without distributor rotation.

Result for the three sensors reveal that, when bed is already under fluidization, the fluid-dynamic regime seems to evolve from a multiple bubble regime to a single bubble regime as all these the regimes are expected to operate far from transport regimes.

The graphic determination of u_{mf} *with* the curve $\sigma_p = A + Bu$ values, fitted by linear regression, for those pressure fluctuations for a bed height of **h_b = 14,4 cm in the plenum and bed with distributor rotation** above σ_p =20 *Pa,* and the intersection with σ_p = 0 *Pa*, at u_{mf} velocity, see Graphic 6.5.3.8., Graphic 6.5.3.9., Graphic 6.5.3.10. , and the mean pressure values in bed, Graphic 6.5.3.11. :

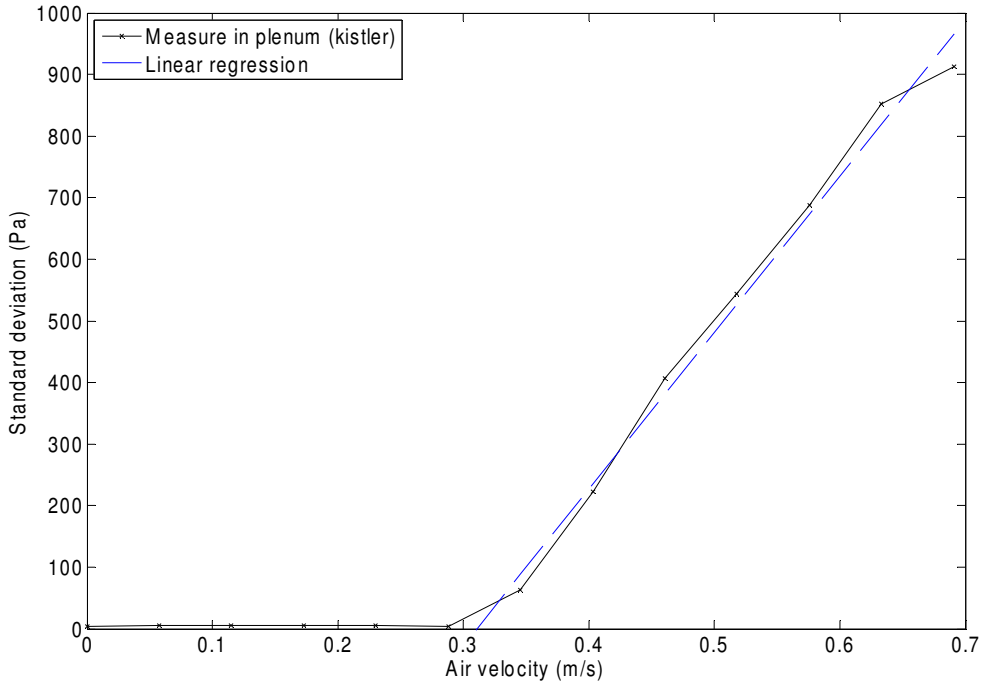

Graphic 6.5.3.8. Standard deviation curve (0 to 1200 lpm) in plenum chamber; and regression curve, with distributor rotation.

Could be observed how the regression curve fit closer to the standard deviation curve from data for plenum chamber. The regression curve has been constructed with those standard deviation values already in fluidization regime (above σ_p =20 *Pa*), see Graphic 6.5.3.8.

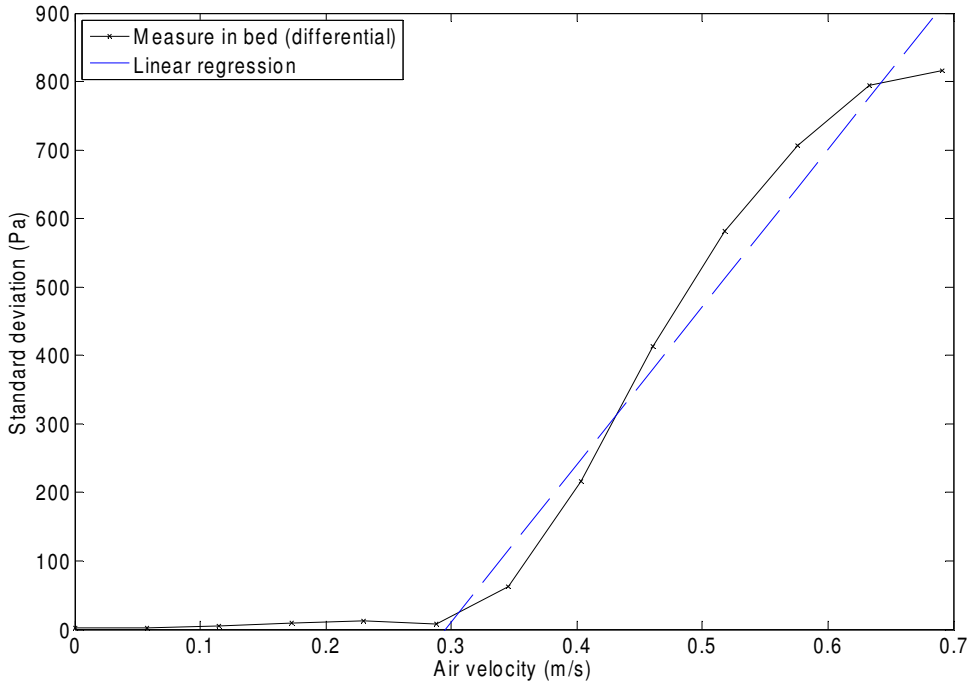

Graphic 6.5.3.9. Standard deviation curve (0 to 1200 lpm) in bed (differential); and regression curve, with distributor rotation.

Could be observed how the regression curve fit closer too the standard deviation curve from data for bed differential sensor, see Graphic 6.5.3.9.

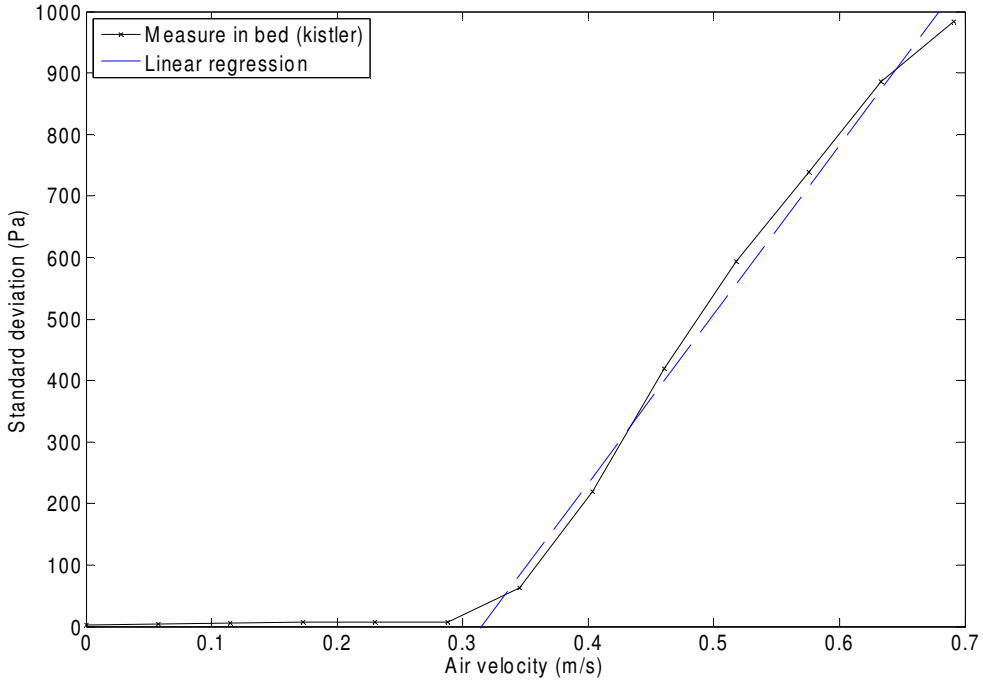

Graphic 6.5.3.10. Standard deviation curve (0 to 1200 lpm) in bed (Kistler); and regression curve, with distributor rotation.

Also, the regression curve for bed *Kistler* sensor fit closer too the standard deviation curve from data, see Graphic 6.5.3.10.

It is presented now graphically the mean pressure in bed for all flow rates, see Graphic 6.5.3.11. :

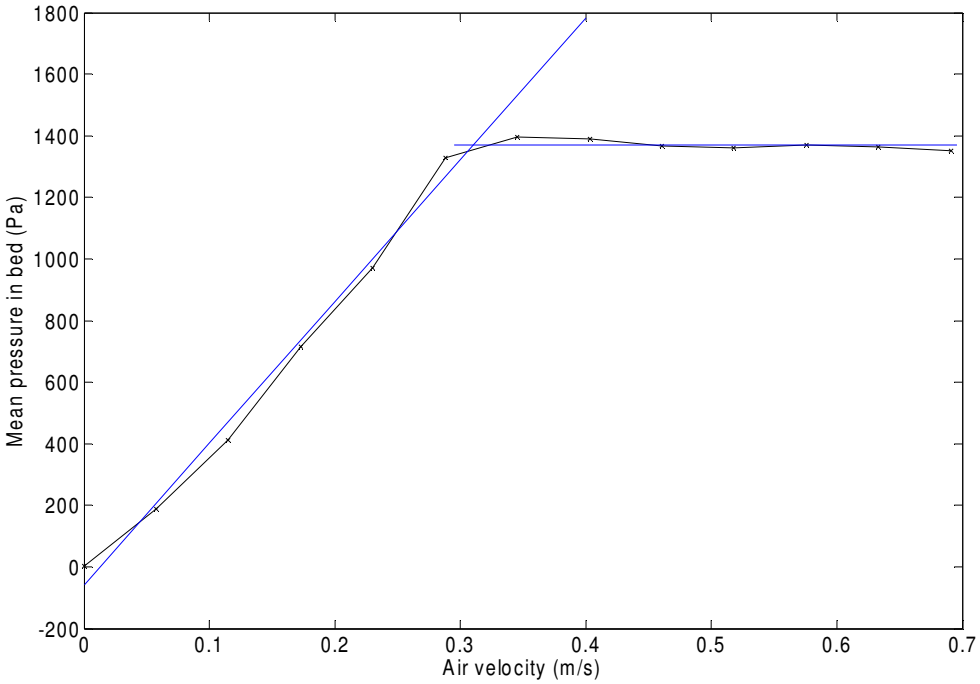

Graphic 6.5.3.11. Mean pressure curve for flow rates from 0 to 1200 lpm in bed; and regression curves for growing and constant pressure values with velocity, with distributor rotation.

As in case of no distributor rotation will be studied too to predict minimum fluidization velocity the mean pressure plot. Remember that pressure grow linearly until fluidization phenomena appears to maintain hydrostatic pressure constant.

One more time, in order to compare this method with deviation one, has been generate two regression curves, see Graphic 6.5.3.11., for linear growing pressure region and for constant pressure region. Intersection of both curves indicates minimum fluidization velocity.

In this case too, despite well fitness between the two different pressure region and its linear regression curves, this method has a greater uncertainty because of the difficulty to decided which pressure data sample belong to which fluid-dynamic region.

Results for the umf determination are summarized on Table 6.5.3.4. The table shows minimum fluidization velocity with the final values extract from *Matlab* both for plenum chamber, bed (with differential sensor and *Kistler* respectively) and the mean value of the three sensors. The u_{mf} calculated with the mean pressure values in bed and the mean is presented too.

	Plenum Chamber	***Bed (differential sensor)***	***Bed (Kistler)***	***Bed Mean Pressure***	***Mean umf Fluctuation Method***	***Mean umf with bed mean pressure value***
(m/s)	0,3104	0,2953	0,3147	0,3109	0,3068	0,3078
lpm	539,2	513,0	546,7	540,1	533,0	534,7

Table 6.5.3.4. Values of u_{mf} for plenum chamber, bed (with differential sensor and Kistler respectively) and the mean value; u_{mf} calculated with the mean pressure values in bed and the total mean.

Results fit well between each other with the pressure deviation method purposed in *Puncochar et al* [20] (*94 %*). This results evidence finally too, that could be used separately any sensor as all of them arrive at the same minimum fluidization velocity, $u_{mf,}$ prediction.

Results from mean pressure deviation method are so close to deviation ones (only *1 %* greater than the mean u_{mf} calculated with the fluctuation method). Knowing that deviation method is a more accurate method for minimum fluidization velocity prediction, could be said that, without distributor rotation, mean pressure method predicts a greater u_{mf}.

Could be observed too, that fitness between data from no distributor rotation are closer each other for three sensors than with distributor rotation. Take into account that a rotational mechanism enter in the system with direct effects in bed performance.

The power spectrum analysis will be carried out, as said, with those flow rates already in fluidization regime. After applied the *FFT*, results obtained from *Matlab* are shown in Graphic 6.5.3.12., 6.5.3.13 and 6.5.3.14 for the three sensors without distributor rotation:

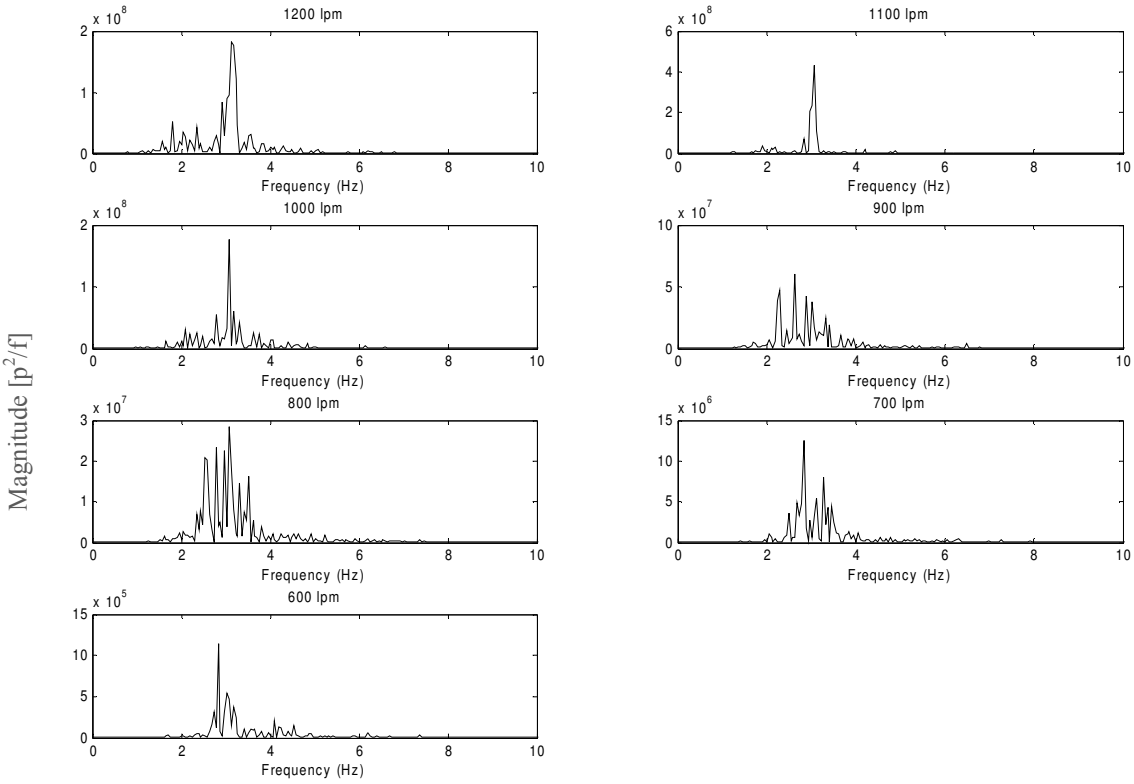

Graphic 6.5.3.12. Power spectra for flow rates from 600 to 1200 lpm in fluidization regime for plenum chamber with Kistler sensor, with distributor rotation .

Results from power spectrum analysis reveal, as *Johnson et al* [13] predicts, that in plenum chamber, with distributor rotation and under fluidization regime all the fundamental frequencies are between 1 to 5 *Hz*.

Because of clarity reasons for document, from now will be show power spectrum analysis in smaller size as all the plots has the same structure than Graphic 6.5.3.12.

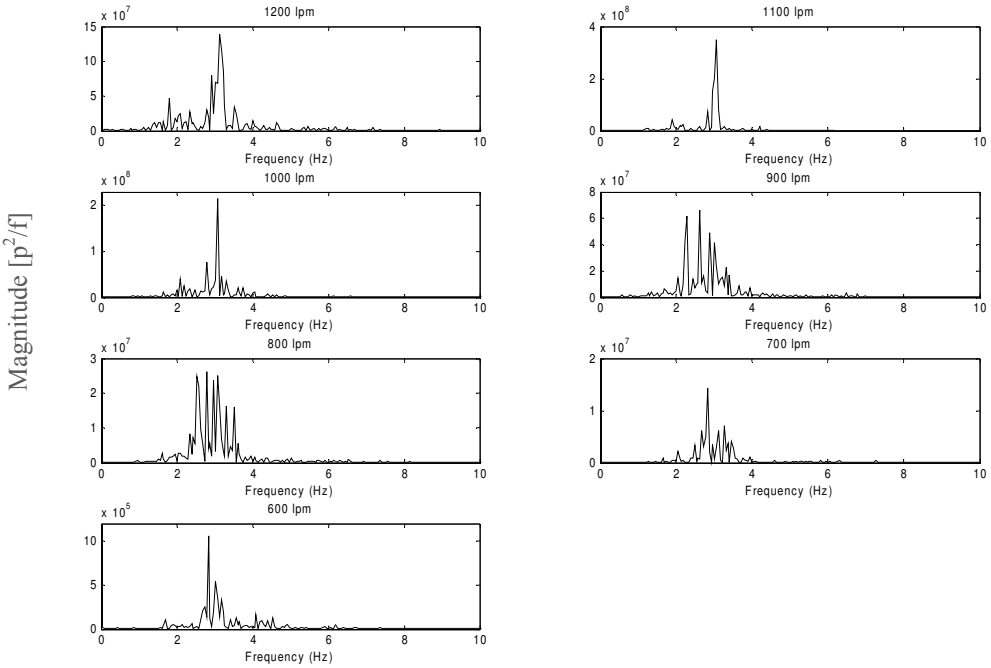

Graphic 6.5.3.13. Power spectra for (600 to 1200 lpm) for bed with differential pressure sensor, with distributor rotation .

Results from power spectrum analysis for bed (with differential sensor) reveal too that and under fluidization all the fundamental frequencies are between 1 to 5 *Hz*.

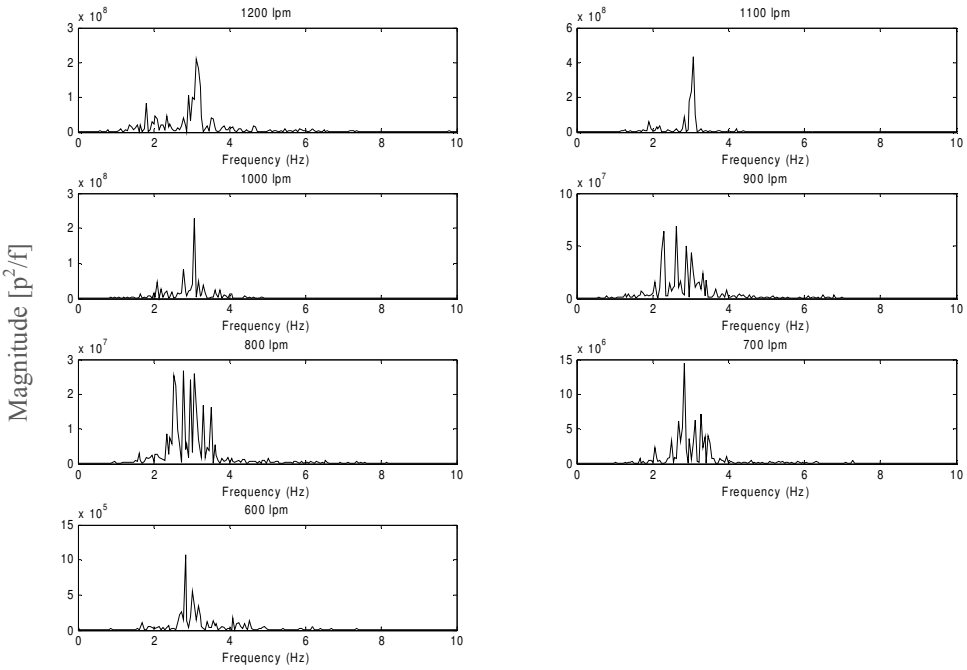

Graphic 6.5.3.14. Power spectra (600 to 1200 lpm) for bed with Kistler sensor, with distributor rotation.

Also, from power spectrum analysis for bed (with *Kistler* sensor) is revealed too that and under fluidization all the fundamental frequencies are between 1 to 5 *Hz*.

Results for the fundamental frequency are summarized on Table 6.5.3.5. The table shows fundamental frequencies with the final values extract from *Matlab* both for plenum chamber, bed (with differential sensor and *Kistler* respectively) and the mean value of the three sensors. Also it is presented the total mean fundamental frequency for plenum and bed.

	[lpm]	***600***	***700***	***800***	***900***	***1000***	***1100***	***1200***	***Mean Frequency [Hz]***
[Hz]	***Plenum Chamber***	*2,8*	*2,8*	*3,1*	*2,6*	*3,1*	*3,1*	*3,1*	***2,9***
	Bed (differential sensor)	*2,8*	*2,8*	*2,8*	*2,6*	*3,1*	*3,1*	*3,1*	***2,9***
	Bed (Kistler)	*2,8*	*2,8*	*2,8*	*2,6*	*3,1*	*3,1*	*3,1*	***2,9***
									2,9

Table 6.5.3.5. Values of fundamental frequencies for plenum chamber, bed (with differential sensor and Kistler respectively) the mean value respectively and the total mean fundamental frequency.

From the *Johnson et al* [13] power spectra plots obtained, the regime has been determine from which prototype evolve from fluidization to maximum flow rate experimented. All the final regimes for plenum chamber, bed (with differential sensor and *Kistler* respectively) for bed without distributor rotation are presented in Table 6.5.3.6.

The fluid-dynamic determination for each flow rate will be carried out by visual analysis by possible correlation of the prototype signal with any of the power spectrum *Johnson et al* [13] ones.

	Flow rate (lpm)	*Fluid-dynamic regime*
Plenum Chamber	600	Multiple Bubble regime
	700	Multiple Bubble regime
	800	Multiple Bubble regime
	900	Multiple Bubble regime
	1000	Multiple Bubble regime
	1100	Single Bubble regime
	1200	Single Bubble regime
Differential Sensor (bed)	600	Multiple Bubble regime
	700	Multiple Bubble regime
	800	Multiple Bubble regime
	900	Multiple Bubble regime
	1000	Multiple Bubble regime
	1100	Single Bubble regime
	1200	Single Bubble regime
Kistler (bed)	600	Multiple Bubble regime
	700	Multiple Bubble regime
	800	Multiple Bubble regime
	900	Multiple Bubble regime
	1000	Multiple Bubble regime
	1100	Single Bubble regime
	1200	Single Bubble regime

Table 6.5.3.6. Final regimes for plenum chamber, bed (with differential sensor and Kistler respectively) for all the flow rates in fluidization regime, with distributor rotation.

Result for the three sensors reveal that, when bed is already under fluidization, the fluid-dynamic regime seems to evolve from a multiple bubble regime to a single bubble regime as all these the regimes are expected to operate far from transport regimes.

6.6. RESULTS SUMMARY

In order to summarize all the information of the experiments, next section will compare results from different test expecting to find new conclusions.

6.6.1. FLOW VELOCITY

Firstly, will be carried out the comparison between all the minimum fluidization velocities predicted with the different sensors and bed dispositions. Next graphic, Graphic 6.6.1.1., shows the values obtain with different sensors for the bed heights of *9,6 cm* and *14,4 cm* without distributor rotation.

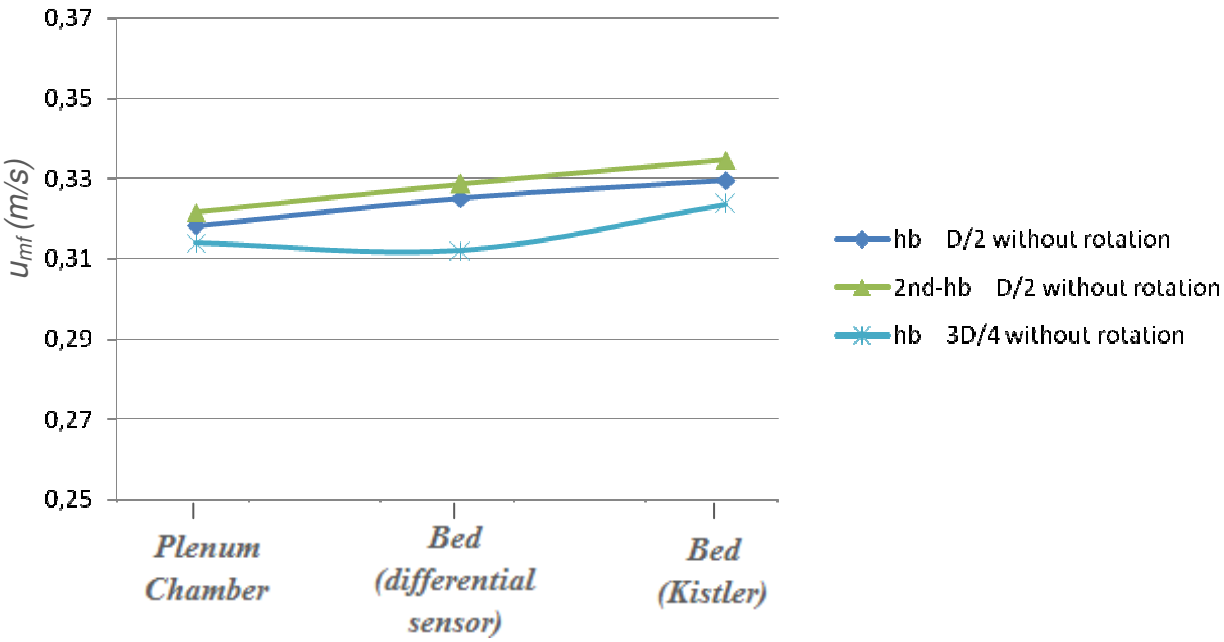

Graphic 6.6.1.1. u_{mf} for the three different sensors for bed heights of 9,6 cm and 14,4 cm without distributor rotation.

Could be observed how u_{mf} takes the lowest values in the plenum chamber with the *Kistler* sensor and the highest in bed with the *Kistler* sensor too. Exist a very good fitness between the ones for first and for the second series of experiments at $h_b = 9,6\ cm$ $(h_b = D/2)$ so in plenum chamber so in bed. Although exist a difference between the experiments at $h_b = 9,6\ cm$ and at $h_b = 14,4\ cm$, department team has associated this

differences with many variables that come into play so difficult to keep under control (ambient temperature, quiet in the room, same equipment disposition, etc.) as this deviation appears without any relation between each others.

Same study will carried out but with distribution rotation, see Graphic 6.6.1.2. :

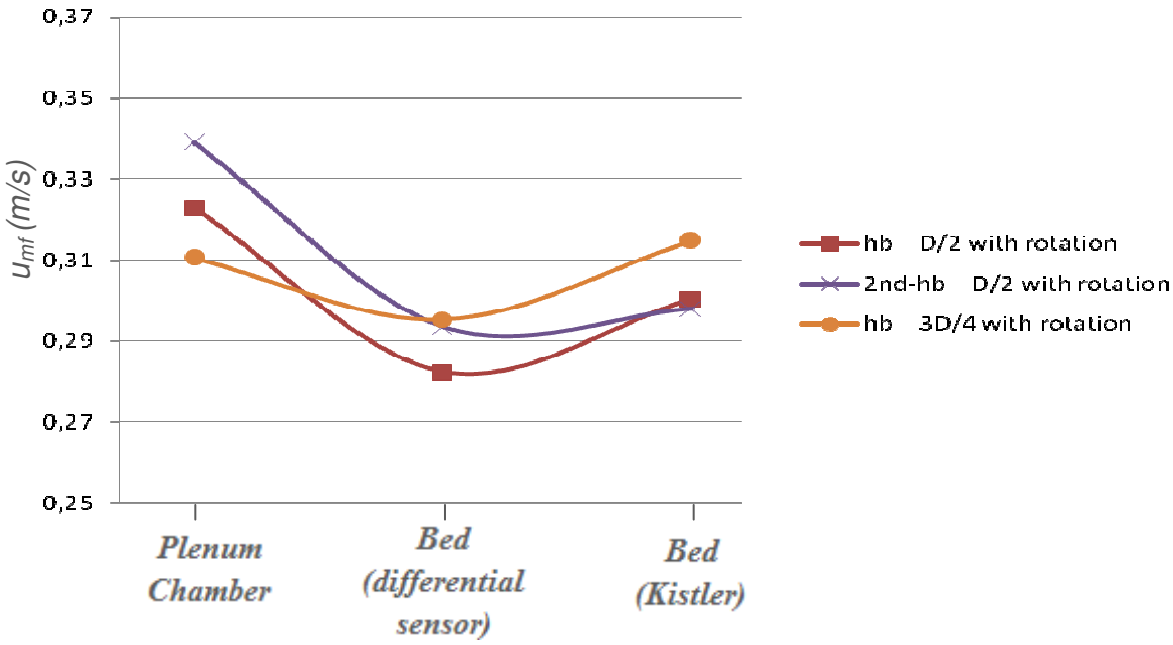

Graphic 6.6.1.2. u_{mf} for the three different sensors for bed heights of 9,6 cm and 14,4 cm with distributor rotation.

Despite from analysis for u_{mf} without distributor rotation, now could be observed how u_{mf} takes the lowest values in the bed with the differential sensor and the highest in the plenum chamber with the *Kistler* sensor. Exist a god fitness too for first and for the second series of experiments at $h_b = 9,6\ cm$ ($h_b = D/2$) so in plenum chamber so in bed. Differences with between experiments at $h_b = 9,6\ cm$ and at $h_b = 14,4\ cm$ comes in this case too because of the natural changes of variables not under control on the previous performance of the experiments.

In addition, could be notice that the mean u_{mf} obtain with rotation is lower than the one without rotation (without rotation: *0,32 m/s* ; with rotation: *0,30 m/s*), see Table 6.6.1.1. and 6.6.1.2. This fact could be explained because of the distributor effect in the sustentation flux. Distributor rotation impress a swirl to the gas flow that makes air

bubbles distribute more homogenize through the bed. In this situation preferred way zones for air circulation are increased, avoiding dead zones under no fluidization, see Figure 6.6.1.1., and letting, then, fluidization start at lower velocities.

	Total Means -without rotation-					
	Plenum Chamber	***Bed (differential sensor)***	***Bed (Kistler)***	***Bed Mean Pressure***	***Mean umf Fluctuation Method***	***Mean umf with bed mean pressure value***
(m/s)	0,3178	0,3219	0,3292	0,3489	**0,3230**	0,3295
lpm	552,1	559,1	571,9	606,2	**561,0**	572,3

Table 6.6.1.1. Total mean minimum fluidization velocities for different sensors without distributor rotation.

	Total Means -with rotation-					
	Plenum Chamber	***Bed (differential sensor)***	***Bed (Kistler)***	***Bed Mean Pressure***	***Mean umf Fluctuation Method***	***Mean umf with bed mean pressure value***
(m/s)	0,3240	0,2903	0,3043	0,3283	**0,3062**	0,3117
lpm	562,8	504,4	528,6	570,4	**531,9**	541,5

Table 6.6.1.2. Total mean minimum fluidization velocities for different sensors with distributor rotation.

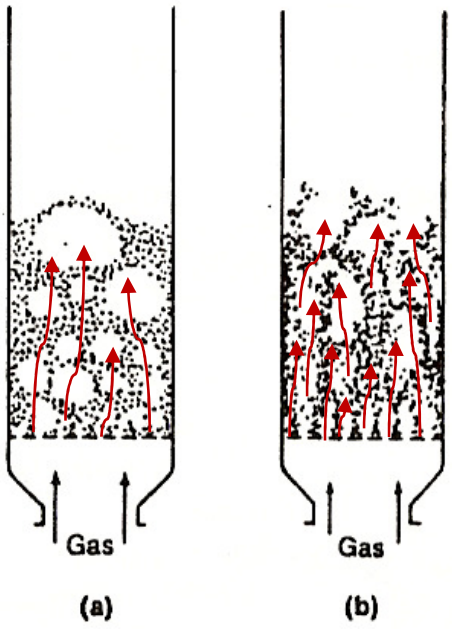

Figure 6.6.1.1. Air distribution in bed without distributor rotation (a) and with distributor rotation (b)..

Gas bubbles rise, despite reactor without distributor rotation (a), along more numerous paths (b) because of the spin that has been printed by distributor swirl in the air before entering the bed.

Finally, the mean values for the three sensors and the mean values for u_{mf} with and without distributor rotation could be seen in the next table, see Table 6.1.1.1. :

	Total Means					
	Plenum Chamber	***Bed (differential sensor)***	***Bed (Kistler)***	***Bed Mean Pressure***	***Mean umf Fluctuation Method***	***Mean umf with bed mean pressure value***
(m/s)	0,3209	0,3061	0,3168	0,3386	**0,3146**	0,3206
lpm	557,5	531,7	550,3	588,3	**546,5**	556,9

Table 6.6.1.3. Total mean minimum fluidization velocities for different sensors for distributor rotation and not.

One time the u_{mf} means are already obtained, in order to compare definitely the three of sensors behavior with the total mean minimum fluidization velocity (so with distributor rotation, so without distributor rotation) could be observe that the u_{mf} velocity obtain with the *Kistlers* is little bit higher than with the differential sensor.

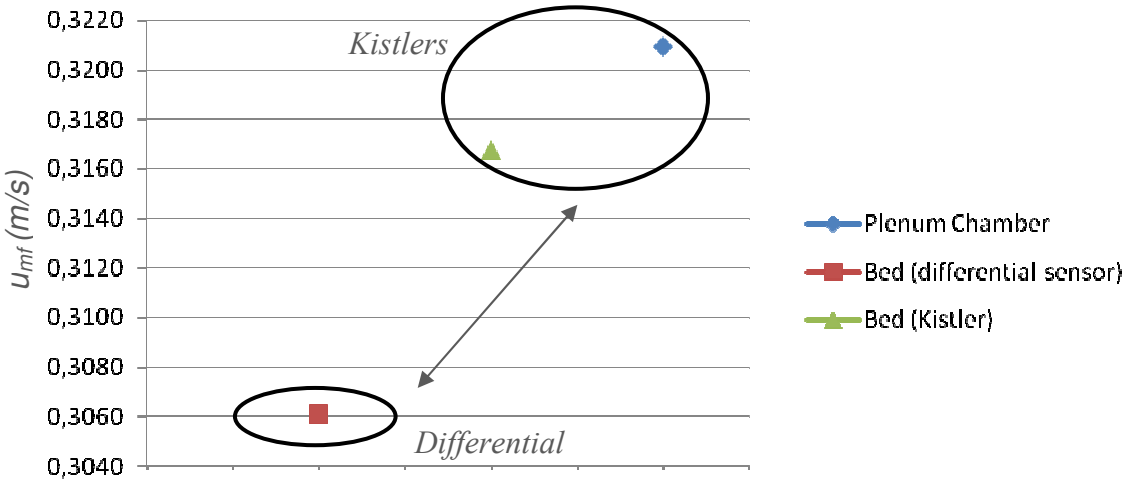

Graphic 6.6.1.3. Total mean fluidization velocity calculated by the three sensors, the two Kistlers and the differential one.

The difference between the total u_{mf} mean calculated with the *Kistlers* and with the differential is no higher than a *4 %*, deviation perfectly assumable as, apart form other uncontrolled variables, are two measures systems with a total different nature of technology that interpret pressure data by different ways.

6.6.2. FREQUENCY DOMAIN

For the frequency spectra data summary, will be observe the mean values of the characteristics frequency of each sensor for the different bed heights of *9,6 cm* and *14,4 cm* without distributor rotation, see Graphic 6.6.2.1. The values represented the characteristic frequencies for all velocities.

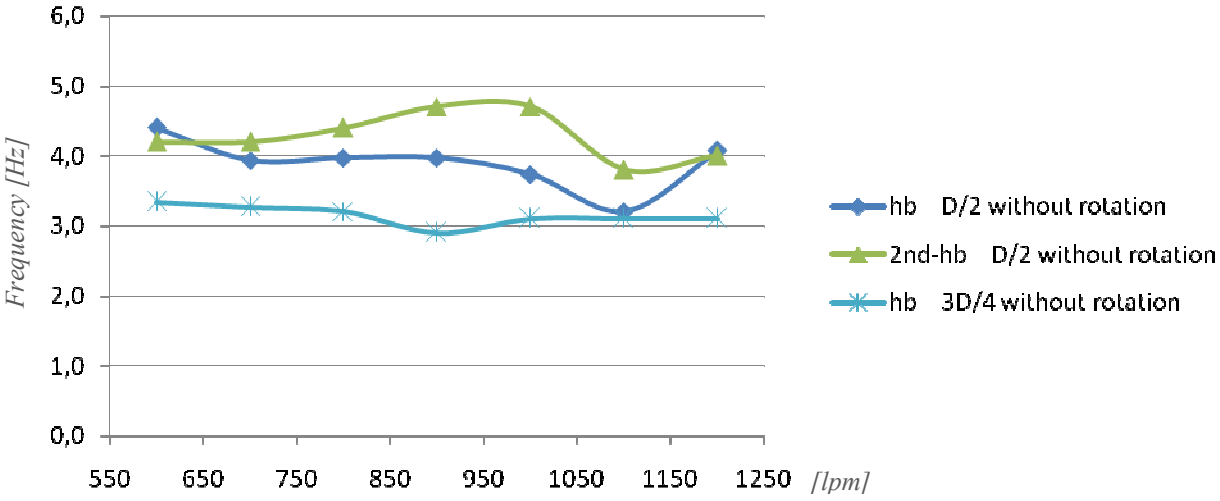

Graphic 6.6.2.1.Characteristic frequency for the three different sensors for bed heights of 9,6 cm and 14,4 cm without distributor rotation.

Could be observed how characteristic frequency takes the lowest values at *14,4 cm* bed height ($^{3D}/_{4}$) and the highest with the second series of experiments for a bed height of *9,6 cm* ($^{D}/_{2}$). Mean values for this two different tests differ a *28 %* for its characteristic frequencies, see Table 6.6.2.1. :

	[lpm]	*600*	*700*	*800*	*900*	*1000*	*1100*	*1200*	*Mean Frequency [Hz]*
[Hz]	***hb = D/2***	*4,4*	*3,9*	*4,0*	*4,0*	*3,7*	*3,2*	*4,1*	***3,9***
	2nd-hb = D/2	*4,2*	*4,2*	*4,4*	*4,7*	*4,7*	*3,8*	*4,0*	***4,3***
	hb = 3D/4	*3,3*	*3,3*	*3,2*	*2,9*	*3,1*	*3,1*	*3,1*	***3,1***
	Mean	***4,0***	***3,8***	***3,9***	***3,9***	***3,8***	***3,4***	***3,7***	***3,8***

Table 6.6.2.1.Characteristic frequency for the three different sensors for bed heights of 9,6 cm and 14,4 cm without distributor rotation.

Same study will carried out but with distribution rotation, see Graphic 6.6.2.2. :

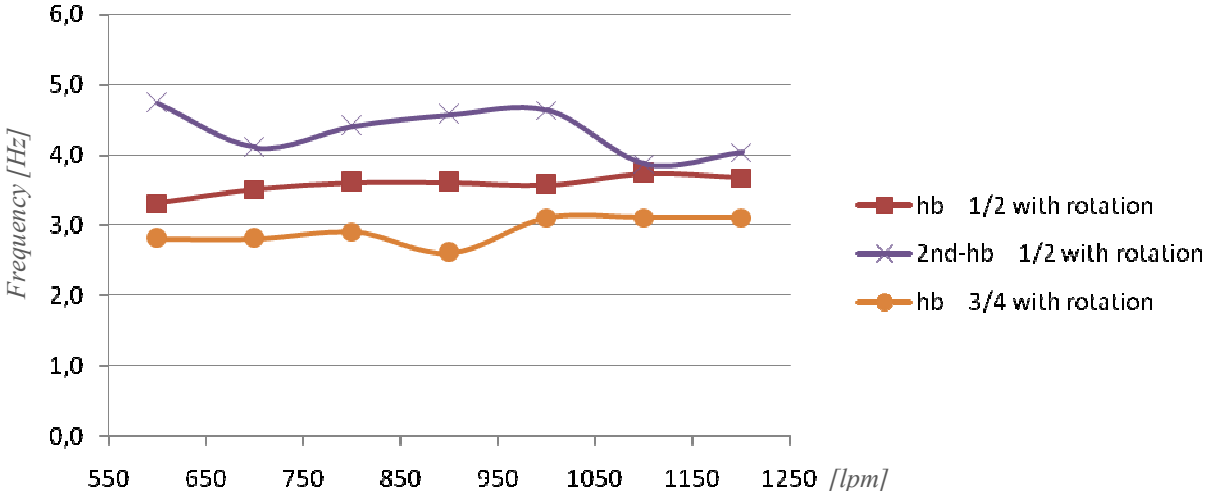

Graphic 6.6.2.2.Characteristic frequency for the three different sensors for bed heights of 9,6 cm and 14,4 cm with distributor rotation.

Could be observed too, how characteristic frequency takes the lowest values at *14,4 cm* bed height ($^{3D}/_{4}$) and the highest with the second series of experiments for a bed height of *9,6 cm* ($^{D}/_{2}$). Mean values for this two different tests differ a 33 *%* for its characteristic frequencies, see Table 6.6.2.1. :

	[lpm]	*600*	*700*	*800*	*900*	*1000*	*1100*	*1200*	*Mean Frequency [Hz]*
[Hz]	*hb = D/2*	*3,3*	*3,5*	*3,6*	*3,6*	*3,6*	*3,7*	*3,7*	***3,6***
	2nd-hb = D/2	*4,7*	*4,1*	*4,4*	*4,6*	*4,6*	*3,9*	*4,0*	***4,3***
	hb = 3D/4	*2,8*	*2,8*	*2,9*	*2,6*	*3,1*	*3,1*	*3,1*	***2,9***
	Mean	***3,6***	***3,5***	***3,6***	***3,6***	***3,8***	***3,6***	***3,6***	***3,6***

Table 6.6.2.2.Characteristic frequency for the three different sensors for bed heights of 9,6 cm and 14,4 cm with distributor rotation.

Both analysis reveal that at *14,4 cm* height ($^{3D}/_{4}$) the frequencies are lower than at *9,6 cm* ($^{D}/_{2}$). This attenuation, although all tests are under the theoretical limits from *1-5 Hz* [13], could be a result of the higher mass to pass trough for the same air flow.

Same air pressure at plenum chamber but different inertia on bed to overcome makes bed material movement to happen at lower velocities, and therefore, at a lower characteristic frequency, see Figure 6.6.2.1. :

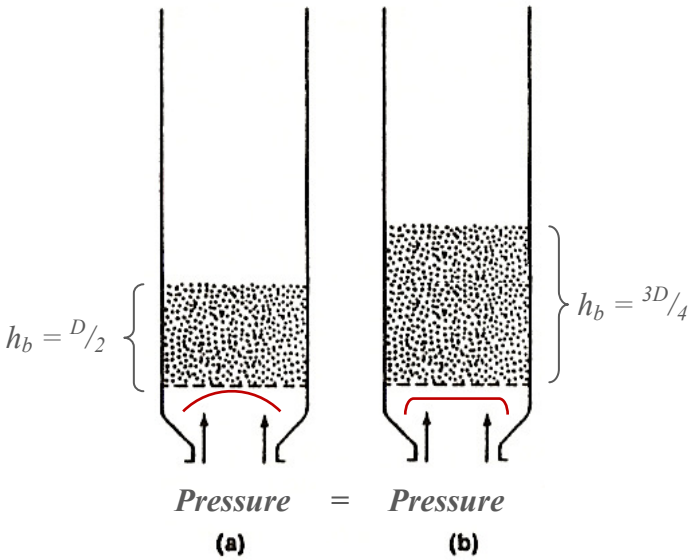

Figure 6.6.2.1. For bed height of 9,6 cm ($^{D}/_{2}$) (a) and for bed height of 14,4 cm ($^{3D}/_{4}$) (b) same pressure at plenum chamber for different material inertia in reactor.

When analyzed the means characteristic pressure by sensors, indifferently with or without distributor rotation and the bed heights ($^{D}/_{2}$ and $^{3D}/_{4}$), results Graphic 6.6.2.3.:

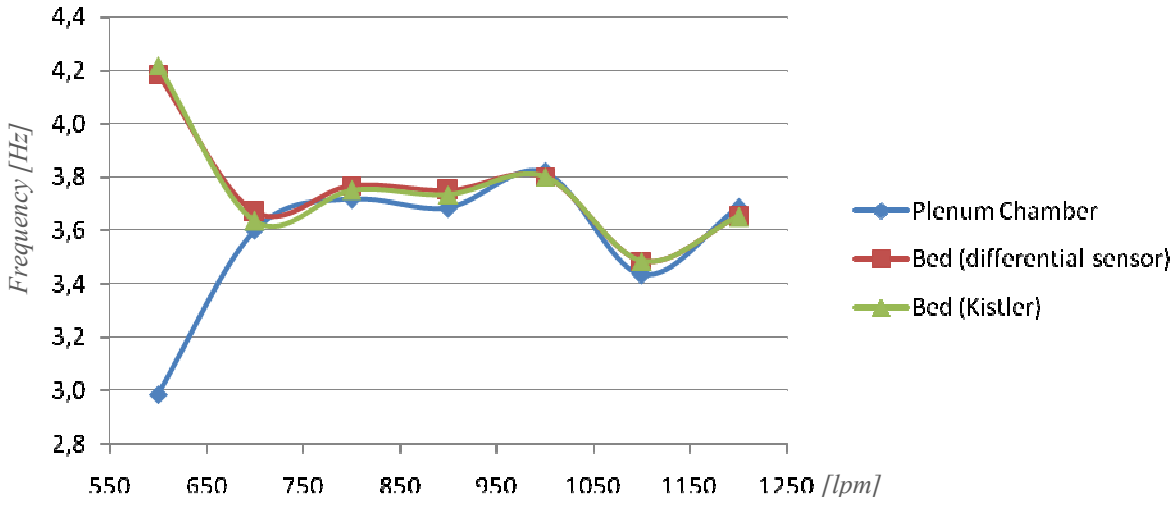

Graphic 6.6.2.3. Mean characteristic frequency by sensors for all tests with and without distributor rotation.

It clearly recognizable the same behavior for all the measured characteristics frequencies. Could be observe that at lower flow velocities are measured the highest frequencies before and attenuation at mid-high flow rates. This effect could be explained because is at this low air velocities when particles move up-down faster than at higher flows when equilibrium between dragged particles and falling velocities makes frequency stabilized, see Figure 6.6.2.2. :

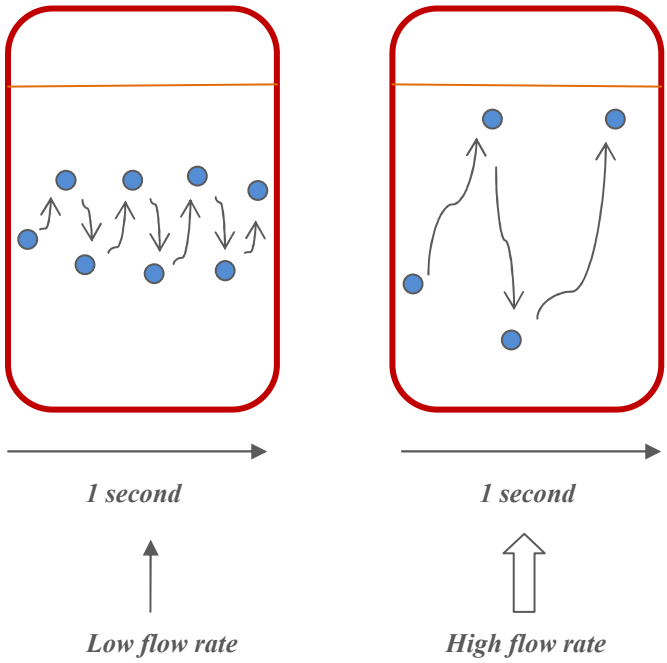

Figure 6.6.2.2. For the same bed height and different flow rate particles frequency of up-down movements .

However, do exist a very low value for the frequency measured at plenum chamber that is sure to have relation with the nature of wave propagation. When lower wavelengths more difficulties to pass trough object with same longitude without distortions [23]. So, when higher frequencies lower wavelengths, increasing then the probability of distortion when transmitted through the perforated plate.

Means values for the characteristic frequencies are also shown divided by sensors in Table 6.6.2.3. :

	Total Means								
	[lpm]	600	700	800	900	1000	1100	1200	Mean Frequency [Hz]
[Hz]	Plenum Chamber	3,0	3,6	3,7	3,7	3,8	3,4	3,7	**3,6**
	Bed (differential sensor)	4,2	3,7	3,8	3,8	3,8	3,5	3,7	**3,8**
	Bed (Kistler)	4,2	3,6	3,8	3,7	3,8	3,5	3,7	**3,8**
									3,7

Table 6.6.2.3. Total mean characteristic frequencies for different sensors for distributor rotation and not.

As has been said, could be observed the higher means values measured in bed versus the ones in plenum chamber. Finally, could say too that all the means values for the characteristic frequencies are between the theoretical ones for this kind of fluidized beds.

8. MODAL ANALYSIS

8.1 VIBRATION MODES

Vibration is the propagation of elastic waves may producing strains and stresses on continuous medium. Any force applied on an object will create disturbance. In its simplest form, a vibration can be considered as the "swing" or repetitive motion of an object around its equilibrium position [27] .

Probably, the most important phenomenon related to vibrations, from the standpoint of engineers, is the resonance, as serious harm could appear in short to medium term in all kind of structures and machines.

Resonance is a phenomenon that occurs when a body capable of vibrating is under the action of a periodic solicitation, which period much with the characteristic period of vibration of the body. In these circumstances, the body vibrates, gradually increasing the amplitude motion after each successive force application [25]. Any solid body excited near its natural frequency origins a characteristic vibrating wave which dynamic amplitude is multiplied without necessarily increasing the value of the external applied load. This large amplitude vibrating wave creates tensions within the material that could collapse itself [28].

The modal analysis is a technique used to determine the characteristics of a vibrating structure with linear elastic or plastic behavior, providing frequencies and natural deformation of the structure while vibrating one time the initial solicitation is gone. It is the most important dynamic analysis that should be done before further analysis, since the characteristics of a vibrating structure determine how it is going to respond to future dynamic solicitations. This study is fundamental to avoid or reduce the possibility of structure to come into resonance [25].

Based on the amplitude of the signal for these natural frequencies, a simple indicator of the internal conditions of the machine that could show changes in the structure vibration state could be obtained. **These changes could affect definitely in the fluid-dynamic behavior of the reactor elements under study and in the critical transmission system**.

It is intended in the next chapter to determine what vibration modes of the prototype structure are found critical for the framework integrity. During the prototype experimental lifetime the possibility of founding frequencies coming closer to the resonance ones exist.

8.2 MODAL SIMULATION TEST

This section will describe in simple terms the procedures by which a structure comes into vibration and the basic parameters that define these phenomena. These will be keys to understand the spectrum on which the diagnostic is used.

Will start by repeating that any structure has some vibration modes themselves, so called natural modes of vibration, with associated values of the frequency showing the vibration modes, these values are called natural frequencies of vibration. In any structure is observed that, when the drive has a frequency coinciding with one of these natural frequencies, the structure presents a much more violent vibration.

It must also be known that in any vibration, vibration-free structure are governed primarily by the forces of inertia and recovery, so that, after any shift in the structure, the force will make it recovers again to its equilibrium position. The recovery force is proportional to the displacement characteristic of each mode. In addition, the forces of inertia of a structure are governed by their mass and are proportional to its velocity. Both forces are easily performable in terms of speed and acceleration of the structure, according to the basic laws of mechanics [27].

However, a model based only on the forces of inertia and the recovery is not definitely real. After removal of the drive was observed that the vibrations are becoming

progressively weaker until it disappeared. This is because the forces of resistance that, although sometimes small in magnitude, have an important role and emerge as a result of internal friction in the structure. So that, the simulation is require to calculate in terms of inertia, recovery and resistance.

8.2.1 FINIT ELEMENTS [27]

Finite element analysis is a method to predict how an approximation of the real world object, a generic mechanical system, will behave face to the usual mechanical parameters: forces, torques, temperature fields, magnetism, electrical currents and so on, in order to find if whether it will break or not, wear out or work in the manner for which it was designed. This type of analysis is used in the product design cycle to predict what will happen when it is in use.

The finite element method discretized the physical properties of a real object in a large number of elements. The behavior of each little element, which has a regular shape, is predicted by the equations of mathematical behavior. Then the computer sums all individual behaviors to predict the actual behavior of the object.

Previously, engineers used the differential and integral calculus which divides the object into a finite number of elements. Finite element analysis is the idea of having a finite number of elements in a finite element model:

a. The continuous material is divided by imaginary lines, surfaces or volumes, in a number of "finite elements".

b. It is assumed that the elements are connected by a number of discrete points, called nodes that are located in its boundaries. The displacements of these nodes are the fundamental unknowns of the problem, as for example in the analysis of simple structures.

c. It takes a set of equations that uniquely define each element. In the case of structural analysis is the field inside each "finite element" in terms of nodal displacements of the element.

These displacement functions defined in a unique way the state of internal element deformation in terms of nodal displacements. These strains, together with the initial deformation and the constitutive properties of the material, define the state of tension throughout the element and also in their contours. Furthermore, for the final defining problem, it is necessary the imposition of corresponding boundary conditions, which can be applied to these nodes, edges or surfaces of a model.

8.2.2 ALGOR [27]

The *MEF Software: Version 23.1 Algor. "ALGOR FEMPRO: Finite Element Modeling, Results Evaluation and Presentation Interface*" is a toolset for a wide field of mechanical or structural analysis, supplemented in Visual Basic language and based on the finite element method (FEA). It was one of the first software FEA (finite element analysis) on PC, the first mass analysis, low cost, the first code FEA implemented in NT, and many other landmarks that have always stood out as the analysis tool FEA more versatile.

Algor provides a "virtual laboratory" for the study of scenarios and situations so that engineers from many disciplines could understand how their designs will work during the operation in real world.

To introduced into *Algor* environment and describe each options that were needed to analyze the prototype, next procedure was followed:

• Define item type: in this step must be selected the type of finite element more appropriate to model the physical system.

• Grid model: the mesh is made according to the type of finite element which is determined in advance.

• Define material: *Algor* has an extensive database of materials that can be assigned to each part of the model.

• Define contour conditions: boundary conditions must be defined (constraints) to be preformed the analysis.

• Calculation of the analytical study.

Before starting to perform the analysis of the element must be designed in a CAD tool (Computer Aided Design). Therefore the prototype is designed with this type of software with the same magnitude as the real facility, and it is exported to the 3D design program for finite element analysis.

8.2.3 SOLID EDGE

CAD (Computer Aided Design) is the use of a wide range of computational tools that assist engineers, architects and other design professionals in their respective activities. These tools can be divided basically in drawing programs in two dimensions (2D) and three-dimensional model (3D). The 2D drawing tools are based on vector geometric entities as points, lines, arcs and polygons, which can be operated via a graphical interface. 3D models added surfaces and solids.

SolidEdge Version 19 is a CAD software design automation. Could be schematize and experiment with different ideas and designs to create 3D models. It is a basic and essential tool in today's industry and can transform a real object into a file with all its geometric dimensions, in order to handle it later in another program.

This program was chosen because is fully integrated with the structural analysis program used in this project. The geometric model could be create and exported directly to the program of analysis, since the latter is unable to generate a 3D geometry.

The first step was taken, with the help of a gauge, measures directly on the prototype to move the plane on which later work. It also took a series of photographs

and general details of the whole and of the parts that compose the mechanism to serve as a complement to help define more precisely the prototype structure.

In practice due to limitations of software and especially hardware available at the *University Carlos III of Madrid* a schematic model has been obtained with all the information needed to carryout further studies with all the essential information required to sustain the validity of the model from the real one.

Thus, the final result on which work is performed and where the different simulations will be carried out are shown in Figures 8.2.3.1. and 8.2.3.2. in the final disposition to be framed in the original set.

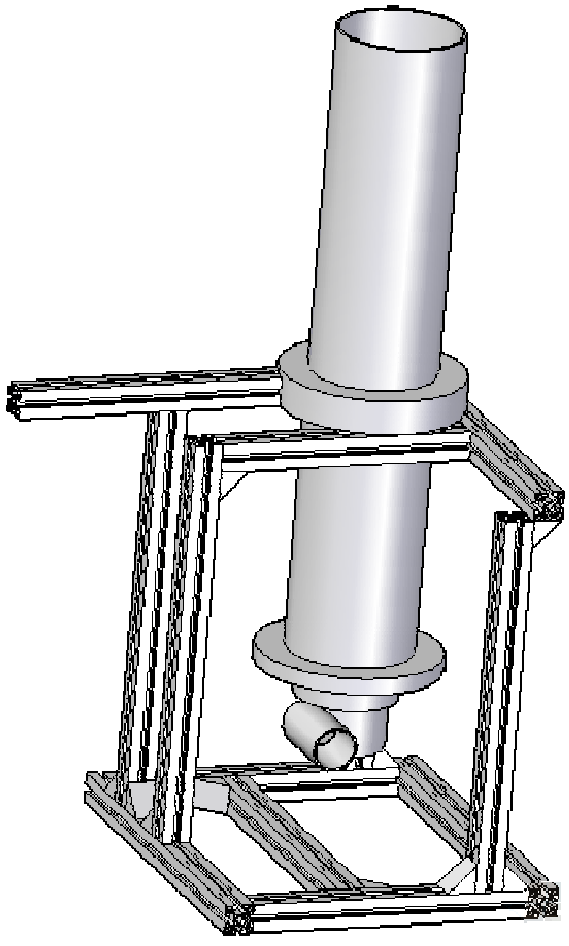

Figure 8.2.3.1 View of the structural schematic model from the CAD program Solid Edge.

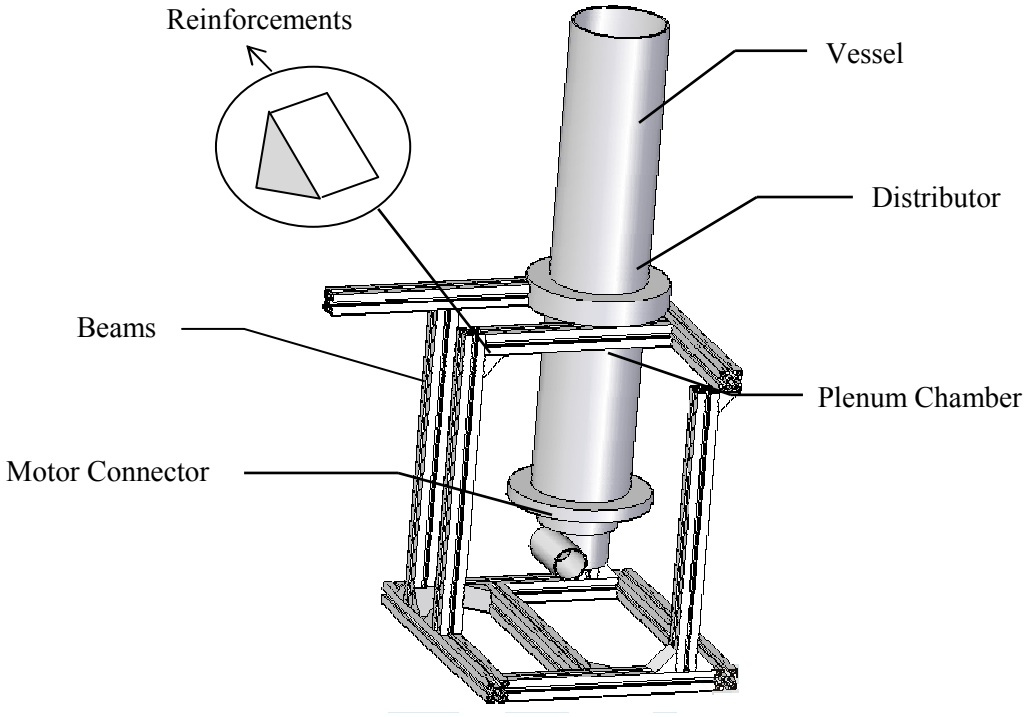

Figure 8.2.3.2 View of all the elements of the prototype and structure.

As could be seen, the whole structure and prototype has barely changed, maintaining the proportionality between its different elements and respect the functionality of all its parts.

To achieve the end of the set have been used the following parts:

Pieces	Units	Pieces	Units	Pieces	Units
Beam 405 mm	1	Reinforcements	11	Motor connector	1
Beam 450 mm	2			**Total pieces**	**28**
Beam 510 mm	1	Base cylinder	1		
Beam 600 mm	5			**Sets**	**Units**
Beam 645 mm	2	Plenum cylinder	1		
		Distributor	1	Prototype	1
Beam adequate	1	Vessel	1	Structure	1
				Total sets	**2**

Table 8.2.3.1 Breakdown of all the pieces that appear on the device.

8.2.4 ANALYSIS AND RESULTS

The model design schematically is used to find the vibration modes. The number of vibration modes will be limited to the first 50 modes as a certain number of frequencies obtained are quite high and is more likely to find the lowest work-life as has been demonstrated in previous in modal analysis investigations [26].

The simulation program *Algor* provides the assistance necessary to meet the objectives exposed. This will create the mesh for the entire volume of the whole mechanism. Once the value of mesh size is set, it is solved offering the following result, see Figure 8.2.4.1. :

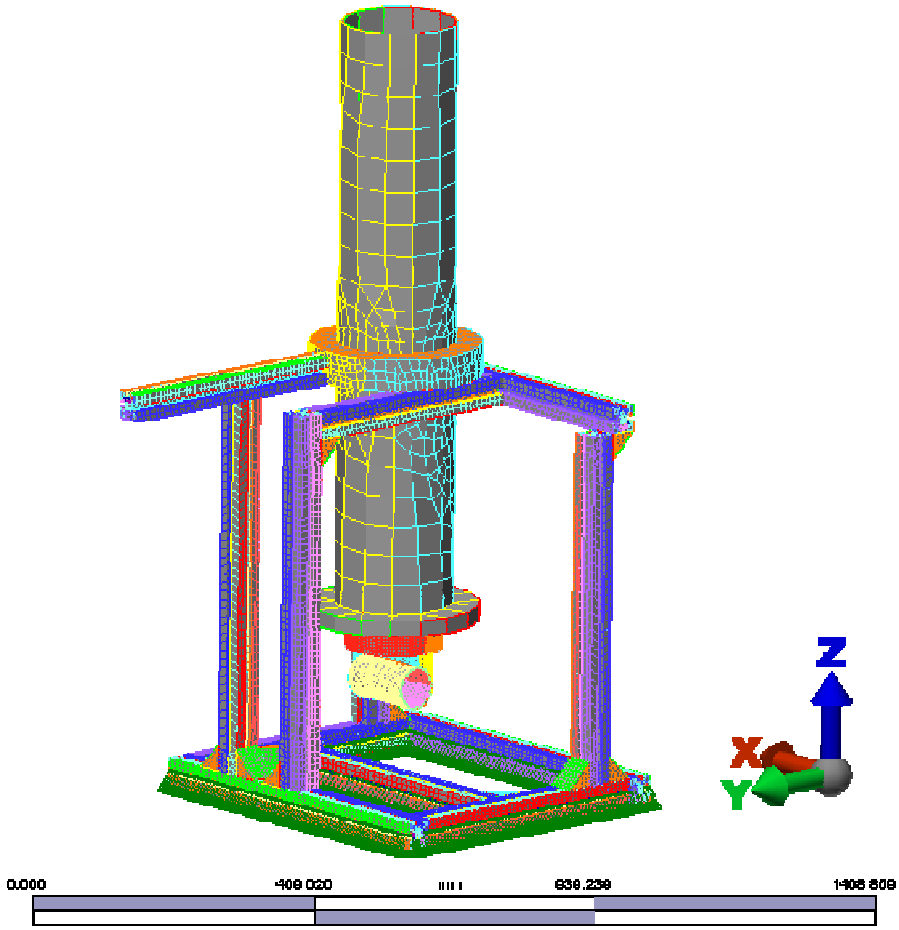

Figure 8.2.4.1. View of the prototype and structure already meshed.

Once everything is meshed, next step will be to determine the properties of materials that composed the prototype structure. To this end, the same program *Algor*, as already mentioned, has a library with a wide variety of materials and their mechanical properties determined. If the program did not provide in its library the type of material one looked for, it offers the possibility to create a new material with the features that are required to define it. This case has not been necessary to design any additional material as the program provides the actual material to determine the complete set. Except the air inlet, design in steel, and the reactor tower, design in PVC, the entire structure is designed in aluminum, with the characteristics shown in the following tables, see Tables 8.2.4.1., 8.2.4.2., 8.2.4.3. and 8.2.4.4. :

AISI 1005 Steel -Brick	
Material model	Standard
Source material file	Algor Material Library
Last actualization date	2004/10/28-16:02:00
Material description	None
Mass density	7,872.10-9 Ns2/mm/mm3
Elasticity modulus	200000 N/mm2
Poisson Coefficient	0,29
Shear elastic modulus	80000 N/mm2
Thermal dilatation coefficient	1,2.10-5 1/ºC

Table 8.2.4.1 Steel properties.

The selected steel is common for parts that continuously are exposed to stress load during their working lives. Thus, as can be verified later, the pieces have been previously selected for a structural function of remarkable mechanical solicitations.

Because it particular functionality, a material that provide both resistance and lightweight is needed for the structure. It should be hardy because the whole installation will hold the prototype and light, because, as seen in anterior chapters, has had to relocate as this is a laboratory element subject to all sorts of eventualities. That condition was resolved by choosing two types of aluminum. For beams under the 5052-H32 Aluminum and for reinforcements the 7075-O Aluminum.

Aluminum 5052-H32 -Brick	
Material model	Standard
Source material file	Algor Material Library
Last actualization date	2004/10/28-16:02:00
Material description	None
Mass density	2,68.10-9 Ns2/mm/mm3
Elasticity modulus	70300 N/mm2
Poisson Coefficient	0,33
Shear elastic modulus	25900 N/mm2
Thermal dilatation coefficient	2,38.10-5 1/ºC

Table 8.2.4.2 Aluminum 5052-H32 properties for beams.

Aluminum 7075-O -Brick	
Material model	Standard
Source material file	Algor Material Library
Last actualization date	2004/10/28-16:02:00
Material description	None
Mass density	2,81.10-9 Ns2/mm/mm3
Elasticity modulus	71700 N/mm2
Poisson Coefficient	0,33
Shear elastic modulus	26900 N/mm2
Thermal dilatation coefficient	2,36.10-5 1/ºC

Table 8.2.4.3 Aluminum 5052-H32 properties for reinforcements.

A plastic material has been selected for the reactor tower. The tower is going to work under wear projection sand, so it is needed to avoid fragile or easy to scratch materials. The one that match better the specifications of the real reactor tower has been the PVC. The material proprieties are shown in Table 8.2.4.4.

Plastic- PVC (Molded) -Brick	
Material model	Standard
Source material file	Algor Material Library
Last actualization date	2004/09/30-16:00:00
Material description	Polyvinyl Chloride
Mass density	1,3038.10-9 Ns2/mm/mm3
Elasticity modulus	2757.9 N/mm2
Poisson Coefficient	0,36
Shear elastic modulus	1013.9 N/mm2
Thermal dilatation coefficient	7,5005.10-5 1/ºC

Table 8.2.4.3 Plastic- PVC (Molded) properties for reactor tower.

Once the properties of all materials of the elements have been already determined, the appropriate conditions necessary to finally determine the set, should also establish. The 6 degrees of freedom will be block (displacements in x, y, z and rotations in x, y, z) of the lower surface of the base on which rests the device.

After specifying all the parameters required to completely determine the mechanical system, the program is ready to obtain the first 50 modes of vibration.

8.2.5 RESULTS

In order to express clearly all the results obtained in *Algor* code, in Table 8.2.5.1., will appear the 50 first modes of vibration and their own frequencies, as also the weighed total characteristic displacements in each one respectively:

Mode	Frequency (Hz)	Maximum displacement (mm)
1	28,9	8,99
2	33	11,30
3	61,9	16,07
4	70,4	14,15
5	115,9	26,47
6	147,8	25,47
7	156,3	38,75
8	163,7	31,12
9	224,6	33,00
10	265,7	33,36
11	336	17,06
12	346,8	17,86
13	365,2	24,23
14	380,2	21,58
15	396,5	43,13
16	470,1	33,18
17	479,8	30,81
18	497,1	40,40
19	509,2	25,49
20	524,8	29,13
21	527	21,84
22	559,4	59,73
23	561,3	25,32
24	582,6	28,76

Table 8.2.5.1 Modes, frequencies and maximum displacements.

Table 8.2.5.1 continuation

Mode	Frequency (Hz)	Maximum displacement (mm)
25	623,8	36,44
26	672,1	37,78
27	734,6	27,90
28	742,7	38,14
29	790,4	48,91
30	807,1	37,83
31	945,3	41,85
32	955,7	40,65
33	1019	67,83
34	1075	56,40
35	1136	52,06
36	1182	41,81
37	1272	35,22
38	1307	38,82
39	1318	28,16
40	1340	24,28
41	1364	63,85
42	1372	51,31
43	1387	53,32
44	1438	32,85
45	1463	36,69
46	1477	29,40
47	1514	33,89
48	1518	41,04
49	1567	46,07
50	1572	42,01

Table 8.2.5.1 Modes, frequencies and maximum displacements.

It will be highlighted here that, in the first 50 vibration modes, in most of all the elements of structure the maximum tension appear at about the mid height of the beams of the structure or in the mid height of the reactor tower. This situation is not a simple coincidence as the geometrical and constructive proprieties of this elements offer less resistance to oppose any forced of vibration within the set.

To illustrate the information described above two graphs are shown, Graphic 8.2.5.1 and 8.2.5.2, which represent frequencies versus modes and displacements versus frequency respectively.

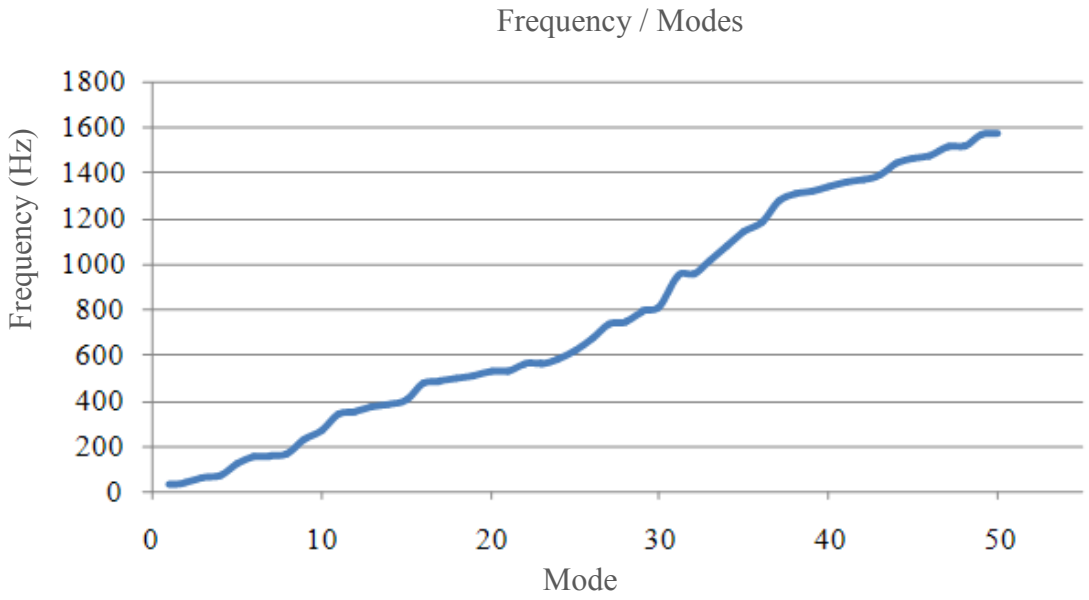

Graphic 8.2.5.1. Frequency face to modes.

Thanks to this first chart it could be understood how the resonance frequencies increase gradually from the first mode frequency up to linear approximately until the last mode calculated. It is observed how the frequencies are grouped around certain values so that there is no sudden leap between their resonance frequencies, which shows that indeed all of them might belong to a single system. As can be seen below, could be solved by the jump shown in the chart because it is precisely in the manner 13 in which there is a considerable increase in the percentage of mass displaced, this being the second highest percentage of mass shifted from all modes.

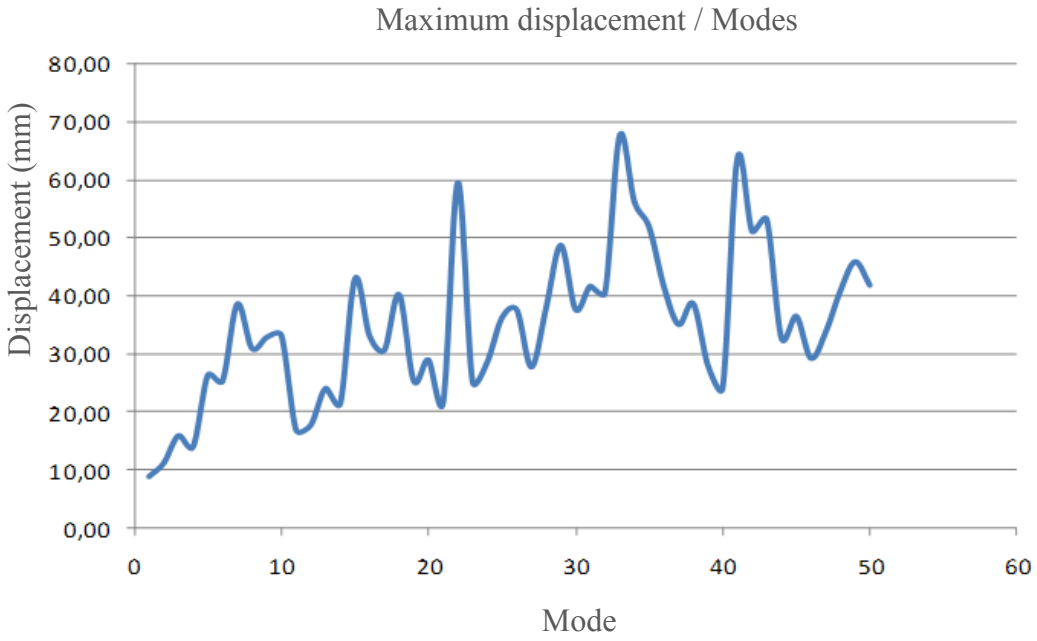

Graphic 8.2.5.2. Displacements face to modes.

Actually the displacements offers by *Algor* for each mode of vibration are weighted values that attempt to measure the effect that happens when energy is released by vibration to compare the degree of deformation of the structure in the different cases studied. It could be seen how this relatives displacements grow with the resonance frequency of the set.

For a complete analysis, the results obtained from the *Algor* program related to physical movement in percentage of mass for each mode.

Mode	Modal mass (%)			Cumulative mass (%)		
Number	X-dir.	Y-dir.	Z-dir.	X-dir.	Y-dir.	Z-dir.
1	1,37	68,16	0,31	1,37	68,16	0,31
2	50,28	1,72	0,08	51,65	69,88	0,39
3	4,98	1,73	0,72	56,63	71,61	1,12
4	6,91	2,55	0	63,54	74,16	1,12
5	6,92	0,02	0,23	70,45	74,19	1,35
6	1,26	0,71	24,62	71,72	74,9	25,97

Table 8.2.5.2 Modes, modal mass and cumulative mass.

Table 8.2.5.2 continuation

Mode	Modal mass (%)			Cumulative mass (%)		
Number	X-dir.	Y-dir.	Z-dir.	X-dir.	Y-dir.	Z-dir.
7	0,02	0	8,76	71,74	74,9	34,73
8	0,48	0,38	20,35	72,22	75,28	55,09
9	0	0	0	72,22	75,28	55,09
10	0,04	0,19	0	72,27	75,47	55,09
11	0	0,31	0,44	72,27	75,78	55,53
12	0,02	0,27	0,41	72,29	76,05	55,94
13	0,06	0,05	0,01	72,35	76,1	55,95
14	0,03	0,03	0,49	72,37	76,13	56,44
15	0,03	0,21	2,42	72,4	76,34	58,86
16	0,35	0,07	0,79	72,76	76,41	59,64
17	0,03	0,6	0,01	72,78	77	59,65
18	2,84	0	0,05	75,62	77	59,7
19	0	0	0,1	75,63	77	59,8
20	1,38	0,07	0,26	77,01	77,08	60,06
21	0,94	0,51	1,67	77,95	77,59	61,73
22	0,03	0,1	2,02	77,98	77,69	63,75
23	0,41	0,43	0,06	78,38	78,12	63,81
24	0,08	0	0,01	78,46	78,12	63,82
25	0,03	0,12	0,04	78,49	78,25	63,86
26	0,02	0,04	0	78,52	78,29	63,86
27	0,01	0,25	0,58	78,53	78,53	64,44
28	0	0,41	0,47	78,53	78,95	64,92
29	0,15	0	0,08	78,67	78,95	65
30	0,01	0,03	0	78,68	78,98	65,01
31	0	0	0,01	78,69	78,98	65,01
32	0	0,01	0,01	78,69	78,98	65,02
33	0	0	0	78,69	78,98	65,02
34	0	0	0	78,69	78,98	65,02
35	0,11	0,03	0,05	78,8	79,01	65,08
36	0,17	0,17	0,18	78,97	79,19	65,26
37	0,03	0,32	0,39	79	79,51	65,64

Table 8.2.5.2 Modes, modal mass and cumulative mass.

Table 8.2.5.2 continuation

Mode	Modal mass (%)			Cumulative mass (%)		
Number	X-dir.	Y-dir.	Z-dir.	X-dir.	Y-dir.	Z-dir.
38	0,04	0,06	0,07	79,04	79,57	65,71
39	0,04	0,45	0	79,08	80,02	65,71
40	0,05	0	0,1	79,13	80,02	65,81
41	0,02	0,04	0,24	79,15	80,06	66,05
42	0,02	0	0,27	79,17	80,06	66,32
43	0	0	0,05	79,17	80,06	66,36
44	0,15	0,04	0,29	79,32	80,1	66,65
45	0,04	0	0,91	79,36	80,1	67,57
46	0,27	0,06	0,71	79,63	80,16	68,28
47	0	0	0,34	79,63	80,16	68,61
48	0,02	0	0,08	79,65	80,16	68,69
49	0	0	0,04	79,65	80,17	68,73
50	0	0	0,04	79,65	80,17	68,77

Table 8.2.5.2 Modes, modal mass and cumulative mass.

In reality it is intent to discover, through knowledge of the mass displacement of set for each mode, which is the degree of intensity that gives each mode by comparing the results of the mass displacement of otherwise modes of the same set. In those cases *Algor* gives mass percentage equal to X-dir .= 0.00%, Y-dir. = 0.00%, Z-dir. = 0.00% , will understand that in this way the percentage of mass that moves in any of the 3 axes is less than 0.01% and thus *Algor* do not reflect it in the report.

In this analysis, it can be seen that the mode in which is greater the percentage of displacement of modal mass is for the first mode, and their respective percentages are as follows:

Modal mass (%)			Cumulative mass (%)		
X-dir.	Y-dir.	Z-dir.	X-dir.	Y-dir.	Z-dir.
1,37	68,16	0,31	1,37	68,16	0,31

Table 8.2.5.3 Modal mass and cumulative mass for first mode.

In mode 2 there is a significant percentage of mass in the displacement compared with other percentages, and their respective values are as follows:

Modal mass (%)			Cumulative mass (%)		
X-dir.	**Y-dir.**	**Z-dir.**	**X-dir.**	**Y-dir.**	**Z-dir.**
50,28	1,72	0,08	51,65	69,88	0,39

Table 8.2.5.4 Modal mass and cumulative mass for second mode.

It is noteworthy that in the first mode coincides precisely the lowest frequency resonance mechanism of 28,90 *Hz* with the highest percentage of displaced mass, which gives an idea of the magnitude of vibration, thereby enabling to know which is the discriminating more critical to the system according to this criterion. However, it is had also highlighted the second mode, but in this case the vibration is a frequency of 33,00 *Hz* slightly higher, reaching a rate close to the mass displacement of the first mode but in direction *"Y-dir"*.

In both cases, the *modal analysis* shows that it would be advisable to avoid the appearance of vibrations particularly near the first and second resonance modes for these systems. If the system is going to work under the possibility of appearance of applied loads with frequencies near those ones, because of integrity prototype reasons, should need to provide systems for absorption of unwanted waves or improve the design of the facility.

8.3 MODAL ANALISYS

The study of the direct effect that the different resonance frequencies may cause in the mechanism will be carried out. That is, it will be located those that, between all the modes, have special relevance for their characteristic mode of vibration that could significantly affect the proper performance of the mechanism and for the future fluid-dynamic investigations.

8.3.1 TRANSMISSION MECHANISM

Those modes that meet an acceptable risk for the distributor transmission system of prototype, the most critical mechanism, because of their particular form of vibrating are presented. Next figures have a color code for going from maximum displacements, red colors, to minimum displacements, deep blue color. It could easily locate maximum displacements in next figures, red color, in the region from the motor connector to the distributor, as is along the plenum chamber where this mechanism is locate.

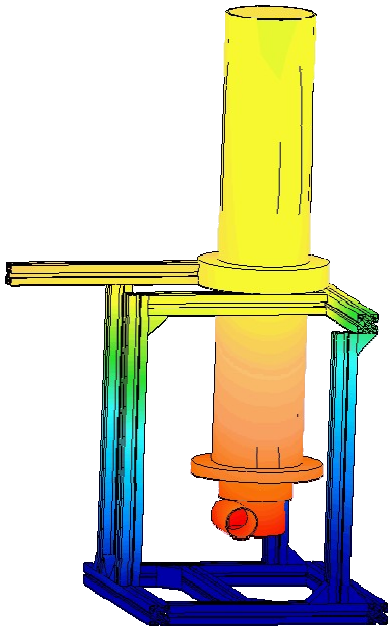

Figure 8.3.1.1. Displacements for the mode 1.

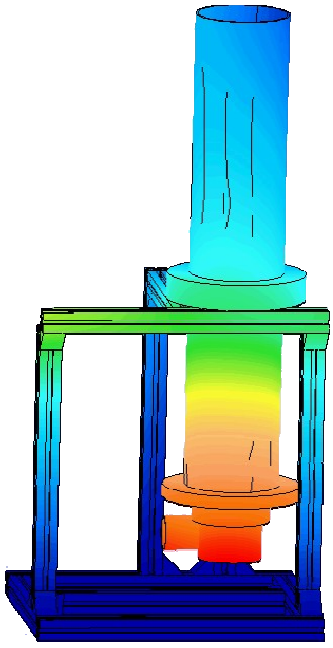

Figure 8.3.1.2. Displacements for the mode 2.

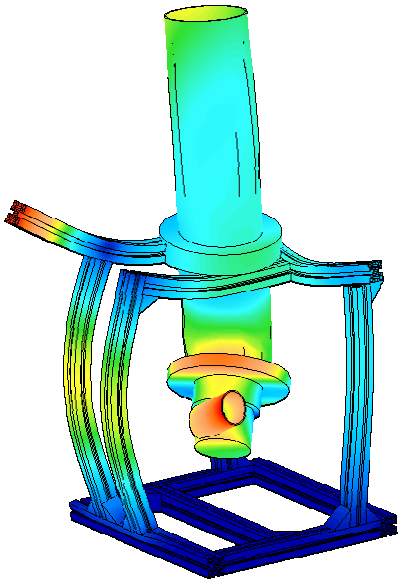

Figure 8.3.1.3. Displacements for the mode 11.

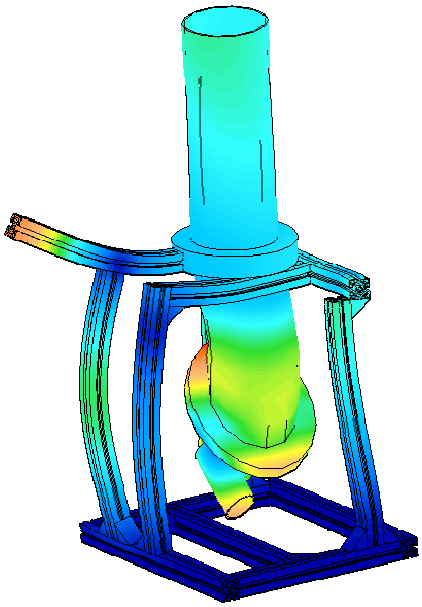

Figure 8.3.1.4. Displacements for the mode 12.

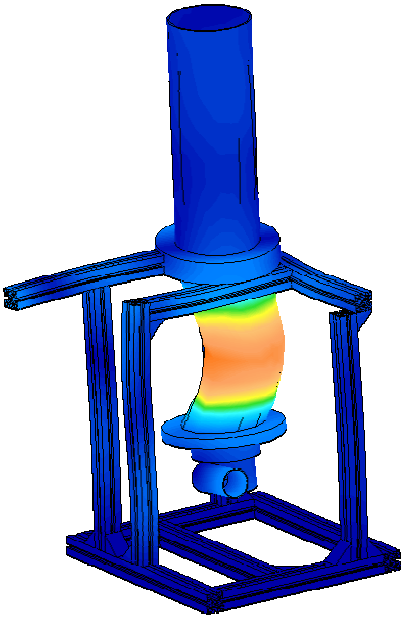

Figure 8.3.1.5. Displacements for the mode 31.

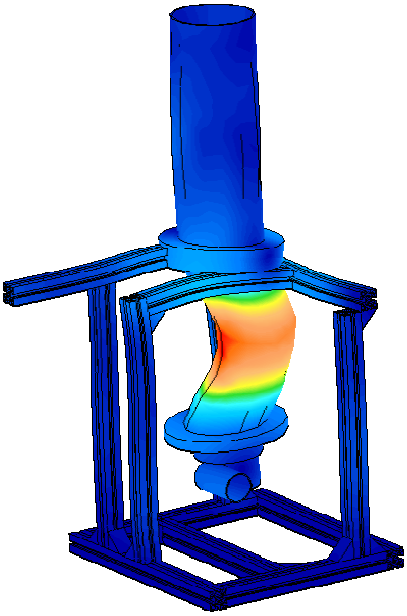

Figure 8.3.1.6. Displacements for the mode 32.

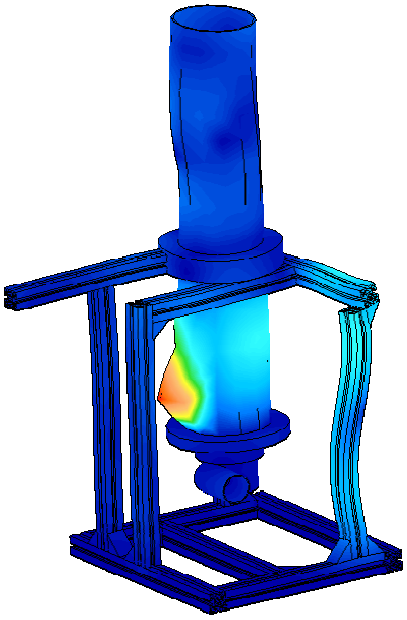

Figure 8.3.1.7. Displacements for the mode 41.

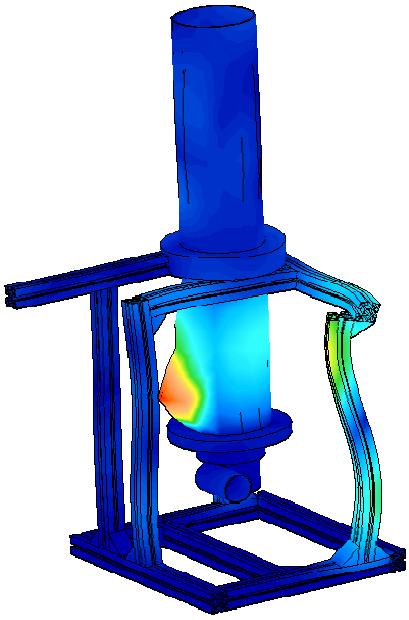

Figure 8.3.1.8. Displacements for the mode 42.

In all previous modes of vibration, corresponding to modes 1, 2, 11, 12, 31, 32, 41 and 42, it would come into resonance with direct consequences for the proper operating of the transmission system. When come into resonance, maximum displacements could appear in the region between the driving engine and the distributor, the two sides of the transmission mechanism, with fatal consequences for the transmission system work live.

8.3.2 VESSEL

In particular modes of vibration that directly affect the future fluid-dynamic study of the different elements that are within the reactor (vessel) will be studied. Thus, there are presented just, as was done in the previous study, all modes of the top 50 in those who are affected in one way or another to the vessel.

Next figures have a color code too for going from maximum displacements, red colors, to minimum displacements, deep blue color. It could easily locate maximum displacements in next figures, red color, in the vessel where future fluid-dynamic experiments will take place.

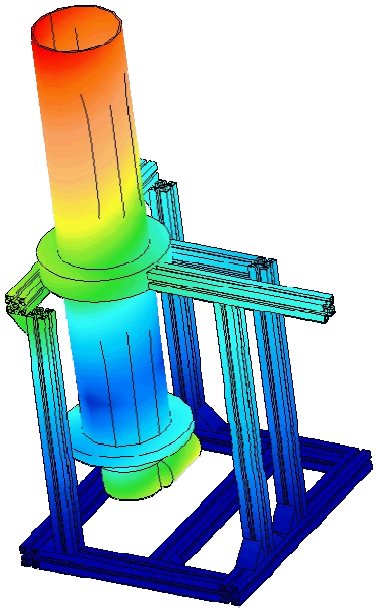

Figure 8.3.2.1. Displacements for the mode 3 .

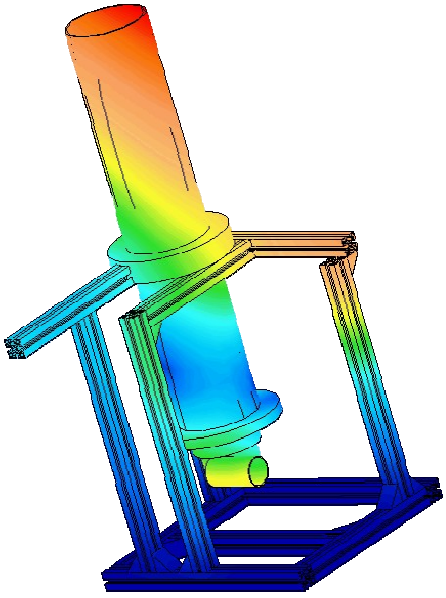

Figure 8.3.2.2. Displacements for the mode 4.

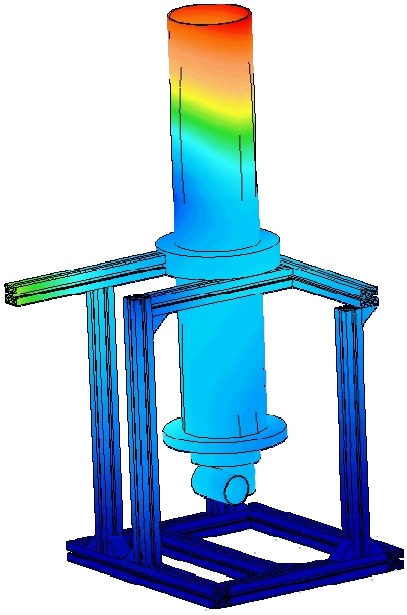

Figure 8.3.2.3. Displacements for the mode 6.

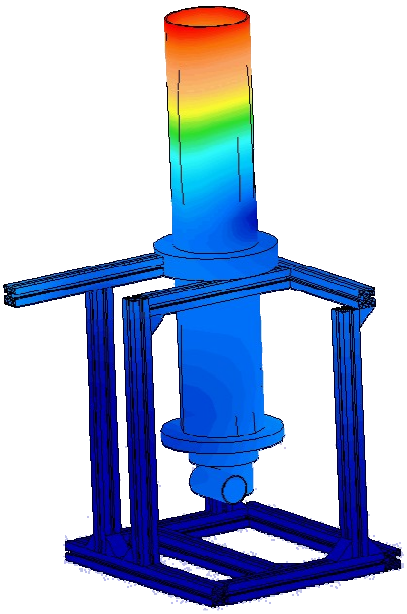

Figure 8.3.2.4. Displacements for the mode 7.

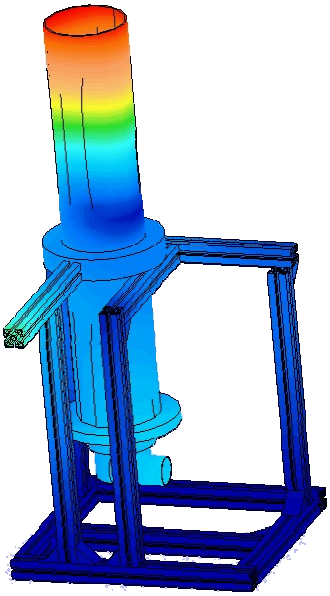

Figure 8.3.2.5. Displacements for the mode 8.

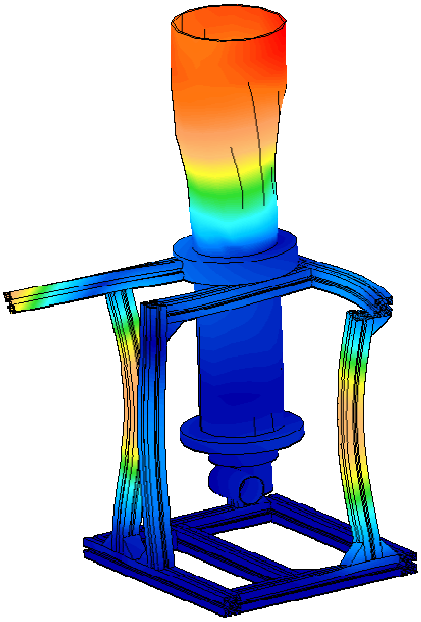

Figure 8.3.2.6. Displacements for the mode 19.

Besides these modes there are 13 more modes of the top 50 modes (24, 25, 26, 27, 33, 34, 38, 39, 43, 45, 46, 47, 49) which modes of vibration also affects directly the vessel, which affect, as has been said directly to study fluid-dynamic future, and which are not shown for clarity and simplicity in the document.

For the remainder of the 23 modes, the mode of vibration occurs typically with peaks in the different beams, being a representative mode of vibration number 22 which is presented below in Figure 8.3.2.7.

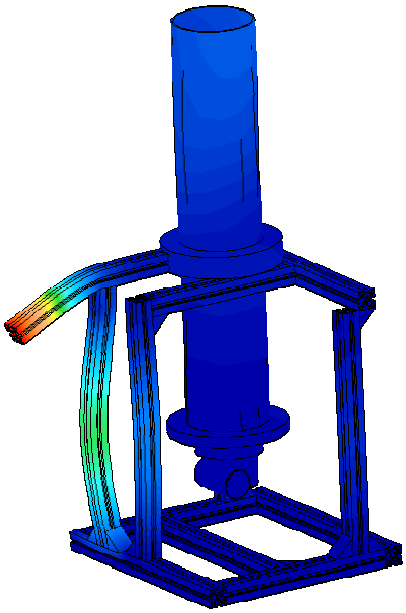

Figure 8.3.2.7. Displacements for the mode 22.

8.4 FREQUENCY ANALISYS

Once determined those frequencies to which the fluidized bed may suffer structural damage, and then disabling prototype to continue offering the same operating conditions to which it was designed, it should try now to ascertain the possibility for those frequencies to appear in the set during in its normal work operation.

Possible sources of frequencies production near the resonance frequencies calculated above, is the electrical engine of the distributor. While any other external source of production of vibrations with frequencies close to resonance may damage the structure, the study will focus on the features characteristic of the prototype fluidized bed.

The other possible source of frequencies is the main reactor while operating. That is, as already has been seen in the power spectra analysis, because of the normal operation of the fluidized bed those frequencies could easily appear during experimental process.

The modal analysis shows how actually appears as a real risk if the system became especially resonant in the first mode, since, although the maximum displacement in this case are generally somewhat lower than the rest of the modes (D_{max1} = 8.99 *mm* <D_{max} mean for the rest of the modes = 35.36 *mm*), the resonance frequency is the lowest of all of them, f_1 = 28.90 *Hz*, and thus increases the chances of achieving it more easily due to the lower energy required for that vibration.

8.4.1 PROTOTYPE, SOURCE OF FREQUENCIES

To verify the adverse effects of vibrations transmitted by the electrical engine it is needed to viewed it from its mechanical behavior. First, will be calculated the frequency of work from the working speed which operates as the main engine.

$$\left.\begin{array}{l} n = 100\ rpm \\ f = \dfrac{100\ rpm}{60\ s/min} \end{array}\right\} \qquad f = 1{,}67\ Hz$$

The other source of frequencies is the reactor, in the base vessel. From the power spectra analysis could be obtain the main frequencies appeared while operating in fluidization regime. Those frequencies are typically from 1 to 5 *Hz* [13].

Knowing that the frequency of the vibration sources are closer to the first and second mode of vibration, and they have a natural frequency of vibration of 28,90 *Hz* and 33,00 *Hz* respectively, it could be said that the motor during operation is not going to be apparently a risk to the integrity of the structure because its frequency is around one twentieth of the resonant frequency of the system. Same conclusion could be obtained for reactor, as it higher frequencies are one sixth of the lower resonant frequency mode. For other modes of vibration frequencies are further away for both vibration sources.

Given the potential damage that may be caused to the transmission, one of the most sensitive system, has to especially highlighted first two modes, corresponding to modes 1 and 2, which vibration mode directly affected to the transmission system. Once they enter into resonance, it would be maximum throughout the driving motion and at lower frequencies (28.90 and 33.00 *Hz*), but far away from the working frequency of the engine and from the frequencies form reactor while fluidization regime. The remaining modes, corresponding to modes 11, 12, 31, 32, 41 and 42, would have a direct impact too but lower probability of occurrence due to the higher frequencies of the modes (336 - 1372 *Hz*) rarely and difficult to find during the working operations.

To assess the potential damage that may arise in the vessel (future head of fluid-dynamics research) due to the occurrence of resonant frequencies, attention should be paid to 3 and 4 modes. It is need to attend their frequencies which are still low (61,9 *Hz* and 70,4 *Hz* respectively), although far from the operating frequency of fluidized bed.

Although beginning to have significant effects in terms of mass movements, all of them are related to higher frequencies not relative ease to happen during work operations.

In this way, it is shown that the **normal operation of the electrical engine and frequencies from working operations should not cause any structural damage for the critical transmission system in terms of vibrations** with possible frequencies close to resonance operating at the work speed.

Could also be ensure that, **for fluid-dynamic investigations, frequencies from electrical engine and working operations will not affect in terms of resonance to the vessel integrity**, hereafter source of investigations.

Moreover, prototype has been hold to the structure with three reinforcements near engine connector, see Figure 8.4.1.1., that will reduce impact of the mode vibration as will decrease maximum displacements and percentage of modal mass movement. These reinforcements do not modify modes as changes introduced are not structural changes.

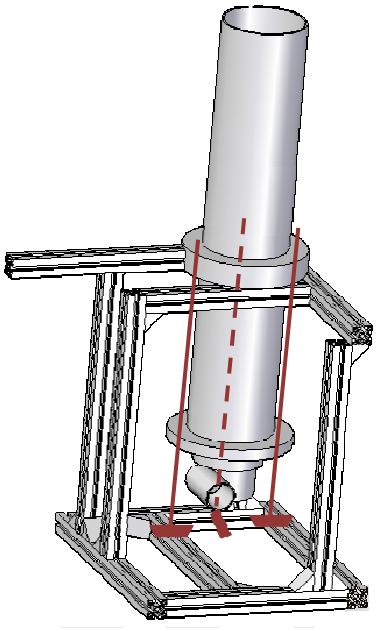

Figure 8.4.1.1 Prototype reinforcements.

9. CONCLUSIONS AND FINDINGS

Since the aim of the project was firstly to design the supporting of the fluidization bed, based on theoretical models, and characterize the fluid-dynamic behavior, basing on the minimum fluidization velocity analysis, it could be said that this investigation has amply fulfilled the objective.

As the experiments carried out by the department team has revealed, **the design of the fluidized bed based on theoretical models has finally given as a result a system capable of fluidizing the inside bed reactor material**. In addition, it has to be said that the prototype has behaved with integrity during all the experiments, demonstrating the reliability of the facility constructed. Particularly, the complex design of the distributor has revealed, after all, a very good accommodation to the fluidized bed system as has worked always properly under the different test situations.

Also, thanks to the two methods of analysis, the standard deviations for pressure signals and the bed mean pressure monitoring, **the fluid-dynamic characterization has been successfully carried out**. All the tests reveal that the minimum fluidization velocity determined for the fluidized bed prototype of *Carlos III University of Madrid* are values not distanced to each other for more than *2,7 %*, in the case of distributor rotation with deviation method, and no more than *10,6 %*, in the case of distributor rotation with mean pressure method. So that, it could be affirmed that the great accuracy between results from all the test and analysis, give the certain of the precise fluid-dynamic characterization method followed, validating, at time, the obtained data and analysis results.

It could be also found, that **minimum fluidization velocity does not depend on bed height**. The higher deviation on u_{mf} is no greater than *1,9 %* between the u_{mf} calculated without distributor rotation by measuring at $h_b = {}^{D}/_{2}$ and at $h_b = {}^{3D}/_{4}$, with pressure deviation method, and of *0,5 %* with mean pressure method. When the distributor rotates, the deviation on u_{mf} is no greater than *1,1 %* between the u_{mf}

calculated by measuring at $h_b = {}^{D}/_{2}$ (second test series) and at $h_b = {}^{3D}/_{4}$, with the pressure deviation method, and *9,6 %* with mean pressure method.

It was found too that u_{mf} **depends weakly with distributor rotation**. It has been explained that when distributor rotates, a better homogenization of air and particles in bed is reached, and sooner achieving of u_{mf}. But, reality is that, although the rotation of distributor effect is perceived, the gain on getting sooner to the minimum fluidization velocity is not higher than *5,5 %* lower than fluidization without rotation.

When data is analyzed, it was observed that the **minimum fluidization velocity do not depend on the sensor used**. The difference between the total u_{mf} mean calculated with the *Kistlers* sensors and with the differential one is no higher than *4 %*, deviation perfectly assumable as, apart form other uncontrolled variables, are two measures systems with a total different nature of technology that interpret pressure data by different ways.

Also, when comparing minimum fluidization velocities determined by measuring at different heights, it could be seen that u_{mf} **prediction does not depend on a specific zone for intake data pressure**. When contrast results for no distributor rotation, the u_{mf} prediction deviate from zones (bed – plenum chamber; with data for second series of test for $h_b = {}^{D}/_{2}$) no more than *3,9 %*. When contrast results with distributor rotation, the u_{mf} prediction deviate from zones (bed – plenum chamber; with data for second series of test for $h_b = {}^{D}/_{2}$) no more than *13,8 %*. The mean deviation is not higher than a *5 %*, being able to affirm that u_{mf} is not dependent on the intake data position.

So that, a definitive **value for minimum fluidization velocity** for the *Carlos III University of Madrid* prototype could be given as the mean value resulting from all the test carried out, as any variable used (bed height h_b, distributor rotation, sensor used, intake samples point) is determinant for calculate u_{mf}. An upper and lower limit for the election of this velocity could be fixing as an evaluation margin. The lower limit could be fixing by the mean of the u_{mf} for prototype with distributor rotation, *3,5 %* lower than the total mean, and the upper limit could be fixed by the mean of the u_{mf} for prototype without distributor rotation, *1,87 %*. As the condition imposed for the lower limit gives

a higher margin, the **minimum fluidization velocity** (a) calculated with the deviation pressure method, the most accuracy method, would be:

a) $u_{mf} = 0{,}31 \pm 0{,}011$ *m/s* $Q_{mf} = 546 \pm 19$ *lpm*

Also, it is shown the **minimum fluidization velocity** (b) for prototype **without distributor rotation** calculated with the deviation pressure method means, by applying same limits:

b) $u_{mf} = 0{,}32 \pm 0{,}011$ *m/s* $Q_{mf} = 560 \pm 19$ *lpm*

It is shown, too, the **minimum fluidization velocity** (c) for prototype **with distributor rotation** calculated with the deviation pressure method means, applying same limits than below:

c) $u_{mf} = 0{,}30 \pm 0{,}011$ *m/s* $Q_{mf} = 531 \pm 19$ *lpm*

From the *Johnson et al.* [13] in its "*Investigation Journal of Multiphase Flow*" it was predicted that **most of the fluidized bed systems has their main frequencies in the order of *1 - 5 Hz***. Actually, **the *Carlos III University* prototype is in this frequency range in all the test carried out** (*2,6 - 5,2 Hz*, for $h_b = {}^{3D}/_{4}$ with distributor rotation and $h_b = {}^{D}/_{2}$ with distributor rotation second series experiments respectively). That supports the theory of a right design to get fluidization on bed prototype.

As a consequence of that, it could be said that the **frequencies measured do not depend on bed height**. Depending on the test carried out, characteristic frequency varies from *2,8 Hz* to *5,2 Hz*, between the ones calculated with distributor rotation by measuring at $h_b = {}^{D}/_{2}$ and at $h_b = {}^{3D}/_{4}$. All frequencies are in the margin establish by *Johnson et al.* [13], and, in addition, would be permitted to grow up to a *14 %* for the higher mean frequency measured and decrease *66 %* for the lower ones and still prototype would be in the establish rage.

It is found too that **frequency depends weakly on distributor rotation**. The difference between the characteristic frequency when rotation and when not is only *5,3*

% making difficult to establish a clear relation between frequency and distributor rotation. However, it might say that the distributor frequency of rotation is *100 rpm*, or what is the same, *1,67 Hz*, which may partly explain the small decrease in the value of frequency.

The **frequency measured does not depend on the sensor used**. Except for the mean main frequency of *600 lpm* commented in next paragraph, differences between total mean frequencies calculated with *Kistlers* and differential sensors is no higher than *2,9 %*. Has to be said that is this a very low margin for the frequency spectra.

Although it is seen obviously, by comparing frequencies data measured at different heights, that the **frequency measured do not depend on a specific zone for intake data pressure**, **nevertheless a zone that do not fulfill this condition at certain flow rates could exist.** When contrast results for no distributor rotation, the mean frequency measured deviates from zones (bed – plenum chamber; with data for second series of test for $h_b = {}^{D}/_{2}$) no more than *9,1 %*. When contrast results with distributor rotation, the u_{mf} prediction deviate from zones (bed – plenum chamber; with data for second series of test for $h_b = {}^{D}/_{2}$) no more than *6,8 %*. This evidence the no frequency dependence on the intake data point. But, when the mean frequency measured with the *Kistler* sensor at plenum chamber is observed deviation is *28,6 %*, when, as has been said in the paragraph above, the maximum difference for sensor measured frequency was no higher than *2,9 %*. First approximation is to assume that this phenomena has a relation with the nature of wave propagation. Lower wavelengths find more difficulties to pass trough object with same longitude without distortions [23]. So, when higher frequencies lower wavelengths, increasing then the probability of distortion when transmitted through the perforated plate and bed material. In the "*Future Works*" chapter a possible experiment to clarify this phenomenon will be commented. Also, has to be appreciated the fact that bed material at low flow rates (around 6*00 lpm*) is theoretically under incipient fluidization, as the analysis revealed that fluidization starts at around *550 lpm*. So that, is at those *600 lpm* flow rates where frequency spectra is evolving from incipiently to the fluidization spectra one, making this situation difficult for a clear reading frequency.

So that, a **definitive value for main frequency** for the *Carlos III University of Madrid* prototype under fluidization could be given as the mean value resulting from all the test carried out, as any variable used (bed height h_b, distributor rotation, sensor used, intake samples point) is determinant for measured frequencies but omitting the chamber plenum for 6*00 lpm* data. Upper and lower limits for the election of this frequency could be taken as an evaluation margin. The lower limit could be fix by the mean of the main frequencies for prototype with distributor rotation measured with second series of test for $h_b = {}^{D}/_{2}$, *3,1 %* lower than the total mean, and the upper limit could be fix by the mean of the main frequencies for prototype without distributor rotation, also *3,1 %*. As the condition imposed for both limits gives the same margin, the characteristic frequency would be, using means values (a), using means values without distributor rotation (b) and using mean values with distributor rotation (c) respectively:

a) f = 3,72 ± 0,12 Hz ***b) f = 3,83 ± 0,12 Hz*** ***c) f = 3,60 ± 0,12 Hz***

But, if plenum chamber 6*00 lpm* data is taken for frequency evaluation of prototype, limits would be the same but with different total mean, resulting next main frequency for same a), b) and c) cases:

a) f = 3,69 ± 0,12 Hz ***b) f = 3,77 ± 0,12 Hz*** ***c) f = 3,62 ± 0,12 Hz***

The fluid-dynamic determination for each flow, carried out by correlation of the prototype signal with any of the power spectrum *Johnson et al* [13] ones, demonstrate that, for the three sensors, when bed is already under fluidization, the **fluid-dynamic regime seems to evolve from a multiple bubble regime** (for flow rates from *600 – 1000 lpm*) **to a single bubble regime** (for flow rates from *1100 – 1020 lpm*). This result is coherent as all these the regimes are expected to operate far from transport regimes. The fluid-dynamic behavior repeats a patron of multiple bubble regime till *1000 lpm* to the single bubble regime at *1200 lpm*. Also, inside this fluid-dynamic patron transition regimes could be seen between that ones (multiple - single regime). But out good approximations to the single or multiple regime has been carried because no description of intermediates regimes was studied in *Johnson et al* [13] and because these approximations permit a better understanding of fluidization behavior.

Although it has been widely discussed in previous chapters, **experiments carried out for a bed height of $h_b = 4.8$ cm could not be studied** because the facility does not have a good setup for data taking in the bed (remember that the sensors in the vessel were at the freeboard height). Moreover, it seems that it has reached a limit in the amount of bed material, as it is evidently not able to get a wide enough volume under fluidization due to the gas turbulence which causes greatly material voids that, especially at high speeds, do not permit a clearly fluidized zone. This eventuality did not have consequences in the characterization study or in the frequency domain analysis.

Attending to the modal analysis, it shows that at **nominal electrical engine operation and frequencies from working operations should not cause any structural damage, not also for the entire fluidized bed structure, but for the critical transmission system too in terms of vibrations** as those frequencies (*1 - 5 Hz*) are far from the lower frequencies of vibrations modes (*28,9-33.0 Hz,* those ones that would affect directly to the transmission system).

It could also be ensure that, **for fluid-dynamic investigations, frequencies from electrical engine and working operations will not affect in terms of resonance to the vessel integrity**, hereafter source of investigations, as, this time too, those frequencies (*1 - 5 Hz*) are far from the lower frequencies of vibrations modes that would affect to the vessel directly (*61,9 -70,4 Hz*).

But this entire project was circumscribed in a greater aim far from these specific findings. The final objective was to settle the conditions that let enlarge the current understanding of the fluid-dynamic behavior of a fluidized bed (FB) by developing experimental and theoretical studies working with a FB prototype in the *Carlos III University* of Madrid. And actually, this FB prototype will be focus of the *thesis* develop by *Antonio Soria,* in the *Thermal and Fluids Department* of the *Carlos III University* of Madrid, as its studies are carried out and based on this preliminary work.

10. FUTURE WORKS

Firstly, as in this way was planned, it has to be ensure that for a bed height of $h_b = 4.8\ cm$ and lower, experiments could not be carried out because of lack of material to fluidized. A simple experiment could be done by carrying out the same minimum fluidization velocity experiments but adjusting the amount of material from, for example, $h_b = 6 - 5 - 4 - 3\ cm$. If the obtained deviation pressure curves appears distorted earlier when increasing the flow rate and decreasing the bed height, then a material quantity variable would have to be taken into account for future experiments.

A parallel solution for this eventuality is to reposition the sensor in bed, as the freeboard oscillation at same data intake height could cause distortions in pressure signal monitoring. To solve the problem, a lower conditioned space for sensor in vessel has to be made by using, for example, the same drill as for the current sensor position. To avoid loosing material trough the original space, as sensor would be in the new conditioned one, a tampon dispositive has to be positioned is this way.

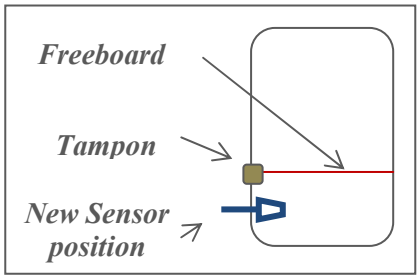

Figure 10.1. New sensor position tampon and freeboard.

In order to clarify if the high frequencies measured in the plenum chamber at low flow rates are distorted by the distributor or not because of it propagation nature, frequency spectra analysis should be object of study in the experiment purposed below for bed heights of $h_b = 6 - 5 - 4 - 3\ cm$. If frequencies measured in plenum camber are lower in all experiments than the ones measured in bed, then distributor or grid, because its orifice dimensions, possibly would interacting with the pressure wave emitted in the bed dissipating it until arrive sensor. If finally so, new distributor or grid redesign would have to carry out by taking into account this new variable.

Despite all these studies, it is always advisable to repeat the experiments first proposed to clarify the doubt about a possible bad performance of them. In fact, after the tests programmed for this project were finished, the experiment for a bed height of

$h_b = 4,8\ cm$ was repeated, and its fluid-dynamic study also proved negative. It would be advisable also to make a frequency spectrum study on this experiment to continue getting results.

In the modal analysis, new prototype models could be proposed. Prototype has been hold to the structure with three reinforcements near engine connector that will reduce impact of the vibration mode as will decrease maximum displacements and percentage of modal mass movement. Despite these reinforcements do not modify modes as changes introduced are not structural changes, a new study with the three reinforcements is advisable to ensure the prototype is out of risk in terms of vibrations.

Knowing that the aim of the project is the fluid-dynamic characterization, nevertheless would be interest to model without simplifications the structure of the prototype. This task need to possess almost unlimited hardware resources that support the simulation, modifying in very low percentage the obtained results, but making more accuracy the solution looked for.

Finally, when the project was programmed, the possibility of doing a fluid-dynamic study using computer software was evaluated. The software chosen would be *Fluent*, a Computational Fluid Dynamics (CFD) software, which met all the necessities require for the analysis, as this software also is used in the *Carlos III University* of Madrid. In fact, the study was started and leaded by personal of the *Thermal and Fluids Department* that, actually, is working in similar objectives. After consult appropriate faculty and literature that were so related with the case, the first simulations were performed, yielding encouraging results. The goal was to design a bed of the same dimensions in a *2D* plane with a fixed bed height. The sequence of the study would be to elevate the gas flow rate until getting the fluidization conditions. The fluidized bed conditions would be the same as in the actual experiment, in which the mean pressure would remain constant in bed once fluidization appears. But the department team realizes that simulations for a determined flow rate take several hours (the average was about 4-5 hours per simulation without the setup that, if it was the first of the series, it could reach up to 1 hour). Surely, with the successive performing of the simulations

would have gain experience and, thus, computation time reduced. But if there were needed 4 different flows rates per different heights carried out, for 4 heights it would have taken more than 80 hours only on simulation. After 2 weeks of simulation performing and three simulations carried out, departmental team realize that must redirect their efforts on achieving the primary objective of making a fluid-dynamic characterization of the bed with the experimental tools and theoretical models of study. Of course, it is now purpose this arduous task as it has a great interest for the *Thermal and Fluids Department* and because is a very helpful tool for complement the characterization. This work, in addition, will amplify the *Carlos III University* of Madrid knowledge in computational fluid dynamics (CFD) software, being an effort that will never be lost since it will remain as a very useful *"Know How"* for the present and the future investigations in the university.

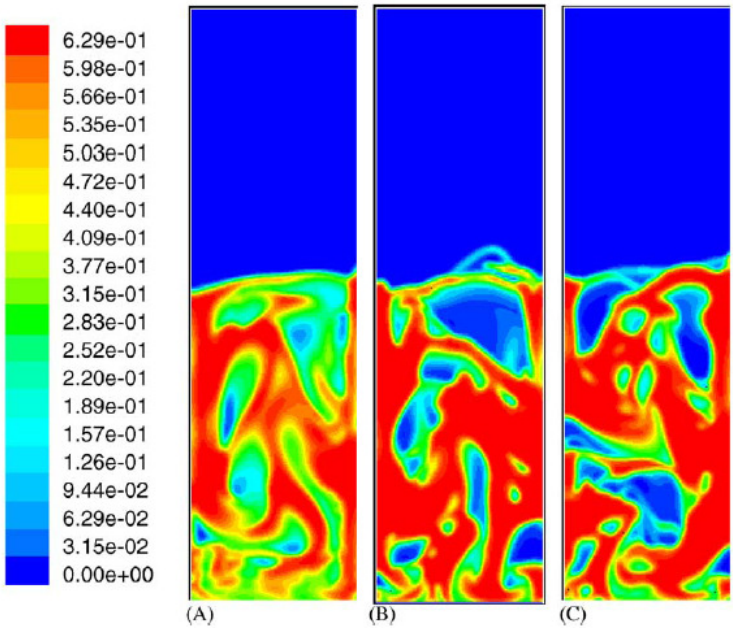

Figure 10.2. Simulated solids volume fraction (U =0.38m/s, drag function: Syamlal–O'Brien, ess =0.9, at 6–7 s; all the simulations started with simulation A at 5 s). (A) First order, 0.001 s time step, 10−3 convergence criterion; (B) second order, 0.001 s time step, 10−3 convergence criterion; (C) second order, 0.0005 s time step, 10−3 convergence criterion) from F. Taghipour et al.[24]

11. ANEX

11.1. BED ASPECT RATIO 1/4

It is shown next the obtained standard deviation for pressure signal graphic for a bed aspect ratio of ¼, a bed height of 4,8 cm, see Graphic 11.1.1. and Graphic 11.1.2., Graphic 11.1.3. and Graphic 11.1.4. :

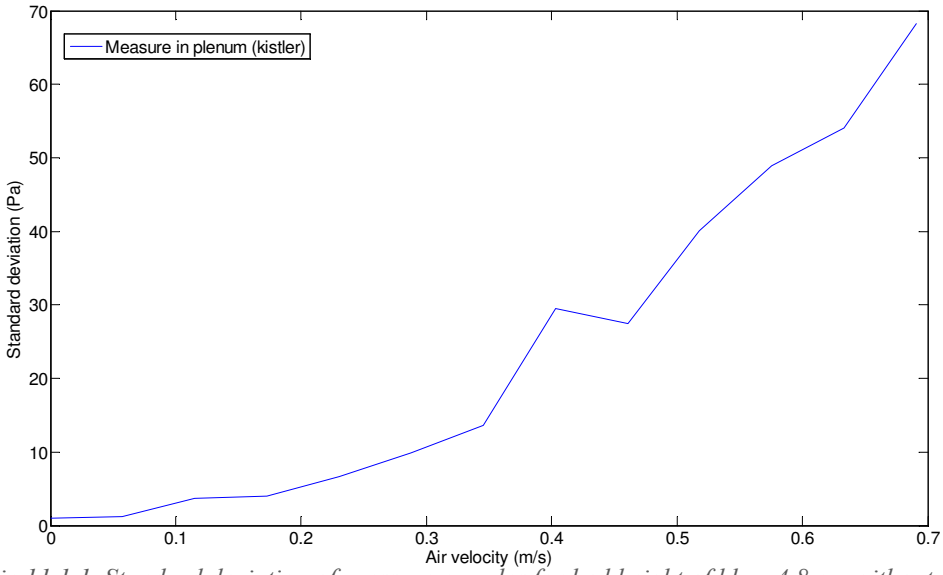

Graphic 11.1.1. Standard deviation of pressure samples for bed height of hb = 4,8 cm without distributor rotation collected by the Kistler sensor at plenum chamber.

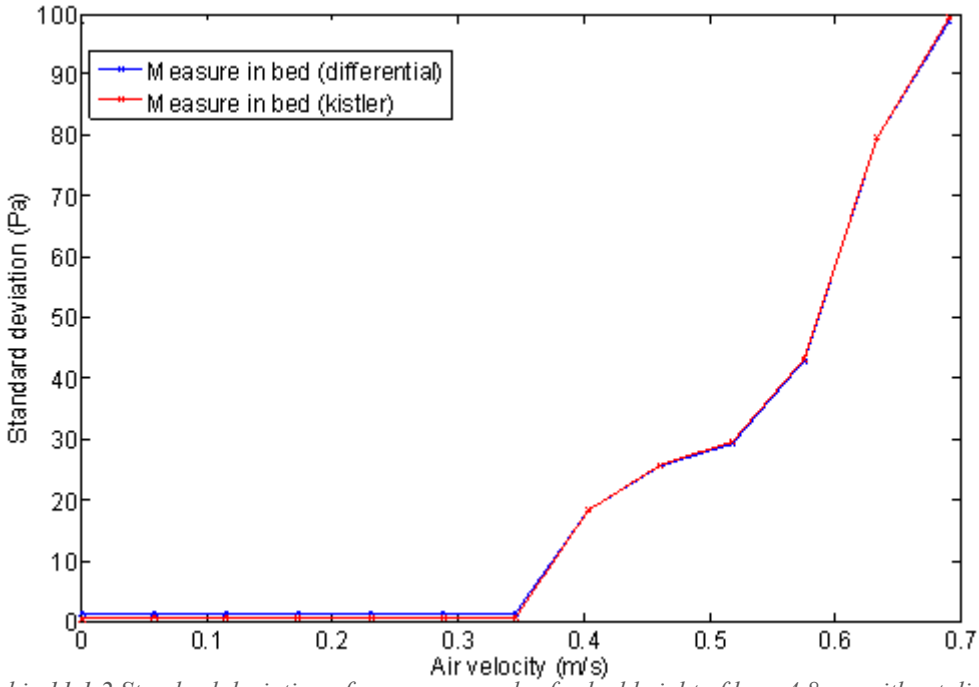

Graphic 11.1.2.Standard deviation of pressure samples for bed height of h_b = 4,8 cm without distributor rotation collected by the Kistler sensor and differential sensor at bed height h_b = 4,8 cm.

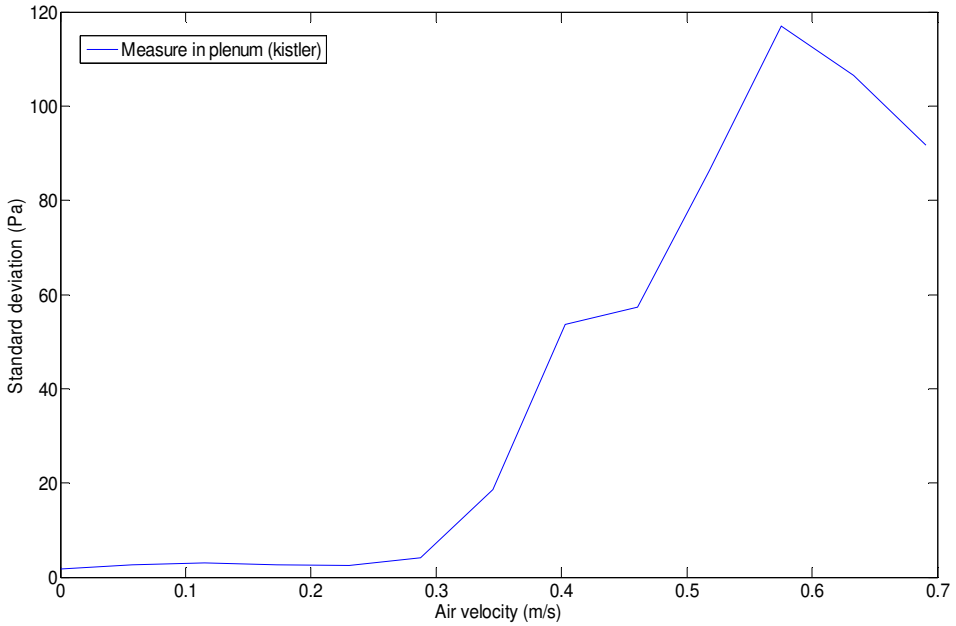

Graphic 11.1.3. Standard deviation of pressure samples for bed height of hb = 4,8 cm with distributor rotation collected by the Kistler sensor at plenum chamber.

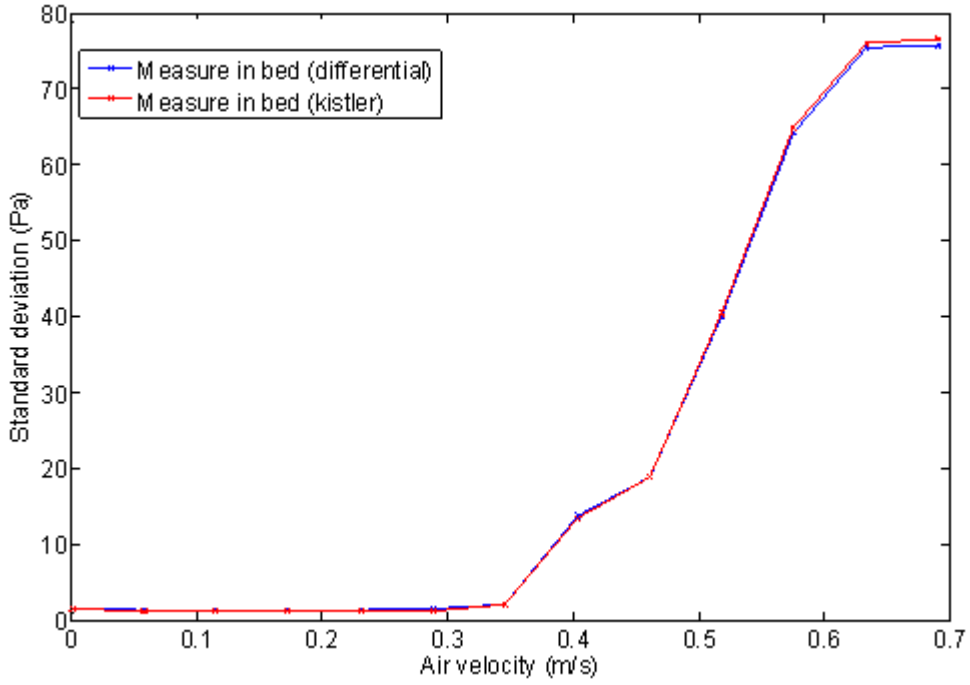

Graphic 11.1.4. Standard deviation of pressure samples for bed height of h_b = 4,8 cm with distributor rotation collected by the Kistler sensor and differential sensor at bed height h_b = 4,8 cm.

11.2. VIBRATION MODES

Are presented now the 40 first vibration modes obtained from ALGOR starting with the number 11, apart form 10 first ones already expose in project,

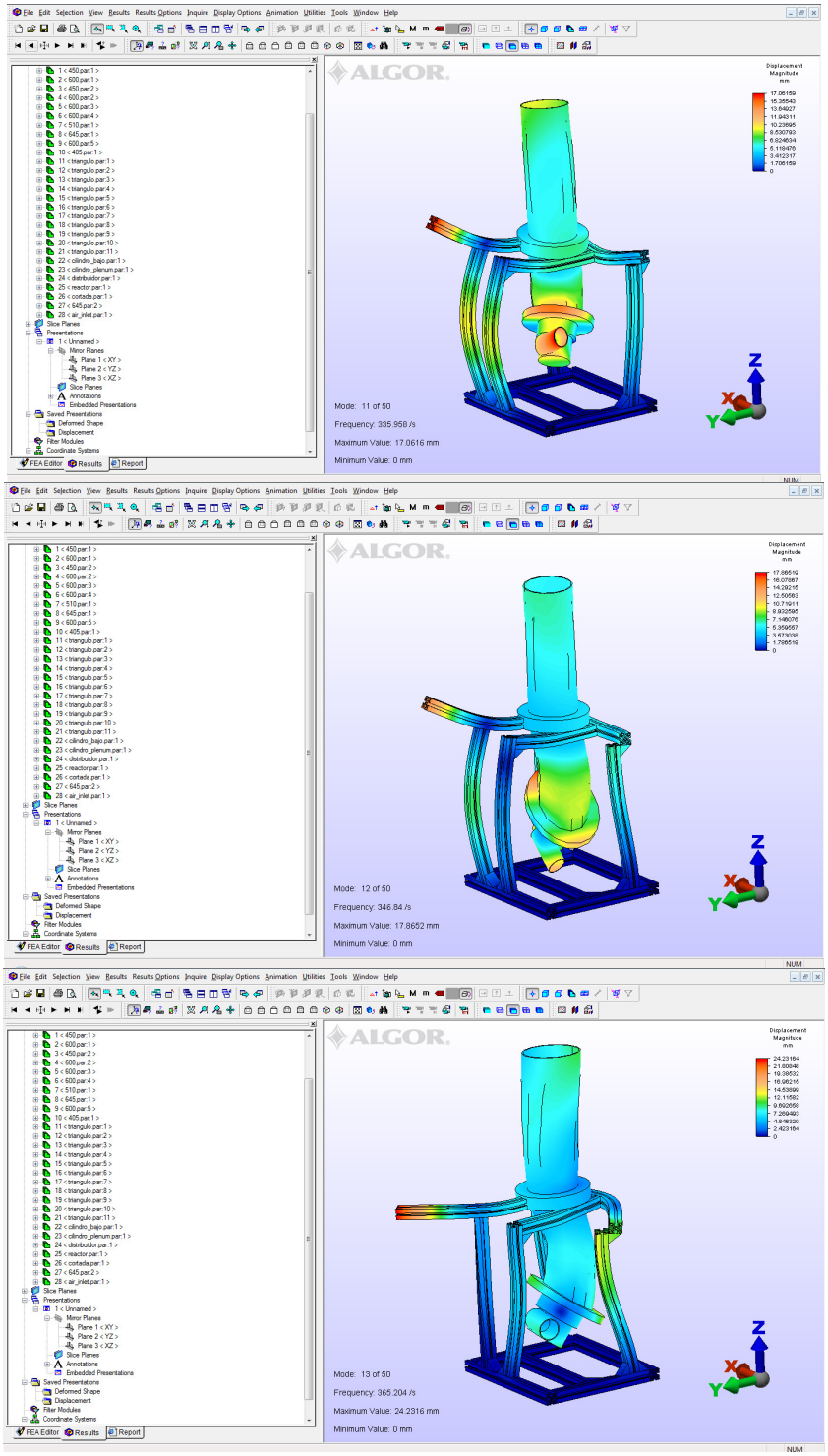

Vibration modes from ALGOR, modes: 11, 12, 13

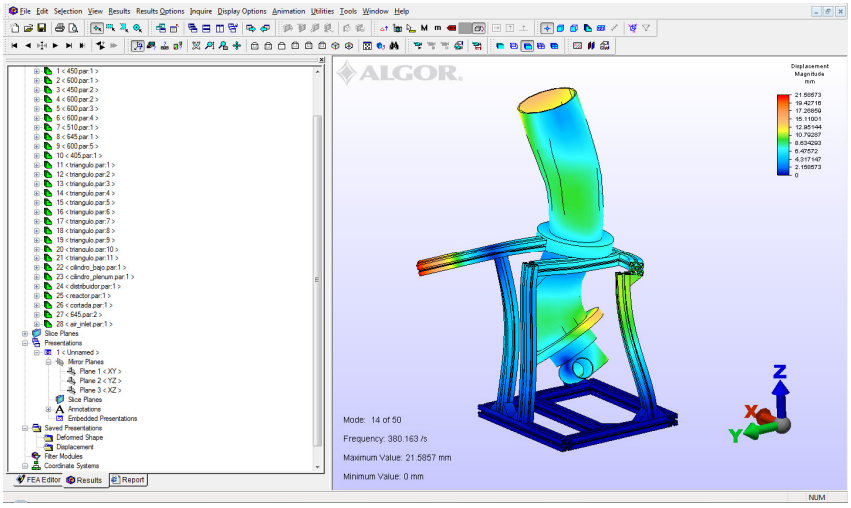

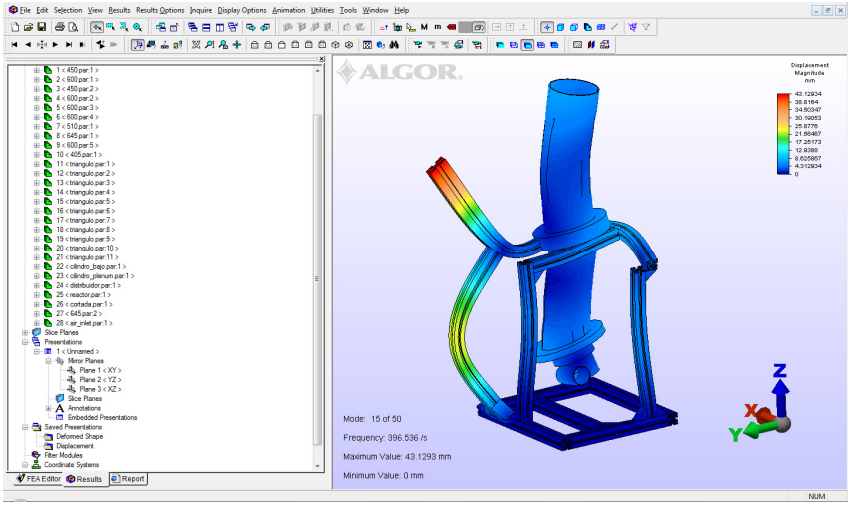

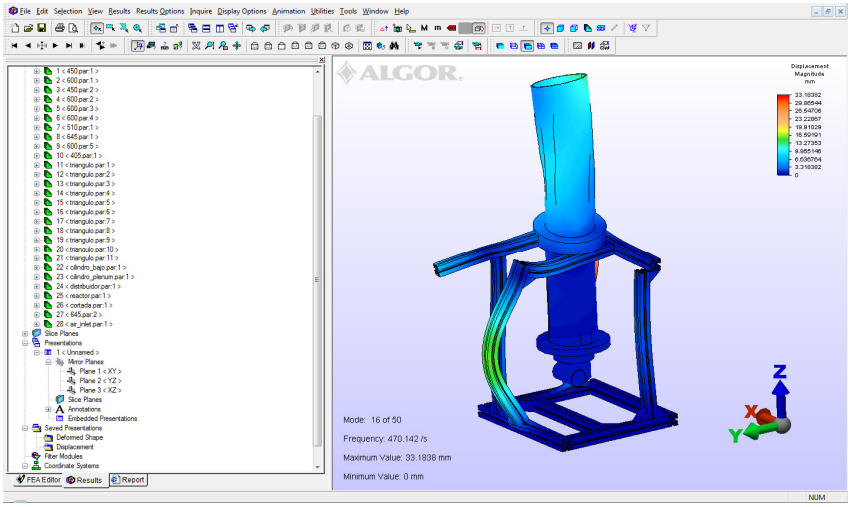

Vibration modes from ALGOR, modes: 14, 15, 16

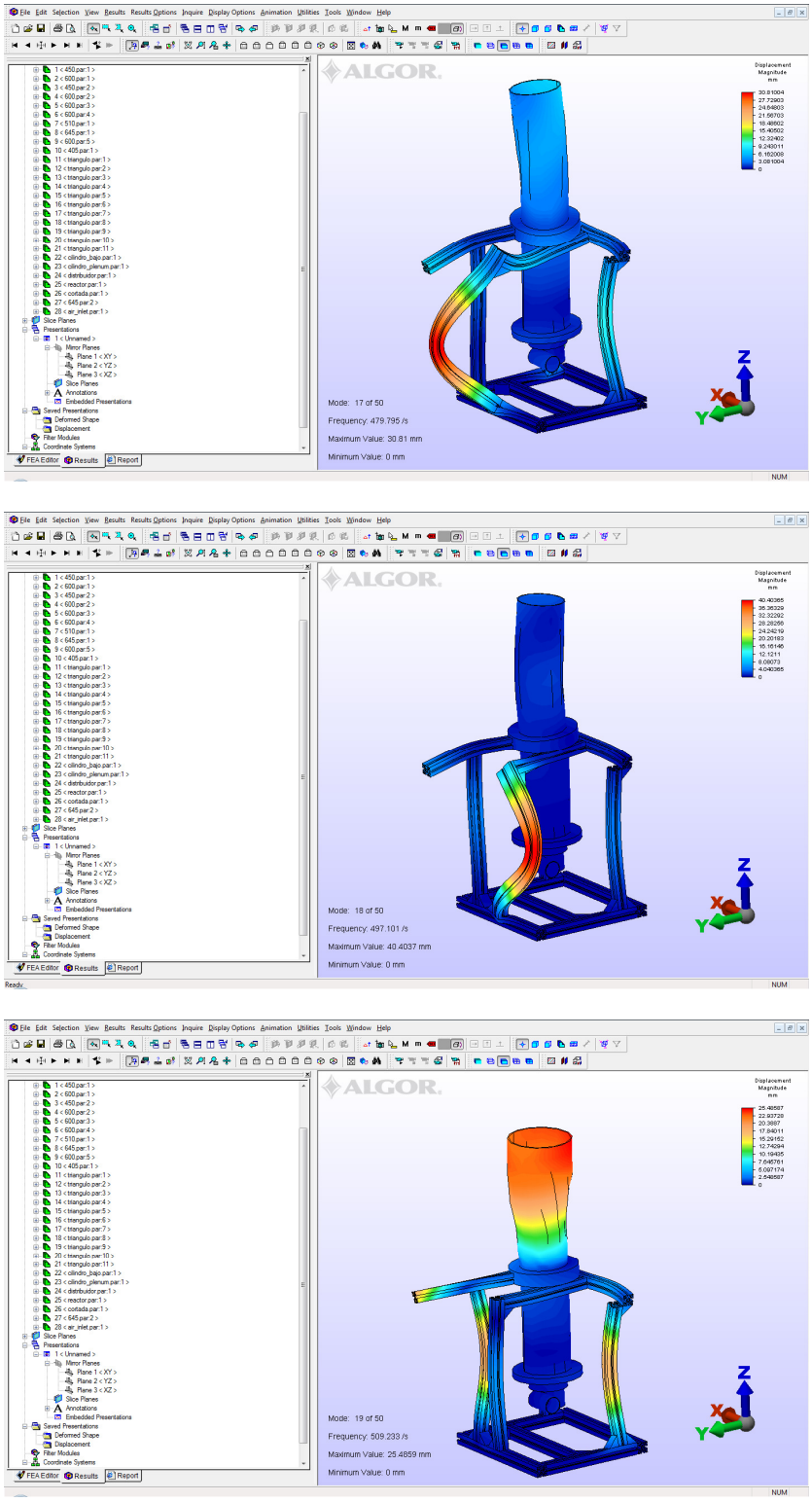

Vibration modes from ALGOR, modes: 17, 18, 19

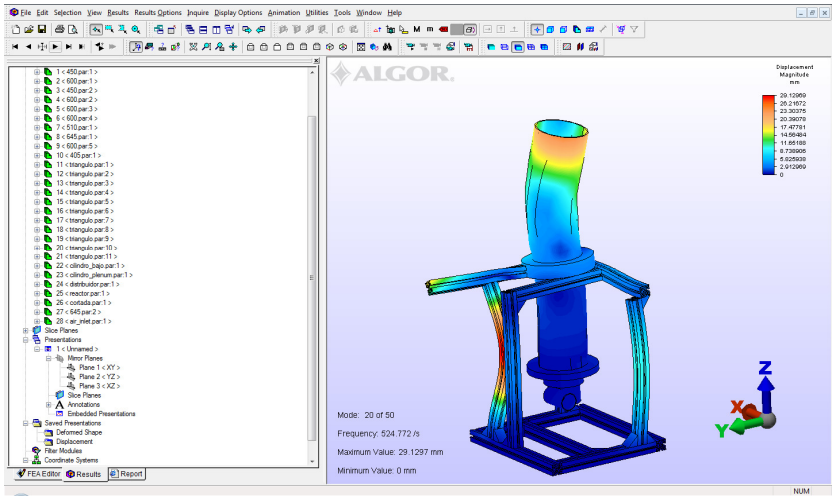

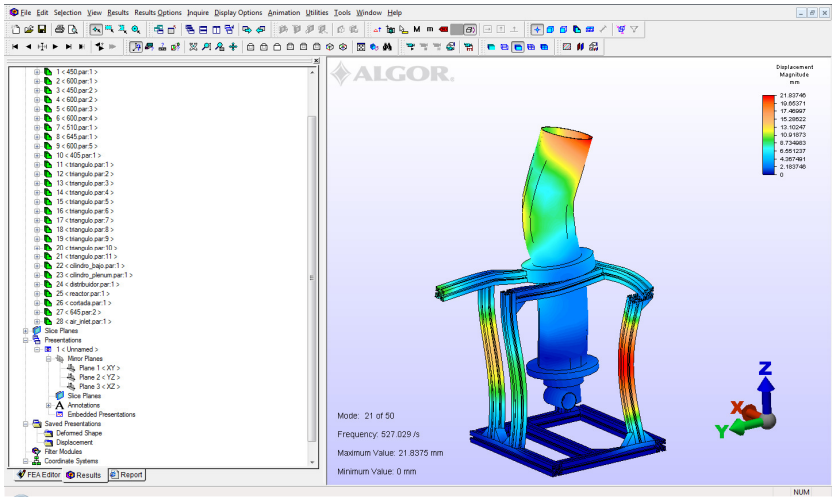

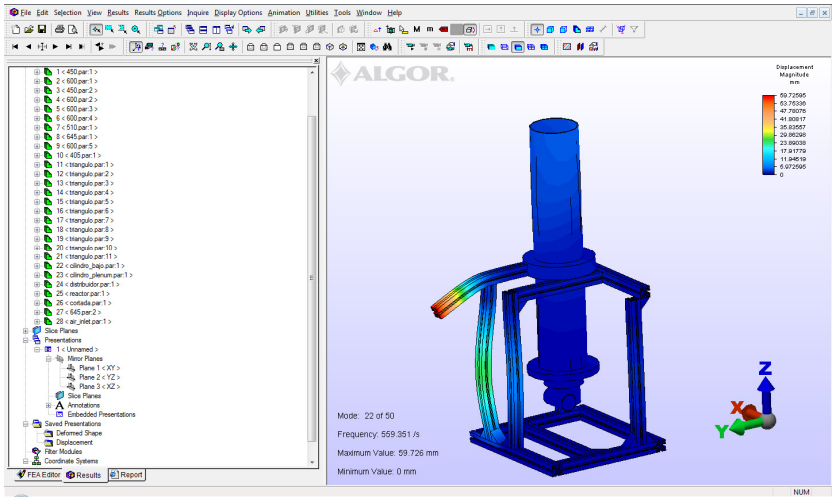

Vibration modes from ALGOR, modes: 20, 21, 22

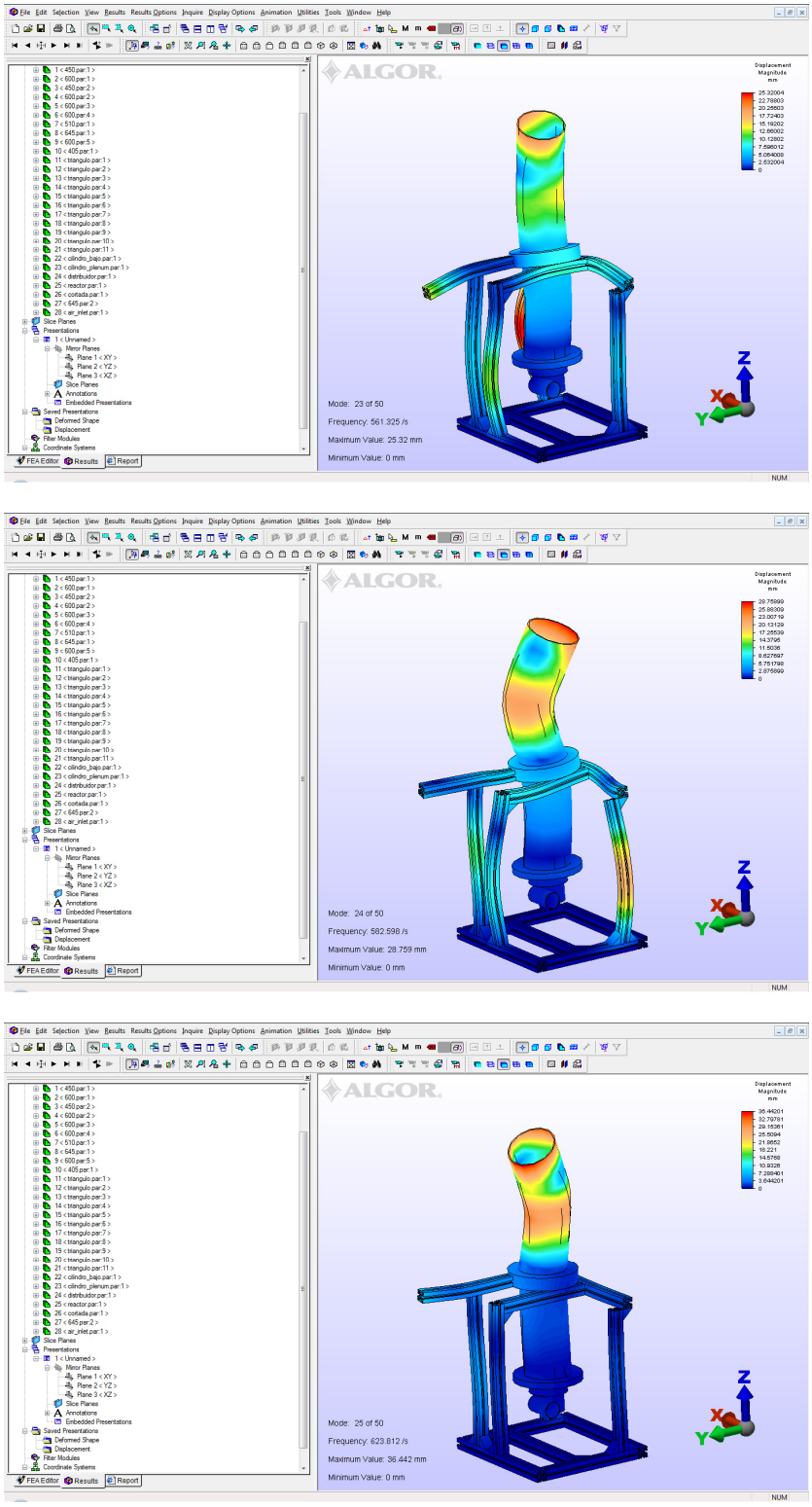

Vibration modes from ALGOR, modes: 23, 24, 25

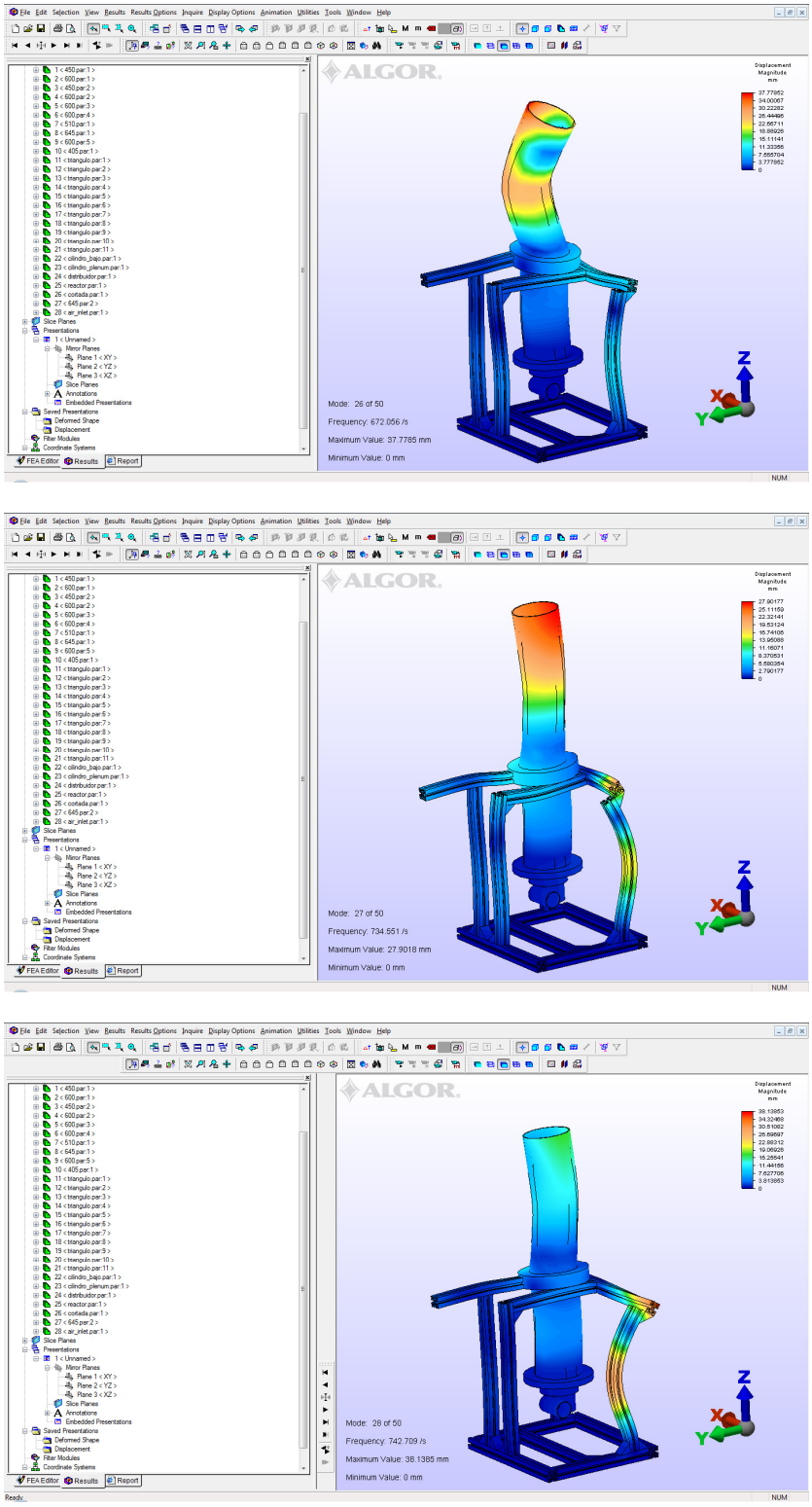

Vibration modes from ALGOR, modes: 26, 27, 28

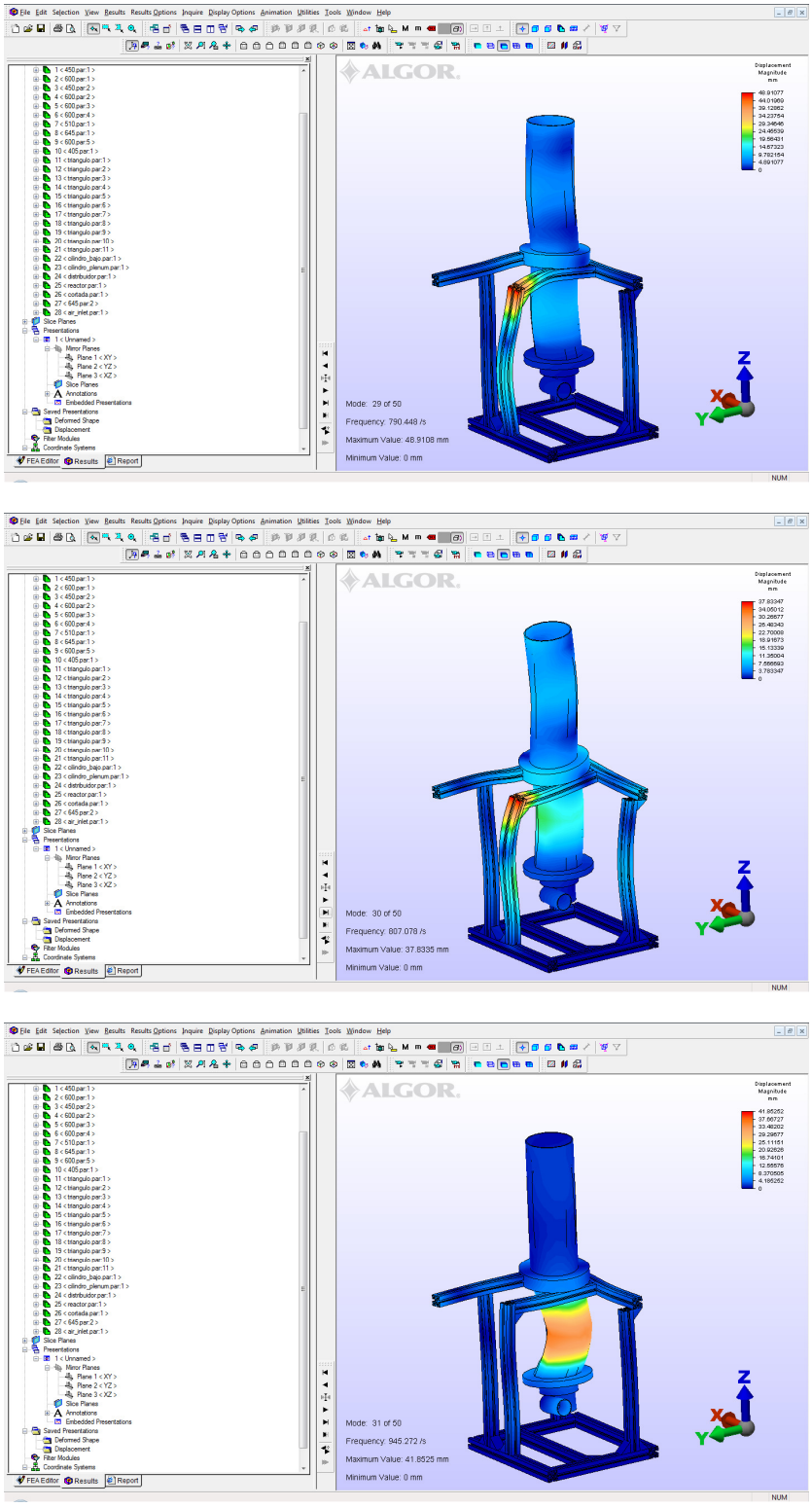

Vibration modes from ALGOR, modes: 29, 30, 31

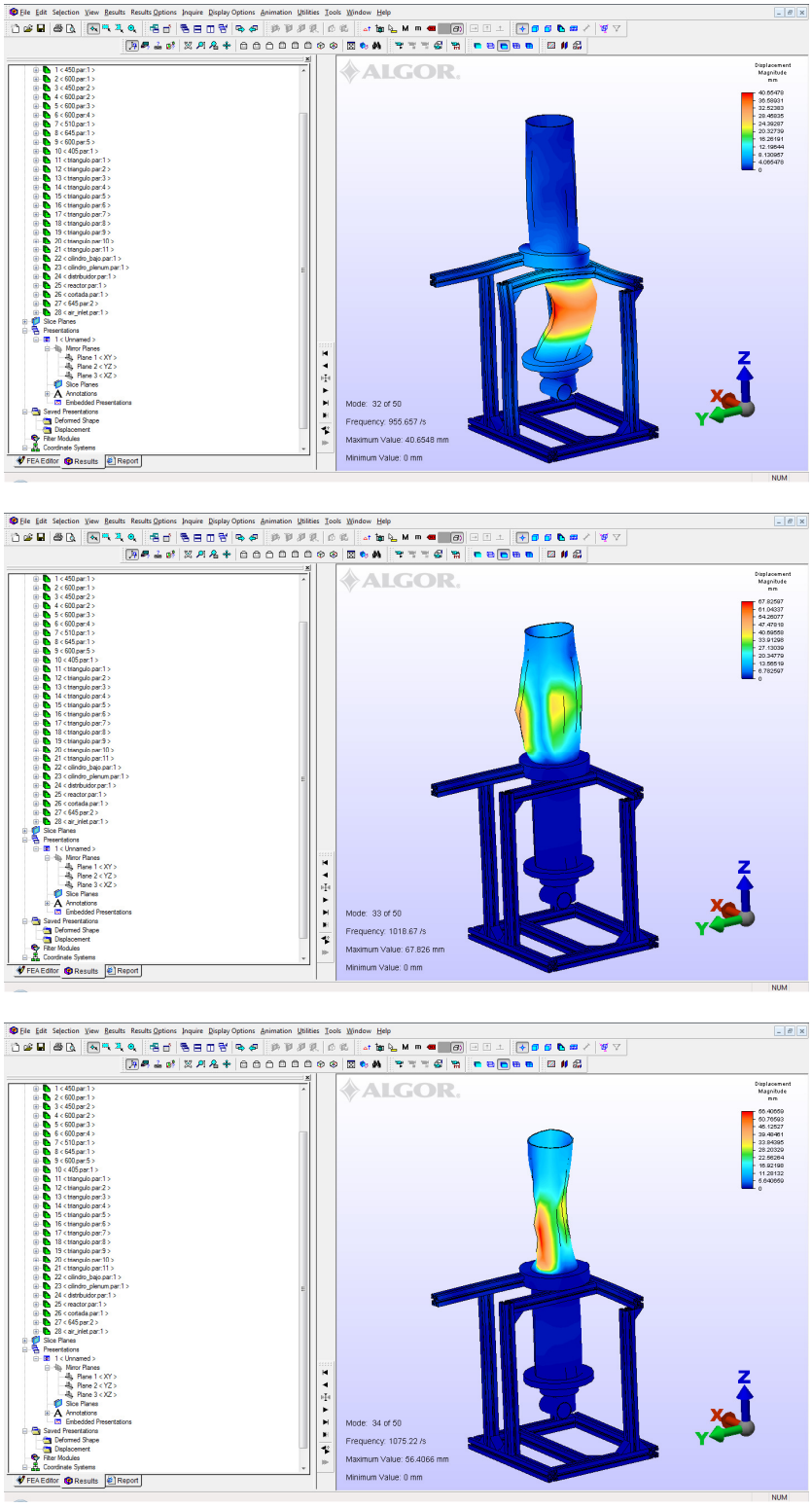

Vibration modes from ALGOR, modes: 32, 33, 34

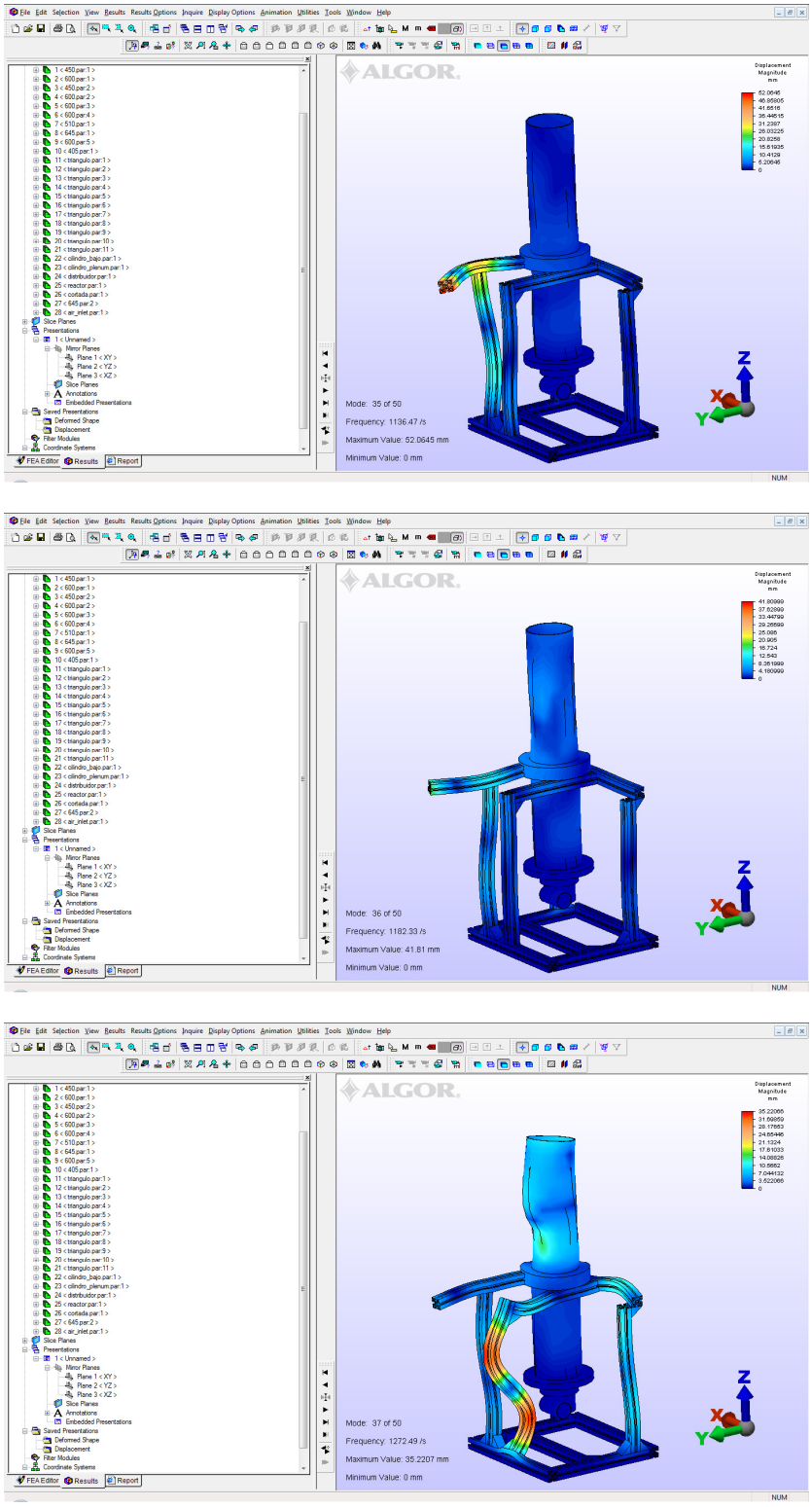

Vibration modes from ALGOR, modes: 35, 36, 37

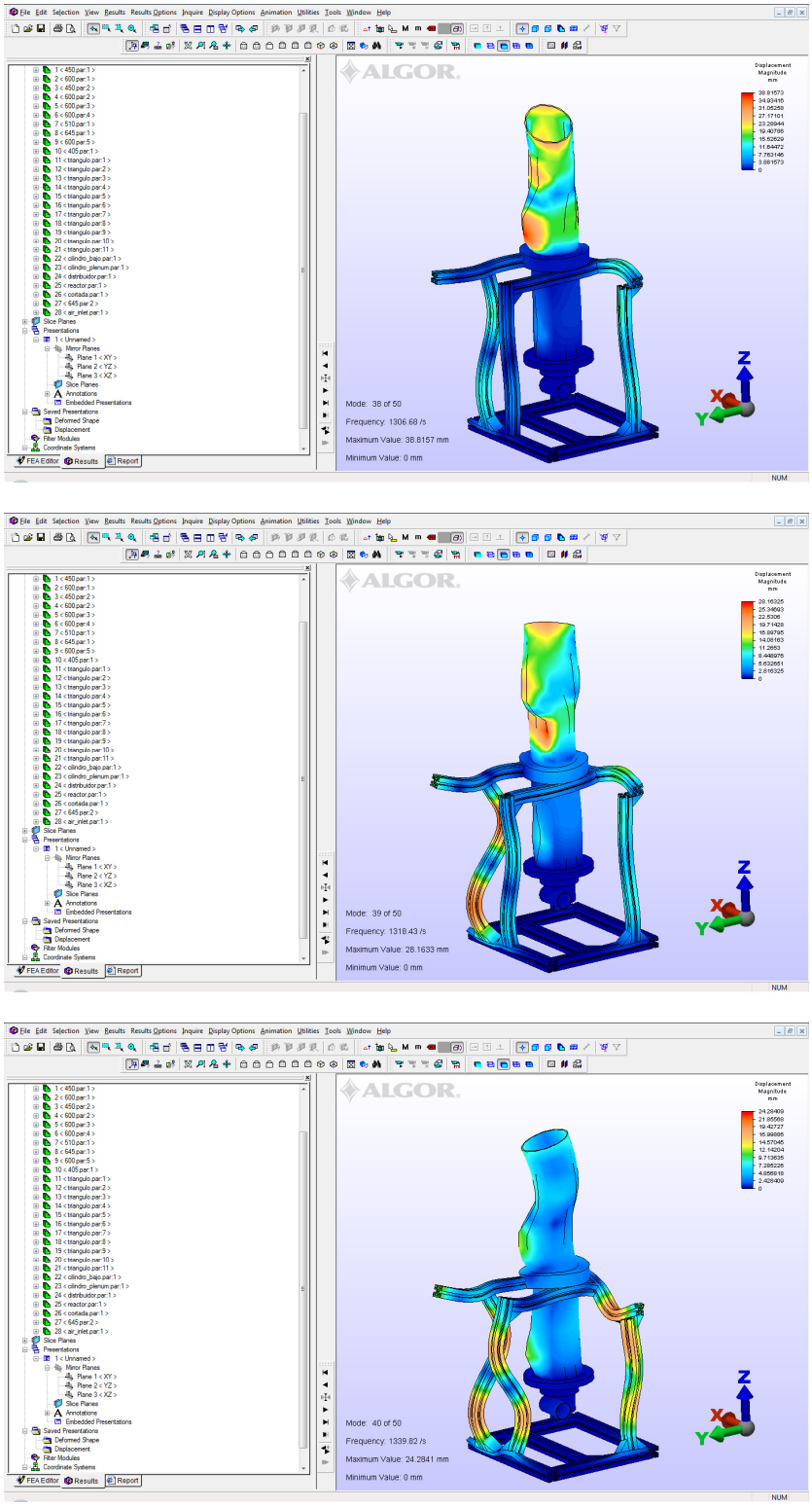

Vibration modes from ALGOR, modes: 38, 39, 40

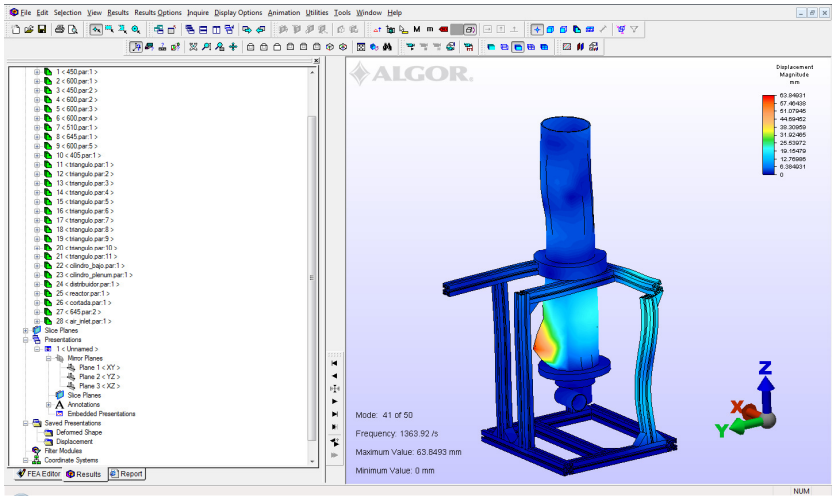

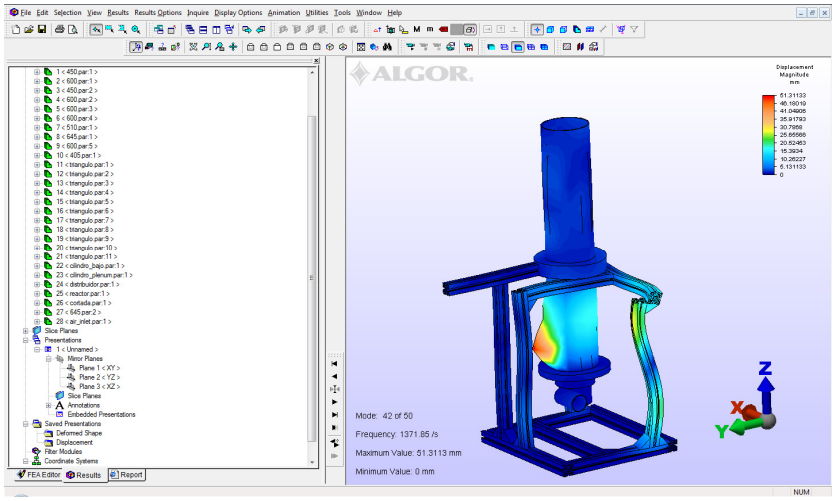

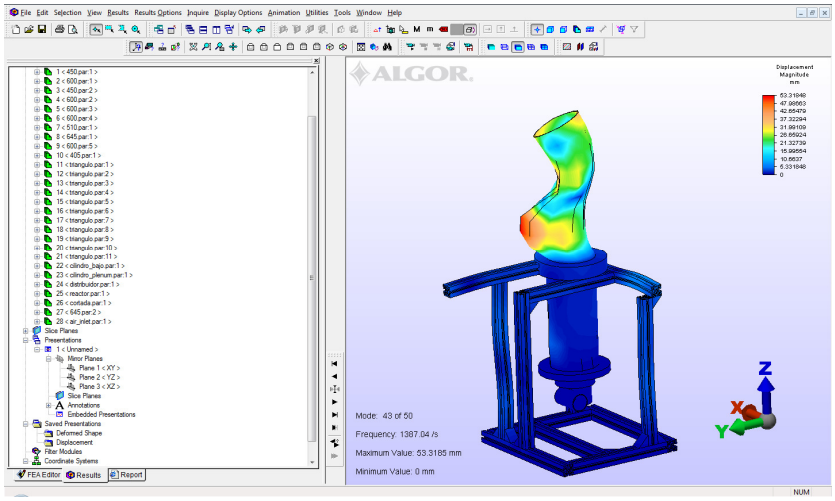

Vibration modes from ALGOR, modes: 41, 42, 43

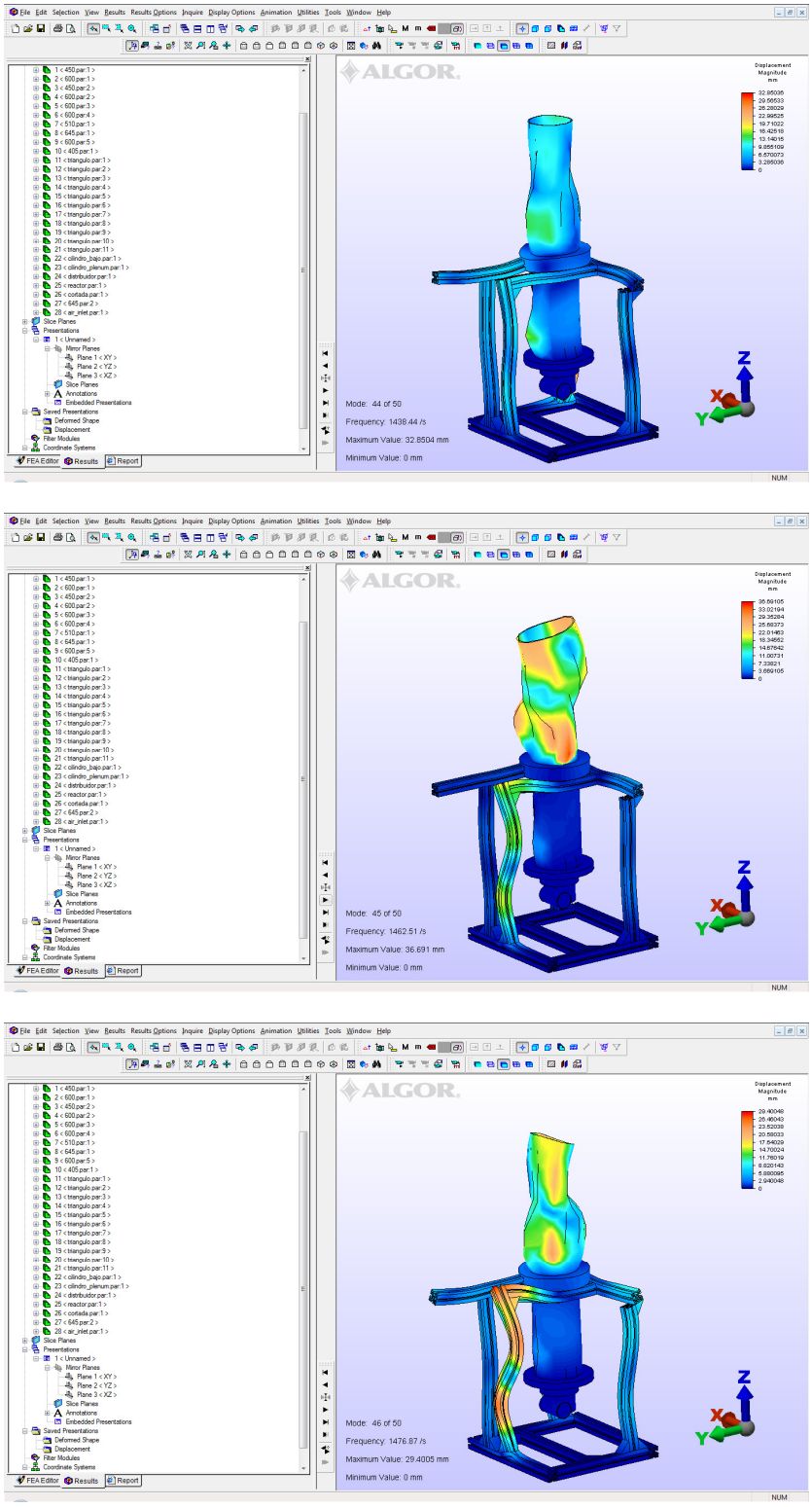

Vibration modes from ALGOR, modes: 44, 45, 46

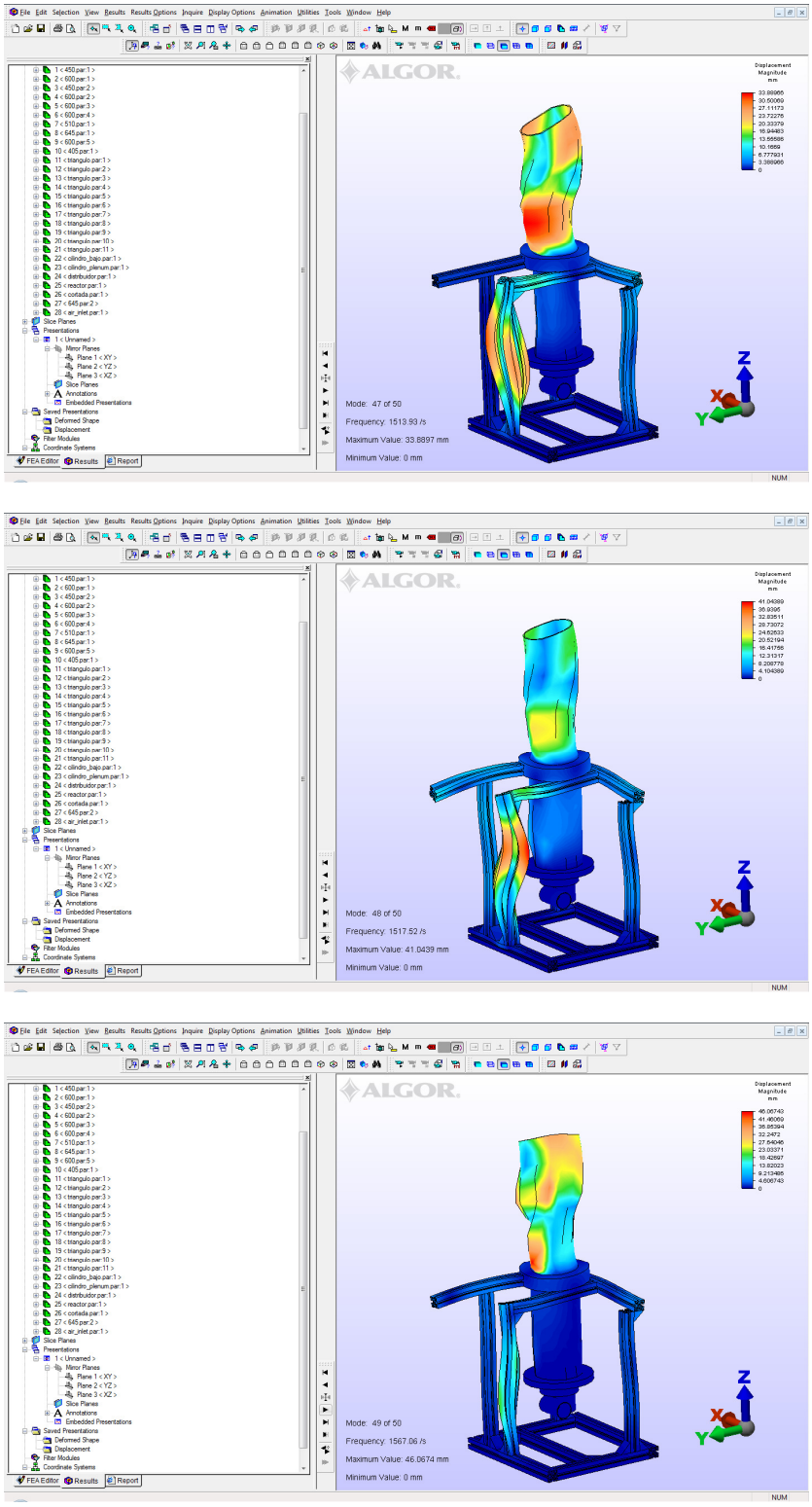

Vibration modes from ALGOR, modes: 47, 48, 49

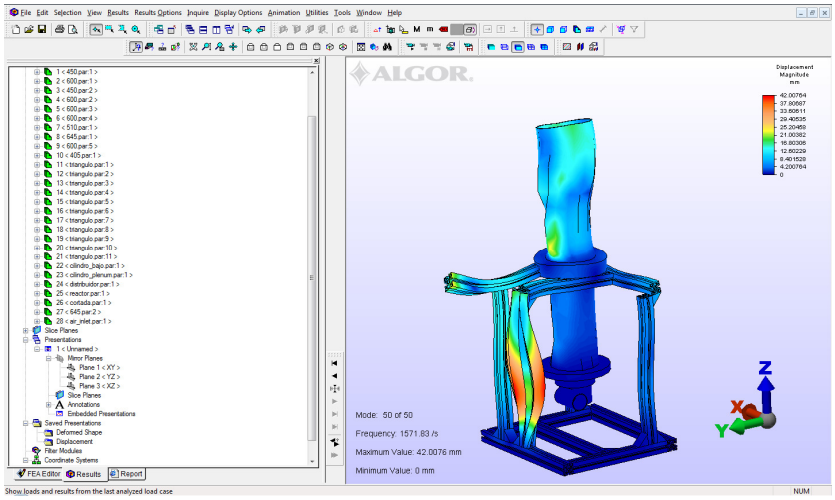

Vibration modes from ALGOR, mode: 50

11.3. KISTLER CHARGE METER

Finally, it is presented technical documentation from *Kistler* charger meter from *Kistler Instruction Manual* [29], see Figure 11.3.1, Figure 11.3.2, Figure 11.3.3. and Figure 11.3.4.:

Measuring mode DC (Long), LP filter off • Bandwidth[17] • Group delay	 kHz µs	 ≈0 ... 200 ≈10

Figure 11.3.1 Frequency response

Analog high-pass filter (1st order)

Time constant, DC (Long) Range FS charge, (voltage) • ≥2 pC, (mV) • ≥1 000 pC, (mV)	 s s	 10 000 100 000
Time constants • Medium[18] • Short[19] Tolerance	s s %	10/100/1 000/2 200 0,1/1/10/220 <±20

Figure 11.3.2 High-pass filter 1st order

Digital low-pass filter functions computed by DSP

Characteristic[20] ▪ Filter type ▪ Order		IIR[21], linear phase 2nd or 5th	
Cutoff frequency (–3 dB) ▪ Steps ▪ Tolerance	Hz %	5 ... 30 000 1/2/3/5 <±10	
Group delay		LP filter 2nd order	5th order
Cutoff frequency (–3 dB) ▪ fg = 30 kHz ▪ fg = 10 kHz ▪ fg = 3 kHz ▪ fg = 1 kHz ▪ fg = 300 Hz ▪ fg = 100 Hz ▪ fg = 30 Hz ▪ fg = 10 Hz	 µs µs µs µs ms ms ms ms	 ≈36 ≈52 ≈330 ≈480 ≈2,5 ≈4,0 ≈25 ≈40	 ≈45 ≈85 ≈450 ≈800 ≈3,5 ≈7,0 ≈35 ≈70

Figure 11.3.3 Low-pass filter

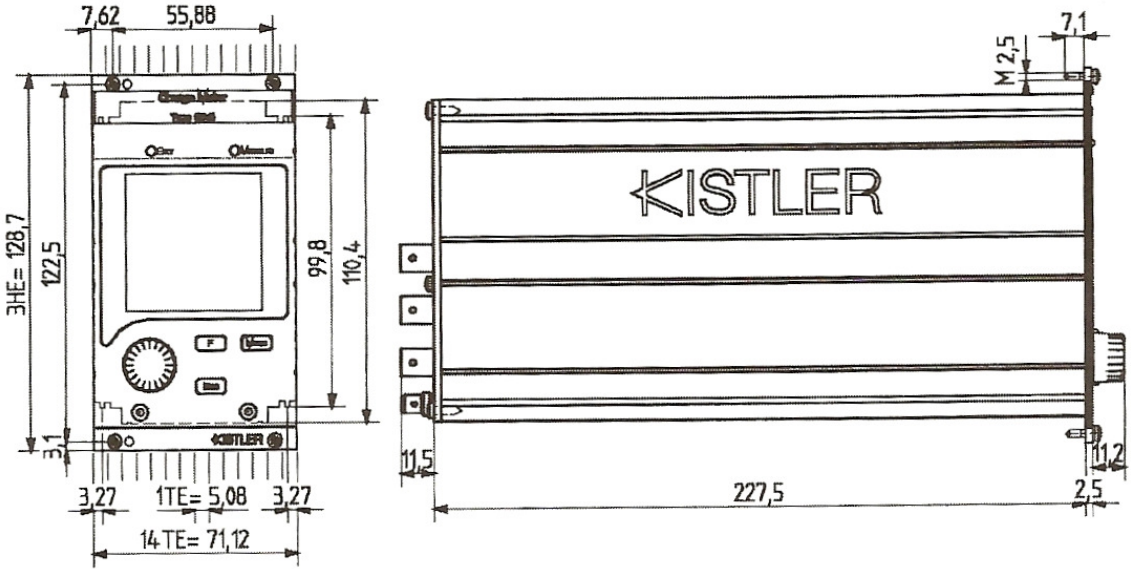

Figure 11.3.4. Kistler 19" plug-in Type 5015A0

12. BIBLIOGRAPHY

[1] Derived from *Ciemat renewable energy reports*, (Web site: *http://www.energiasrenovables.ciemat.es/especiales/energia/index.htm*)

[2] National Energy National Laboratory (USA). Department of energy office of fossil energy. (Web site: *http:// www. netl . doe . gov / technologies / coalpower / combustion / FBC / fbc-benefits.html*)

[3] Derived from Energy Information Administration (EIA). Energy Annual 2004 (May-July 2006). (Web site: *http://www.eia.doe.gov.iea*)

[4] "*Fluidization Engineering"*, Second Edition. Kunii, Octave Levenspiel. USA: Butterworth-Heinemann Edition.

[5] Fluidized bed combustion (USA). Department of energy office of fossil energy. (Web site*: http://en.wikipedia.org/wiki/Fluidized_bed_combustion*)

[6] Trambouze, P., & Euzen, J. (2004). ‘*’Chemical Reactors: From Design to Operation*.’’ (R. Bononno, Trans.). Paris: Editions Technip.

[7] Derived from National Energy National Laboratory (USA). Department of energy office of fossil energy.

[8] Derived from International Journal of Chemical Reactor Engineering.

[9] Derived from *University of Zaragoza*, Master of *"Generación eléctrica: Ciclos Combinados, Cogeneración y Sistemas avanzados de Generación*", "*7.4 Sistemas de Combustión en Lecho Fluido*"

[10] Derived from The University of Akron, Author: George G. Chase, SOLIDS NOTES 5 (Web site: *http: //www.engineering.uakron.edu/~chem./fclty/chase/ Solids / SolidsNotes5%20Fluidization.pdf*)

[11] Derived from Fluid Bed Technology in Materials Processing. Authors: C. K. Gupta, D. Sathiyamoorthy (Web site: *http:// books.google.es/books?id = pnwsQb1WPqwC&pg= PA360&lpg= PA360&dq= bed+aspect+ ratio&source= bl&ots= HekZ4uqG1v&sig =5OH- rQF5MtZhJhmrPXTfopUGZI&hl =es&ei= FJAvStKKIOXPjAfc6MCKCw&sa =X&oi =book_result&ct = result&resnum = 1#PPA360,M1)*

[12] *"Response characteristics of probe–transducer systems for pressure measurements in gas–solid fluidized beds: how to prevent pitfalls in dynamic pressure measurements",* J. Ruud van Ommen, Jaap C. Schouten, Michel L.M. vander Stappen, Cor M. van den Bleek. (Year 1999).

[13] *"Characterization of fluidization regimes by time-series analysis of pressure fluctuations",* F. Johnson, R.C. Zijerveldb, J.C. Schoutenb, C.M. van den Bleekb, B. Lecknera. (Year 2000)

[14] "*Kistler Instruction Manual*, *Charge Meter Type 5015A"*, 2008, *Kistler Instrumente AG.*, Switzerland.

[15] D. Park, O. Levenspiel, and T.J, Fitzergerald, Fuel, 60, 295 (1981); 61, 578 (1982).

[16] *"Flow Resistance: A Design Guide for Engineers"*, Author: *I.E. Idelchik;* pag 265.

[17] *"Flow Resistance: A Design Guide for Engineers", Chemical Industries, Author: Wen-Ching Yang.*

[18] *"Flow Resistance: A Design Guide for Engineers", Chemical Industries, Author: "Geldar And baeyens".*

[19] *"Engineering B45 Sand Sieve Analysis Lab Report", (web site: http:// www2 .bakersfieldcollege.edu/ mrozell/ documents/ Engr%20B45 /sand%20sieve.pdf).*

[20] *"Evaluation of minimum fluidizing velocity in gas fluidized bed from pressure fluctuations"*, Authors: *M. Puncochar, J. Draho§, J. Cbermak and K. Selucky*, Institute of Chemical Process Fundamentals, Czechoslovak Academy of Science.

[21] *H.Y. Sohn and J. Szekely, Chem. Eng. Sci., 27, 763 (1972).*

[22] *Ergun Equation*, (web site: *http :// web 2. Clarkson .edu / projects / Subramanian / ch301 / notes /packfluidbed.pdf*).

[23] Derived from: *http: / / www . fisica . uh . cu / biblioteca / revcubfi / 2000 / Vol.%2017,% 20 No. % 201 y 2/171y2010.pdf*

[24] *"Experimental and computational study of gas–solid fluidized bed hydrodynamics"*, Authors: Fariborz Taghipour, Naoko Ellis, ClaytonWong.

[25] *"Análisis de los modos de vibración de un banco de ensayos de rodamientos"*, Author: *Miguel Ángel de Lucas Hernández*, Trabajo dirigido, Departamento de Ingeniería Mecánica, Universidad Carlos III de Madrid.

[26] "*Resonance, Tacoma Narrows Bridge Failure, and Undergraduate Physics Textbooks"*, Authors: K. Billah and R. Scanlan (1991), American Journal of Physics, 59(2), 118—124.

[27] *"Análisis de vibraciones de un rodamiento con elementos en fase dinámica bajo la acción de una fuerza de desbalance"*, Author: Alfonso Vilches Serrano, Final Proyect, Ingeniería Industrial, Departamento de Ingeniería Mecánica, Universidad Carlos III de Madrid.

[28] *"Caracterización de defectos localizados en sistemas mecánicos rotativos mediante análisis de vibraciones"*, Author: *Higinio Rubio Alonso;* Tesis doctoral, Departamento de Ingeniería Mecánica, Universidad Carlos III de Madrid.

[29] "*Kistler Instruction Manual, Charger Meter Type 5015A…",*

FIGURE INDEX

GRAPHIC INDEX

TABLE INDEX